Author:
Sherrard, Alice

Title:
The role of nuclear F-actin in chromatin organisation

The role of nuclear F-actin in chromatin organisation

Alice Louisa Sherrard

A dissertation submitted to the University of Bristol in accordance with the requirements for award of the degree of Doctor of Philosophy in the Faculty of Life Sciences, Department of Cellular and Molecular Medicine.

October 2018

Word count: 29,481

Abstract

Re-establishment of nuclear structure and chromatin organisation after cell division is essential for genome regulation and cell function. However, the mechanisms underlying these events remain incompletely understood. Previous research identified the transient formation of filamentous actin (F-actin) that arises in the nucleus after mitosis, in several mammalian cell types. Given that the emergence of these filaments coincides with nuclear expansion and chromatin de-condensation, it was hypothesised that nuclear F-actin may drive these processes. Accordingly, this work describes the development of three assays to measure chromatin compaction and/or nuclear structure; through the combined use of fluorescence lifetime imaging (FLIM), electron microscopy (EM) and atomic force microscopy (AFM), a robust platform to detect changes in chromatin compaction was developed. These systems were then deployed to dissect the role of nuclear F-actin in nuclear re-organisation after cell division. AFM and live cell imaging were used to show that nuclear F-actin promotes nuclear expansion after cell division, a process which was impaired by the expression of a nuclear-targeted non-polymerisable actin mutant (NLS-actin^{R62D}). Additionally, FLIM and quantitative EM showed that these actin mutant cells have defective chromatin de-condensation after mitosis, compared to wild-type cells. This increase in chromatin condensation was further confirmed by MNase assays, and the analysis of epigenetic markers associated with chromatin de-condensation. These results also suggest a potential role for nuclear F-actin in the regulation of chromatin re-modelling complexes, including Aurora B. In light of these results, the biological consequences of this increase in chromatin compaction was investigated under conditions, in which polymerisation of nuclear actin after cell division was inhibited (NLS-actin^{R62D}). Using immunofluorescence, it was shown that transcription and progression through G1 was impaired in the daughter cells. Further, using flow cytometry and immunofluorescence to dissect the fate of these cells, defects in the timing of DNA replication were identified, as well as the pronounced accumulation of γH2AX foci in S phase. Finally, these defects were linked to the increase in chromatin compaction observed in G1. Collectively, these findings identify a novel role for nuclear F-actin, which contributes to the re-establishment of an interphase nucleus after cell division. This work has potential implications in the global regulation of chromatin structure throughout the cell cycle, and further emphasises the importance of post-mitotic genome organisation on healthy nuclear function and genome stability.

Acknowledgments

The Kaidi and Grosse lab

Firstly, I would like to thank the members of the Kaidi lab; particularly Melanie, Maria and Paul, for making this such an enjoyable experience. I learnt, and most certainly laughed a lot with you all; for this, I will look back at this time very fondly.

I would also like to thank my previous PhD supervisor, Abderrahmane Kaidi, for his provision of space, finances, collaboration and the opportunity to do this work. Importantly, I would like to thank Robert Grosse, and the members of his laboratory, especially Matthias and Christian. I am very grateful for this experience, and the opportunity to work on such a brilliant project. In addition to scientific input, I would also like to personally thank Robert, for the support that he showed me.

The Roberts lab

I would like to thank Stefan Roberts for supporting me academically, providing career advice, and for always having time to chat. In addition, I thank you for taking over my supervision and all the help you have provided this year. I would also like to thank current and previous lab members; Lyndsey, Sam, and Amy for their help during both my undergraduate and PhD.

The Verkade lab

I would next like to thank Paul, Lorna, Jen Judith and Hugh for welcoming me into their lab. I learnt a lot from you all, and was very lucky to work with such great people. I really enjoyed my time here! And not forgetting Tania and Catherine, it was great to share an office with you!

The Wolfson Bioimaging facility

I thank the Wolfson Bioimaging facility, particularly, Dom, Stephen, Chis, Tom, Gini, and Judith, for providing such brilliant training. Some of the most important skills that I learnt here were provided by this facility, and I can't thank you all enough for all you have taught me. Tom, EM wouldn't have been the same without you. Chris, you are a nutter. Dom, I will miss you greatly, and will remember all our FLIM hours very fondly. I also thank Christoph for being a great panel member and providing support during my PhD.

The G66 slags

To all of the G66 slags; Adam, Alex, Rhys, Madhu, Amy, Danny, Elle, Steve, Mel, Paul, Maria; you are a bunch of legends and it was a pleasure to share a lab space with you all!!

Other

Finally, I thank George Smith for cooking me dinner, picking me up late at night and generally looking after me for all these years! In addition, I thank Ana Rubio for making all my balls.

Declaration

I declare that the work in this dissertation was carried out in accordance with the requirements of the University's Regulations and Code of Practice for Research Degree Programmes and that it has not been submitted for any other academic award. Except where indicated by specific reference in the text, the work is the candidate's own work. Work done in collaboration with, or with the assistance of, others, is indicated as such. Any views expressed in the dissertation are those of the author.

SIGNED: ..... DATE: .....

Alice Sherrard

Abbreviations

- **2DG:** 2-deoxy-D-glucose
- **AFM:** Atomic force microscopy
- **ANOVA:** Analysis of variance
- **APC:** Anaphase promoting complex
- **APS:** Ammonium persulfate
- **ATR:** Ataxia telangiectasia and Rad3-related
- **ATM:** Ataxia-telangiectasia-mutated
- **ATP:** Adenosine triphosphate
- **ATRIP:** ATR interacting protein
- **BAF:** Brg/Brm-associated factor
- **BFP:** Blue fluorescent protein
- **Cdc25:** Cell division cycle 25
- **Cdc45:** Cell division cycle 45
- **Cdc6:** Cell division cycle 6
- **CdcA2:** Cell division cycle associated 2
- **CDK:** Cyclin dependent kinase
- **cDNA:** Complementary DNA
- **CDT1:** Chromatin licensing and DNA replication factor 1
- **ChIP:** Chromatin immunoprecipitation
- **CHK2pS345:** Checkpoint kinase 2 phosphorylated serine 345
- **CRISPR:** Clustered regularly interspaced short palindromic repeats
- **Cryo-FIB-SEM:** Cryogenic-focussed ion beam-scanning electron microscopy
- **Ct:** Cycle threshold
- **CTCF:** CCCTC-binding factor
- **CTD:** C-terminal repeat domain
- **C-terminus:** Carboxyl terminus
- **DAPI:** 4′,6-diamidino-2-phenylindole
- **DMEM:** Dulbecco's modified eagle's medium
- **DMSO:** Dimethyl sulfoxide
- **DNA:** Deoxyribonucleic acid
- **DNA-PK:** DNA-protein kinase
- **mTOR:** Mammalian target of rapamycin
- **PI3K:** Phosphoinositide 3-kinase
- **DNase:** An enzyme which digests DNA
- **DSB:** Double strand break
- **DTT:** Dichloro diphenyl trichloroethane
- **E2F:** E2 Transcription factor
- **EDTA:** Ethylenediamine tetraacetic acid
- **EM:** Electron microscopy
- **ER:** Endoplasmic reticulum
- **LAP2β:** Lamin-associated protein 2 β
- **EDU:** 5-Ethynyl-2´-deoxyuridine
- **ETP:** Etoposide
- **EU:** 5-ethynyl uridine
- **FACS:** Florescence activated cell sorting

- **F-actin:** Filamentous actin
- **FBS:** Foetal bovine serum
- **FISH:** Fluorescent in situ hybridisation
- **FLIM:** Fluorescence lifetime imaging
- **FRAP:** Fluorescence recovery after photobleaching
- **FRET:** Fluorescence (Förster) resonance energy transfer
- **G1:** Gap 1
- **G2:** Gap 2
- **G-actin:** Globular actin
- **GFP:** Green fluorescent protein
- **GTP:** Guanosine-5'-triphosphate
- **H2A:** Histone 2A
- **H2AX:** Histone 2AX
- **H2B:** Histone 2B
- **H2B2^{1FP}:** Histone 2B labelled with GFP
- **H2B2^{2FP}:** Histone 2B labelled with GFP and mCherry
- **H3:** Histone 3
- **H3K27ac:** Histone 3 lysine 27 acetylation
- **H3K9me2/3:** Histone 3 lysine 9 di/tri methylation
- **H3S10ph:** Histone 3 serine 10 phosphorylation
- **H3S28ph:** Histone 3 serine 28 phosphorylation
- **H3T11ph:** Histone 3 threonine 11 phosphorylation
- **H3T3ph:** Histone 3 threonine 3 phosphorylation
- **H4:** Histone 4
- **H4ac:** Histone 4 acetylation
- **H4K16ac:** Histone 4 lysine 16 acetylation
- **H4K20me1/2/3:** Histone 3 lysine 20 mono/di/tri methylation
- **HDAC:** Histone deacetylase
- **HiC:** Chromatin conformation and capture and high throughput sequencing
- **HMTase:** Histone methyltransferase
- **HRP:** Horse radish peroxidase
- **HSV VP16:** Herpes simplex virus protein 16
- **INCENP:** Inner centromere protein
- **INM:** Inner nuclear membrane
- **Kat5:** Lysine acetyltransferase 5
- **ko:** Knock out
- **LAD:** Lamin-associated domain
- **Lat:** Latrunculin B
- **LINC:** Linker of nucleoskeleton and cytoskeleton
- **MCM:** Minichromosome maintenance protein complex
- **mDia:** Diaphanous-related formin
- **MNase:** Micrococcal nuclease
- **mRNA:** Messenger RNA
- **nAC:** Nuclear actin chromobody
- **NAD:** Nicotinamide adenine dinucleotide
- **NaN_3:** Sodium azide
- **NE:** Nuclear envelope
- **NEB:** Nuclear envelope breakdown

- **NLS:** Nuclear localisation signal
- **NM1:** Nuclear myosin 1
- **NPC:** Nuclear pore complex
- **NPL4:** Nuclear protein localization protein 4 homolog
- **N-terminus:** Amino terminus
- **ONM:** Outer nuclear membrane
- **PBS:** Phosphate buffered saline
- **PCNA:** Proliferating cell nuclear antigen
- **PCR:** Polymerase chain reaction
- **PDMS:** Polydimethylsiloxane
- **PEI:** Polyethyleneimine
- **PFA:** Paraformaldehyde
- **PI:** Propidium iodide
- **PIP2:** Phosphatidylinositol 4,5-bisphosphate
- **PP1:** Protein phosphatase 1
- **PP2A:** Protein phosphatase 2A
- **pRPAs33**: Replication protein A phosphorylation at serine 33
- **PVDF:** Polyvinylidene difluoride
- **qPCR:** Quantitative PCR
- **R62D:** Arginine 62 replaced with glutamic acid
- **RAD:** RIF1 associated domain
- **Rb:** Retinoblastoma
- **RNA:** Ribonucleic acid
- **RNase:** An enzyme which digests RNA
- **RNAP:** RNA polymerase
- **ROI:** Region of interest
- **rRNA:** Ribosomal RNA
- **tRNA:** Transfer RNA
- **RT:** Room temperature
- **RUVBL1:** RuvB-like 1
- **RUVBL2:** RuvB-like 2
- **SDS:** Sodium Dodecyl Sulfate
- **SEM:** Scanning electron microscopy
- **siRNA:** Small interfering RNA
- **SIRT2:** NAD-dependent deacetylase sirtuin-2
- **SMC:** Structural Maintenance of Chromosomes
- **SRF:** Serum response factor
- **SUN1:** SUN domain containing protein 1
- **TAD:** Topologically associated domain
- **TDP:** Timing decision point
- **TEM:** Transmission electron microscopy
- **TEMED:** Tetramethylethylenediamine
- **TSA:** Trichostatin A
- **UFD1:** Ubiquitin recognition factor in ER associated degradation 1
- **VCP:** Valosin-containing protein
- **WT:** Wild type
- **YM:** Young's Modulus
- **γH2AX:** Histone H2AX phosphorylation

Contents

Chapter 1 : Main introduction 1

1.1 Background 2

1.2 The nuclear envelope 3

1.2.1 Nuclear envelope breakdown 3

1.2.2 Nuclear envelope reformation 4

1.2.3 Nuclear lamina reformation 4

1.3 Chromatin condensation 6

1.3.1 Histone modifications 6

1.3.2 Chromosome associated proteins 9

1.4 Chromatin de-condensation 11

1.4.1 Removal of Aurora B 11

1.4.2 Chromatin de-compaction proteins 12

1.5 Nuclear re-organisation 12

1.6 Nuclear bodies 15

1.7 Nuclear actin 16

1.7.1 Nuclear actin and transcription 17

1.7.2 Formation of nuclear actin filaments 18

1.8 Nuclear F-actin and chromatin organisation 20

1.9 Manipulating nuclear F-actin 21

1.10 Project Aims 24

Chapter 2 : Materials and Methods 25

2.1 Cell lines 26

2.1.1 NIH-3T3 26

2.1.2 NIH-3T3-BFP-NLS-Actin$^{WT/R62D}$ cells 26

2.1.3 NIH-3T3-FLAG-NLS-Actin$^{WT/R62D}$ cells 26

2.1.4 NIH-3T3-GFP-H2B and NIH-3T3-GFP-H2B-mCherry cells 27

2.1.5 NIH-3T3-BFP-NLS-Actin$^{WT/R62D}$+nAC-mCherry-H2B cells 27

2.1.6 RPE1 control and ATM ko cells 27

2.1.7 HEK293 cells 28

2.2 Cell culture 28

2.3 Cell synchronisation 28
2.3.1 Mitotic synchronisation 28
2.3.2 S phase synchronisation 29
2.4 Cell treatments 29
2.4.1 VCPi 29
2.4.2 Chromatin compaction and de-compaction 29
2.4.3 DNA damage 29
2.4.4 Flavopiridol 29
2.5 siRNA 29
2.6 Production of lentivirus 30
2.7 Fluorescence activated cell sorting (FACS) 30
2.8 Transfections 30
2.9 Nucleofection 31
2.10 Primary antibodies and dilutions 31
2.11 Secondary antibodies and dilutions 33
2.12 Western blotting 34
2.13 qPCR 35
2.13.1 qPCR primers: 35
2.14 MNase Assay 36
2.15 Immunocytochemistry/ immunofluorescence 36
2.16 CLICK chemistry 37
2.16.1 EDU flow cytometry staining protocol 37
2.16.2 EDU imaging staining protocol 37
2.16.3 EU staining protocol 38
2.17 Flow cytometry 38
2.17.1 Flow Jo (flow cytometry analysis) 39
2.18 Light microscopy 39
2.18.1 Widefield (Delta Vision) 39
2.18.2 Confocal (FLIM system) 40
2.18.3 IncuCyte microscope 40
2.19 Fluorescence lifetime imaging (FLIM) 40
2.19.1 Cell line generation and staining 40

2.19.2 Data acquisition 41
2.19.3 Fitting of FLIM data 41
2.20 Electron microscopy (EM) 41
2.20.1 Sample preparation: cell fixation 41
2.20.2 Sample preparation: high pressure freezing 42
2.20.3 Imaging 43
2.21 Atomic force microscopy (AFM) 43
2.21.1 Peak force AFM 45
2.21.2 Sample preparation 47
2.21.3 Imaging 47
2.22 Image Analysis 48
2.22.1 Cell profiler. 48
2.22.2 Fiji. 49
2.22.3 MATLAB 49
2.23 Statistics 50
Chapter 3 : Development of assays to measure chromatin compaction 51
3.1 Introduction 52
3.2 Results 55
3.2.1 Fluorescence lifetime imaging 55
3.2.2 Electron microscopy 74
3.2.3 Atomic force microscopy (AFM) 76
3.3 Discussion 80
Chapter 4 : Nuclear F-actin promotes nuclear re-organisation after cell division 84
4.1 Introduction 85
4.2 Results 89
4.2.1 Nuclear F-actin promotes post-mitotic chromatin de-condensation 89
4.2.2 Nuclear F-actin promotes histone modifications that are associated with chromatin de-condensation 97
4.2.3 Regulation of Aurora B 102
4.2.4 Nuclear F-actin promotes post-mitotic nuclear expansion 104

4.2.5 Re-establishment of nuclear bodies 110
4.3 Discussion 112
Chapter 5 : Consequences of nuclear F-actin assembly 115
5.1 Introduction 116
5.2 Results 119
5.2.1 Polymerisation of nuclear actin after cell division is important for mRNA transcription in G1 119
5.2.2 Inhibition of nuclear actin polymerisation after cell division results in reduced progression through G1 125
5.2.3 NLS-actin^{R62D} cells have dysregulated replication timing 133
5.2.4 NLS-actin^{R62D} cells show replication stress 139
5.2.5 NLS-actin^{R62D} post-mitotic cells show perturbations in replication machinery 142
5.3 Discussion 146
Chapter 6 : General discussion 149
Chapter 7 : Appendix 158
7.1 Hooke's law 159
7.2 Atomic force microscopy (AFM) image resolution 159
7.3 Resolution limits of a light microscope 159
7.4 FRET efficiency 162
7.5 Fluorescence lifetime 162
7.6 Chromatin FLIM 162
7.7 Conversion of fluorescence lifetime to FRET efficiency 163
Chapter 8 : References 164

List of figures

Figure 1-1. The nuclear envelope....5
Figure 1-2. Mitotic chromosome formation....10
Figure 1-3. 3D chromatin structure....14
Figure 1-4. Manipulating nuclear F-actin....23
Figure 2-1. Constructs to manipulate nuclear F-actin....27
Figure 2-2. The Atomic force microscope (AFM)....44
Figure 2-3. Peak force AFM....46
Figure 3-1. Validation of FLIM cell lines....56
Figure 3-2. FLIM outputs....58
Figure 3-3. Testing the detection of chromatin compaction and de-compaction....60
Figure 3-4. FACS sorting improves fluorescence lifetime measurements 62
Figure 3-5. FLIM can be combined with immunofluorescence to detect chromatin structures....64
Figure 3-6. Live cell FLIM....66
Figure 3-7. DNA damage induces ATM dependent chromatin relaxation. 68
Figure 3-8. ATM induces chromatin compaction....71
Figure 3-9. In absence of DNA damage, ATM activity involves histone acetylation and does not signal through CHK2....73
Figure 3-10. Quantitative electron microscopy confirms FLIM results....75
Figure 3-11. Nuclear stiffness correlates with chromatin compaction....77
Figure 3-12. ATMko cells have increased nuclear stiffness....79
Figure 4-1 Nuclear F-actin arises after mitosis....87
Figure 4-2 MNase assay shows decreased chromatin accessibility in actin mutant cells....90
Figure 4-3 Electron microscopy shows an increase in condensed chromatin in post mitotic cells unable to polymerise or turnover nuclear actin....93
Figure 4-4 Fluorescence lifetime imaging (FLIM) shows reduced fluorescence lifetime in cells unable to polymerise nuclear actin after cell division....96
Figure 4-5 Nuclear F-actin promotes chromatin re-modelling....99

Figure 4-6 Nuclear F-actin regulates chromatin modifying enzymes. 101
Figure 4-7. Nuclear F-actin regulates VCP 103
Figure 4-8 Nuclear F-actin promotes nuclear expansion. 105
Figure 4-9 Polymerisation of nuclear F-actin affects nuclear stiffness and roughness. 107
Figure 4-10 Nuclear F-actin promotes nuclear protrusions. 109
Figure 4-11 Nuclear F-actin does not affect the formation of nuclear bodies 111
Figure 5-1. Inhibition of nuclear F-actin after cell division reduces transcriptional elongation 120
Figure 5-2. Inhibition of nuclear actin polymerisation after cell division does not affect global RNA production 122
Figure 5-3. Inhibition of transcription does not affect chromatin de-condensation 124
Figure 5-4. Actin mutant cells progress slower through G1 126
Figure 5-5. Actin mutant cells have perturbed cyclin expression 129
Figure 5-6. Actin mutant cells de-condense chromatin by the entry to S phase 132
Figure 5-7. Actin mutant cells prematurely enter S phase 134
Figure 5-8. Early initiation of DNA replication is linked to mitosis 136
Figure 5-9. Actin mutant cells have early initiation of late replicating origins 138
Figure 5-10. Actin mutant cells show replication stress 141
Figure 5-11. Inhibition of nuclear actin polymerisation after mitosis impairs the formation of the pre-replication complex 143
Figure 5-12. Actin mutant cells have reduced chromatin bound RIF1 145
Figure 6-1. Thesis model 152
Figure 7-1. Jablonski diagrams of fluorescence, intersystem crossing and FRET 160
Figure 7-2. Factors which influence FRET efficiency 161
Figure 7-3. Chromatin FLIM 162

List of tables

Table 2-1. Primary antibodies and dilutions 31
Table 2-2. Secondary antibodies and dilutions..... 33
Table 2-3. Components of polyacrylamide gels 34
Table 2-4. Components of a 4% Stacking gel 34
Table 2-5. Composition of buffers used for Western Blotting 35

List of equations

Equation 7-1. Hooke's law 159
Equation 7-2. Resolution of an AFM image 159
Equation 7-3. Abbe's equation 159
Equation 7-4. Förster theory 162
Equation 7-5. Fluorescence lifetime 162
Equation 7-6. Conversion of fluorescence lifetime to FRET efficiency ... 163

List of publications

- Sherrard, A., Bishop, P., Panagi, M., Alibhai, D., Kaidi, A. streamed lined Fluorescent lifetime imaging approach identifies a role of ATM in chromatin compaction, Biology Open, 2018.
- Baarlink, C*., Plessner, M*., Sherrard, A*., Morita, K., Misu, S., Virant, D., Kleinschnitz, E.M., Harniman, R., Alibhai, D., Baumeister, S., Miyamoto, K., Endesfelder, U., Kaidi, A., Grosse, R. A transient pool of nuclear F-actin at mitotic exit controls chromatin organization. Nature Cell Biol. 2017; 1389-1399. *Equal contribution.
- Kollareddy. M., Sherrard, A., Park, J.H., Szemes, M., Gallacher, K., Melegh, Z., Oltean, S., Michaelis, M., Cinatl, J Jr., Kaidi, A., Malik, K. The small molecule inhibitor YK-4-279 disrupts mitotic progression of neuroblastoma cells, overcomes drug resistance and synergizes with inhibitors of mitosis. Cancer letters, 2017; 403:74-85.

Chapter 1 : Main introduction

1.1 Background

In 1953 Watson and Crick reported that DNA forms a double helix (Watson and Crick, 1953); observations which lead to an understanding of how the genome is stored and copied. Since this time, it has become clear that genome organisation and gene regulation cannot be predicted from this sequence alone (Misteli, 2013). Thus, future challenges are to understand how DNA is packaged, organised and read within the nucleus. In vitro experiments have suggested a hierarchical folding model, where chromatin is progressively folded into more compact structures, ultimately forming a 30nm chromatin fibre (Tremethick, 2007). These models have been validated by the recently developed RICC-seq method (Risca et al., 2017), which obtains nucleosome resolution interaction maps. However, the first visualisation of chromatin, at nucleosome resolution in intact cells (Ou et al., 2017), disputes these models and argues that DNA packaging is uniform, and it is the local concentration of DNA fibres that defines heterochromatin (condensed structure, low gene expression) and euchromatin (de-condensed structure, high gene expression).

Our understanding of chromatin compaction is therefore unclear but given the importance of modulating this structure during nuclear processes, understanding the transition between condensed and de-condensed states will likely provide insights into gene regulation and the maintenance of genome stability. Indeed, chromatin compaction is correlated with gene silencing; at the nuclear periphery, chromatin is marked by repressive histone modifications such as H3K9me3 and in general, is transcriptionally inactive (Fiserova et al., 2017). Likewise, the compact chromatin environment at centromeres (Mizuno et al., 2011) and mitotic chromosomes, are also largely inhibitory to transcription (Antonin and Neumann, 2016; Palozola et al., 2017). Chromatin de-condensation is therefore important for transcription. In addition, the compartmentalisation of heterochromatin and euchromatin aids the coordination of DNA replication, by defining distinct timings of origin activation (Kim et al., 2003; Lima-de-Faria and Jaworska, 1968).

Given the pronounced change in chromatin compaction after cell division, studying post-mitotic chromatin de-condensation may shed light on the mechanisms which produce and maintain chromatin compaction states. Furthermore, the link between mitotic progression and gene re-positioning (Shachar and Misteli, 2017) suggests as potential link between chromatin de-

condensation and the establishment of the elusive 3D genome. The work within this thesis develops and adapts imaging methods to measure chromatin compaction and uses these methods to understand how the nucleus expands and chromatin de-condenses after cell division, as well as the relevance of these to transcription and DNA replication.

1.2 The nuclear envelope

The nuclear envelope is composed of two membranes; the inner nuclear membrane (INM) and the outer nuclear membrane (ONM), which is continuous with the endoplasmic reticulum (ER). Below the INM is a structure referred to as the nuclear lamina, which contains a large array of proteins, including lamins (lamin A/C and lamin B), emerin and motor proteins (reviewed in (Simon and Wilson, 2011)). Gaps in these membranes allow for the insertion of nuclear pore complexes (NPC), which facilitate transport between the nuclear and cytoplasmic compartments. The nucleus and cytoplasm are also mechanically coupled through the linker of nucleoskeleton and cytoskeleton (LINC) complex; KASH-domain containing proteins nesprin 3 and giant isoforms of nesprin 1 and 2 are found in the ONM, and interact with cytoskeletal proteins, including F-actin and microtubules. In the perinuclear space, nesprins interact with SUN-domain proteins, which reside within the INM and interact with the nuclear lamina (Figure 1-1A). As such, mechanical cues are believed to transmit to the nuclear lamina via the LINC complex, resulting in alterations in gene expression (Crisp et al., 2006).

1.2.1 Nuclear envelope breakdown

During prophase, the nuclear envelope is broken down (NEB), which allows access of the mitotic spindle to chromatin. These early processes are largely driven by phosphorylation events, predominantly by CDK1. One target of CDK1 is lamin A/C, which becomes depolymerised in early prophase as a result of this phosphorylation (Fields and Thompson, 1995). Later, nucleoporins dissociate from NPCs, leaving holes in the nuclear membrane which causes membrane permeability and the dissociation of lamin B, as well as INM proteins (Dultz et al., 2008; Guttinger et al., 2009). These proteins enter the ER membrane, which is converted from membrane sheets into tubule structures (Puhka et al., 2007).

1.2.2 Nuclear envelope reformation

During telophase, ER tubules, containing INM and chromatin binding proteins, flatten into sheets around de-condensing chromatin (Figure 1-1B) (Anderson and Hetzer, 2007). This attracts other INM proteins and NPC components, which fill gaps between the flattened tubules to form a continuous sheet. Finally, holes between the two membranes are sealed by annular fusion (Burke and Ellenberg, 2002), which requires both the removal of Aurora B (Hetzer et al., 2001) and the activity of the CHMP2A/ESCRT-III complex (Olmos et al., 2015). Upon completion of these processes, the nucleus expands from its smallest to largest state. This is related to the size of the cell (Webster et al., 2009), membrane availability (Anderson and Hetzer, 2007) lipid synthesis (Siniossoglou, 2009), and nuclear membrane proteins such as SUN1 (Walters et al., 2012; Webster et al., 2009). The relationship between nuclear and cell size suggests that nuclear size is important for cell function and the re-initiation of interphase processes. Indeed many protein complexes are effected by macromolecular crowding (Hancock, 2004), which is related to nuclear volume.

1.2.3 Nuclear lamina reformation

During telophase, INM proteins such as LAP2β binds nuclear lamina components to anchor them into the membrane. These include lamin B and emerin, thus these are the first proteins to comprise the nuclear lamina (Schirmer and Foisner, 2007), both of which are able to directly interact with chromatin and chromatin associated proteins (Towbin et al., 2009). Therefore, this structure is critical for many nuclear processes, including chromatin organisation, transcription and DNA replication. Indeed, whereas A-type lamins are primarily responsible for nuclear rigidity (Lammerding et al., 2006), B-type lamins have direct roles in transcription (Tang et al., 2008). Although some components of the nuclear lamina bind chromatin at the end of mitosis, the nuclear lamina is not fully re-constituted until nuclear transport is re-established during early G1, when lamin A/C incorporates into the nuclear lamina (Moir et al., 2000). Therefore, lamin proteins are not required for nuclear envelope formation. Instead, given that lamin import increases nuclear expansion, these proteins are suggested to be involved in this process (Newport et al., 1990).

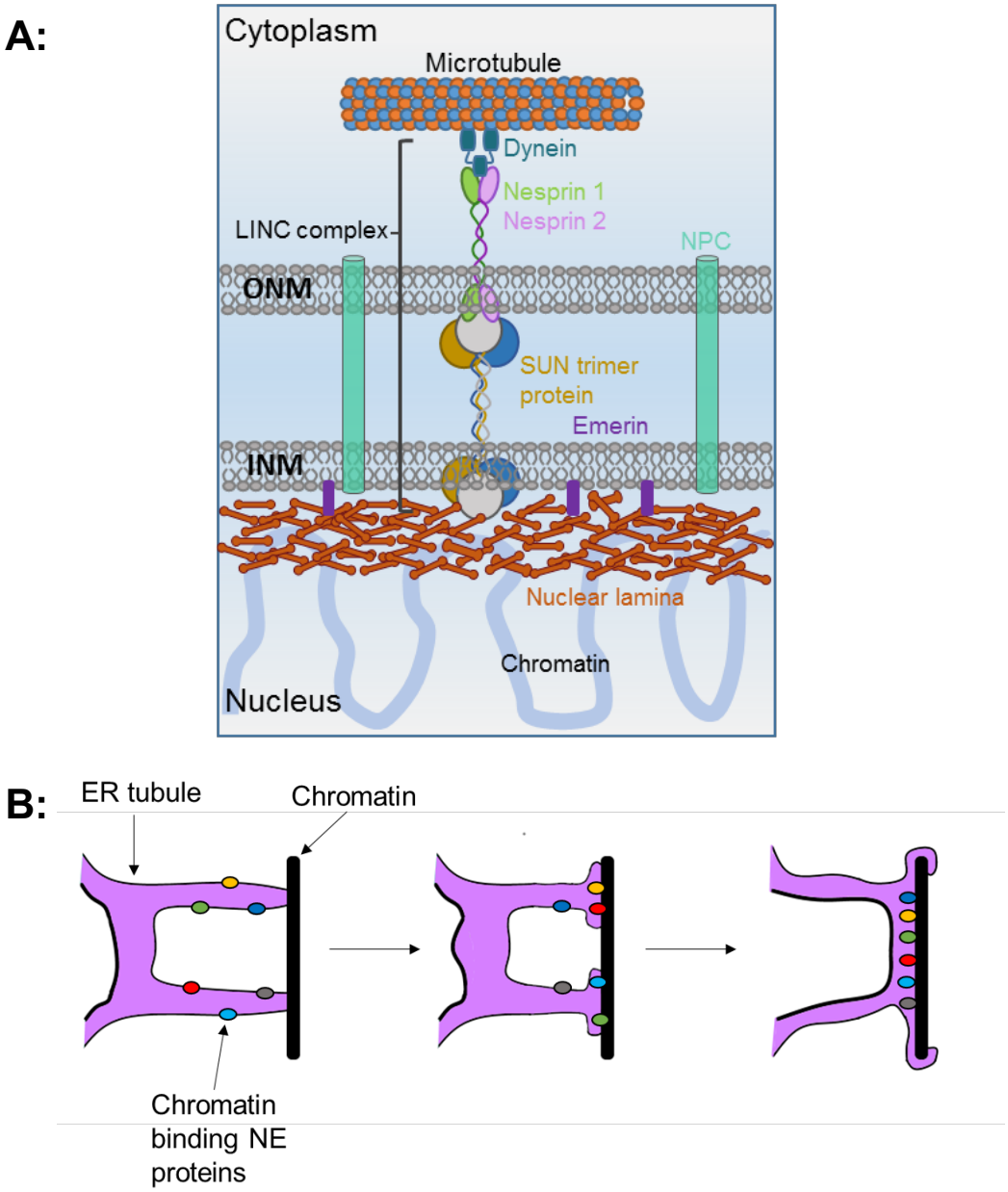

Figure 1-1. The nuclear envelope.

***A**, shows a diagram of the nuclear envelope (NE), consisting of the outer nuclear membrane (ONM) and inner nuclear membrane (INM), with nuclear pore complexes (NPC) spanning both membranes. In the ONM, are the KASH-domain containing proteins nesprin 1 and nesprin 2, which through the motor protein dynein, interact with microtubules. In perinuclear space (between the INM and ONM), these proteins interact with SUN-domain containing proteins in the INM. These proteins comprise the linker of cytoskeleton and nucleoskeleton (LINC) complex. Below the INM is the nuclear lamina, containing proteins such as lamins and the INM protein emerin. Lamina proteins interact with SUN-domain proteins, as well as chromatin. As such, mechanical signals are transmited from the cytoplasm, to the nucleus and chromatin. Image made by Maria Beatriz Villagomez-Torres. **B**, shows the binding of endoplasmic reticulum (ER) tubules, which contain chromatin binding proteins, to chromatin during nuclear envelope (NE) reformation. Arrows indicate the stages of this process, where the tubules first bind chromatin, and progressively flatten into sheets. Adapted from Webster et al, 2009.*

1.3 Chromatin condensation

Changes in nuclear structure are therefore associated with cell division. In addition, progress through the cell cycle is associated with pronounced chromatin remodelling, making the structure of chromatin an accurate predictor of cell cycle stage (Nagano et al., 2017). This is most defined at the entry to mitosis, where chromatin is condensed into mitotic chromosomes (Paulson and Laemmli, 1977) and genomic compartments can no longer be observed (Nagano et al., 2017). This unique chromatin structure aids the equal division of genetic material between daughter cells (Gibcus et al., 2018) and begins to emerge in prophase, prior to NEB. After NEB, chromosomes become shorter and fatter (Champoux, 2001), and then progress through expansion/compaction cycles, reaching maximum compaction at metaphase (Kleckner et al., 2004). At anaphase, the anaphase promoting complex (APC) cleaves securin to release seperase. Seperase subsequently dissociates the functional SMC1 and SMC3 domains of cohesin, resulting in separation of sister chromatids, which have been linked since the previous S phase (Hagting et al., 2002). Although the transition between interphase and mitosis remains incompletely understood, several proteins and histone modifications have been shown to be important.

1.3.1 Histone modifications

The primary structure of chromatin is referred to as ‘beads on a string’; which consists of nucleosomes (histone octamers wrapped by approximately 146bp of DNA) that are separated by linker DNA. These histone octamers are composed of two copies of four core histone proteins; H3, H4, H2A and H2B, as well as a single copy of histone H1. In addition, variants of all histones, excluding histone H4, can also contribute to forming a histone octamer (Talbert and Henikoff, 2010). In this way, the primary structure of chromatin, and therefore maximum de-condensation, is inherently limited by the hindrance produced through the incorporation of histones into DNA. Furthermore, these histone proteins have tails which extend from the core particle and can be modified by the addition of various chemical groups, producing residues that are for example; acetylated, methylated, ubiquitinated, phosphorylated or sumoylated. Combined, these modifications produce a unique signature which affects both chromatin-chromatin and protein-chromatin interactions. Thus, histone modifications and nucleosome remodelling are well documented to exert changes in chromatin structure (Bannister and Kouzarides, 2011; Clapier et al., 2017).

1.3.1.1 Histone phosphorylation

Phosphorylation of histone H3 is one of the earliest signs of mitotic preparation, prior to the formation of prophase chromosome morphology (Hendzel et al., 1997). During mitosis, H3 is phosphorylated at threonine 3 (H3T3) and 11 (H3T11), as well as serine 10 (H3S10) and 28 (H3S28) (Bonenfant et al., 2007; Garcia et al., 2005). Serine 10 and 28 are recognised by the protein kinase Aurora B, which is part of the passenger complex (Sawicka and Seiser, 2012); the passenger complex is composed of Aurora B, INCENP, Borealin and Survivin (Cooke et al., 1987; Ruchaud et al., 2007), and functions to both regulate chromatin structure and modulate chromosome segregation (Ruchaud et al., 2007). In late G2, the kinase haspin phosphorylates centromeric chromatin at H3T3 (Dai et al., 2005). Once phosphorylated, survivin recognises and binds this residue, and by doing so, directs the passenger complex to this site (Wang et al., 2010). Aurora B subsequently phosphorylates H3S28 and H3S10 (Kelly et al., 2010), which by metaphase, spreads across the entire length of the chromosome (Hendzel et al., 1997). These phosphorylations are highly important for mitosis, indeed chromosomes segregate abnormally when these phosphorylation events are reduced (Wei et al., 1999).

Once phosphorylated, H3S10ph serves several functions which support chromosome condensation. Importantly, H3S10ph promotes the recruitment of the supercoiling protein condensin I during early metaphase (Adams et al., 2001; Collette et al., 2011), and the ejection of HP1 from chromatin (Fischle et al., 2005). In budding yeast, H3S10ph also recruits the histone deacetylase HST2P. This removes acetyl groups from H4K16, which otherwise counteracts chromatin compaction (Wilkins et al., 2014). H3S10ph is therefore generally considered to be important for chromatin condensation. However, H3S10ph is also associated with gene activation and in some species, chromosomes form normally in absence of H3S10ph. Thus, the importance of H3S10ph in chromatin condensation has been debated (Johansen and Johansen, 2006; Mahadevan et al., 1991; Sawicka and Seiser, 2012). In addition, treatment with okadaic acid, which inhibits the protein phosphatases PP1/PP2a, results in increased H3S10ph but does not induce mitotic chromosomes, suggesting that this modification is not sufficient to promote chromosome formation (Van Hooser et al., 1998). Despite this, the correlation between H3S10ph and chromatin compaction is evident in many species (Giet and Glover, 2001; Hsu et al., 2000; Kaszas and Cande, 2000; Wei et al., 1998; Wei et al., 1999), thus it has been suggested that it is the

combination of this modification with other chromatin marks and proteins that is important for the formation of a mitotic chromosome (Ernst et al., 2011).

1.3.1.2 Histone acetylation

Acetylation of histones at lysine residues is the most prevalent histone modification (Zhang et al., 2003), and its status also has roles in chromosome formation. Addition of this group removes the positive charge on lysine residues (Zheng and Hayes, 2003), which can alter chromatin structure in several ways; firstly, the acetylation status can affect the proteins which interact with chromatin. For example, Bromodomain proteins specifically interact with acetylated histones, whereas other proteins are specifically excluded from acetylated regions (Dhalluin et al., 1999). In addition, histone acetylation has a more direct role in regulating chromatin structure; H4K16 is of particular importance, as this residue falls within the basic patch of the H4 tail. Therefore, its deacetylation allows the H4 tail to interact with the acidic patch of the H2A-H2B dimer and promote high order chromatin folding (Dorigo et al., 2003). The deacetylation of H4K16 and other lysine residues, which are generally associated with gene activation (Taylor et al., 2013), therefore accompanies chromosome formation.

1.3.1.3 Histone methylation

Several methylation events are involved in forming a mitotic chromosome. Methylation of histone tails at lysine 9 is well known to be associated with chromatin compaction (Towbin et al., 2012), but its levels remain unchanged through mitosis (Fischle et al., 2005), suggesting it is not involved in chromosome formation. Other histone methylations, such as H4K20me, have a more direct role. Due to both the mitosis specific stabilisation of PR-Set7 methyltransferase (Wu et al., 2010), and dissociation of the H4K20me PHF8 demethylase (Liu et al., 2010), H4K20 methylation rises at the entry to mitosis. Here it recruits and interacts with the chromosomal protein condensin II and antagonises H4K16ac (Liu et al., 2010), thus promoting chromatin condensation.

Therefore, histone modifications have important roles in promoting chromatin compaction. However, chromosomes can still form in absence of these modifications, thus their roles in chromosome formation are likely a cooperation between the modifications themselves, and other proteins which independently promote chromatin compaction, many of which are recruited by these modifications and hydrolyse ATP (Vagnarelli, 2012).

1.3.2 Chromosome associated proteins

As discussed, mitosis associated histone modifications begin to emerge in late G2, and chromosome structures can be observed in prophase, prior to NEB. These early events are linked to the activation of the CDK1-cyclin B complex (Gavet and Pines, 2010), which targets the condensins (Kimura et al., 1998). Higher eukaryotes have two types of condensin complexes; condensin I and condensin II, which share common ATP-hydrolysing SMC2 and SMC4 subunits (Melby et al., 1998), but also have different non-SMC proteins as part of the complex (Hirano et al., 1997). Condensin II localises to the nucleus and therefore participates in earlier events than condensin I, which localises to the cytoplasm and thus only gains access to chromatin after NEB (Hirota et al., 2004; Ono et al., 2004). These condensins therefore have distinct roles in chromosome formation, where condensin II forms a central scaffold of 400kb loops, which are subdivided into 80kb loops by condensin I (Figure 1-2). This scaffold subsequently spirals during progress into prometaphase, which is influenced by condensin mediated loop extrusion, resulting in chromosome shortening (Gibcus et al., 2018).

Lack of condensins does not alter chromatin compaction *per se*, but cells cannot form proper chromosomal architecture or successfully divide without these proteins (Gibcus et al., 2018). Condensins are therefore fundamental in the formation of chromosomes and coat the central chromosome axis. Two other proteins are also found within this axis. Firstly, the chromokinesin KIF4 has been shown interact directly with condensins and therefore has overlapping regions within the chromosome axis (Mazumdar et al., 2004). KIF4 influences the localisation of condensin complexes and facilitates chromosome formation by promoting lateral chromosome compaction (Samejima et al., 2012). In this respect, the role of KIF4 acts in opposition to another protein in the central chromosome axis, topoisomerase II alpha. Topoisomerase II alpha is well known to promote relief from topological stress throughout the cell cycle (Champoux, 2001), and this function may also be important during chromosome formation. It is found in an alternating pattern to condensins within the chromosome axis, where it promotes axial chromatin compaction (Farr et al., 2014). Depletion of Topoisomerase II alpha therefore results in deformed chromosomes which misalign at the spindle pole, but have normal lateral compaction (Chang et al., 2003).

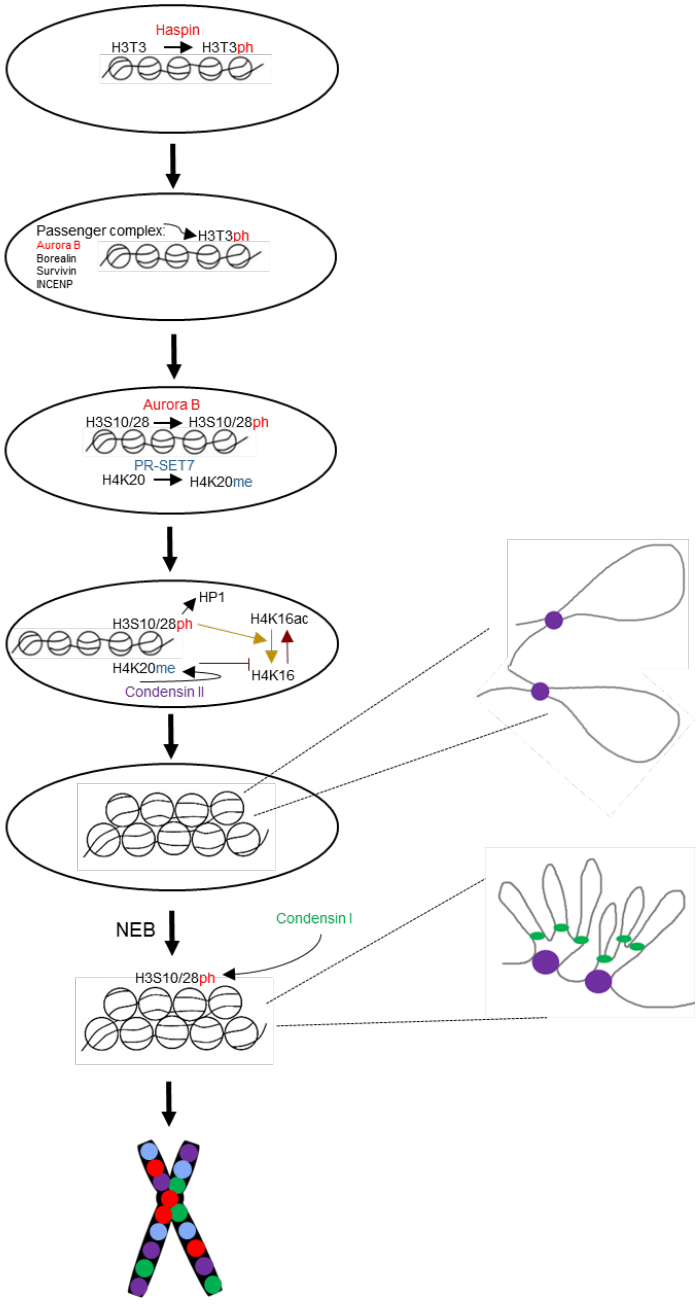

Figure 1-2. Mitotic chromosome formation.

During the early stages of mitotic chromatin condensation, prior to nuclear envelope breakdown (NEB), H3T3 is phosphorylated by the protein kinase Haspin (H3T3ph). This attracts the passenger complex, containing Aurora B, to this site. Aurora B then phosphorylates H3S10 (H3S10ph), which leads to the ejection of heterochromatin protein 1 (HP1) from chromatin. H4K20 is also methylated (H4K20me) by PR-set7 histone methyltransferase (HMTase), which leads to the recruitment of condensin II (purple). Condensin II subsequently forms 400kb loops in the chromatin fibre. Further, both H3S10ph and H4K20me promote the deacetylation of H4K16, by recruiting histone deacetylates and preventing its re-acetylation, respectively. This in turn leads to chromosome compaction, by allowing this region to interact with the H2B/H2A dimer. After NEB, condensin I (green) gains access to chromatin and interacts with H3S10ph. This segregates the condensing II mediated 400kb loops into 80kb loops to further condense chromatin. KIF4 (red) and Topisomerase II alpha (blue) also bind and become part of the chromosome axis, where they aid the lateral and axial compaction, respectively.

1.4 Chromatin de-condensation

Although the mechanism of chromatin compaction prior to mitosis is now well defined, research into the events that evoke chromatin de-compaction have been difficult to examine and remain under-investigated. Such research has predominantly been studied in the context of sperm chromatin remodelling after fertilisation, which requires the oocyte specific protein NPM2, and therefore uses an alternative mechanism (Philpott et al., 1991). However, pronounced chromatin de-condensation and nuclear re-organisation after mitosis are evident (Nagano et al., 2017). Intuitively, this requires the removal of chromosome associated proteins, such as condensins. How exactly this occurs is not known, but a reduction in CDK1 activity, which during mitosis activates condensins, may be important (Kimura et al., 1998). Mitotic histone modifications, such as histone phosphorylation, must also be removed, through the activation of the protein phosphatases PP1 and PP2A (Landsverk et al., 2005; Schmitz et al., 2010) and the inactivation of mitotic kinases, such as Aurora B.

1.4.1 Removal of Aurora B

During mitosis, Aurora B inhibits NE formation and chromatin de-condensation (Ramadan et al., 2007), highlighting the importance of its removal post-mitosis. VCP, a member of the AAA protein family, cooperates with its heterodimeric co-factor (Ufd1-Npl4) to promote sealing of the NE around de-condensed chromatin in Xenopus laevis egg extracts (Hetzer et al., 2001). Later research (Ramadan et al., 2007) demonstrated a physical interaction between $VCP^{Ufd1\text{-}Npl4}$ and ubiquitinated Aurora B on chromatin, and a requirement for this interaction in the extraction of Aurora B from chromatin. However, unlike the typical mode of VCP mechanism, it does not appear to affect Aurora B degradation, thus it is likely involved in promoting its de-ubiquitination, which may in turn affect its localisation (Ye, 2006). $VCP^{Ufd1\text{-}Npl4}$ mediated removal of Aurora B therefore promotes chromatin de-condensation and NE reformation.

It is tempting to speculate that the removal of Aurora B begins a cascade of events which lead to chromatin de-condensation. Firstly, this may impact the removal of condensins, as well as other proteins, which during mitosis are regulated by Aurora B (Takemoto et al., 2007). In addition, the removal of Aurora B decreases H3S10ph (Ramadan et al., 2007), and this can in turn promote other changes to chromatin structure. Importantly, this may influence the re-

establishment of H4K16ac after cell division, which is associated with de-condensed chromatin. H4K16ac marks active enhancers, (Taylor et al., 2013), promotes chromatin accessibility during S phase (Iizuka et al., 2006a) and in *C.elegans*, promotes X chromosome de-condensation during dosage compensation (Lau et al., 2016). H4K16ac is therefore associated with de-condensed chromatin, and may in fact have an active role in chromatin de-condensation, by reducing inter/intra nucleosomal contacts (Dorigo et al., 2003).

1.4.2 Chromatin de-compaction proteins

However, chromatin de-condensation is not simply a reversal of mitotic events. It is an active process, requiring both ATP and GTP (Magalska et al., 2014). Although the requirement for GTP remains unclear, RUVBL1 and RUVBL2, members of the AAA+ superfamily, have been identified as critical chromatin de-compaction factors (Magalska et al., 2014). These proteins localise to chromatin in early G1 and promote chromatin de-compaction, which is dependent on their ATPase activity. The requirement for ATP is not related to VCP, as the defects in chromatin de-compaction remained in the absence of ATP, regardless of Aurora B activity. Furthermore, the role of these ATPases in chromatin de-compaction is independent of the recruitment of other proteins, including CDCA2, which is involved in PP1 recruitment. How these proteins promote chromatin de-condensation is not clear but given that these proteins cannot de-condense chromatin alone, and are known to form large protein complexes, they may co-operate with currently unknown co-factors. For example, they may promote histone exchange to facilitate de-compaction, a mechanism known to occur in sperm cells (Philpott and Leno, 1992).

1.5 Nuclear re-organisation

During interphase, chromatin exists in several levels of organisation. This organisation is lost at the entry to mitosis and therefore, must be re-established after cell division (Nagano et al., 2017). Most distinctly, DNA paint has shown that chromosomes occupy defined regions of the nucleus, referred to as chromosome territories (Cremer et al., 2006). Within these territories, the chromatin fibre is thought to be folded into loop arrays at CTCF boundaries (Weintraub et al., 2017) which are tethered by proteins such as cohesin (Barrington et al., 2017) and YY1 (Weintraub et al., 2017). This looping promotes interactions between sequences, such as promotors and enhancers, which are spatially distant within the linear

DNA sequence, and therefore has implications for gene regulation. These loop arrays produce transcriptional hubs which are clustered together to form what is known as a topologically associated domain (TAD), in which multiple ranges of genetic interactions take place (Dixon et al., 2012). Collectively, these domains are separated into euchromatin (open chromatin structure, gene rich) and heterochromatin (closed chromatin structure, gene poor), known as A/B compartments (Lieberman-Aiden et al., 2009) (Figure 1-3).

Heterochromatin is preferentially localised to the nuclear periphery, nucleolus and centromeres, whereas euchromatin is found throughout the nucleoplasm (Federico et al., 2006). Gene position can therefore influence gene expression. Indeed, artificial tethering of chromosomes to nuclear membrane proteins relocates these chromosomes to the nuclear periphery. This process requires progress through mitosis and leads to repression of previously expressed genes near the tethering site (Finlan et al., 2008). The association of gene repression at the nuclear periphery is related to the nuclear environment, which is generally marked by repressive histone modifications (Fiserova et al., 2017). In addition, INM proteins and lamina components can bind chromatin remodelling complexes; Lamin-associated domains (LADs) are regions where lamins are in contact with heterochromatin. LADs contain a specific sequence called the lamin-associated sequence (LAS) that is sufficient to target genes to the nuclear periphery. Lamin B1 binds these sequences in late anaphase, along with the transcriptional repressor cKrox, which induces transcriptional repression through interaction with HDAC3 (Zullo et al., 2012). Of note, the localisation of genes to the nuclear membrane does not necessarily repress gene expression, indeed active gene transcription has been found to be stimulated at nuclear pore complexes (Pascual-Garcia et al., 2017). This illustrates the importance of cell division in the co-ordination of gene position, 3D chromatin structure and therefore gene regulation.

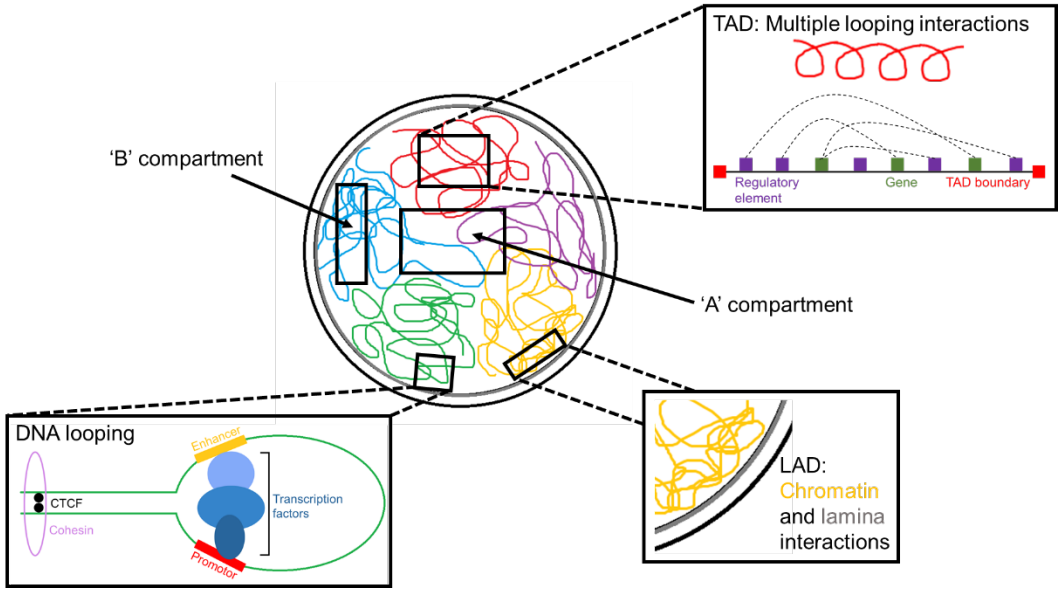

Figure 1-3. 3D chromatin structure.

This figure shows the organisation of DNA within the nucleus. Chromosomes occupy distinct territories within the nucleus (indicated by colours; blue, red, green, yellow, purple). Broadly, chromatin is segregated into condensed (heterochromatin, B compartment) and de-condensed (euchromatin, A compartment) regions. At a finer scale, DNA loops allow the interaction of sequences which are far apart within the linear sequence, for example allowing promotors and enhancers to interact through transcription factors. These regions are linked by cohesin at CTCF boundaries. Collectively, multiple looping interactions cluster together to form a topologically associated domains (TAD). At the nuclear lamina, chromatin-lamina contacts are made, and are known as a lamin-associated domains (LAD).

1.6 Nuclear bodies

Another aspect of nuclear reorganisation after cell division is the reformation of nuclear organelles, collectively referred to as nuclear bodies (reviewed in (Mao et al., 2011)). These bodies are devoid of membranes and are thought to be generated by the sequential binding of components in a stochastic or ordered manor. Due to the lack of membranes, these bodies spatially confine themselves by compartmentalising high concentrations of necessary substrates to create an isolated nuclear environment (Kaiser et al., 2008). This has important implications for nuclear processing, by providing regions where reactions are more likely to take place. For example, the nucleolus is the site of rRNA transcription (Pederson, 2010), polycomb bodies are repressive regions containing polycomb repressive complex I and II proteins (Pirrotta and Li, 2012) and nuclear speckles contain high quantities of splicing factors (Spector and Lamond, 2011).

The formation of an interphase nucleus is therefore a complex process that must be tightly regulated. Given that the assembly of nuclear bodies are sensitive to protein concentration, and chromatin de-condensation is sufficient to re-locate genes (Therizols et al., 2014), the process of chromatin de-condensation and nuclear expansion may impact the formation of these nuclear structures and compartments. Indeed, chromatin mobility is high during early G1, where genes are readily switching radial compartments. This therefore suggests that chromatin organisation is not inherited, but re-established after cell division (Thomson et al., 2004). High-content imaging screens have been used to identify proteins that are important in the establishment of this structure, revealing a requirement for proteins involved in chromatin remodelling, DNA replication, and the nuclear envelope (Shachar et al., 2015). However, these observations tended to be gene specific, as no one protein affected the organisation of all the regions tested. Therefore, as yet unidentified proteins are likely involved. Given the dramatic changes that occur within the nucleus after cell division, as well as the emerging roles of nuclear actin, it is conceivable that filamentous actin may promote these processes.

1.7 Nuclear actin

Actin is a 42 kDa protein which is, along with several of its regulators (Baarlink et al., 2013), detected in the nucleus and cytoplasm of cells (Baarlink et al., 2013). Actin is imported into the nucleus via importin 9 in a complex with cofilin (Dopie et al., 2012) and exported via exportin 6 in a complex with profilin (Stuven et al., 2003), highlighting the importance of actin in both compartments. Nucleation of monomeric actin (G-actin) leads to the generation of actin filaments (F-actin), which have structural polarity, due to the orientation of the actin monomers (Bonder et al., 1983). There are three main types of actin nucleators, which are activated during different conditions and lead to the generation of branched or linear arrays. These include formins, ARP2/3 complexes and spire proteins (Plessner and Grosse, 2015). In a resting state, most of the nuclear actin pool is monomeric, but it is estimated that in a heterogeneous cell population, 20% of nuclear actin is polymeric (Simon and Wilson, 2011). The constant shuttling of actin monomers between nuclear and cytoplasmic compartments means polymerisation events can affect shuttling in either direction (Grosse and Vartiainen, 2013).

Within the cytoplasm, actin filaments are readily visualised using fixed samples and dyes such as Phalloidin using light microscopy (Lengsfeld et al., 1974). For live cell actin imaging, several probes have been developed, including F-tractin, GFP-actin, SIR-actin and LifeAct, all of which have context dependent advantages (Melak et al., 2017). The ease of detection has assisted the validation of the cytoplasmic functions of F-actin, which includes major cellular processes such as cell motility (Mogilner and Oster, 1996) and intracellular transport (Cramer, 2008). In contrast, visualisation of nuclear actin is more challenging. This is due to the lower concentration of nuclear actin compared to in the cytoplasm, shuttling of actin between compartments, and the transient single-dependent nature of nuclear actin filament assembly (Baarlink et al., 2013; Grosse and Vartiainen, 2013). In addition, visualisation of nuclear actin requires novel methods such as actin chromobodies, tagged with an NLS and fluorescent proteins (Plessner et al., 2015; Riedl et al., 2008). These methods have only recently been developed and therefore, the role of nuclear F-actin is relatively unexplored. Indeed, despite the knowledge that G-actin is found in the nucleus, confirmation of the presence of nuclear F-actin in somatic cells has only recently been achieved. Since this discovery, many roles of nuclear F-actin have been

identified, including during cell spreading (Plessner et al., 2015) and in the giant *xenopus laevis* oocyte, stabilisation of the nucleus itself (Bohnsack et al., 2006). Although the functions of nuclear F-actin are only recently emerging, nuclear functions of G-actin are well established and are involved in all stages of transcription.

1.7.1 Nuclear actin and transcription

Two main lines of evidence support a requirement for nuclear actin in transcription. First came from observations of transcriptional activity following nuclear actin depletion by anti-actin antibodies in salamander oocytes, which lead to similar effects as transcriptional inhibitors (Scheer et al., 1984). Later, actin was found to be a component of the pre-initiation complex and required to initiate RNAP II (Hofmann et al., 2004), as well as RNAP III transcription (Hu et al., 2004). Indeed, it is likely that actin is required by all three RNA polymerases, as actin binds the subunits RPABC2 and RPABC3, which are common to all three RNA polymerases (Fomproix and Percipalle, 2004; Hu et al., 2004; Visa, 2005). Secondly, actin is a component of several chromatin remodelling complexes, including INOS80, BAF and TIP60 and the actin nuclear family ARPs are an evolutionary conserved component of chromatin modifiers (Bettinger et al., 2004; Cairns et al., 1998; Peterson et al., 1998). In the BAF complex, actin and the actin related protein BAF53 stimulates the ATPase activity of the brg1 subunit. Furthermore, both actin and PIP2 enhance the binding of brg1 to the nuclear matrix and chromatin (Zhao et al., 1998). Nuclear actin can therefore co-operate with other nuclear lipids and proteins to impact the activity and localisation of chromatin remodelling complexes, thus effecting transcription.

Actin therefore influences many aspects of transcription. In fact, actin may be involved with the whole transcriptional path including splicing (actin co-localises with SM-proteins) and RNA export (actin-antibodies inhibit RNA export) (Shumaker et al., 2003). Importantly, it is monomeric actin that is presumed to be associated with these complexes. Though given the co-occupancy and requirement for nuclear myosin 1 (NM1) and nuclear actin in transcription (Fomproix and Percipalle, 2004), it is possible that actin polymerisation and nuclear transport are also important during transcription. Indeed, it has recently been shown that nuclear actin polymerisation influences the activity and localisation of β-catenin to target genes (Yamazaki et al., 2016). Furthermore, nuclear and cytoplasmic polymerisation events can affect the localisation of

transcription factors, including the transcriptional co-activator MAL during serum stimulation (Baarlink et al., 2013).

1.7.2 Formation of nuclear actin filaments

1.7.2.1 Serum stimulation

MAL is a mechanotransducive transcriptional co-activator. In a resting state, MAL resides in the cytoplasm, by interaction with G-actin via its RPEL domain, coupled with constitutive nuclear export. Following mechanical stimulation, RhoA mediates actin polymerisation, resulting in the release of MAL from actin monomers, exposure of its NLS and consequent nuclear localisation. MAL then transactivates serum response factor (SRF), leading to MAL-SRF driven transcription and activation of mechanotransducive genes (Hirano and Matsuura, 2011; Ho et al., 2013). In addition, mDia1/2 has been found in the nucleus, where it mediates the polymerisation of nuclear actin within 15s of serum stimulation (Baarlink et al., 2013). Similar to events in the cytoplasm, this results in the release of MAL from actin, allowing it to interact with SRF to stimulate transcription. This process may be in turn related to the organisation of the nuclear lamina, as LMNA deficient cells have altered MAL translocation. It is thought that this is in fact an indirect consequence of lamin depletion, as in the absence of lamins, the actin capping protein emerin becomes mis-localised. Due to its ability to polymerise actin, mislocalised emerin leads to a reduction in nuclear actin polymerisation and the consequent increased nuclear export of MAL. This in turn affects cytoplasmic actin, as MAL-SRF are master regulators of many cytoskeletal proteins (Ho *et al*, 2013).

1.7.2.2 Cell spreading

Another example of nuclear F-actin formation is via integrin activation following cell spreading or fibronectin stimulation (Plessner et al., 2015). This signal is transmitted to the nucleus via the LINC complex, resulting in mDia1/2 mediated nuclear actin polymerisation, release of MAL and transcription of MAL-SRF-controlled genes. However, less than 80% of cells produced these filaments upon stimulation, thus unknown factors, such as the cell cycle are likely involved. The actin filaments formed by integrin stimulation differed from those formed following serum stimulations, despite being nucleated by the same formins; they were shorter, thicker and more persistent, suggesting that different signalling pathways lead to different types of filaments.

1.7.2.3 Genetic reprogramming

In addition, several pieces of evidence point to a role of nuclear F-actin in development. Firstly, the Xenopus oocyte contains large amounts of nuclear actin, equating to 6% of all nuclear protein (Clark and Merriam, 1977). This remarkably high concentration is achieved through the delayed expression of exportin 6, which is only expressed from meiotic maturation. This forms a complex nuclear F-actin network which is fundamental in the stabilisation of the oocytes large nuclei (Bohnsack et al., 2006).

Secondly, somatic nuclear transfer of mouse nuclei into Xenopus oocytes stimulates Toca-1 mediated nuclear actin polymerisation. These filaments are required for the transcriptional re-activation of Oct-4, and subsequent acquisition of a pluripotent state. Actin was found directly at the Oct-4 promotor and its localisation, as well as the BAF complex, was increased by Toca-1. The authors thus proposed a mechanism whereby Toca-1 stimulates the polymerisation of actin, which subsequently interacts with the Oc-t4 promotor to open chromatin, allowing the BAF and RNAP II complex to bind (Miyamoto et al., 2011).

1.7.2.4 DNA damage

The above examples all implicate nuclear F-actin in promoting transcription, through a range of different stimuli. Another instance of nuclear F-actin formation differs from these, where DNA damage has been shown to promote formin-2 and spire-1/2 mediated actin polymerisation, which is required for DNA double strand break (DSB) repair (Belin et al., 2015b). The precise function of these filaments in DNA repair was not identified, but it is possible that nuclear F-actin may play a role in the localisation of components of the repair pathway or the organisation of chromatin to allow repair to occur. Indeed, further research has shown that nuclear actin and NM1 promote contact between homologous chromosomes at the site of a DSB (Evdokimova et al., 2018), and that DNA repair based relocation of heterochromatin breaks requires nuclear F-actin and myosins (Caridi et al., 2018); this may be linked to a role for nuclear F-actin in the clustering of γH2AX foci (Schrank et al., 2018).

1.7.2.5 Stress induced nuclear actin filaments

During times of cellular stress, specific actin-cofilin structures emerge in the nucleus (Nishida et al., 1987; Pendleton et al., 2003). These structures are morphologically unconventional, when compared to the actin filaments transiently

observed in response to DNA damage, cell spreading and serum stimulation, appearing as thick rod structures (Serebryannyy et al., 2016c). These can be initiated by a range of stimuli including heat shock (Welch and Suhan, 1985), high salt concentrations (Iida and Yahara, 1986), ATP depletion and treatment with latrunculin B (Pendleton et al., 2003). Upon removal from the stimuli, these filaments rapidly disassemble.

1.8 Nuclear F-actin and chromatin organisation

Several stimuli which induce the polymerisation of nuclear actin have thus been identified, but little is known about their function in chromatin organisation. Evidence that suggests a role for nuclear actin in organising the genome comes from a study in budding yeast (Spichal et al., 2016b). In this publication, actin dynamics were perturbed using an actin monomer-sequestering drug, Latrunculin A (Lat). The movement of genes positioned at the nuclear periphery, as well as in the nuclear interior, were both reduced in the presence of Lat. This suggests a potential role for nuclear and cytoplasmic actin in chromosome movement. Similarly, in mammalian cells, nuclear actin polymerisation has been shown to promote movement of the U2 locus during transcriptional activation (Dundr et al., 2007). Such a function has also been noted during homologous recombination, where actin is suggested to promote clustering of damaged foci to facilitate repair (Evdokimova et al., 2018). Further, stress induced nuclear actin filaments alter chromatin organisation, RNAP II localisation and co-localise with heterochromatin (Serebryannyy et al., 2016c). The role of nuclear F-actin in chromatin organisation may therefore be mechanical. However, the forces generated by actin polymerisation may not be exerted directly to chromatin. Indeed, nuclear actin polymerisation has been found to promote HDAC activity, which subsequently effects genome organisation (Serebryannyy et al., 2016a).

Alternatively, nuclear actin filaments may not pose mechanical stresses to chromatin, and instead be involved in molecular transport, as is the case in the cytoplasm. Cytoplasmic transport along actin filaments is orchestrated by the ATP hydrolysing motor proteins, myosins. Indeed, although the transport of myosins along nuclear actin filaments is yet to be observed, myosin I, II, V, VI, X, XVI and XVIII have been detected in the nucleus, where the first discovered was nuclear myosin 1 (NM1) (de Lanerolle, 2012; Pestic-Dragovich et al., 2000). Here they may have similar functions, as studies show that intranuclear

movement is too fast to be due to diffusion, suggesting an active nuclear transport mechanism (Chubb et al., 2002). Indeed, myosin XVI has been found in interact with polymerised actin (Cameron et al., 2007) and Myosin Va localises to nuclear speckles (Pranchevicius et al., 2008). Interestingly, research has suggested that chromosome movement is an active process which requires polymerised nuclear actin and NM1 (Chuang et al., 2006). This complex may also be required for the movement of RNAP, as antibodies against this myosin inhibits RNA synthesis (Shumaker et al., 2003).

1.9 Manipulating nuclear F-actin

Links between nuclear F-actin and chromatin organisation have therefore been suggested, but this has not been fully investigated. Several systems have been developed to interfere with nuclear F-actin and can be used to uncover the role of nuclear actin filaments in chromatin organisation. Historically, inhibition of actin filaments has used compounds such as Cytochalasin D and Latrunculin B, which disrupt actin filaments through binding directly to the polymer or monomer, respectively (Casella et al., 1981; Morton et al., 2000; Wakatsuki et al., 2001). However, these methods are not specific to nuclear actin, and therefore cannot be used to uncouple the independent functions of cytoplasmic vs nuclear F-actin. To specifically interfere with nuclear actin, a common approach is the over expression of non-polymerising actin mutants. These mutations include G13R and R62D actin, as well as the fusion of HSV VP16 to the C-terminus of actin, which also inhibits actin polymerisation (Posern et al., 2002).

Of these mutants, R62D actin was found to shuttle between the nucleus and cytoplasm with similar dynamics to wild type and was completely excluded from phalloidin staining (Posern et al., 2002). This mutant system is thus considered most favourable. R62D actin is a well-documented polymerisation deficient mutant actin (Kabsch et al., 1990; Otterbein et al., 2001; Posern et al., 2002) which produces a form of actin monomer that is unable to polymerise, likely due to disruption of salt bridges between subdomains 2 and 4 (McCormack et al., 2001). Researchers have thus utilised this mutant to manipulate nuclear F-actin through the generation of plasmid constructs, which consist of the wild type (WT) or mutant (R62D) actin sequence, tagged to an nuclear localisation sequence (NLS) and a tag to aid the detection of positively transduced cells (Baarlink et al., 2017; Baarlink et al., 2013). Through the NLS, these proteins traffic to the

nucleus, where the mutant actin dilutes the nuclear pool of incorporable actin and largely prevents the emergence of nuclear actin filaments (Figure 1-4A).

One limitation of the method just described is the potential effects that the mutant actin may have on cytoplasmic actin, particularly during NEB when these proteins are no longer confined to the nucleus. To address this limitation, nuclear F-actin assembly can also be inhibited by manipulation of actin nuclear-cytoplasmic shuttling. Actin is imported into the nucleus via importin 9, in complex with cofilin (Dopie et al., 2012), and exported out of the nucleus via exportin 6 in complex with profilin (Stuven et al., 2003). Therefore, overexpression of exportin 6 leads to increased actin export, and reduced actin filament assembly. Likewise, depletion of importin 9 decreases actin nuclear import, and therefore its polymerisation (Figure 1-4B). Although this method has its own limitations, as exportin 6 and importin 9 also traffic other proteins in and out of the nucleus, combined these approaches have strength and can be used to unravel the function of nuclear F-actin.

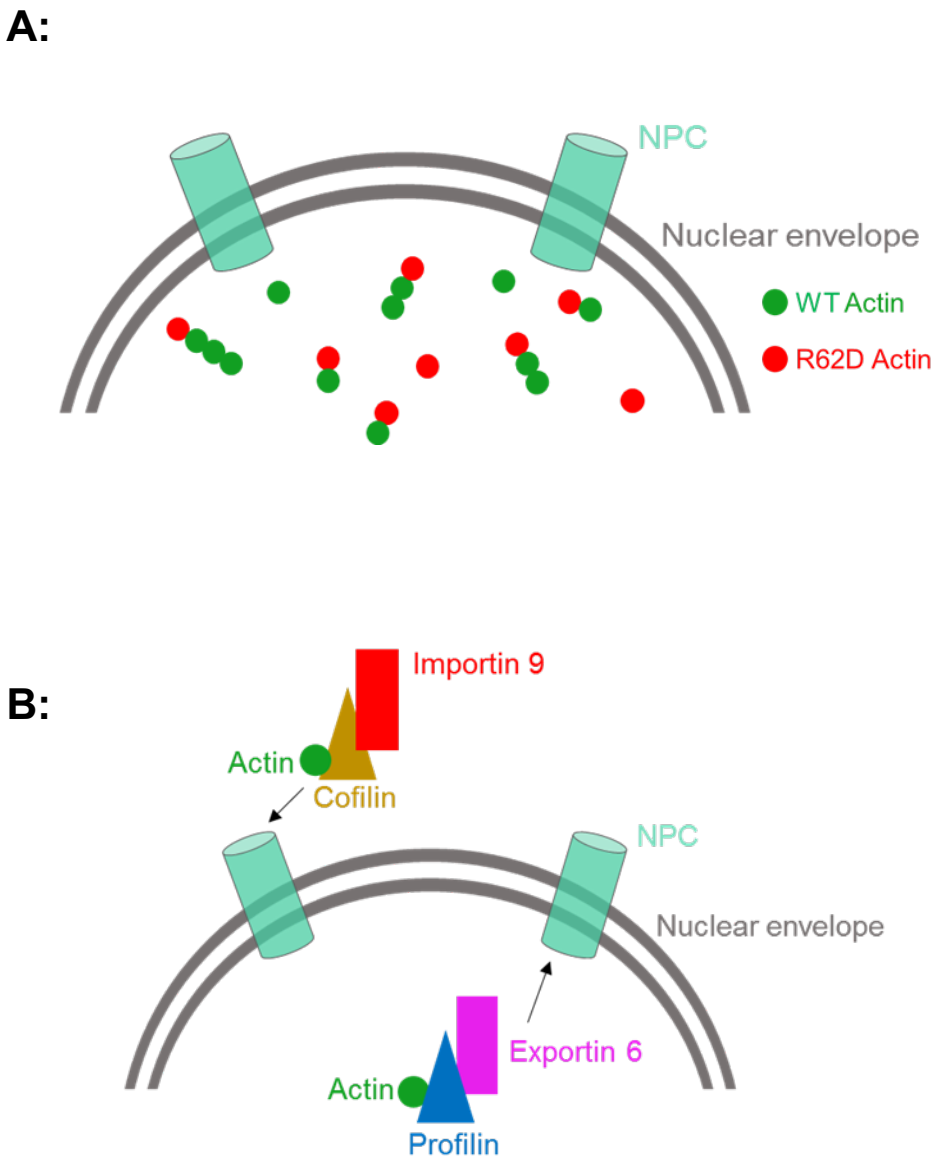

Figure 1-4. Manipulating nuclear F-actin.

This figure shows diagrams which illustrates two methods of manipulating nuclear actin polymerisation. The nuclear envelope and nuclear pore complexes (NPC) are indicated. ***A****, shows the expression of NLS-tagged wild type (WT, green) and mutant (R62D, red) actin, which is unable to polymerise. Through the NLS, these proteins are localised in the nucleus, where the R62D actin has a dominant affect, and largely inhibits nuclear actin polymerisation.* ***B****, shows actin trafficking through NPC's. Actin is in complex with cofilin and importin 9 during nuclear import, and with profilin and exportin 6 for nuclear export. Depletion of importin 9, or overexpression of exportin 6, therefore reduces actin import and increases actin export, respectively. Both reduce the pool of nuclear actin.*

1.10 Project Aims

The re-organisation of the nucleus and genome after cell division is therefore a complex process, which is under strict spatial-temporal control. However, contrary to the events which govern chromatin compaction, relatively less is known about chromatin de-condensation. Given the dramatic changes that occur to the nucleus after cell division, and the suggested roles of nuclear actin filaments in chromatin dynamics, it is conceivable that nuclear F-actin may be involved in these processes. Indeed, work from Robert Grosse's laboratory identified the formation of a nuclear F-actin network after cell division. Using the systems described to manipulate nuclear F-actin, the work within this thesis builds on the initial observations of the Grosse laboratory, with three research aims:

1. Develop assays to visualise and measure chromatin compaction.
2. Identify the role of post-mitotic actin filaments in the reformation of an interphase nucleus.
3. Identify the biological significance of these nuclear actin filaments.

Chapter 2: Materials and Methods

2.1 Cell lines

2.1.1 NIH-3T3

Parental embryonic mouse fibroblasts. Purchased from ATCC and provided by Professor Robert Grosse, University of Marburg, Germany.

2.1.2 NIH-3T3-BFP-NLS-Actin$^{WT/R62D}$ cells

NIH-3T3 cells that were transduced with lentivirus which expresses the wild type (WT) or mutant (R62D) actin sequence, linked to a nuclear localisation signal (NLS) and blue fluorescent protein (BFP), under the control of a doxycycline regulated promoter (Figure 2-1A). Upon addition of doxycycline, these sequences are expressed, and through the NLS, traffic into the nucleus. The R62D mutation produces a form of actin monomer which is unable to polymerise, and therefore dilutes the pool of incorporable actin within the nucleus. For a homogeneous population, these cells were purified by Fluorescence Activated Cell Sorting (FACS), based on BFP. Cell lines were provided by Professor Robert Grosse, University of Marburg, Germany.

2.1.3 NIH-3T3-FLAG-NLS-Actin$^{WT/R62D}$ cells

Generated using lentivirus. These are the same as described above, but instead of a BFP tag, there is a flag-tag to detect expression. A self-cleavable SNAP tag was also added to this sequence to aid the selection of positively transduced cells (Figure 2-1B). This tag is spontaneously cleaved upon protein translation, thus does not interfere with the protein function and was detected by live cell ANTI-SNAP dyes, facilitating FACS . Cell lines were provided by Professor Robert Grosse, University of Marburg, Germany.

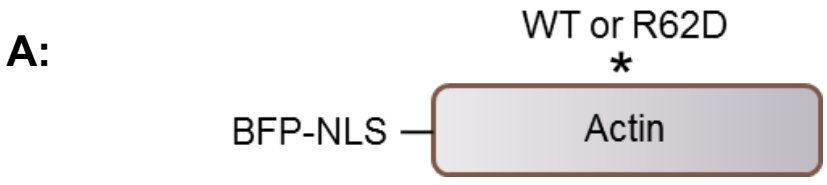

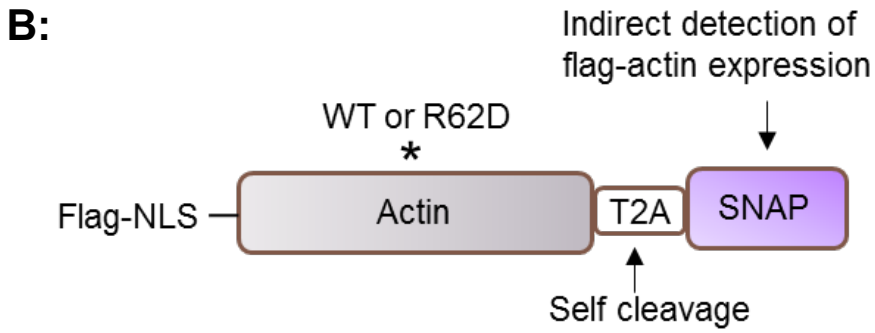

Figure 2-1. Constructs to manipulate nuclear F-actin.

***A**, shows the design of BFP- and NLS-tagged wildtype (WT) or mutant (R62D) actin derivatives*. ***B**, shows the design of Flag- and NLS-tagged actin derivatives, linked to the SNAP-tag by a T2A peptide. The T2A peptide is cleaved upon translation, resulting in equimolar expression of Flag-NLS-actin and the SNAP-tag. Live cell anti-SNAP dyes were used to indirectly detect Flag-NLS-actin.*

2.1.4 NIH-3T3-GFP-H2B and NIH-3T3-GFP-H2B-mCherry cells

These are parental NIH-3T3 cells which have been transduced with lentivirus to express GFP-H2B, or both GFP-H2B and mCherry-H2B. The PGK-H2B-mCherry and PGK-H2B-GFP vectors (Addgene) were used to produce lentivirus. One week after infection, GFP-positive and mCherry expressing NIH-3T3 cells were purified using FACS. For FLIM experiments, the double positive cells were first subdivided into eight subpopulations, and these were matched to corresponding single colour populations.

2.1.5 NIH-3T3-BFP-NLS-Actin$^{WT/R62D}$+nAC-mCherry-H2B cells

These are NIH-3T3-BFP-NLS-actin$^{WT/R62D}$ cells (2.1.2), which have been transduced with lentivirus to also express mCherry-H2B and GFP-tagged nuclear actin chromobody (nAC). This consists of the variable heavy (V_HH) domain of an actin specific antibody, fused to an NLS and GFP (Plessner et al., 2015). Cell lines were provided by Professor Robert Grosse, University of Marburg, Germany.

2.1.6 RPE1 control and ATM ko cells

These are human retinal pigment epithelial cells (ATCC) which have been modified with a control CRISPR plasmid or an ATM CRISPR plasmid to genetically knockout the ATM gene. These cell lines were provided by Professor Steve Jackson, University of Cambridge, UK.

2.1.7 HEK293 cells

Parental human embryonic kidney cells, purchased from ATCC.

2.2 Cell culture

NIH-3T3 cells were cultured in Dulbecco's Modified Eagles Medium (DMEM) (Gibco), containing 2mM glutamine (Sigma), 100units/ml Penicillin (Gibco), 100μg/ml Streptomycin (Gibco) and 10% foetal bovine serum (FBS) (Gibco). RPE1 cells were cultured in Dulbecco's Modified Eagles Medium F12 HAM (DMEM/F12) media (Gibco), containing 2mM glutamine, 100units/ml Penicillin, 100μg/ml Streptomycin and 10% FBS (Gibco). Cells were maintained in T25 flasks (CytoOne) and incubated at 37°C and 5% CO_2 in dry humidified incubators. Cells are passaged several times per week, using Trypsin-EDTA (Sigma).

2.3 Cell synchronisation

2.3.1 Mitotic synchronisation

For IF samples, cells were first synchronised at the G1/S border by single thymidine block (2mM thymidine, diluted in water, for 18 hrs). After this time, cells were washed three times in PBS, and left in normal media containing 500ng/ml doxycycline (dissolved in DMSO), for 10 hrs. Cells were then fixed and processed as seen in IF. Mitotic cells were subsequently detected by eye. All other mitotic synchronisations were performed as follows; cells were synchronised to the G1/S border by thymidine block, using 2 mM thymidine (dissolved in water) for 20 hrs. Cells were then washed three times in PBS, before adding normal media containing 500 ng/ml Doxycycline. After 4 hrs, analysis of flow cytometry data, using the Watson (Pragmatic) model, determined that 40% of cells had completed S phase. This time point was therefore chosen to add 1μM of CDK1i (RO-3306, Sigma, dissolved in DMSO), for a period of 4 hrs. After this time, cells were washed three time in PBS, and then returned to normal media containing 500 ng/ml Doxycycline. Thirty minutes later, mitotic cells were isolated by mitotic shake off; in this process, the dishes were tapped, and the media was aspirated, and washed over the cells several times. This media was then centrifuged at 1000 x g for 5 minutes, to pellet the mitotic cells which had rounded up, and were floating in the media. Cells were then plated onto PLL-coated 35 mm dishes or #1.5 coverslips. Cells were subsequently fixed, lysed or frozen at the desired timepoint after mitotic shake off.

2.3.2 S phase synchronisation

Cells were blocked at the G1/S border using single thymidine block (18 hrs, 2mM). To look at the S phase population, cells were washed 3 x in PBS, and released for 2 hrs, before being fixed.

2.4 Cell treatments

2.4.1 VCPi

Cells were synchronized by thymidine block, and 30nM of VCP inhibitor (VCPi) (NMS-873, Calbiochem) was added to half of the culture at thymidine release. Cells were subsequently washed, fixed and stained.

2.4.2 Chromatin compaction and de-compaction

Cells were treated with 1μM Trichostatin A (TSA) (Sigma) for 16 hrs and 50mM 2-deoxy-D-glucose (2DG) and 10mM sodium azide (NaN_3) (Sigma) for 30 minutes before being fixed.

2.4.3 DNA damage

Cells were treated with 10μM ATMi (Abcam, KU-55933) or 1.5μM CHK2i (Sigma, C3742), for 18 hrs, and treated with 10μM etoposide (Sigma) for 1 hr before being fixed.

2.4.4 Flavopiridol

Cells were synchronized by thymidine release. 1 hr before fixation, 1μm Flavopiridol (Santa Cruz) was added to half the culture. Cells were then fixed.

2.5 siRNA

siRNAs were designed using sfold software and obtained from MWG eurofins.
ATM siRNA sequences:
5'-3': CAUCUAAUGGUCUAACGUA[dTdT]
3'-5': UACGUUAGACCAUUAGAUG[dTdT]
Luciferase siRNA sequences:
5'-3': CGU ACG CGG AAU ACU UCG A[dTdT]
3'-5': UCG AAG UAU UCC GCG UAC G[dTdT]

2.6 Production of lentivirus

6 million HEK293 cells were seeded in a 10mm dish, using Sigma media. The next day, transfection mixtures were prepared; 2.5ml of plain filtered DMEM was added to a Bijou. 10µg of the viral vector of interest, 2.5µg of pMD2.G (expresses the VSV-G envelope protein) and 7.5µg of p8.91 (helper vector) was added to produce the DNA-DMEM mixture. To produce the PEI-DMEM mixture, 2.5ml of plain filtered DMEM was added to a 15ml falcon tube. 24µl of 1mg/ml PEI (Polyethylenimine) was then added for each ml of DMEM and mixed by inverting several times. This mixture was then sterile filtered and left at RT for 2-3 minutes. The PEI-DMEM mixture was mixed again by inverting several times. Solutions were then combined and left at RT for 30 minutes. Meanwhile, HEK293 cells were washed twice in 3ml of warm plain DMEM. DMEM was then removed and 5ml of the transfection mixture was added to the cells. Cells were left in the incubator for 4 hrs. After 4 hrs, the transfection mixture was replaced with 7ml of warm, sterile-filtered media, and cells were put back into the incubator. The virus was harvested 48 hrs post-transfection, by removing the media into a 15ml falcon tube. This was then centrifuged at 1500g for 10 minutes to remove dead cells. The supernatant was then filtered with a 0.45µM filter and stored at -80°C. To produce stable cell lines, 25µl/cm^2 was added to cells, which were then left in the incubator for 72hrs.

2.7 Fluorescence activated cell sorting (FACS)

Viable cells were identified based on light scatter and the exclusion of propidium iodide (PI). In addition, single cell gating was used to exclude doublets and aggregated cells. GFP and mCherry expressing cells were sorted using 488nm laser excitation and 510-550nm emission, and 552nm excitation with 600-620nm emission, respectively, using a Becton Dickinson InFlux cell sorter (BD Biosciences, Franklin Lakes, NJ) running BD Sortware version 1.2.

2.8 Transfections

Cells were split into a 6cm dish (Corning) in 2ml of antibiotic free media (5% FBS and 2mM glutamine only). Once prepared, the transfection mixture was added directly to these cells; 250µl of Opti-MEM (Gibco) was added to two separate Eppendorf tubes. To one Eppendorf, 2µg of the plasmid or 0.8µM of siRNA was added. To the other, 8µl of lipofectamine 2000 (Invitrogen), or lipofectamine RNAiMAX (Invitrogen) was added, respectively. Mixtures were then vortexed and

left at RT for 5 minutes, before combining. The combined mixture was then vortexed and left for 15 minutes at RT. The cells were left in the incubator for 4 hrs. After this, the media was removed, cells were washed, and normal, complete media was added. Samples were taken at 24, 48 and 72 hrs to check transfection/ knockdown efficiency. For exportin 6 FLIM experiments, the 48 hr time point was chosen.

2.9 Nucleofection

100µl of re-suspension buffer, containing 1 million cells and 5µg of plasmid DNA was used per reaction. Control cells were put through the same process but had an empty DNA vector. The nucleofection was performed using recommended protocols in a Neon Transfection system (Invitrogen), using asynchronous cells.

2.10 Primary antibodies and dilutions

Table 2-1. Primary antibodies and dilutions

Antibody Name	Species	Supplier	Cat #	Dilution in WB	Dilution in IF
H3S10ph	Rabbit	Abcam	ab32107	1/2500	1/1000
H4K16ac	Rabbit	Active Motif	39167	1/1000	1/250
H4 ac	Rabbit	Active Motif	39926	1/1000	1/250
H3K27me3	Rabbit	Cell Signalling	#9733S	1/1000	1/1600
H3K9me2	Mouse	Abcam	ab1220	1/1000	1/200
H3K9me3	Rabbit	Abcam	ab8898	1/1000	1/500
H4K20me1	Rabbit	Abcam	ab17788	1/1000	1/200
H4K20me2/3	Mouse	Abcam	ab78517	1/1000	1/200
yH2A.X	Mouse	Millipore	05-636	1/1000	1/500
H2A.X	Rabbit	Abcam	ab124781	1/1000	N/A
H3	Rabbit	Cell Signalling	#4499P	1/2000	N/A
H4	Rabbit	Cell Signalling	#13919P	1/1000	N/A
H2A	Rabbit	Cell Signalling	#12349P	1/1000	1/500
Cyclin A	Mouse	bd biosciences	554174	1/500	1/100
Cyclin E	Mouse	Santa Cruz	SC-247	1/200	N/A
Cyclin D	Rabbit	Cell Signalling	#2978	1/1000	N/A
RNAPIIpS2	Rabbit	Abcam	ab5095	N/A	1/500

RNAPIIpS5	Rabbit	Abcam	ab5131.50	N/A	1/200
MOF	Rabbit	Abcam	ab200660	1/1000	1/2000
KAT5		Abcam	ab23886	1/1000	1/1000
Aurora B	Rabbit	Bethyl Laboratories	A300-431A-T	1/1000	1/200
PP1	Rabbit	Bethyl Laboratories	A300-904A	1/1000	1/200
PP2A	Rabbit	Bethyl Laboratories	A300-732A-T	1/1000	1/200
VCP	Mouse	BD Biosciences	612183	1/1000	1/100
Tropomyosin4	Rabbit	Millopore	AB5449	1/1000	1/500
BRD4	Rabbit	Bethyl Laboratories	A301-985A-T	1/1000	1/100
NUMA	Rabbit	Bethyl Laboratories	A301-509A	1/1000	1/100
CAF1	Rabbit	Abcam	ab126625	1/1000	1/100
HMGB1	Rabbit	Abcam	a301-509A-t	1/1000	1/1000
Phalloidin-594	N/A	Thermo Fisher	A12381	N/A	1/100
53BP1	Rabbit	Novus Biologicals	NB100-304	1/1000	1/250
pCHK1s345	Rabbit	Cell Signalling	#2348	1/500	N/A
Total CHK1	Mouse	Santa Cruz	sc-8408	1/200	N/A
pATRs428	Rabbit	Cell Signalling	#2853P	1/500	N/A
ATRIP	Abcam	Rabbit	ab3729	1/500	N/A
pRPAs33	Rabbit	Bethyl Laboratories	A300-246A	1/500	1/200
ATM	Rabbit	Abcam	ab32420	N/A	1/250
GFP	Mouse	Roche	11 814 460 001	1/1000	N/A

RFP	Rabbit	MBL life science	PM005	1/1000	N/A
Flag	Mouse	Cell signalling	#98533	N/A	1/1600
MYO1C	Rabbit	Abcam	ab194828	N/A	1/100
Bmi1	Rabbit	Cell Signalling	SC-10745	N/A	1/200
Nucleolin	Rabbit	Bethyl	A300-711A	N/A	1/200
Lamin A/C	Mouse	Santa Cruz	SC-376248	N/A	1/100
Actin	Mouse	Sigma	A4700	1/1000	N/A
MCM7	Mouse	Santa Cruz	sc-9966	N/A	1/100
RIF1	Rabbit	Cell Signalling	#95558S	N/A	1/1000
CDC45	Rabbit	Cell Signalling	#11881	N/A	1/50

2.11 Secondary antibodies and dilutions

Table 2-2. Secondary antibodies and dilutions

Antibody	**Species**	**Supplier**	**Cat #**	**Dilution in WB**	**Dilution in IF**
Alexa fluor 594	Rabbit	Invitrogen	A11037	N/A	1/1000
Alexa fluor 488	Mouse	Invitrogen	A11029	N/A	1/1000
Alexa fluor 647	Mouse/Rabbit	Invitrogen	A21236 /A21245	N/A	1/1000
Alexa fluor 405	Mouse/Rabbit	Abcam	ab175658/ ab175651	N/A	1/1000
DyLight 488	Mouse	Cell signalling	#4316	1/5000	N/A
DyLight 800	Rabbit	Cell signalling	#5151	1/5000	N/A

2.12 Western blotting

Western samples were collected by lysing cells in 2X laemmli buffer (4% SDS and 120mM Tris, pH6.8). Samples were then boiled for 5 minutes, before being passed through a 25G needle using a syringe. Samples were centrifuged at 21,000g for 5 minutes and quantified by nano-drop. Concentrations were normalised, by adding water to produce samples with equal concentration and volume. 4X sample buffer (Thermo Fisher, NP0007) was combined with DTT (Dithiothreitol, Sigma), and diluted to 1X in each sample. The samples were then loaded into a polyacrylamide gel (Table 3). The gel was transferred to a nitrocellulose membrane (Thermo Fisher), which was blocked (table 5) for 1 hr, before being probed with the relevant antibodies (table 1).

Table 2-3. Components of polyacrylamide gels

	Resolving gel percentages					
Solutions	20%	15%	10%	8%	6%	4%
ddH2O	1	3.7	6.3	7.4	8.5	9.5
30% Acrylamide (v/v) (ml)	10.7	8	5.4	4.3	3.2	2.2
Resolving Buffer (ml) *	4	4	4	4	4	4
APS (Ammonium Persulfate, 0.1g/ml) (µl)	80	80	80	80	80	80
TEMED (µl)	8	8	8	8	8	8

Table 2-4. Components of a 4% Stacking gel

4% Stacking gel components	**Volume**
ddH2O	6
30% Acrylamide (v/v) (ml)	1.33
Stacking Buffer ** (ml)	2.5
APS (Ammonium Persulfate, 0.1g/ml) (µl)	65
TEMED (µl)	6.5

***Resolving Buffer:** 1.5M Tris, pH8.8, 0.1% SDS

****Stacking buffer:** 0.5M Tris, pH6.8, 0.1% SDS

Table 2-5. Composition of buffers used for Western Blotting

Buffer	
Running	20mM sodium acetate, 10 mM EDTA (Ethylenediaminetetraacetic acid) (pH 8.0) adjust to pH 7 with NaOH
Transfer	25mM Tris-HCl (pH 7.6), 192 mM glycine, 20% methanol, 0.03% sodium dodecyl sulfate (SDS)
TBST	10mM Tris-HCl (pH7.4), 150mM NaCl, 0.1% TWEEN-20
Blocking	TBST plus 5% (w/v) skimmed milk powder

2.13 qPCR

Cells were synchronized in mitosis by mitotic shake off and collected 5 hrs post-mitotic release. These pellets were used to extract RNA (PureLink™ RNA Mini Kit, life technologies, 12183018A). DNA contaminants were digested by incubation of 10µg of RNA with TURBO DNAse (TURBO DNA-free™ kit, Invitrogen, AM1907), at 37ºC for 30 minutes, in a volume of 50µl. After this time, DNase inactivation agent was added, samples were left at RT for 5 minutes, mixing ever few minutes. Samples were centrifuged at 10, 000g for 1.5 minutes. Supernatant was removed. 0.5µg of clean RNA was then used to make cDNA (iScript™ cDNA Synthesis Kit, BIO-RAD, 170-8891), using a thermocycler (SimpliAmp Thermo Cycler, life technologies, A24811), in a volume of 20µl. These samples were run in duplicate, where one sample did not contain reverse transcriptase (-RT sample). Once complete, 180µl of dH_20 was added, and the –RT samples were run in duplicate in a qPCR machine (Corbett research, Rotor-gene 6000). Components per reaction; 1µl of 5µm FWD and REV primer mix, 7.5µl iTaq (BIO-RAD, 1725120), 1.5µl H_2O, 5µl cDNA. If clean, +RT samples were then run in quadruplicate. Ct values were fitted to a standard curve of known numbers of cDNA molecules. These data were then normalised to the number of RhoGDI molecules.

2.13.1 qPCR primers:

Primer sequences were taken from the publications referenced, and purchased from MWG europhins, with the following sequences:
RhoGDI: Fwd= CGGTGTCCCAAACTAGAGGT, Rev= TCACAGAGTGCTCGTCTTCC

Cyclin D1: Fwd= TGCCATCCATGCGGAAA, Rev= AGCGGGAAGAACTCCTCTTC (Kothapalli et al., 2007).
Cyclin E1: Fwd= AATTGGGGCAATAGAGAAGAGGT, Rev= TGGAGCTTATAGACTTCGCACA (McEvoy et al., 2007).
SKP2: Fwd= AGCGCGTGGGTGAAAGC, Rev= ATCACTGAGTTCGACAGGTCCAT (Stewart et al., 2004).

2.14 MNase Assay

Following synchronization for 15x15cm dishes, samples were washed in 1ml of RSB buffer (10mM Tris pH 7.6, 15mM NaCl and 1.5mM $MgCl_2$) and collected by centrifugation at 300g. Samples were then lysed in 1ml of RSB buffer containing 0.1% TritonX100 and centrifuged at 13,000g for 1 minute to collect nuclei. The pellet was then washed twice in 1ml of buffer A (15mM Tris pH7.5, 15mM NaCl, 60mM KCL, 1x EDTA-free protease inhibiter cocktail and 0.1% β-mercaptoethanol, v/v), and collected by centrifugation at 13,000g for 1 minute. Nuclei were then re-suspended 1x mnase buffer (NEB), containing 1x BSA (NEB), and separated into 100µl aliquots. Aliquots were incubated at 37ºC with 200 gel units of Mnase enzyme (NEB). Samples were subsequently removed, and the reaction was stopped, by addition of 3µl of 0.5M EDTA (made in house) at multiple time points**.** Results showed the 5 minute incubation gave the best digestion, thus this was used for future experiments. Samples were separated on a 1.5% agarose gel.

2.15 Immunocytochemistry/ immunofluorescence

Cells were seeded onto #1.5 coverslips (Bruker), washed 3 x in PBS, and fixed in 4% (v/v) paraformaldehyde (made in house, diluted in PBS) for 10 minutes. Coverslips were then washed another 3 x in PBS, and permeabilised in 0.1% TritonX-100 (v/v) (Sigma, diluted in PBS) for 10 minutes. Coverslips were then washed 3 x in PBS, before blocking them in 3% BSA (w/v) (Thermo Fisher) in PBS for 15-30 minutes. Antibodies were diluted (table 1-2) in 1% BSA (w/v) in PBS. Coverslips were incubated at RT in primary antibodies for 2 hrs, and subsequently washed 3 x in PBS. They were then incubated with secondary antibody in the dark at RT for 45 minutes. Coverslips were then washed three times in PBS and mounted onto microscope slides using fluoroshield (Sigma). The next day, samples were stored at 4°C. Where necessary, cells were fixed

following a 5 minute incubation with CSK buffer (10mM PIPES, pH7, 100mM NaCl, 300mM sucrose, 3mM $MgCl_2$, 0.2% (v/v) TritonX-100, 100mM NaCl).

2.16 CLICK chemistry

Click Chemistry reactions for 5-Ethynyl-2´-deoxyuridine (EDU) and ethynyl uridine (EU) used Click-iT EDU Alexa Fluor 647 Flow Cytometry Assay Kit (Thermo Fisher, C10634) and Click-iT RNA Alexa Fluor 594 Imaging kit (ThermoFisher, C10330), respectively. All centrifugation steps were performed at 800g.

2.16.1 EDU flow cytometry staining protocol

Cells were incubated with 10μM EDU for 15 minutes. Cells were washed in PBS, trypsinised, and centrifuged for 5 minutes. Cells were washed in PBS. Pellets were suspended in 100μl of 4% (v/v) paraformaldhye for 15 minutes. Cells were washed in 1% (w/v) BSA in PBS and centrifuged for 5 minutes. Cells were permeablised in 100μl of saponin-based permeablisation reagent and incubated for 15 minutes at RT. After this, 250μl of Click-iT Plus reaction cocktail was added, containing 219μl PBS, 5μl copper protectant, 1.25μl fluorescent picolyl azide and 25μl of 1X reaction buffer (diluted in water). Samples were left in the dark for 30 minutes at RT. Cells were washed in 3x in saponin permeablisation and wash reagent. After labelling, cells were centrifuged for 5 minutes and resuspended in 300μl of saponin wash buffer, containing 10μg/ml RNAse (Invitrogen) and 20μg/ml Propidium Iodide (PI, Sigma) for 30 minutes.

2.16.2 EDU imaging staining protocol

Cells were seeded onto #1.5 coverslips and treated with 500ng/ml doxycycline overnight. Cells were synchnosnised in S phase by thymidine release (2.3.2) 2 hrs after thymidine release, cells were washed in PBS and fixed in 4% (v/v) paraformaldyde for 15 minutes. Cells were then permeabilised in 0.1% (v/v) Triton X-100 for 10 minutes. Cells were washed 3 x in PBS and incubated with 250μl of Click-iT reaction cocktail, as described. After 30 minutes, cells were washed 3 x in PBS and stained with 1μg/ml DAPI (diluted in PBS) for 10 minutes. Cells were washed 3 x in PBS and mounted onto coverslips, as described.

2.16.3 EU staining protocol

Cells were seeded onto coverslips and synchronised in mitosis by thymidine release (2.3.1). Cells were cultured in 1mM EU for 30 minutes (10 hrs post thymidine release), before being fixed in 4% (v/v) paraformaldehyde for 10 minutes. Cells were washed 3 x in PBS and permeabilised in 0.1% (v/v) Triton-X-100 for 10 minutes. Cells were washed 3 x in PBS and incubated with Click-iT reaction cocktail; 214µl reaction buffer, 10µl $CuSO_4$, 0.9 µl Alexa Fluor Azide and 25 µl reaction buffer additive (diluted in water), then left in the dark for 30 minutes at RT. Cells were then washed 3 x in PBS, stained with DAPI and mounted as described.

2.17 Flow cytometry

Flow cytometry experiments were analysed on a Novocyte (ACEA Biosciences). Cells were stained using the Click-iT EDU Alexa Fluor 647 Flow Cytometry Assay Kit (2.16.1). For staining controls, no $CuSO_4$ was added (required for the Click reaction). Three different flow cytometry experiments were performed:

1. $1x10^6$ NIH-3T3-BFP-Actin$^{WT/R62D}$ cells were seeded in 6cm dishes and induced with 500ng/ml Doxycycline (Sigma) overnight. These cells were then treated with 2mM thymidine for 18 hrs (one dish left as asynchronous). Cells were washed 3x in PBS (one left in thymidine) to release cells from thymidine block. Samples were harvested by trypsinisation and fixed every hour, for a period of 5 hrs. 10uM of EDU was added to cells 30 minutes before each time point. Cells were left in PBS at 4ºC overnight and the next day, the Click-iT EDU flow cytometry protocol was followed, labelling EDU with alexa-647 and staining DNA with PI. Samples were gently vortexed and taken directly to the flow cytometer.
2. $1x10^6$ NIH-3T3-BFP-Actin$^{WT/R62D}$ cells were seeded in 6cm dishes and treated with 2mM thymidine for 18 hrs (one dish left as asynchronous). 500ng/ml Doxycycline (Sigma) was added to the cells, while they are still in thymidine, for 8 hrs. Cells were washed 3x in PBS (one left in thymidine) to release cells from thymidine block. Samples were harvested by trypsinisation and fixed every hour, for a period of 5 hrs. 10uM of EDU was added to cells 30 minutes before each time point. The click it EDU

flow cytometry protocol was then followed, labelling EDU with alexa-647 and PI, as described.

3. $1x10^6$ NIH-3T3, GFP-H2B, GFP-H2B and mCherry-H2B cells were seeded into 6cm dishes. The next day, cells were cultured in 10uM of EDU for 30 minutes. Cells were fixed and stained following the Click-iT EDU protocol. After labelling, cells were centrifuged at 800 g and resuspended in 300µl of saponin wash buffer (part of kit) containing 25µg/ml Hoechst (Thermo Fisher) for 15 minutes. Samples were gently vortexed and taken directly to the flow cytometer.

2.17.1 Flow Jo (flow cytometry analysis)

- Viable cells were gated (FSC-A vs SSC-A)
- Singlets were selected (PI-W vs PI-A).
- Background (647) was then identified using the $–CuSO_4$ samples (FSA vs 647-A).
- PI area vs 647-area was then used to gate the cells based on cell cycle phase (G1, S, G2). Here, the asynchronous gates could not be applied to all populations, due to cell cycle related changes to cell size etc. Therefore, gates were made on the 5 hr time point (distinct populations can be observed by this time point) and applied to all other samples.
- S phase cells were then analysed, looking at the level of 647 (647-A vs histogram, and FSC area vs 647).

2.18 Light microscopy

2.18.1 Widefield (Delta Vision)

Fluorescence imaging within this thesis largely used a Delta Vision microscope (Imsol), equipped with a 63x 1.3 NA oil immersion objective. Illumination was provided by a 4 colour Fluorescent protein InsightSSI module and excitation/emission filters were DAPI (blue), FITCI (green), TRITCI (red) and Cy5 (far red). Images were acquired at an average of 10 Z planes, 1µm apart, using a Cool SNAP camera (Photometrics). These images were then de-convolved and projected (maximum projection) to produce single images, using inbuilt software (softWoRx). De-convolution of these images produced similar resolution to confocal images; the software knows the point spread function of the system and uses rounds of de-convolution to unmix this from the fluorescence from the sample.

2.18.2 Confocal (FLIM system)

Fluorescence lifetime images were acquired on a Leica TCS SP8 system (confocal) attached to a Leica DMi8 inverted microscope (Leica). Excitation was provided by a white light laser with a repetition rate of 80 MHz and an acousto-optical beam splitter (AOBS) selected an excitation wavelength of 488 nm, 405 nm, 594 nm or 647 nm. Images were acquired using a 63×1.4 NA oil immersion objective. Fluorescence of GFP and mCherry was detected using a hybrid detector operating in photon counting mode over an emission range of 495–530 nm or 550-650 nm, respectively. When also using 405 and 647 secondary antibodies, detection used PMT detectors, over an emission range of 400–500 nm or 650-750 nm, respectively. For some experiments, this system was used to run HyVolution software (Leica), which increased the resolution of images, through automatic reduction of the pinhole and rounds of de-convolution.

2.18.3 IncuCyte microscope

Cells were seeded into a 96 well plate. The next day, this plate was put into an InCucyte microscope (Satorius), kept in a tissue culture incubator, maintained at 37°C and 5% CO_2. Images were taken every 2 hrs, using a 10X air objective, for a maximum period of 3 days. NIH-3T3-BFP-NLS-Actin$^{WT/R62D}$+nAC+mCherryH2B cells were treated with or without doxycycline. Growth rates were analysed in terms of fold increase of red cell count (mCherry-H2B), the numbers for which were obtained by normalising each value to the number of red cells at the start of the experiment.

2.19 Fluorescence lifetime imaging (FLIM)

2.19.1 Cell line generation and staining

NIH-3T3-GFP-H2B/ NIH-3T3-GFP-H2B-mCherry cells were generated and purified by FACS, as described in section 2.2 and 2.7. Cells were seeded into glass bottomed 8-well chambers (Ibidi), treated (section 2.4) and fixed in 4% (v/v) paraformaldehyde for 10 minutes. No mounting medium was used; FLIM was performed in PBS. When using transfection, cells were transfected (section 2.8), and this was detected using the relevant primary antibody and Alexa Fluor 405 secondary. For live cell FLIM, cells were imaged in complete phenol red free media (Gibco) and imaged at 37ºC and 5% CO_2.

2.19.2 Data acquisition

Fluorescence lifetime images were acquired on the FLIM system, as described in section 2.18.2. Fluorescence lifetime measurements used a 488 nm laser, with a repetition rate of 80MHz, which continued for 75 s/ FLIM measurement/focal plane. Fluorescence of the H2B-GFP was detected using a hybrid detector operating in photon counting mode over an emission range of 495–530 nm. A notch filter centred on 488 nm minimised any laser scatter into the detector. Time-resolved data were acquired through use of a PicoHarp 300 TCSPC module (PicoQuant) controlled through SymPhoTime64 software (PicoQuant). FLIM Images were acquired with 512×512 pixels and 4096-time bins. For 3D FLIM, FLIM measurements were taken every 1µm, for 10µm in Z.

2.19.3 Fitting of FLIM data

Fitting of FLIM images was performed with the FLIMfit software tool (version 5.0.3) developed at Imperial College London. Temporal binning of the fluorescence decays was performed prior to fitting, resulting in 401-time bins per decay (32ps/bin) and the images were spatially binned 4×4 to ensure sufficient photons were present per pixel prior to the fitting of the data (which compensates for the short acquisition time). Fitting of the fluorescence images was then performed pixelwise with a single exponential model on all pixels above an intensity threshold of 200 photons with a 5×5 smoothing kernel applied, allowing spatial variations in fluorescence lifetime to be visualised. Decay was restricted to the range of 500-1.2x10^4 ps, to ensure each decay was composed of data from only one laser pulse (i.e. the repetition rate if the 80MHz laser is 12ns, so decay after this time is excluded). The instrument response function (IRF) was measured by imaging a solution of 1µM rhodamine 6G with the same settings as data acquisition and then using the ‘Estimate IRF’ function within the FLIMfit software to extract the IRF. Data was fitted using the maximum likelihood algorithm. Data were fitted by myself, or Dr Dominic Alibhai.

2.20 Electron microscopy (EM)

2.20.1 Sample preparation: cell fixation

Cells were seeded into 35mm glass bottomed gridded dishes (Ibidi, low Grid-500), washed in PBS and fixed in 4% (v/v) paraformaldehyde (Electron Microscopy Sciences) for 15 minutes. Cells were washed in PBS and imaged to identify regions of interest (ROI), which were marked at the bottom of the dish.

Cells were then fixed in 1% (v/v) glutaraldehyde (Electron Microscopy Sciences) for 30 minutes. Cells were washed (3 x 5 minutes) in 0.1M phosphate buffer (PB) (81mM Na_2HPO_4, 22mM NaH_2PO_4, pH 7.4). Cells were post-fixed in 1% (w/v) Osmium, diluted in PB, for 20 minutes. Cells were washed (3 x 10 minutes) in 0.1M PB in water (2 x 5 minutes). Cells were stained with 3% (v/v) uranyl acetate (UA, diluted in acetone) for 20 minutes in the dark and washed in water on a rocker (3 x 10 minutes). Cells were dehydrated through an ethanol series; 70%, 80%, 90%, 96%, 100%, 100%, 100%, (v/v) each for 10 minutes. Ethanol was removed and EPON (TAAB-812, combined with the accelerator BDMA and the epoxy hardeners DDSA and MNA) was poured over the cells for 2 hrs, on a rocker. After this time, EPON was poured off the dishes, and fresh EPON was added. Samples were baked at 60ºC for 24 hrs, then a stub was placed over the ROI, and sealed using EPON. After 48 hrs, samples were removed, and the dish was broken using plyers. To remove the central coverslip, the sample was frozen in liquid nitrogen and immediately placed in boiling water. This was repeated until the coverslip was removed. EPON around the ROI was cut using plyers and trimmed to the region using a razor. 70 nm sections were cut using an EM UC6 microtome and a diamond knife (Diatome) and picked up using 3mm copper slot grids (Agar Scientific). Grids were left to dry for at least 1 hr on pioliform coated racks. Samples were then removed and stained with 3% (w/v) aqueous uranyl acetate (diluted in acetone) and lead citrate (containing lead nitrate, sodium citrate and sodium hydroxide, as seen in (Reynolds, 1963)).

2.20.2 Sample preparation: high pressure freezing

Cells were synchronised in mitosis, as described, and mitotic cells were plated onto PLL-coated 35mm dishes. After 1 hr, cells were trypsinised and centrifuged at 1000 x g for 5 minutes. For EM using transfected cells, cells were treated to induce mitotic arrest (2.3.1) 12 hrs after nucleofection. Mitotic cells were collected by mitotic shake off and FACS sorted to obtain a population with homogenous expression. Pellets were re-suspended in complete media containing 10% (w/v) BSA and centrifuged at 1000 x g for 5 minutes. 1µl of this pellet was then put into a 0.1 mm gold membrane carrier and high pressure frozen (Leica EM PAC2). Samples were then freeze-substituted (Leica EM AFS2) in a freeze-substitution acetone mix, containing 0.1% (w/v) uranyl acetate and 1% (w/v) osmium tetroxide, in acetone. During this procedure, samples were first held at -90ºC for 15 minutes, then brought to 0ºC, over a period of 18 hrs (increasing 5ºC per hr). Once at 0ºC, the substitution mix was removed, and samples were first rinsed,

then washed for 5 minutes in acetone (rocking). Samples were then infiltrated with increasing concentrations of EPON, diluted in acetone; 25%, 50%, 75% for 1 hr, then 100% for 2 hrs (rocking). EPON was removed, and fresh EPON was poured in a barrelled sample holder which allows the flow of EPON between compartments. Samples were placed in these holders and baked at 60ºC for 48 hrs. Blocks were then removed from the sample holder, using plyers, and the gold carrier was removed; either by prising with a razor blade, or by freezing the block in liquid nitrogen, waiting for the crystals to start to break, then immediately removing the carrier with a carrier detachment tool, heated to 80 ºC. EPON was trimmed to the area of the cavity, and cells were identified by cutting a 1µm section using an EM UC6 microtome and a glass knife (made using an LKB knife maker) and staining these sections with trypan blue. A razer was used to trim around the ROI. Samples were sectioned and stained as described above.

2.20.3 Imaging

Images were taken on a Tecnai 12 BioTwin Spirt transmission electron microscope (FEI), operated at 120kV, and attached to an Eagle CCD camera (FEI). Images were taken at 2900x.

2.21 Atomic force microscopy (AFM)

In this system, a sharp tip (<10nm radius) is attached to a cantilever linked to a piezo, which controls Z movement of the tip. A laser is aligned to the tip and reflected onto a detector. An xy scanner moves the sample so that the tip scans the desired region in a rasta pattern. Repulsive and attractive forces from tip-surface interactions cause bending of the cantilever and therefore the position of the laser on the detector changes as a function of xy position. This information is used to form an image (Figure 2-2). There are three common modes of AFM; contact, non-contact and tapping, which directly contact, pass over, or tap in and out of contact with the sample, respectively. These methods use a feedback mechanism to maintain the tip at a constant oscillation amplitude, and therefore distance from the sample.

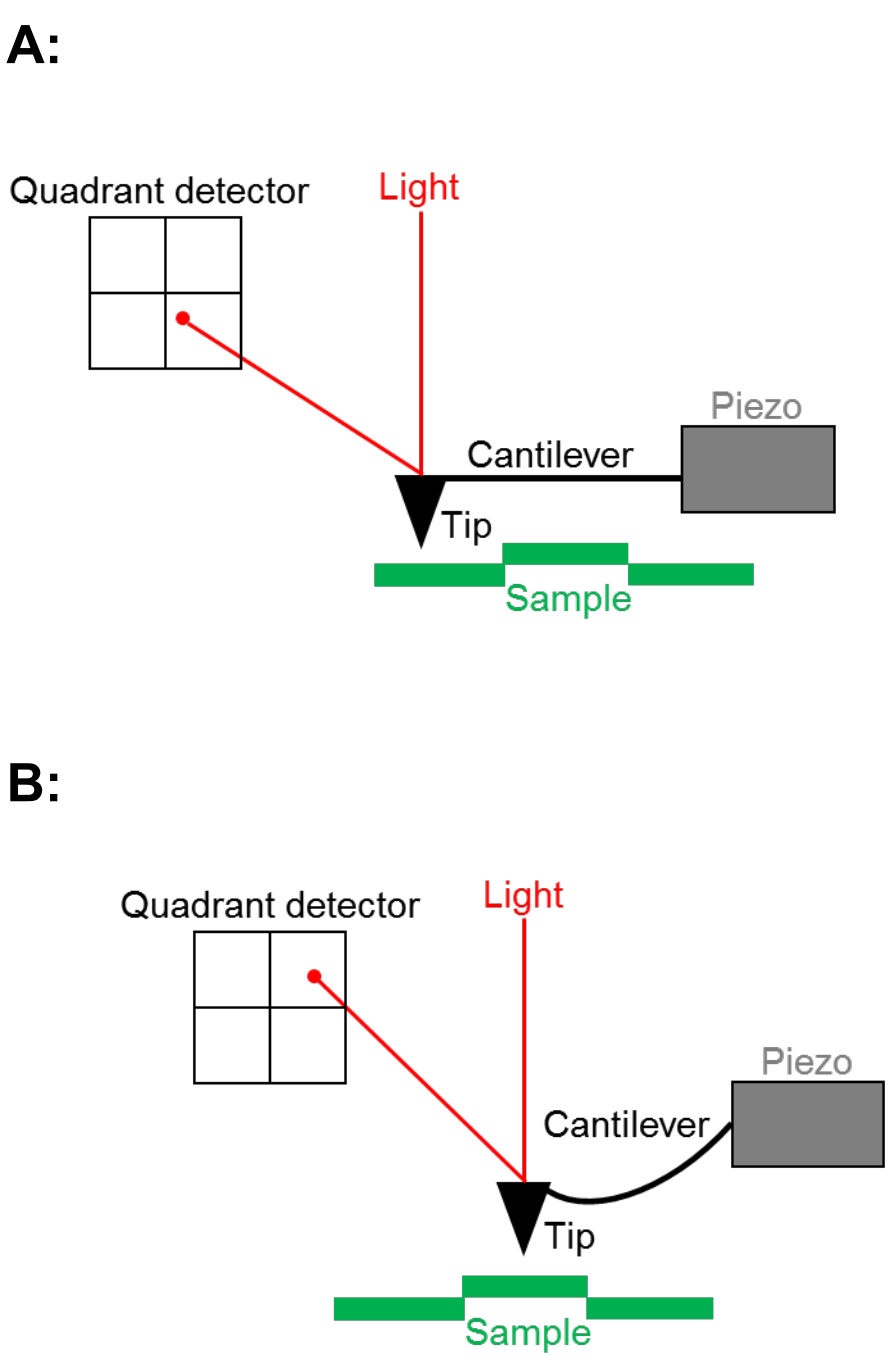

Figure 2-2. The Atomic force microscope (AFM).

A-B *show diagrams of an AFM at two positions over a sample. In this system, a sharp tip is attached to a cantilever, which is linked to a piezo. The piezo controls Z movement of the tip and the sample holder controls X/Y position (driving the tip over the desired region). A light is aligned to the tip, which is deflected onto a quadrant detector (**A**). When a raised surface feature is encountered, this causes bending of the cantilever, meaning the position of the point at the detector changes (**B**). This information is used to form the image, linking height to X/Y position.*

2.21.1 Peak force AFM

Peak force is a variation of AFM, which uses a feedback to control the maximum peak force applied to the sample, opposed to the oscillation amplitude. This allows more precise control, and accurate extrapolation of mechanical properties (Young's Modulus, YM) which are concurrent with topography. The tip maintains contact with the sample, at a specific force, determined by the set point. The x/y scanner moves the sample over the desired scan region, and a force curve is generated for each pixel (Figure 2-3).

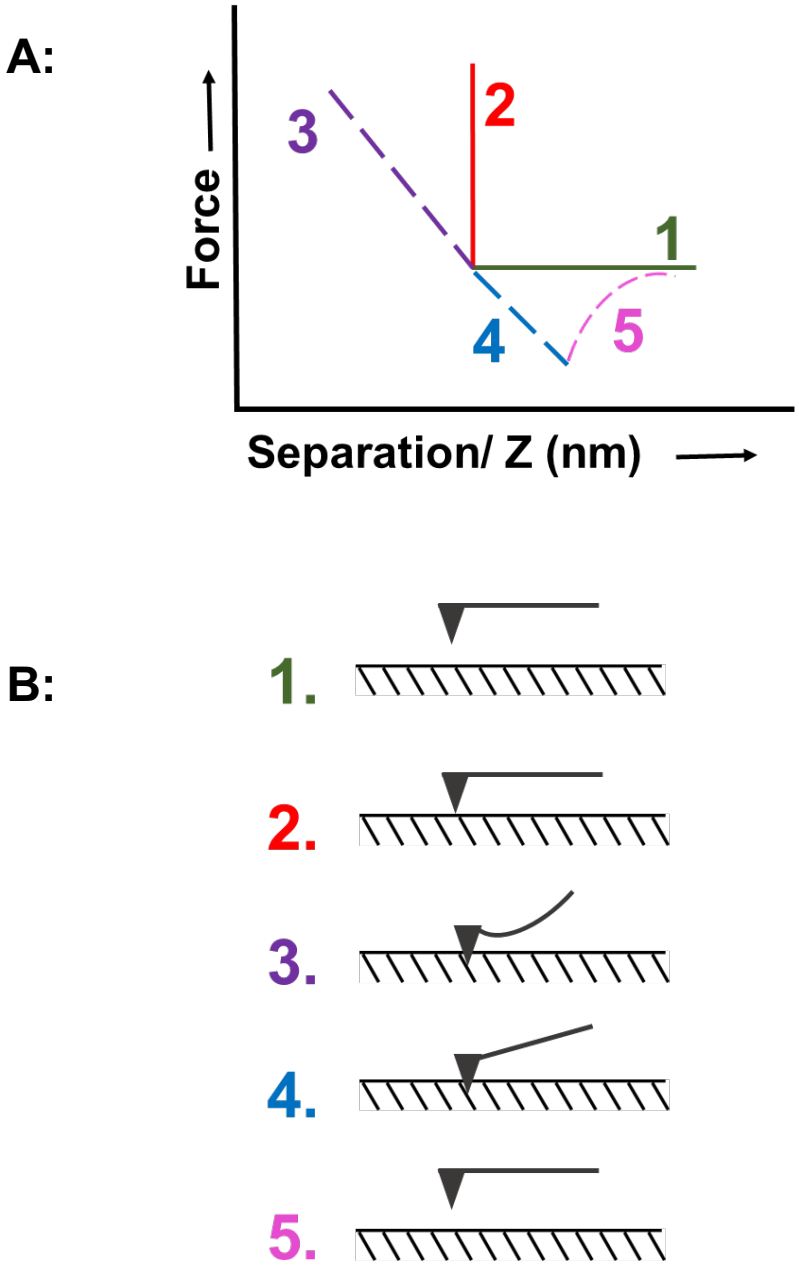

Figure 2-3. Peak force AFM.

***A**, shows a force curve, which is generated each time the tip contacts the sample (i.e. every pixel). **B**, shows the position of the cantilever and tip at each of the stages of the graph shown in a. At position 1, the tip is approaching the surface of the sample. The tip makes contact with the sample in position 2. Once in contact, the tip is deformed into the sample. The amount of force, and therefore indentation into the sample, is determined by the set point put into the system (e.g. apply a force of 5N). Position 3 shows the tip indenting into the sample, at the desired force. As shown, this causes the cantilever to bend, and therefore the position of the laser on the detector changes. This part of the force curve is used to extrapolate Young's Modulus (YM). Once the force curve for that pixel is generated, the cantilever pulls the tip away from the sample (4) and returns to its normal position (5), ready to take a new measurement, according to changes in x/y. The adhesion (stickiness) of the surface effects the characteristics of steps 4-5.*

2.21.2 Sample preparation

2.21.2.1 Ambient (dried cells)

Glass coverslips (#1, 12mm, Menzel) were washed by mechanically rubbing the glass with methanol, using nitrile gloves, and repeating this several times. This process was then repeated, using milli-Q water, before immediately blast drying the coverslips with compressed air. Once cleaned, cells were seeded onto coverslips and treated or synchronised as described. The next day, media was removed, and cells were washed 3x in PBS and fixed in 4% (v/v) paraformaldehyde for 15 minutes. Cells were again washed 3x in PBS then dehydrated through an ethanol series; 25%, 50%, 70%, 80%, 90%, 100% (5 minutes each). Cells were left in 100% ethanol and dried to critical point using 15 cycles of CO_2 exchange in a CPD300 (Leica). Coverslips were removed and stored in sealed containers to prevent re-hydration.

2.21.2.2 Liquid (isolated nuclei)

Cells were synchronised into mitosis by mitotic shake off and seeded onto 35mm dishes. After 1 hr, media was removed, and cells were washed in PBS. Cells were then incubated with hypotonic buffer (10mM HEPES, 1 mM KCl, 1.5 mM $MgCl_2$, 0.5 mM dithiothreitol, and protease inhibitors) for 5 minutes on ice. Cells were then detached using a cell scraper, homogenised with several stokes with a dounce homgeniser, vortexed and left on ice for another 5 minutes. Cells were centrifuged at 700g (5 minutes at 4ºC), and this step was repeated to wash the pellets in hypotonic buffer. The efficiency of isolation was observed by placing some of these nuclei onto a glass slide and sealing with a coverslip. Dark nuclei were observed in bright field. Nuclei were then seeded on to PLL-coated (sigma) cover slips in buffer S (20 mM HEPES at pH 7.8, 25 mM KCl, 5 mM $MgCl_2$, 0.25 M sucrose and 1 mM ATP). For ATM measurements, isolated nuclei remained hydrated in buffer I (20 mM HEPES at pH 7.8, 25 mM KCl, 5 mM $MgCl_2$ and 1 mM ATP) to increase the longevity of the nuclei for investigation (Guilluy et al., 2014), and reduce adhesion from the sucrose.

2.21.3 Imaging

2.21.3.1 Ambient

Atomic force microscopy investigations were conducted in ambient conditions utilizing a Multi-mode VIII microscope with Nanoscope V controller and a

PeakForce feedback control mechanism. Scan assist air cantilevers with a nominal spring constant 0.4 N/m and nominal tip radius 10 nm (Bruker) were used. Before taking YM measurements, the relative method of calibration was used to calibrate the tip on a sample of PDMS gel, which has a YM of 2.5 mPa (Bruker). Using the relative method, the probe was scanned over a 2.5μm region of the PDMS. As per Hook's law (section 7.1); the spring constant, and also tip radius, were modified until the correct YM value (2.5mPa) was obtained. These calibrated tips were then used to take stiffness measurements by indenting the sample to an average of 10nm; the tip was placed over the nucleus of the cell, which was identified using bright field. This tip was then scanned over a 2.5μm region, at a scan rate of 0.5Hz at 256x256 pixels, giving a digital resolution of ~10 nm/pixel (section 7.2). Measurements were converted to YM using the DMT modulus algorithm.

2.21.3.2 Liquid

Atomic force microscopy investigations were conducted in aqueous solution utilising a Multi-mode VIII microscope with Nanoscope V controller and a PeakForce feedback control mechanism with an enclosed liquid cell, to maintain nuclei hydrated in buffer (2.21.2.2). The surface morphologies of nuclei were observed to remain unchanged for several hours under these conditions, allowing multiple nuclei to be tested in each sample and an average surface roughness (Rq) and associated error to be calculated for each nucleus type. Using SCANASYST-FLUID cantilevers (Bruker) of nominal spring constant 0.7 N/m and nominal tip radius 2 nm, the force applied normal to plane of the sample by the AFM tip was kept below 1 nN, thus imaging stability was maintained whilst avoiding tip-induced deformation of the sample. Images were collected over a 5μm area at a scan rate of 0.404 Hz with at 500 x 500 pixels, giving a digital resolution of ~10 nm/pixel.

2.22 Image Analysis

2.22.1 Cell profiler.

Cell Profiler was used to make several plugins used in the image analysis. These include spot detection (yH2AX), and nuclear intensity measurements (EDU). In each of these plugins, nuclei were identified as 'primary objects', using size exclusion and thresholding filters. Foci and signal within the nucleus were identified as secondary objects and measured using in built functions.

2.22.2 Fiji.

1. Nuclear intensity measurements. Nuclei were manually segmented, based on the DAPI channel, and the intensity of respective channels within this region was measured.
2. Segmentation for heterochromatin analysis; nuclei and nucleoli were manually segmented in 2D slice images across the cell using the freehand selection tool of Fiji (Schindelin et al., 2012; Schneider et al., 2012) to create a binary mask of the nucleoplasm. Heterochromatin was then semi-automatically segmented across the nucleoplasmic region using the WEKA Trainable Segmentation plugin for Fiji (Arganda-Carreras et al., 2017). Classification was based on the Gaussian blur, Sobel filter, Hessian, Difference of Gaussians and membrane projections metrics using the built-in fast random forest algorithm. Due to the variability in heterochromatin staining, it was necessary to train a new classification model for each image. Heterochromatin distribution was subsequently analysed in the segmented images using a custom ImageJ/Fiji macro (made by Dr Stephen Cross in the Wolfson Bioimaging Facility), which measured: (1) the total heterochromatin area and perimeter, (2) the area fraction of heterochromatin as a proportion of the total nucleoplasmic area, (3) the mean distance of any heterochromatin-labelled pixel from the edge of the nucleoplasmic area normalised to the maximum distance, (4) the fraction of heterochromatin-labelled pixels within the outermost 5% of the nucleoplasmic area.

2.22.3 MATLAB.

1. A MATLAB coded gel analysing tool was developed by Dr Stephen Cross in the Wolfson Bioimaging Facility. Briefly, this took the intensity profile along a lane, and used the MATLAB ‘peak finding’ function to find the bands. Intensity values were then normalised to the total lane intensity.
2. A MATLAB coded radial analysis tool was developed by Dr Stephen Cross in the Wolfson Bioimaging Facility. First, this tool segmented projected images; using a median filter (preserves edges), a manual threshold, size exclusion filters and a distance watershed transform to split touching objects. The geometric centre of these segmented objects was then determined, and the MATLAB IMprofile function was used to measure the pixel intensity at 100 points on 60 lines emerging from the

centre. Here, the 100 points were equally distributed along each line, where 0 was the centre and 100 was the edge.

3. MATLAB was used to produce line profiles for fluorescence and FLIM data; image registration was used to correct for misalignment in the two channels (H3K9me3 and the GFP lifetime channel), which was caused by scaling from FLIM-fit. The H3K9me3 channel image was scaled to be 128 x128 pixels using bicubic interpolation in ImageJ and rotated to align with the lifetime image. These rotated and scaled images were loaded into MATLAB (*MathWorks*) and registered with an affine transform to ensure best alignment. These data were saved from MATLAB and then a line profile of width 2 pixels was drawn in ImageJ through centromeres, identified as focal regions showing high intensity in the H3K9me3 channel. The same line was then copied onto the lifetime image and a corresponding line profile was extracted. Developed by Dr Dominic Alibhai in the Wolfson Bioimaging Facility.

2.23 Statistics

Statistics were measured using graphpad prism. For two sample experiments, a Student's t-test was used. For group analysis, a one-way ANOVA and Tukey post-test was chosen. In both instances, *=$p \leq 0.05$, **=$p \leq 0.005$, ***=$p \leq 0.0005$.

Chapter 3 : Development of assays to measure chromatin compaction

3.1 Introduction

During interphase, chromatin is visualised in two clearly distinct states: open euchromatin and condensed heterochromatin (Bickmore and van Steensel, 2013). Although these chromatin states seem to be stable at-steady-state conditions, they undergo dynamic reorganisation during genome transduction processes such as transcription (Therizols et al., 2014; Wang et al., 2014) and DNA repair (Murga et al., 2007; Ziv et al., 2006). Therefore, experimental approaches that enable quantitative analysis of global and regional chromatin compaction states will likely advance understanding of the principles that govern genome organisation and regulation. Such approaches largely rely on imaging, which has advantages over biochemical assays through the ability to visualise chromatin in intact cells. However, standard light microscopy is limited by the wavelength of light (diffraction limited), achieving a maximum resolution of ~200nm (section 7.3). This resolution is not sufficient in many instances, and therefore, imaging techniques such as electron tomography (~1nm resolution) (Ou et al., 2017) and super-resolution light microscopy (~10-100nm resolution) (Boettiger et al., 2016; Ricci et al., 2015), have been used extensively to understand the regulation and structure of chromatin.

An alternative approach to measure close distance interactions, which can be applied to study chromatin compaction, is the detection of Förster resonance energy transfer (FRET). FRET occurs when an excited fluorophore transfers its energy to excite a neighbouring fluorophore. This occurs in a non-radiative way, i.e. without emitting a photon, through dipole-dipole coupling (Figure 7.1). For FRET to occur, the two fluorophores must be close (i.e. within ~10nm distance from one another) and in an orientation which allows dipole-dipole coupling (i.e. not perpendicular). In addition, spectral overlap between the emission of the donor fluorophore and the excitation of the accepter fluorophore is required (Figure 7.2) (Lakowicz, 2006; Piston and Kremers, 2007). During FRET, the donor intensity decreases, the accepter intensity increases, and the donor susceptibility to photobleaching also decreases. These parameters can therefore be used to detect changes in FRET efficiency (section 7.4). However, changes in FRET efficiency are often very small and due to low signal to noise, the readout is often binary (i.e. low FRET, high FRET). In addition, FRET measurements are affected by fluorophore brightness, concentration and the stoichiometry of donor: accepter, and therefore several parameters must be tightly controlled. Another

way to measure FRET, which circumvents these issues, is by fluorescence lifetime imaging (FLIM).

The fluorescence lifetime (Tau: τ) of a fluorophore is the average time which it remains in an excited state before returning to ground state. It is defined as the inverse sum of all rates of relaxation from the excited state (section 7.5). In FLIM-FRET experiments, samples are labelled with two fluorophores capable of FRET, which are compared to samples labelled with only the donor fluorophore. If FRET is occurring, the fluorescence lifetime of the donor will decrease in the presence of the accepter. This change can be measured in either the frequency or time domain, both of which provide a quantitative readout of FRET. In biology, FLIM often uses fluorescent proteins tags, which have a fluorescence lifetime time of 2-4ns. Detection at this time resolution is achieved through using short (picosecond or femtosecond) optical pulses and measuring the arrival time of emitted photons at the detector. FLIM can be implemented in either a widefield or confocal geometry, thereby providing fluorescence decay measurements in each pixel, enabling the spatial mapping of fluorescence lifetimes and FRET. To determine chromatin compaction using FLIM, histones can be tagged with FRET-compatible fluorescent proteins. Due to the orientation of histone octamers, FRET is able to occur between nucleosomes (Lleres et al., 2009). Thus, when chromatin compaction increases, nucleosomes become in closer proximity to one another, leading to increased FRET and a decrease in fluorescence lifetime of the donor fluorophore (Figure 7-3). This approach has been previously reported in live Hela cells and C.elegans (Lleres et al., 2017a; Lleres et al., 2009).

Given the requirements for FRET, FRET based assays may give false negative results e.g. two proteins could interact, but the fluorophores could be on the other side of the complex, or in the wrong orientation. Therefore, it is important to validate findings with these methods, using other approaches which do not suffer from this weakness. One such example is electron microscopy (EM), where by cryopreserving the samples, chromatin can be visualised in its unstained, and highly preserved sate. In addition, scanning probe techniques such as Atomic force microscopy (AFM) can be used to take surface measurements, such as nuclear stiffness, in fixed or live cells. These stiffness values can be in turn correlated with chromatin compaction. Indeed, compact structures tend to be stiffer objects, and repressive histone modifications and chromatin condensation have been previously linked to high nuclear stiffness (Mazumder et al., 2008;

Stephens et al., 2018). Although these methods present their own weaknesses; where EM is limited to preserved cells and AFM can only take surface measurements, combined these methods provide a wealth of insight into the organisation of chromatin and the nucleus.

Following the development of these assays, they were used to examine changes in chromatin compaction in response to DNA damage and the protein kinase Ataxia telangiectasia mutated (ATM). ATM has been well studied in respect to the DNA damage response, where it recognises aberrations in chromatin structure (Stephens et al., 2018) and initiates a signalling cascade to promote the repair of DNA double strand breaks (DSB) (Khanna et al., 2001). In addition to the role of ATM in DNA damage signalling, evidence suggests that it may also have functions in chromatin de-condensation. Indeed, biochemical Micrococcal nuclease (MNase) accessibility assays (Ziv et al., 2006) and chromatin-immunoprecipitation (ChIP) (Khanna et al., 2001) have observed chromatin de-condensation after ionising radiation and/or site-specific DNA double stand breaks. Given the role of ATM in promoting DNA repair within condensed heterochromatin (Goodarzi et al., 2008), a potential role for ATM in chromatin de-condensation in response to DNA damage is suggested. However, other reports suggest chromatin condensation in response to DNA damage (Burgess et al., 2014; Oberdoerffer, 2015), and therefore, the role of ATM in chromatin compaction remains incompletely understood.

The results in this chapter report the development of a streamlined chromatin FLIM protocol that is simpler, faster, and more adaptable than current methods. In addition, this method is validated using other approaches, and used to resolve contradictions relating to the role of ATM in modulating chromatin compaction.

The experiments in this chapter have three main aims:

1. Develop a FLIM assay to measure chromatin compaction.
2. Validate this FLIM approach using quantitative electron microscopy and atomic force microscopy.
3. Use these systems to investigate the role of ATM in chromatin compaction.

3.2 Results

3.2.1 Fluorescence lifetime imaging

3.2.1.1 Cell line production

In pursuit of developing a FLIM assay to measure chromatin compaction, NIH-3T3 cells were transduced with lentivirus expressing GFP-H2B ($H2B^{1FP}$) or both GFP-H2B and mCherry-H2B ($H2B^{2FP}$). Given that this system relies on overexpression of histones, and histone protein levels are important in the timing of S phase and cell cycle progression (Gunesdogan et al., 2014), cell cycle phase was compared between these cells, and the parental cell line, by flow cytometry. To this end, asynchronous cells were fixed and stained with EDU to detect replicative cells, and Hoechst as a measure of DNA content. By plotting these parameters, it was found that the three cell line derivatives showed similar cell cycle profiles (Figure 3-1), thus suggesting that overexpression of fluorescent histones does not affect cell cycle phase distribution.

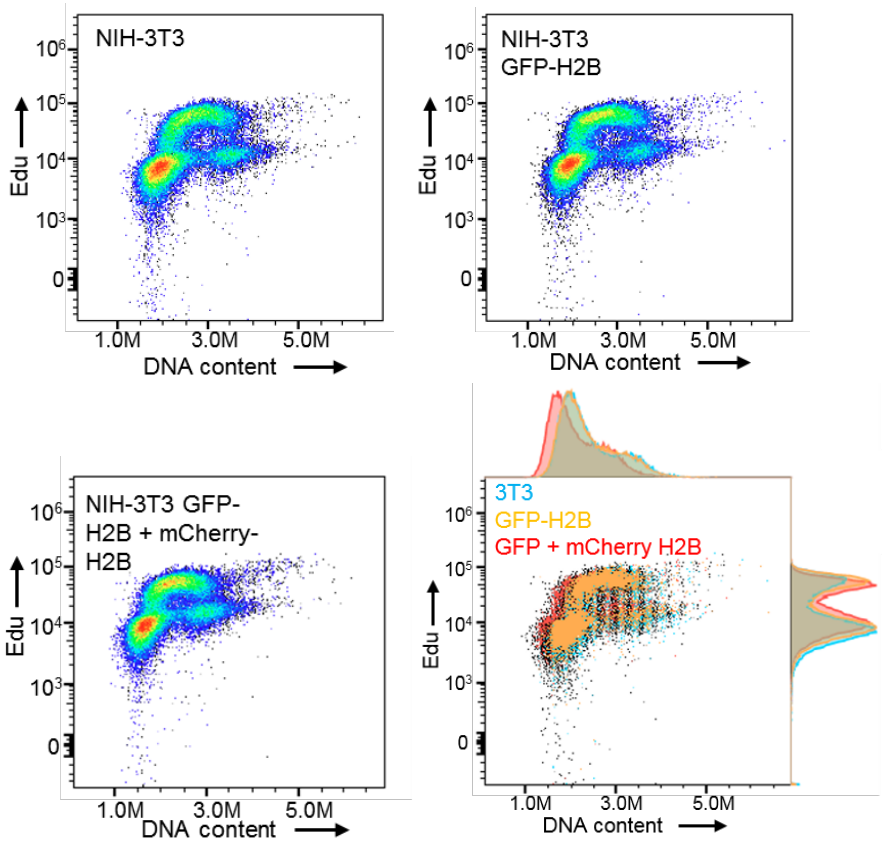

Figure 3-1. Validation of FLIM cell lines.

This figure shows flow cytometry data (acquired on a Novocyte), plotting DNA content (Hoechst) against replicative cells (EDU), of the indicated NIH-3T3 derivatives. Cells were pulsed labelled with EDU for 30 minutes, then fixed and permeabilised for staining with EDU (using Click chemistry) and Hoechst. The final plot (bottom right) shows a merge of the other three plots, revealing similar profiles. Histograms of the indicated channels are also shown. These are representative images from two independent repeats.

3.2.1.2 FLIM outputs

Upon the generation and validation of these cell lines, they were used in a FLIM experiment. As the first control, the florescence lifetimes between $H2B^{1FP}$ cells were compared to $H2B^{2FP}$ cells. The data were analysed using FLIMfit (Warren et al., 2013), an open source software which generates a corresponding fluorescence lifetime (Tau) and intensity map on a pixel-by-pixel basis. A merged map is generated wherein each pixel is represented with a colour, dictated by its fluorescence lifetime, and its brightness determined by the GFP-intensity during FLIM-data acquisition (Tau merge). FLIMfit software also provides graphical representation of chi-squared (Chi^2) values, a statistical test that indicates the extent of variation between the FLIM measurements and the data-fitting model, thereby providing a quality-control for validating FLIM data analyses (Figure 3-2A).

Results showed that the mean GFP fluorescence lifetime was higher in $H2B^{1FP}$, compared to $H2B^{2FP}$, at the single nucleus level (Figure 3-2A). This difference in fluorescence lifetime can also be observed as a shift in the distribution of fluorescence lifetime values of each pixel (Figure 3-2B), which is consistent with specific FRET from GFP-H2B (donor) to mCherry-H2B (acceptor) when they are co-expressed in $H2B^{2FP}$ cells. These fluorescence lifetime values were also converted to FRET efficiency maps (section 7.6), which showed that high FRET efficiency correlates with low fluorescence lifetime. Likewise, by plotting the FRET efficiency as a histogram, higher FRET efficiency was observed in $H2B^{2FP}$ cells (Figure 3-2C). Therefore, FRET is successfully detected by the addition of mCherry-H2B to $H2B^{1FP}$ cells.

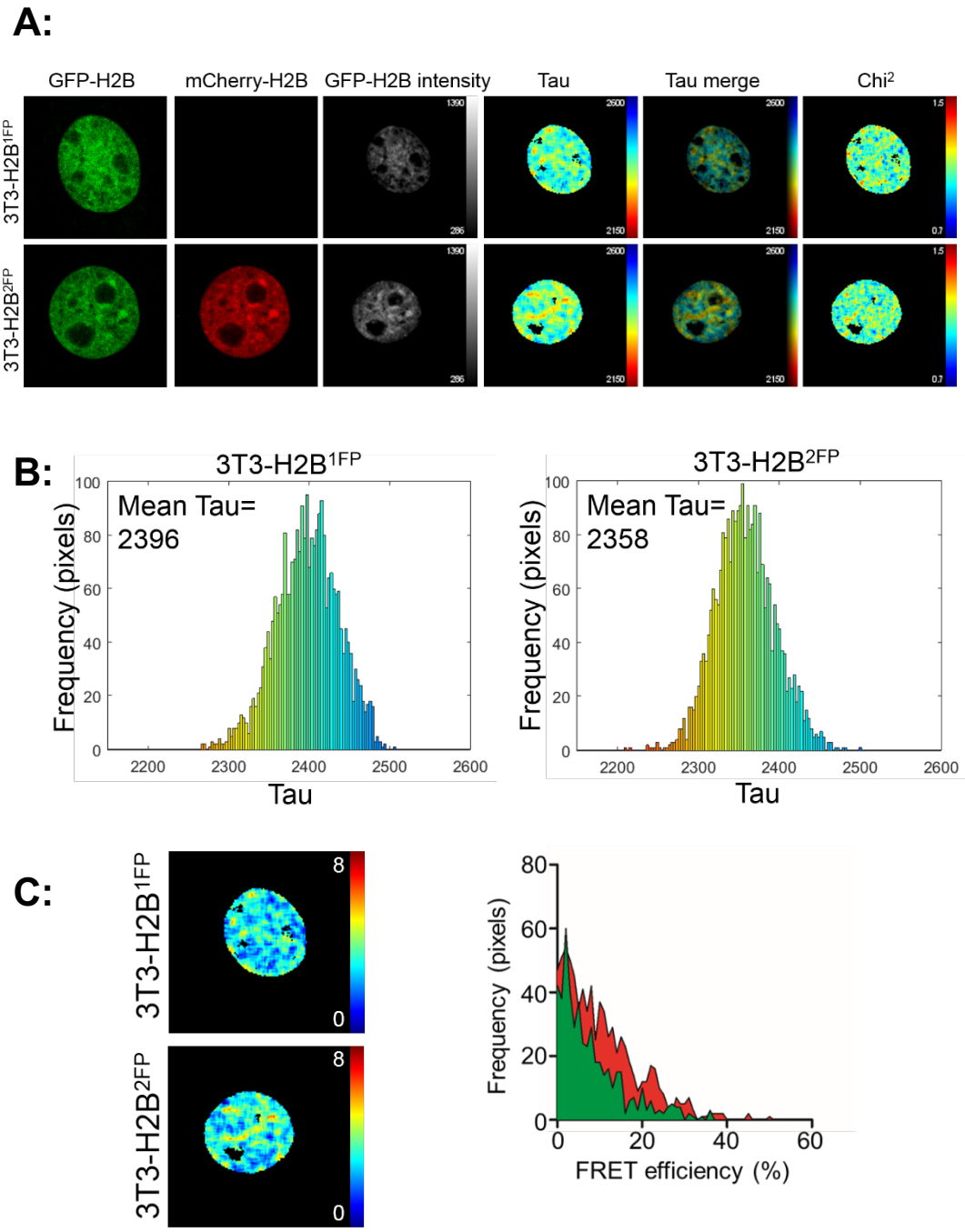

Figure 3-2. FLIM outputs

***A**, shows fixed H2B^{1FP} and H2B^{2FP} cells. GFP and mCherry channels were acquired on a confocal microscope, which was used to generate the FLIM data. Data were analysed using FLIMfit, giving the other outputs within this panel, which show the: corresponding GFP intensity, GFP fluorescence lifetime (Tau), merged fluorescence lifetime and GFP intensity (Tau merged) and chi-squared (Chi^2) nuclear maps. Scale bars show GFP intensity or fluorescence lifetime, as indicated. For Tau merged, the pixel colour is determined by Tau, and its brightness by GFP intensity. **B**, shows the distribution of Tau values on a pixel-by-pixel basis of the same nuclei shown in A. **C left**, shows FRET efficiency maps of the cells shown in A. Scale bar shows FRET efficiency (%). **C right** shows these values as a function of pixel frequency. Green= 3T3-H2B^{1FP}, red= 3T3-H2B^{2FP}.*

3.2.1.3 Optimisation of the FLIM assay to measure chromatin compaction

To validate that this system detects changes in chromatin compaction, as opposed to FRET between free histones, FLIM experiments were repeated using agents that compact and de-compact chromatin. As previously reported (Lleres et al., 2009), chromatin de-condensation and condensation was achieved using the HDAC inhibitor Trichostatin A (TSA) and depletion of ATP, using 2-deoxy-glucose (2DG) and sodium-azide (NaN_3), respectively. Results showed that at the single cell level, the expected changes in chromatin compaction were observed, where TSA treatment increased the fluorescence lifetime due to chromatin de-condensation and therefore decreased proximity and FRET between histones. Conversely, 2DG/NaN_3 treatment decreased the fluorescence lifetime by increasing chromatin compaction and thus FRET between histones (Figure 3-3A).

To identify population heterogeneity, these experiments were repeated in multiple nuclei. Here, the expected decrease in fluorescence lifetime from the addition of mCherry-H2B was observed. However, at the population level, TSA and 2DG/NaN_3 treatment did not show the expected shifts (Figure 3-3B).

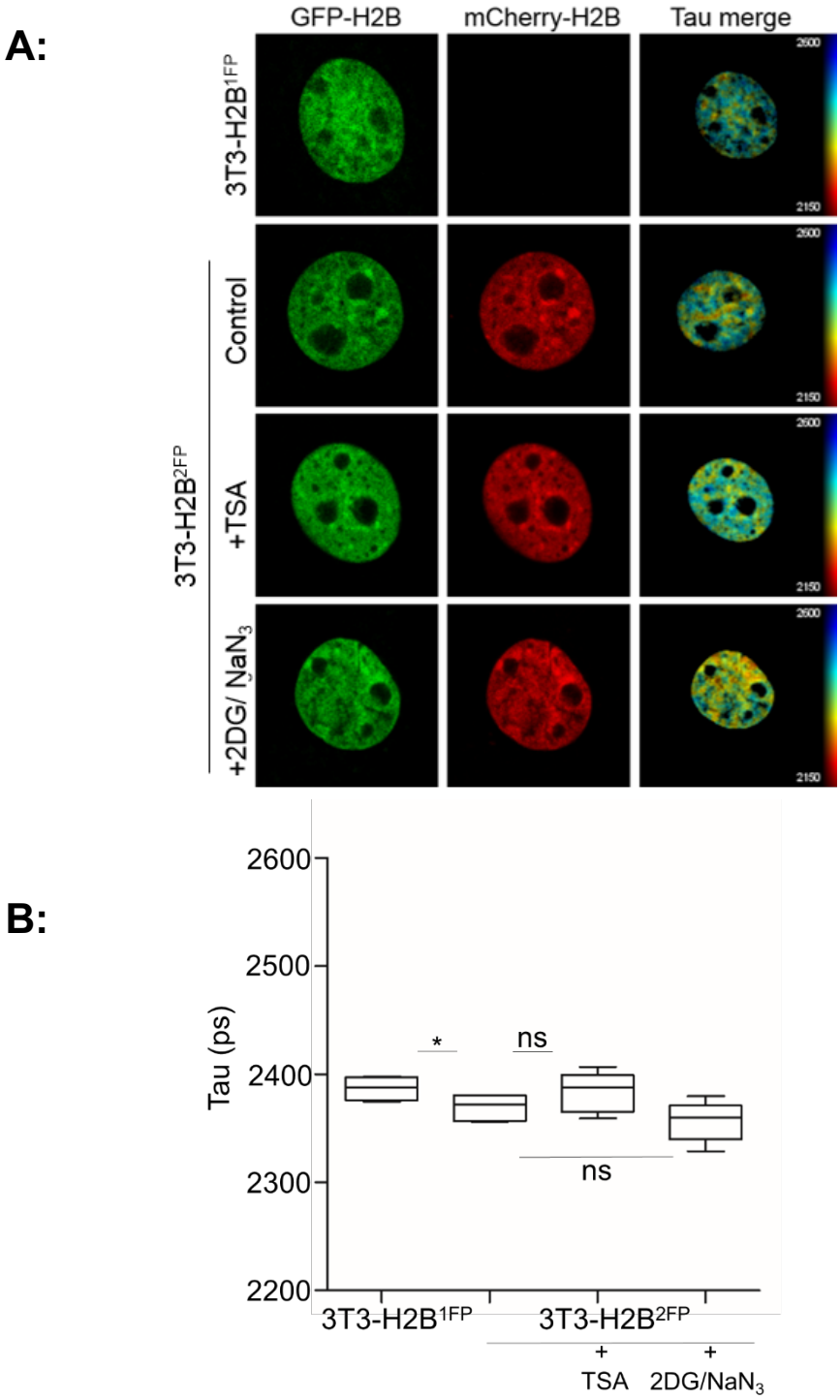

Figure 3-3. Testing the detection of chromatin compaction and de-compaction

***A**, shows 3T3-H2B^{1FP} and 3T3-H2B^{2FP} cells which were treated with DMSO (control), trichostatin A (TSA) or sodium azide and 2-deoxy-glucose (2DG/NaN$_3$), prior to being fixed, as indicated. GFP-H2B and mCherry-H2B channels are indicated and taken with a 63x/1.2 NA water immersion objective lens on a confocal microscope. The final column of panels shows a merge of the fluorescent lifetime and GFP intensity maps (Tau merged). Scale bar shows fluorescence lifetime. **B**, shows a box plot of fluorescence lifetime values (Tau) of the cells shown in A. N=5, one biological repeat. * indicates p=0.042, ns indicates p>0.05, one-way ANOVA.*

Given the heterogeneity of florescent lifetime values observed in these experiments, it was reasoned that the relative levels of GFP-H2B and mCherry-H2B may need to be controlled in this system. To test this, fluorescence activated cell sorting (FACS) was used to generate different $H2B^{2FP}$ cell subpopulations with varying expression levels of GFP-H2B and mCherry-H2B. $H2B^{2FP}$ cells were sorted into eight different subpopulations (Figure 3-4A) and FLIM experiments were performed to determine the extent of heterogeneity in GFP-H2B fluorescence lifetime. Subpopulations 3 and 6 had the lowest degree of variation in GFP-H2B fluorescence lifetime (Figure 3-4B). Out of these two populations, subpopulation 6 was chosen for FLIM experiments due to its higher expression of fluorophores. By using subpopulation 6 in FLIM experiments, TSA treatment resulted in a significant increase in GFP-H2B fluorescence lifetime, at a population level, and 2DG+NaN_3 decreased GFP-H2B fluorescence lifetime (Figure 3-4C). Therefore, by controlling the expression levels and homogeneity of GFP-H2B and mCherry-H2B, comparable lifetime shifts to previous work were obtained.

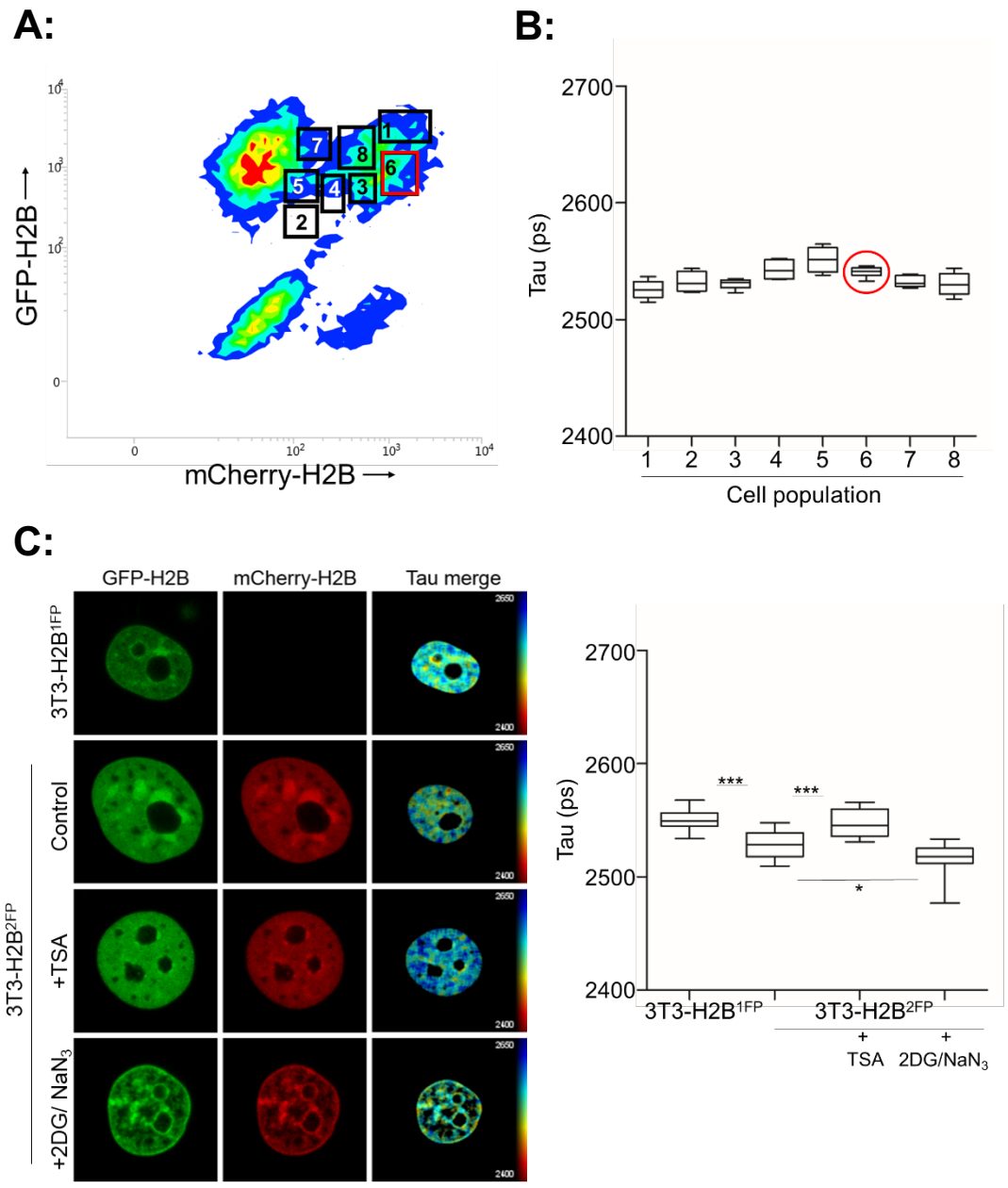

Figure 3-4. FACS sorting improves fluorescence lifetime measurements

***A**, shows a FACS scatter plot of NIH3T3 cells co-expressing H2B-GFP and H2B-mCherry (3T3-H2B^{2FP}). The indicated numbers (1-8) correspond to FACS subpopulations of cells that express varying levels of H2B-GFP and mCherry-H2B. **B**, shows quantification of GFP fluorescence lifetime (Tau) of the FACS-sorted subpopulations, as seen in A. N=5, one biological repeat. **C left**, shows FACS sorted 3T3-H2B^{1FP} and 3T3-H2B^{2FP} cells (population 6) which were treated with DMSO (control), trichostatin A (TSA) or sodium azide and 2-deoxy-glucose (2DG/NaN$_3$), prior to being fixed, as indicated. GFP-H2B and mCherry-H2B channels are indicated and taken with a 63x/1.2 NA water immersion objective lens on a confocal microscope. The final panel shows a merge of the fluorescence lifetime and GFP intensity maps (Tau merged). Scale bar shows fluorescence lifetime. **C right**, shows a box plot of fluorescence lifetime values (Tau) of the cells shown in C left. N>13, two biological repeats. *s indicates results from a one-way ANOVA. *=p<0.05, ***=p<0.0005.*

3.2.1.4 Combination with immunofluorescence

Next, controls were conducted to determine appropriate secondary antibodies which can be combined with FLIM and permit immunostaining. To ensure that the fluorescent secondary antibodies do not interfere with fluorescence lifetime, $H2B^{1FP}$ cells were stained with histone H2A antibody with either no secondary antibody, or AlexaFluor-405 or AlexaFluor-647 secondary antibodies. Fluorescence lifetime measurements were taken, showing that the staining process does not affect GFP-H2B lifetime (Figure 3-5A). When using secondary antibodies, it was found that the presence of AlexaFluor-647 interferes slightly with H2B-GFP fluorescence lifetime whereas using AlexaFluor-405 had less discernible effect (Figure 3-5A). This suggests that AlexaFluor-405 staining is compatible with performing FLIM experiments using the GFP and mCherry FRET pair.

Immunofluorescence was then used to further test the ability of this method to measure high order chromatin compaction. Here, cells were stained with H3K9me3, a marker of condensed chromatin, and the fluorescence lifetime was measured. A line profile was drawn through a H3K9me3 marked chromocenter, as well as the nuclear periphery, both of which contain highly condensed chromatin and therefore should show low fluorescence lifetimes. When this line was positioned to the same region of the fluorescence lifetime map, it was found that H3K9me3 intensity inversely correlates with fluorescence lifetime, as expected (Figure 3-5B). This further validated chromatin FLIM in detecting specific chromatin environments through combination with immunocytochemistry.

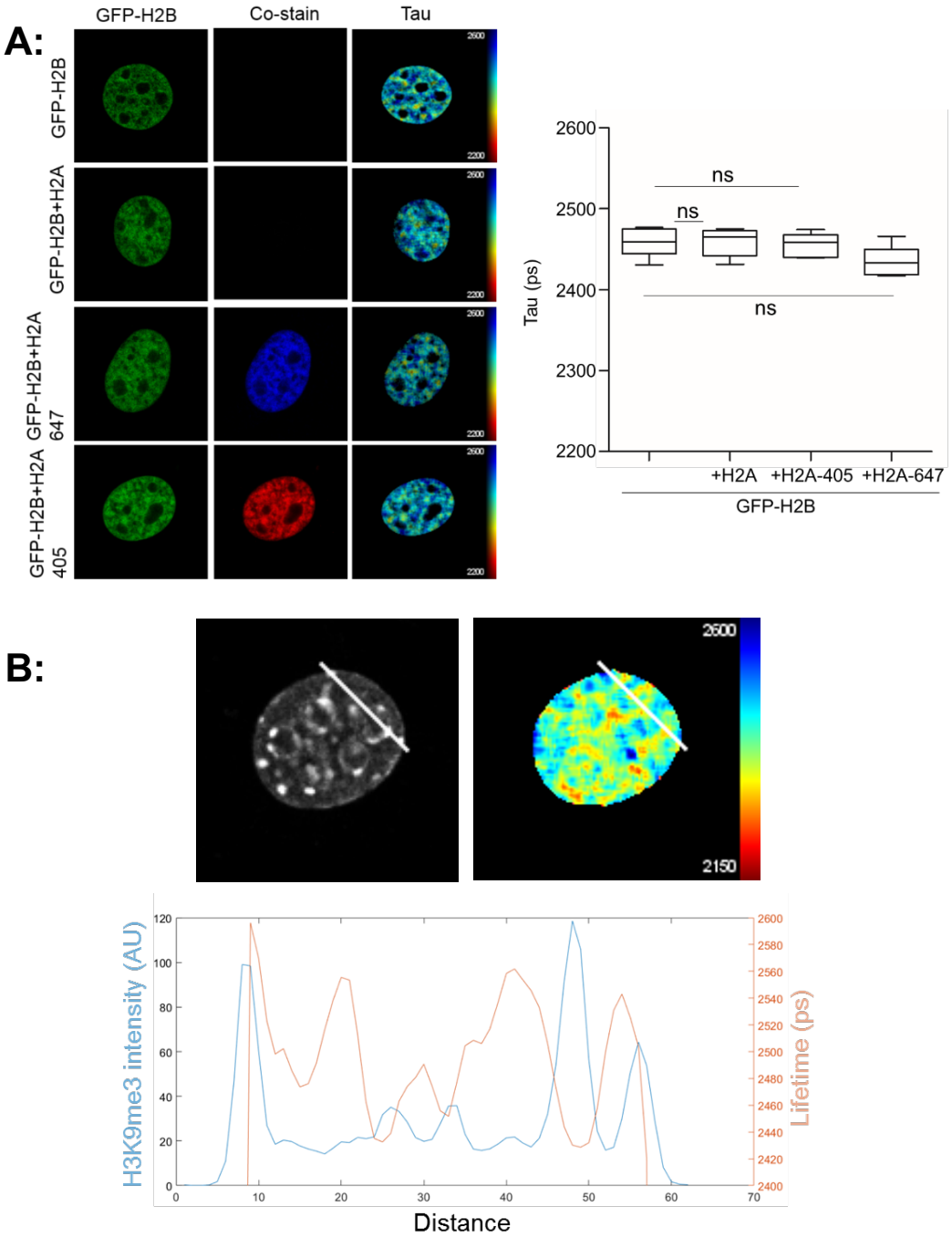

Figure 3-5. FLIM can be combined with immunofluorescence to detect chromatin structures

***A**, shows 3T3-H2B^{1FP} cells which are either: unstained, stained with H2B primary but no secondary antibody, or stained with H2B primary and either Alexa Fluor 405 or 647 secondary antibody. Channels are indicated. The final panel shows a merge of the fluorescence lifetime and GFP intensity maps (Tau merged). Scale bar shows fluorescence lifetime**. A right,** shows a box plot of fluorescence lifetime values (Tau) of the cells shown in A left. N=5, one biological repeat. ns indicates results from a one-way ANOVA, where p>0.05. **B**, shows an image of a cell which was fixed and stained with H3K9me3 and the corresponding fluorescence lifetime map. Colour scale bar shows fluorescence lifetime. A line is drawn over the H3K9me3 image (measuring intensity, AU), and in the corresponding location of the fluorescence lifetime map (measuring lifetime, ps), the values of which are shown in the graph below (where 0 represents the start of the line, i.e. at the top of the image). B, was analysed by Dr Dominic Alibhai.*

3.2.1.5 Live cell FLIM

The discussed pipeline therefore provides a method to perform chromatin FLIM in fixed cells, and a way to combine this with immunostaining. To increase the utility of the method, it was also applied to live cells. For live cell FLIM to capture chromatin changes in real time, it is important that data are acquired as quickly as possible. The speed of acquisition is often limited by the fitting method, which commonly requires fluorescence decay before the next laser pulse, thus using high repetition rates gives falsely short fluorescence lifetimes. By using FLIMfit, which accounts for incomplete fluorescence decay, an increased repetition rate of 80mHz (pulses are separated by 12.5ns) was used. This increased the photon count rate allowed for shorter acquisition times, reaching a maximum speed of 75 seconds per measurement. This provides a scope for rapid chromatin rearrangements to be detected.

In addition, fluorophore stability throughout the FLIM experiment is also an important consideration for live cell experiments. To measure GFP-H2B stability through time, $H2B^{1FP}$ cells were imaged every 75s for 450s, and the GFP intensity and fluorescence lifetimes were compared between these timepoints. In the majority of cells, fluorescence lifetime and GFP intensity remained stable throughout this time period (Figure 3-6A). However, in a proportion of the cells, fluorescence lifetime and GFP intensity both decreased through time (Figure 3-6B). Therefore, when data are combined, there is an overall trend of decreasing fluorescence lifetime through time (Figure 3-6C). An explanation for this may be environmental changes or photobleaching during the experiment. This limitation will need to be overcome in future research.

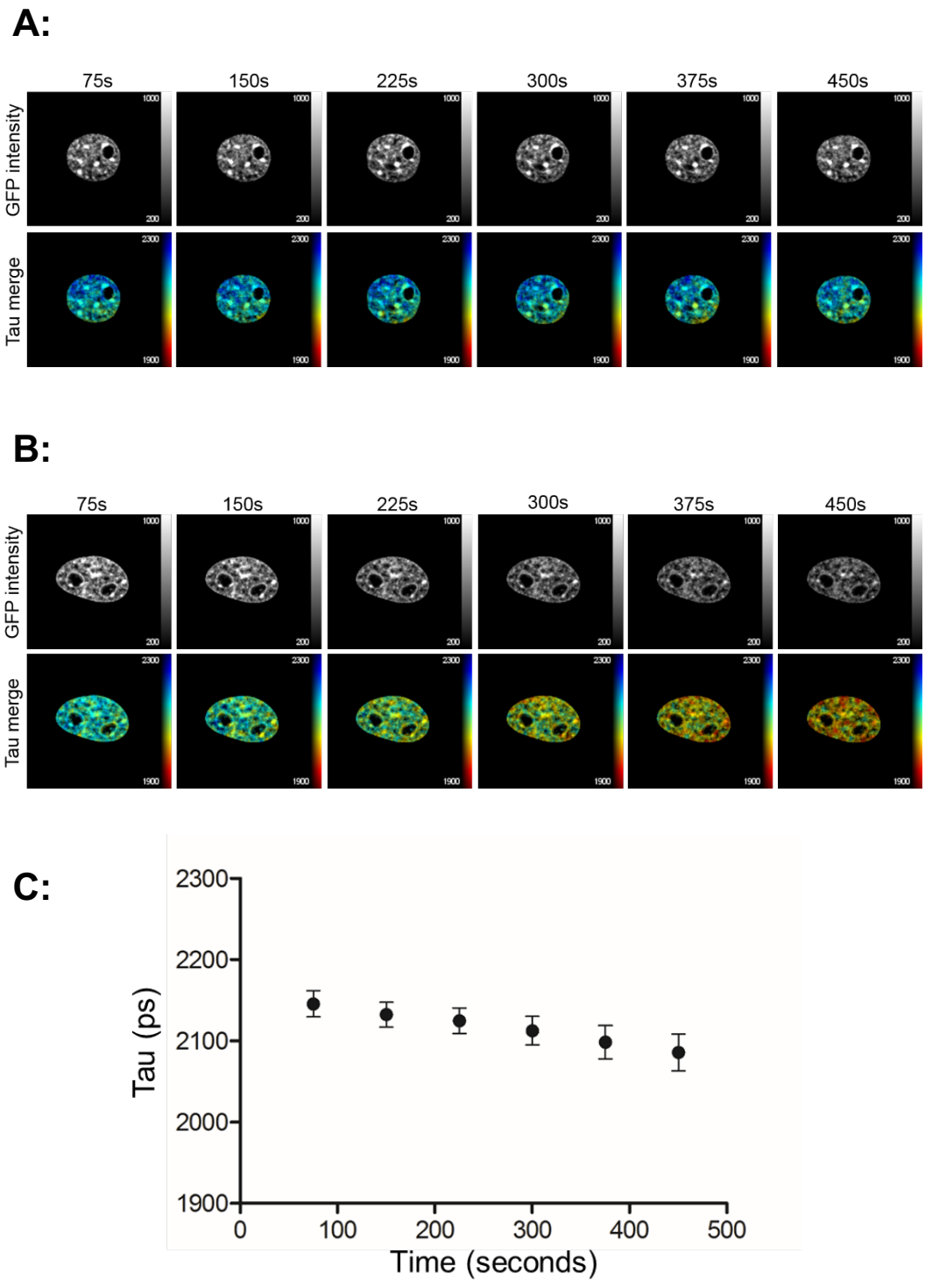

Figure 3-6. Live cell FLIM

A-B *show images during FLIM acquisition of live 3T3-H2B^{1FP} cells, at the indicated time points (seconds). The top panel shows GFP intensity, the bottom panel shows a merge of GFP-fluorescence lifetime and intensity. Colour coded scale bar represents GFP intensity (top) and fluorescence lifetime (bottom).* ***C****, shows a graph of the mean fluorescent lifetime at the indicated timepoints. Error bars show SEM. N=5, one biological repeat.*

3.2.1.6 The role of ATM in DNA damage associated chromatin relaxation

To test the ability of this method to address biological questions, it was applied to visualise changes in chromatin compaction after DNA damage, which has been shown to promote chromatin relaxation (Ziv et al., 2006). Accordingly, $H2B^{2FP}$ cells were treated with the topoisomerase II inhibitor etoposide (ETP) and DNA damage induction was confirmed by the detection of H2AX-phosphorylation at S139 (γH2AX). γH2AX positive cells were selected and used for fluorescence lifetime measurements. Here it was found that DNA damage resulted in increased fluorescence lifetime (Figure 3-7A/B), suggestive of chromatin relaxation after DNA damage. Inhibition of the DNA damage kinase ATM, using the competitive ATM inhibitor ku55933, markedly reduced etoposide-induced chromatin de-compaction (Figure 3-7A/B), consistent with previous reports of ATM-dependent chromatin relaxation after DNA damage (Ziv et al., 2006). These results highlight the usefulness of the chromatin FLIM approach in detecting and validating known structural changes of chromatin in response to genotoxic stress.

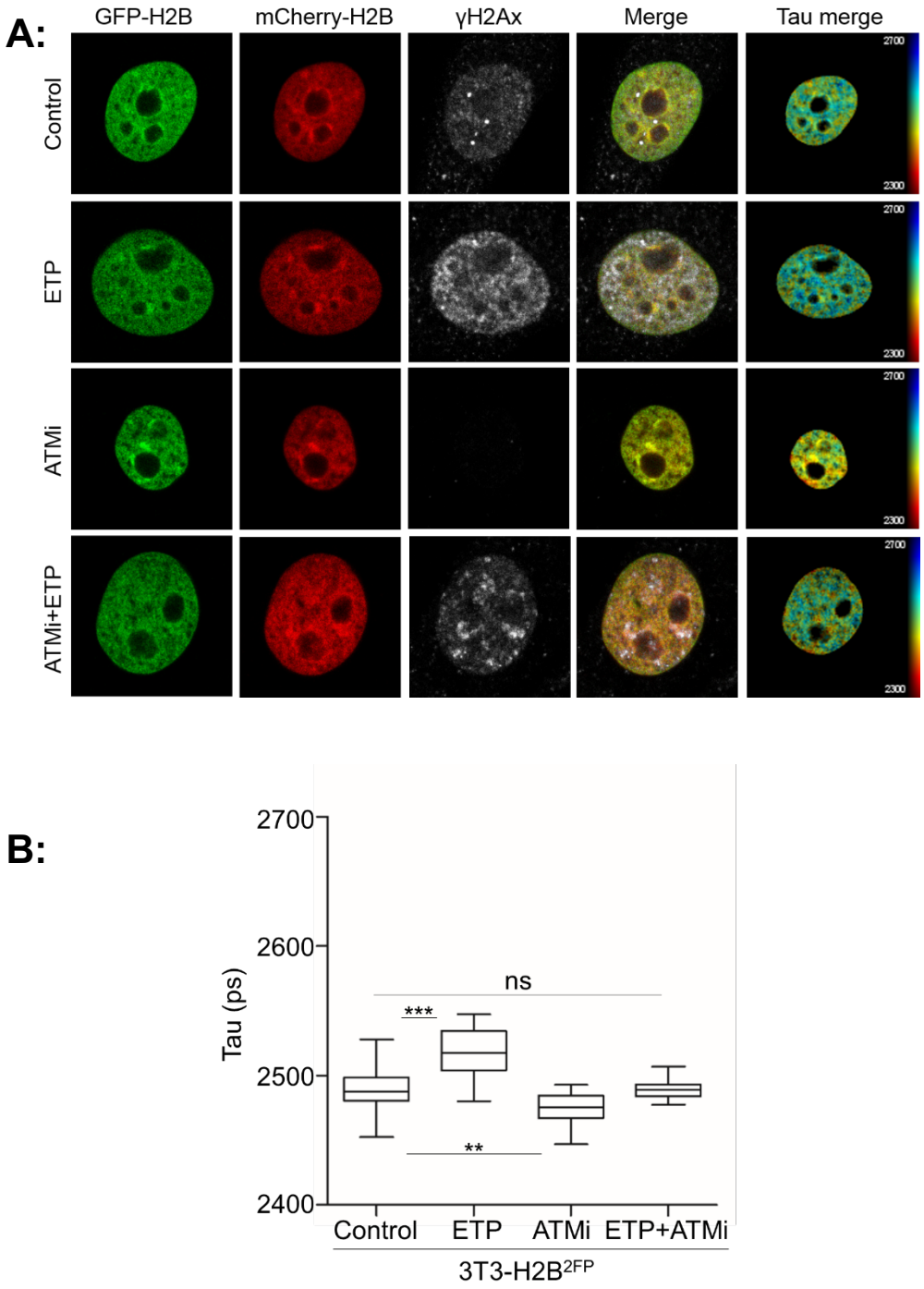

Figure 3-7. DNA damage induces ATM dependent chromatin relaxation

A, *shows FACS sorted 3T3-H2B^{1FP} and 3T3-H2B^{2FP} cells (population 6) which were treated with DMSO (control), etoposide (ETP), ATM inhibitor (ATMi) or both, prior to being fixed. Cells express GFP-H2B and mCherry-H2B and were stained with γH2AX to confirm induction of DNA damage. Channels are indicated. The final panel shows a merge of the fluorescence lifetime and GFP intensity maps (Tau merged). Scale bar shows fluorescence lifetime.* ***B****, shows a box plot of fluorescence lifetime values (Tau) of the cells shown in A. N>18, two biological repeats. *s indicate significance from one-way ANOVA, where **=p<0.005, ***=p<0.0005, and ns=p>0.05.*

3.2.1.7 Inhibition of ATM induces chromatin compaction in absence of DNA damage

Interestingly, these FLIM experiments also showed that inhibition of ATM in the absence of ETP induced chromatin compaction (Figure 3-7A/B). Such a function for ATM in basal conditions has not been previously reported and therefore was of particular interest. Indeed, this increase in chromatin condensation was also visualised in both fixed and live cells at multiple focal planes (Figure 3-8A). Further, these affects were not likely to be due to non-specific targets of the ATM inhibitor, which has weak specificity to DNA-PKcs, mTOR, ATR and PI3K, as the same result was observed after ATM siRNA (Figure 3-8B). In addition, by combining FLIM with H3K9me3 immunostaining, it was found that when fluorescence lifetime and H3K9me3 intensity were measured in the same cells, these parameters were inversely correlated (Figure 3-8C-E). These results provide further evidence that ATM promotes chromatin relaxation, both in the presence and absence of clear DNA damage.

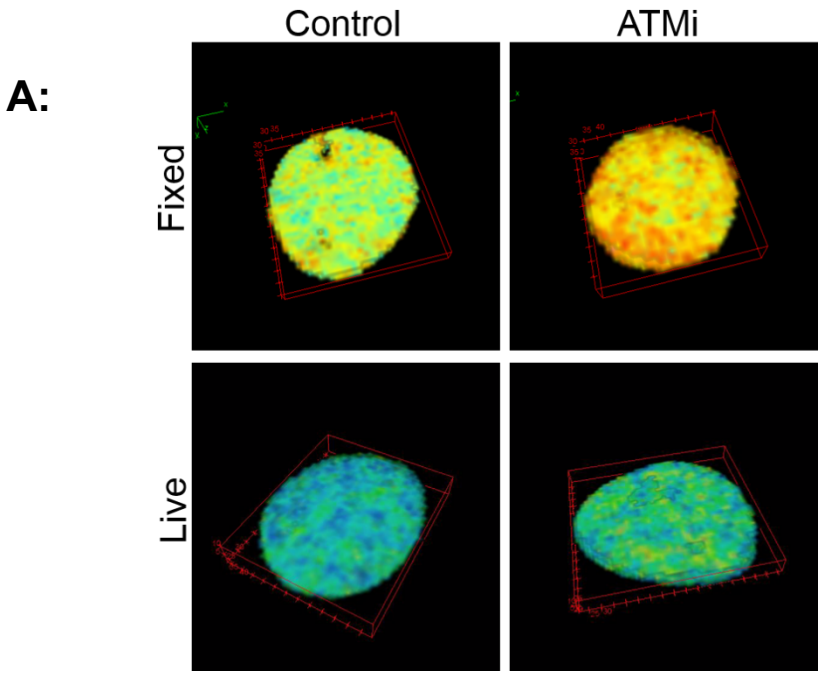
A:
Control
ATMi
Fixed
Live

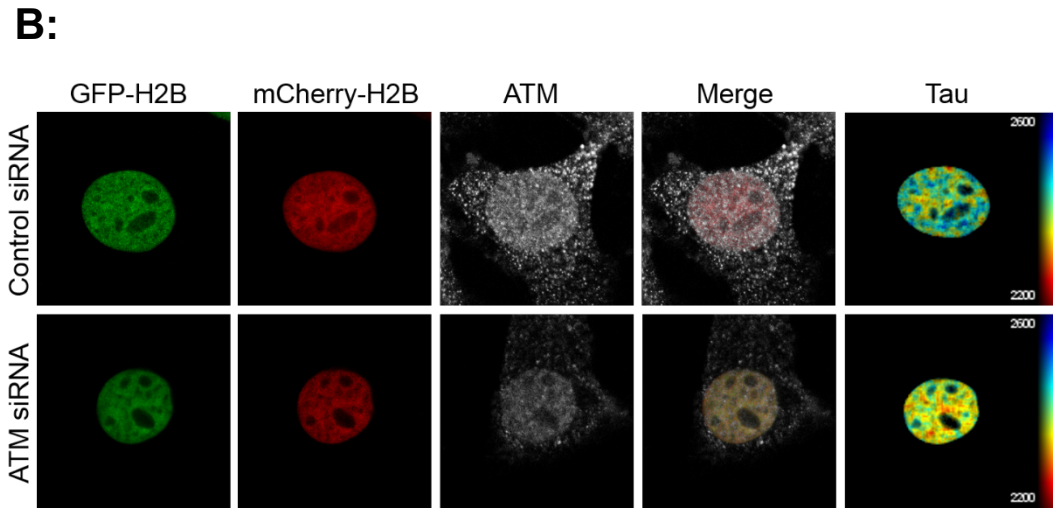
B:
GFP-H2B
mCherry-H2B
ATM
Merge
Tau
Control siRNA
ATM siRNA
2600
2200

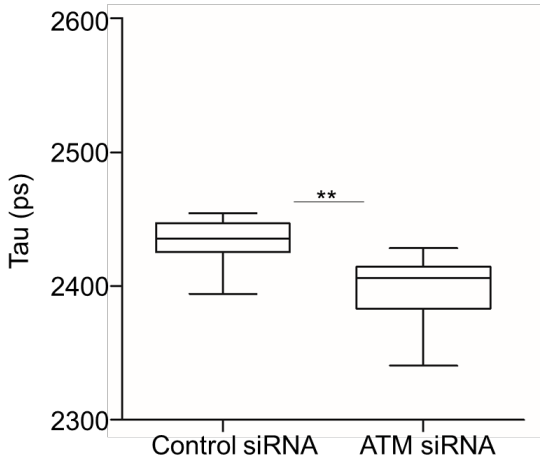
2600
2500
2400
2300
Tau (ps)
**
Control siRNA
ATM siRNA

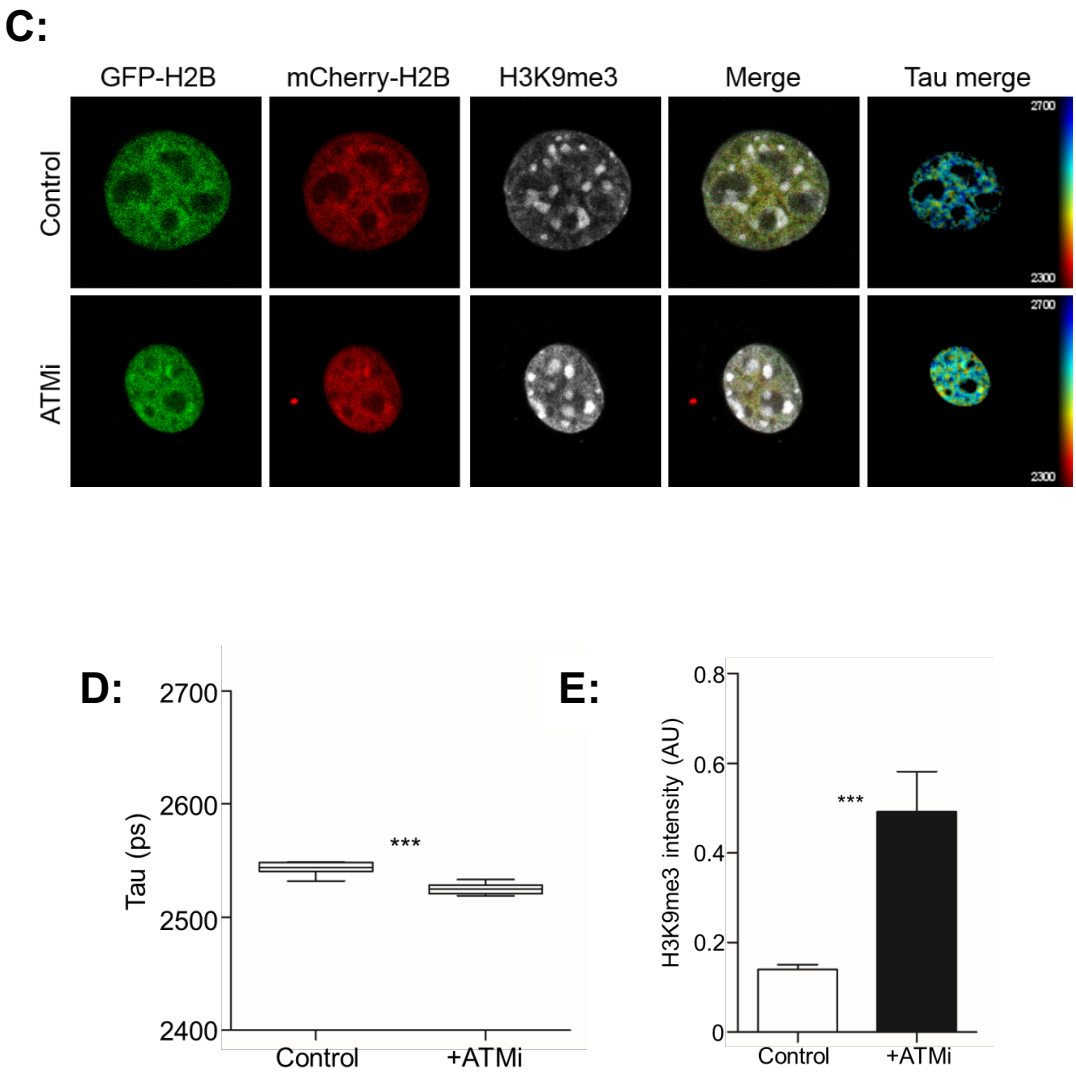

Figure 3-8. ATM induces chromatin compaction

***A**, shows 3D projections of 3T3-H2B^{2FP} cells which were treated overnight with DMSO, or ATM inhibitor (ATMi), before being fixed or imaged live, as indicated. FLIM was performed at a total of 8 focal planes, 1µm apart. **B**, shows FACS sorted 3T3-H2B^{2FP} cells (population 6) which were transfected with control (luciferase) or ATM siRNA 48hrs before being fixed. Cells express GFP-H2B and mCherry-H2B and were stained with ATM to confirm successful knockdown. Channels are indicated. The final panel shows a merge of the fluorescent lifetime and GFP intensity maps (Tau merged). Scale bar shows fluorescence lifetime. **B bottom** shows a box plot of fluorescence lifetime values (Tau) of the cells shown in A. N=10, two biological repeats. ** indicates p=0.002, Student's t-test. **C**, shows FACS sorted 3T3-H2B^{2FP} cells (population 6) which were treated overnight with ATMi or DMSO before being fixed and stained with H3K9me3. Channels are indicated. The final panel shows a merge of the fluorescence lifetime and GFP intensity maps (Tau merged). Scale bar shows fluorescence lifetime. **D**, shows a box plot of fluorescence lifetime values (Tau) of the cells shown in C. N=10, two biological repeats. *** indicates p<0.0001. **E**, shows a graph measuring H3K9me3 intensity (AU) of the cells shown in C. *** indicates p=0.0007, Student's t-test.*

3.2.1.8 ATM mediated chromatin compaction

In light of these results, it was of interest to determine if ATM signals through its canonical pathway when promoting chromatin relaxation in the absence of DNA damage. During DNA damage, ATM signals through a number of interacting partners, ultimately resulting in activation of the effector kinase CHK2 (Khanna et al., 2001). It was therefore speculated that inhibition of CHK2 would result in a similar effect to inhibition of ATM. However, this was not the case, as pharmacological inhibition of CHK2, using competitive inhibitor with high specificity to CHK2 kinase, did not affect chromatin compaction (Figure 3-9A). Therefore, this may suggest that in a non-damaged context, ATM regulates chromatin structure through non-canonical signalling.

Given that ATM-dependent chromatin relaxation in response to DNA damage is thought to involve lysine acetylation (Ziv et al., 2006), it was hypothesised that this may also be involved in ATM's basal functions. Indeed, treatment with the lysine deacetylase inhibitor, TSA, partially rescued the ATMi cell phenotype. However, TSA did not fully alleviate the higher chromatin compaction in ATM inhibited cells (Figure 3-9B), suggesting other mechanisms are involved. Combined, these results suggest that basal ATM activity may somewhat be required for maintaining chromatin organisation in interphase cells, in a manner that is at least partially independent from typical signalling and involves histone acetylation.

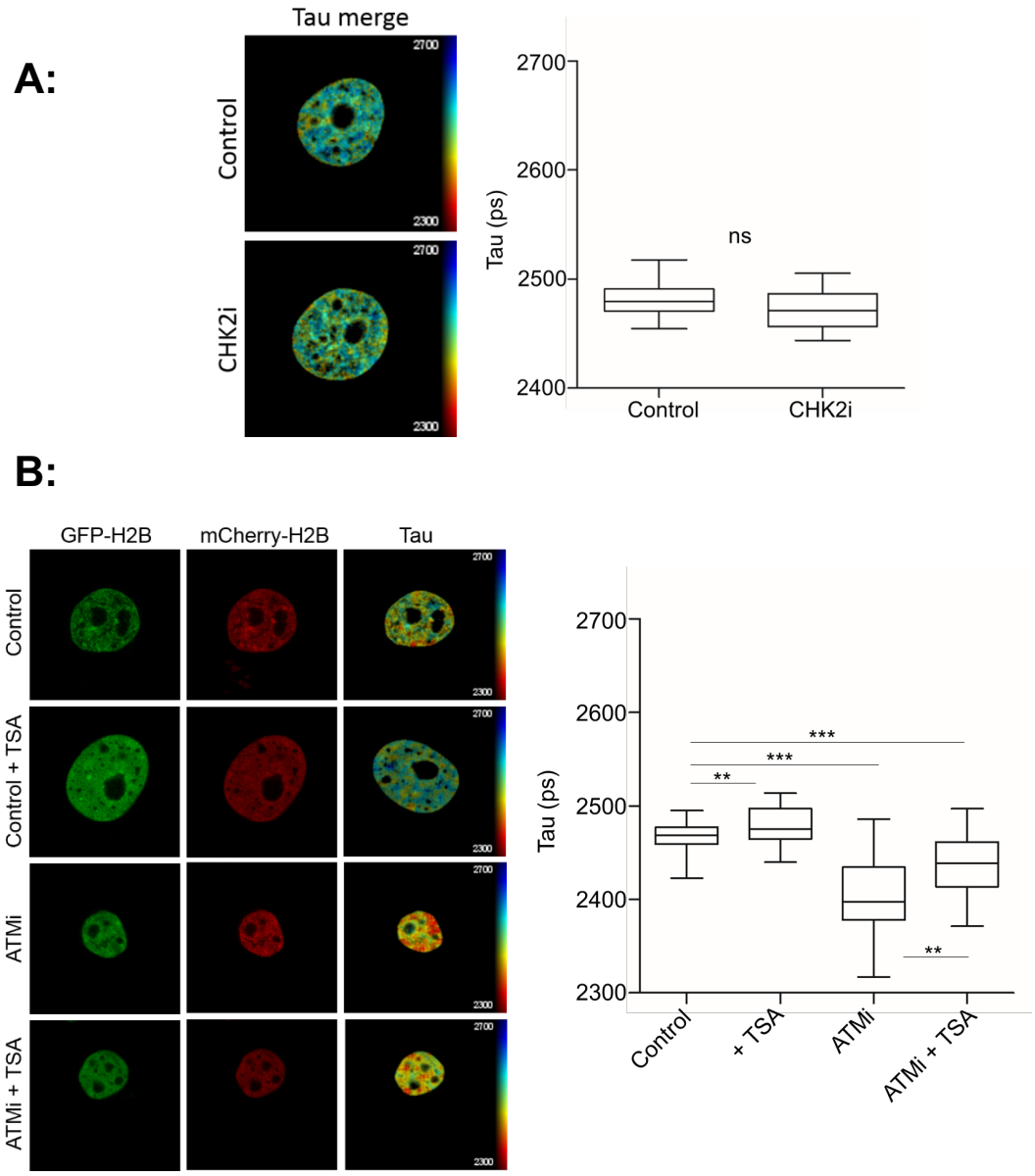

Figure 3-9. In absence of DNA damage, ATM activity involves histone acetylation and does not signal through CHK2

***A left**, shows a merged fluorescence lifetime and intensity map of FACS sorted 3T3-H2B^{2FP} cells (population 6) treated overnight with CHK2 inhibitor (CHK2i) and fixed. Colour scaled bar shows fluorescence lifetime. **A right**, shows quantification of fluorescence lifetime (Tau) of the cells in A left. N>16 in two biological repeats. ns indicates p>0.05, Student's t-test. **B left**, shows FACS sorted 3T3-H2B^{2FP} cells (population 6) which were treated with DMSO (control), Trichostatin A (TSA), ATM inhibitor (ATMi) or both, prior to being fixed. GFP and mCherry channels are indicated. The final panel shows a merge of the fluorescence lifetime and GFP intensity maps (Tau merged). Scale bar shows fluorescent lifetime. **B right**, shows a box plot of fluorescence lifetime values (Tau) of the cells shown in B left. N=25, three biological repeats. *s indicate significance from one-way ANOVA, where **=p<0.005, ***=p<0.0005.*

3.2.2 Electron microscopy

Given that the FLIM approach described above is somewhat novel, it was important to develop another way of measuring chromatin compaction which validated these findings. To directly visualise internal cellular structures, such as heterochromatin, without labelling, electron microscopy (EM) must be used. Methods were thus optimised to establish a robust quantitative imaging platform to measure heterochromatin by EM. First, the method of cell preservation was tested. Cells were either fixed in a combination of paraformaldehyde and glutaraldehyde, or high pressure frozen. Samples were embedded and cut into 70nm sections, before being stained with uranyl acetate and lead citrate to enhance contrast. Figure 3-10A shows that high pressure freezing cells clearly results in better preservation and distinction of heterochromatin. This appears as a dark staining within the nuclei, due to the staining of histone proteins by uranyl acetate. Therefore, high pressure freezing was chosen as the preservation method for future experiments. To quantitatively measure condensed chromatin, an analysis platform was developed. This involved manually segmenting the nuclei and nucleolus, then using a FIJI machine learning plugin (Trainable Weka Segmentation) to define four classes: heterochromatin, euchromatin, nucleolus and background. Finally, a macro was used to quantify properties of the region classed as heterochromatin (Figure 3-10B). This provided a number of measurements including the total nuclear area, the proportion of the nucleus occupied by heterochromatin and its spatial distribution.

Once this assay was developed, it was used to confirm the FLIM results which identified chromatin compaction upon ATM inhibition. NIH-3T3 cells were treated overnight with ATMi or DMSO. Cells were then high pressure frozen and prepared for EM (section 2.20). Images were taken on a transmission electron microscope (TEM) and quantified as described above. Figure 3-10C shows that at the single cell and population level, inhibition of ATM increases chromatin compaction. To confirm that the expression of GFP-H2B and mCherry-H2B does not affect chromatin dynamics in response to ATMi, the $H2B^{2FP}$ FLIM cells line was also treated overnight with ATMi or DMSO and prepared for EM. As previously shown, ATM inhibition increased chromatin compaction (Figure 3-10C). Therefore, expression of fluorescent histones in this system does not affect the ability of chromatin to remodel in response to ATMi, or chromatin condensation in basal conditions. This presents a robust way to confirm FLIM findings and visualise and quantify chromatin condensation in its native state.

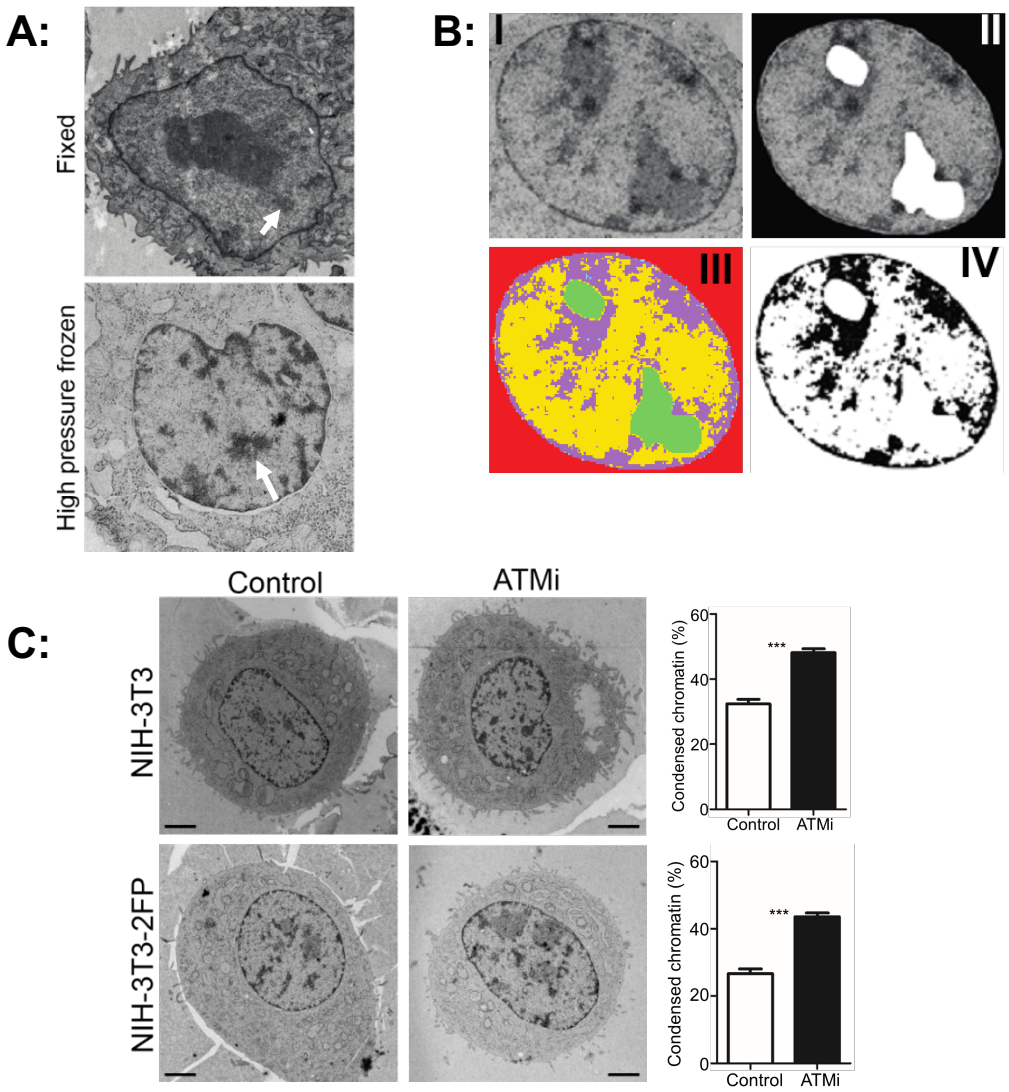

Figure 3-10. Quantitative electron microscopy confirms FLIM results

The images in this figure were taken with a transmission electron microscope (TEM). In all cases, after preservation, cells were embedded in EPON, using standard protocols (section 2.20), and cut into 70nm sections. These sections were then stained with uranyl acetate and lead citrate to visualise heterochromatin (white arrows). ***A****, shows TEM images of NIH-3T3 cells which were fixed or high pressure frozen, as indicated.* ***B****, shows example images illustrating the pipeline used for the quantification of condensed chromatin in electron microscopy images. Based on raw images (I) nuclei and nucleoli were manually segmented (II). The image was then classified using wekka trainable software into four classes; background, heterochromatin, euchromatin and the nucleolus (III). The regions classed as heterochromatin are then used to produce a binary image (IV), allowing for an assessment of its distribution using a custom ImageJ/Fiji macro (made by Dr Stephen Cross).* ***C left****, shows images of NIH-3T3, or NIH-3T3^{2FP} cells which were treated overnight with DMSO (control) of ATM inhibitor (ATMi). Cells were high pressure frozen 18 hrs after treatment and prepared for EM as described.* ***C right****, shows the quantification of condensed chromatin of the cells in C left, using the method shown in B. Graphs are pooled from two biological repeats, using 15 (NIH-3T3) or 20 (NIH-3T3^{2FP}) cells. *s indicates p<0.0001, Student's t-test. Image quantification used a Fiji plugin, made by Dr Stephen Cross.*

3.2.3 Atomic force microscopy (AFM)

As a final technique to investigate nuclear and chromatin structure, atomic force microscopy (AFM) was used. This uses a sharp tip to scan over the sample and detect surface features, and has advantages over the other techniques discussed, due to its non-invasive ability to study nuclear structure and mechanics, in fixed or live cells, at high resolution. Given that previous reports have suggested a correlation between chromatin compaction and increased nuclear stiffness, it was reasoned that AFM may be able to detect changes in stiffness, that correlate with chromatin compaction. To test this, cells were treated with TSA or 2-DG/NaN_3 to induce chromatin compaction or de-compaction, respectively. Cells were then fixed and dehydrated to collapse the cell membrane over the nucleus. This enables nuclear measurements to be taken with minimal effect from the cytoplasm, as previously reported (Francis et al., 2010). Bright field imaging was used to localise the probe over the nucleus (Figure 3-11A), which was then scanned over a 2.5µm region. A defined force was applied to the sample, using a calibrated tip to accurately determine stiffness (defined as Young's Modulus, YM). Figure 3-11B shows that treatment with TSA, which de-condenses chromatin, decreases nuclear stiffness. Likewise, treatment with 2-DG/NaN_3, which increases chromatin compaction, increases nuclear stiffness. Therefore, this suggests that this method can be used to detect changes in chromatin compaction in intact cells.

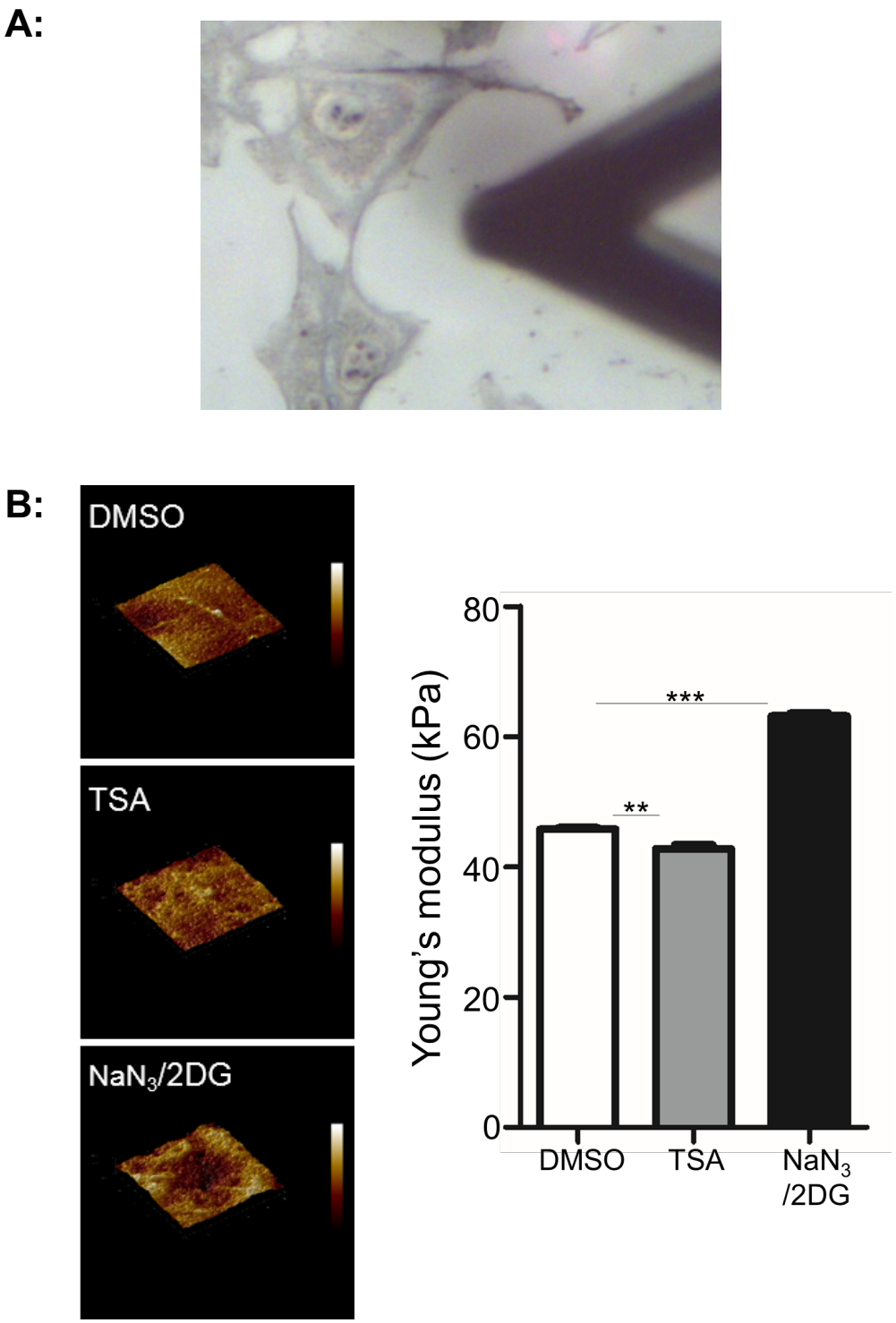

Figure 3-11. Nuclear stiffness correlates with chromatin compaction

***A**, shows a bright field image of a cell which was used during an AFM experiment. The probe is visualised to the right of this cell and is placed over the nucleus during the imaging. **B left**, shows 3D AFM images, scale bar shows height, where the maximum (white) is 300nm. Cells were treated, as indicated, fixed and then dehydrated through an ethanol series and dried to critical point. The AFM probed scanned a 2.5µm region over the nucleus of cells. **B right**, shows a graph of the pooled stiffness values (Young's Modulus, kPa). N=3, one biological repeat. *** indicates p<0.0005, ** indicates p<0.005, one-way ANOVA. AFM imaging was in collaboration with Dr Robert Harniman.*

Using this method, nuclear stiffness measurements were next taken on WT and ATMko cells. Results showed that ATMko cells had significantly increased nuclear stiffness, compared to WT (Figure 3-12A). As stated above, increased nuclear stiffness has been correlated with increased chromatin compaction, in previous reports (Mazumder et al., 2008; Stephens et al., 2018) and also in figure 3-11. Therefore, this approach corroborated the findings within this chapter, confirming an increase in chromatin compaction in ATMko cells, in absence of clear DNA damage.

Finally, given that this technique detects surface features, cytoplasmic variation between samples may preclude the detection of nuclear specific changes in stiffness, when taking measurements on intact cells. In such cases, measurements would be taken on isolated nuclei. To this end, nuclei were isolated and imaged by light microscopy, as well as scanning electron microscopy (SEM), to visualise the efficiency of the nuclear isolation (Figure 3-12B). Upon the development of a robust nuclear isolation protocol (section 2.21.2.2), experiments were conducted to optimise AFM measurements in these conditions (section 2.21.3.2).

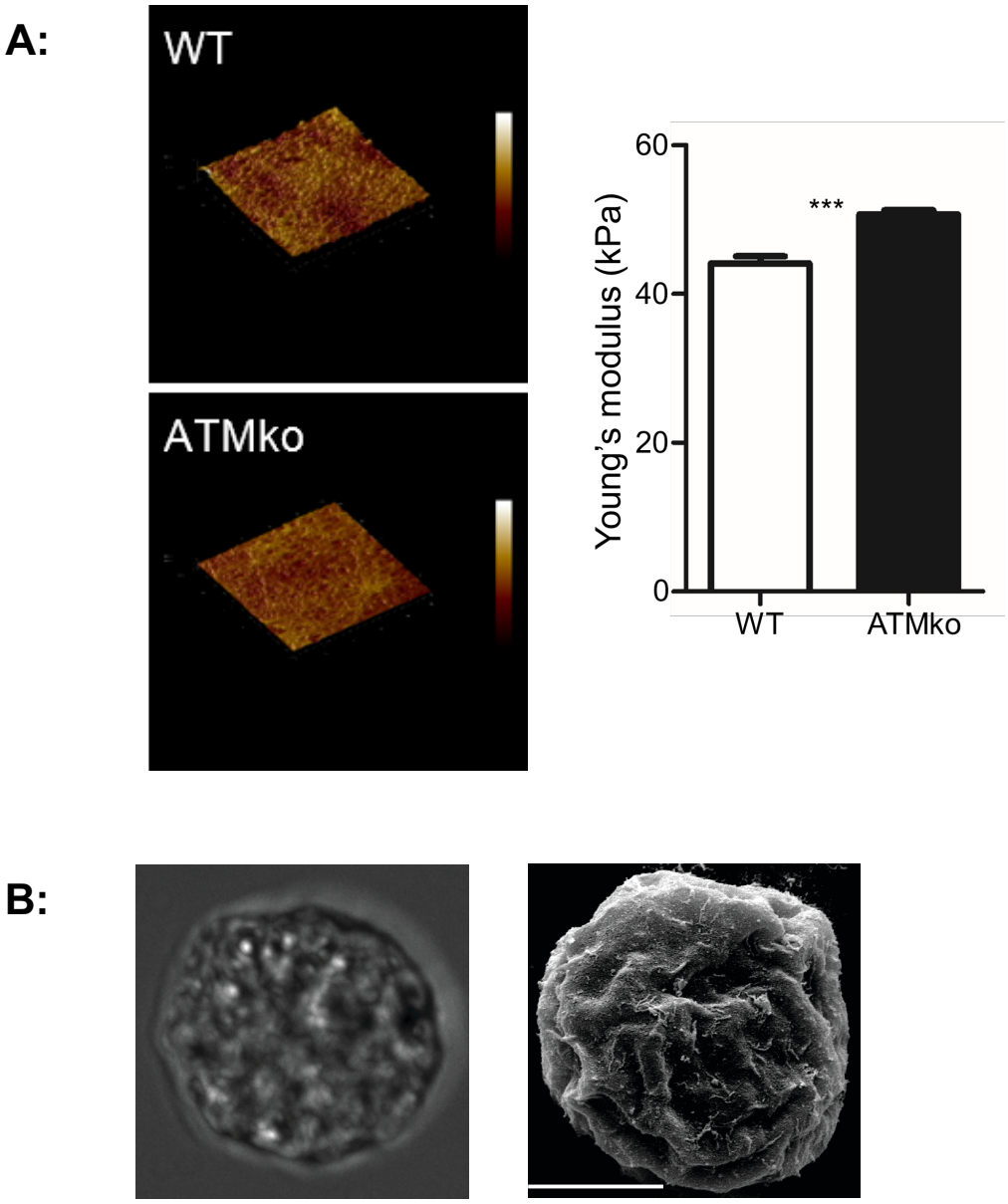

Figure 3-12. ATMko cells have increased nuclear stiffness

A right *shows a graph of the pooled stiffness values (Young's Modulus, kPa). N=6, two biological repeats. *** indicates p=0.0001, Student's t-test. AFM imaging was in collaboration with Dr Robert Harniman. Cells were provided by Melanie Panagi.* ***A left****, shows 3D AFM imagees taken over a 2.5μm region over the nucleus of RPE1 wild type (WT) or ATM knockout (ATMko) cells. Scale bar shows height, where the maximum (white) is 300nm.* ***B****, shows images of isolated nuclei. Left, is a nucleus imaged by bright field (DIC), right is a nucleus imaged by scanning electron microscopy (SEM), scale bar is 10μm.*

3.3 Discussion

The results in this chapter present a streamlined chromatin FLIM method for visualising chromatin compaction states in live and fixed mammalian cells. This approach produced similar results to previous work (Lleres et al., 2017b; Lleres et al., 2009), and extends this through the combination with immunofluorescence. Additionally, this method is amenable to automation for the purpose of screening, which may be useful to identify agents that influence chromatin structure, with potential to reveal the mechanisms underlying genome organisation. This is particularly relevant given that FLIMfit software (Warren et al., 2013) is part of the Open Microscopy Environment (OME) which integrates large data sets from phenotypic screens.

Furthermore, the previous work reported FLIM measurements as FRET efficiency, and used thresholding to present these data as FRET efficiency maps, which were segmented into 'high FRET', 'medium FRET' and 'low FRET' populations (Lleres et al., 2009). In this work, confocal scanning and pixel-based fitting was used to obtain pixel resolution fluorescence lifetime maps. This allowed visualisation of the diverse range of chromatin structures within the nucleus, beyond the simplistic view of heterochromatin and euchromatin. These FLIM data were also converted into FRET efficiencys (Padilla-Parra et al., 2015; Zeug et al., 2012), and gave results consistent with known observations, where nuclear regions of lower GFP-H2B fluorescence lifetime were associated with higher FRET efficiency. In addition, through combination with immunofluorescence, this method detected chromatin compaction within H3K9me3-rich chromatin. This could in turn be adapted to provide insights into the association of condensed/de-condensed chromatin with sub-nuclear domains, or chromosome territories, thus increasing our understanding of genome compartmentalisation.

A robust chromatin FLIM assay was thus developed in this chapter. However, the observed shifts in fluorescence lifetime are small, potentially obscuring the detection of subtle changes in chromatin structure. This is not necessarily the case, as fluorophores have a relatively narrow window of fluorescence lifetimes, and the results obtained are comparable to those seen previously. Nevertheless, increasing the magnitude of difference between the conditions would be of benefit. A potential dilution of FRET signal could arise from a sample existing in

two populations, where the donor is either interacting or not interacting with the accepter. Fitting the data using a double exponential fit allows distinct quantification of fluorescence lifetime in both populations, as well as the proportion of the FRETing vs non-FRETing component. This may be a useful approach to dissect smaller changes. Likewise, post-fitting segmentation, assigning a colour to a range of lifetime values, could be an informative way of spatially visualising compaction and potentially identifying regional 'hot spots'.

A disadvantage of this FLIM-FRET approach is that it requires genetic tagging with large fluorescent proteins. This size (4.2nm long with 2.4nm barrel) occupies much of the useful FRET distance, resulting in a maximum FRET efficiency of 40% and a potential cause of false negative results (Kremers et al., 2011). Therefore, the method could be improved by using modified fluorescent proteins such as mTurquoise (donor) and mCitrine (accepter), which have higher FRET efficiency (Bajar et al., 2016). Alternatively, because the problems associated with FRET are most prevalent with fluorescent proteins and FLIM relies only on the donor fluorophore, the use of a non-fluorescent accepter molecule (Murakoshi and Shibata, 2017) may improve some of these issues and allow more of the spectrum to be used for additional probes or co-staining. In addition, antibody FLIM has been previously reported and could be a useful method to perform FLIM in fixed cells, for example using secondary antibodies tagged with Quantum dots, which are small, have a high quantum yield and low susceptibility to photobleaching (Resch-Genger et al., 2008). Although antibodies are smaller than fluorescent proteins, they often have a high degree of non-specific binding. Therefore, more specific labelling techniques, such as click-chemistry, may replace such approaches in the future (Chen and Ting, 2005).

In addition to the development of this method, this chapter also showed global chromatin de-condensation after DNA damage, as well as partial ATM dependency in this process, confirming previous studies (Khanna et al., 2001; Ziv et al., 2006). Of particular interest, FLIM, quantitative EM and AFM showed that ATM inhibition or depletion results in genome-wide chromatin compaction, in absence of clear DNA damage, suggesting a role for ATM in chromatin surveillance. Although ATM-dependent chromatin relaxation has been shown to occur during DNA damage and apoptosis (Schou et al., 2008; Ziv et al., 2006), this is the first evidence of this dependency during resting conditions. These results may thus explain previous studies, such as the reported ATM-dependent

transcriptional inhibition (Shanbhag et al., 2010), which may somewhat be mediated through the regulation of chromatin compaction by ATM. However, it cannot be excluded that the cells were experiencing low level DNA damage and are therefore not truly 'resting'; indeed, the absence of γH2AX foci was likely due to the inhibition of ATM, which phosphorylates this residue, and therefore does not necessarily indicate absence of DNA damage in this context. Therefore, induction of DNA damage could be assessed by directly measuring DNA double strand breaks, using click chemistry, and cannot be confirmed by measuring the phosphorylation of ATM targets. Linked to this, it is possible that the expression of fluorescent histones in the FLIM cell lines lead to low level DNA damage. However, this is unlikely, as parental NIH-3T3 cells behaved similarly to the FLIM cell lines, in response to ATM inhibition, as measured by EM.

Given that phosphorylation of KAP1 by ATM has been linked to chromatin de-condensation after DNA damage (Ziv et al., 2006), it would be of interest to see if ATM also uses this canonical signalling whilst regulating chromatin compaction under basal conditions. Evidence against this is presented in Figure 5-10A, which shows that CHK2 inhibition (also downstream of ATM) does not affect global chromatin condensation. However, the efficiency of this inhibitor was not confirmed, thus to understand these results, future work would require the comparison of phosphorylations of CHK2 targets before and after inhibition, the use of a different inhibitor, or another target downstream of ATM. Future investigation to understand the role of ATM in chromatin surveillance may provide insights into genome regulation and diseases where ATM is mutated. Given that figure 5-10B showed that ATM-induced chromatin compaction was partially restored by addition of TSA, and ATM inhibited cells showed elevated H3K9me3, the role of ATM in chromatin de-condensation may mechanistically involve histone acetylation and de-methylation.

Furthermore, the AFM data showed that cells depleted of ATM have increased nuclear stiffness. Figure 3-12B potentially explains the increased nuclear stiffness, through correlating it with an increase in chromatin compaction, consistent with previous studies which link histone modifications and chromatin de-condensation to decreased nuclear stiffness (Mazumder et al., 2008; Stephens et al., 2018). However, it cannot be excluded that this change in mechanical property is due another factor, such as alterations in lamin proteins. Indeed, studies have shown that both chromatin compaction and lamin A/C

contribute to nuclear rigidity (Stephens et al., 2017). To uncouple the effects of lamin A/C and chromatin compaction in nuclear rigidity, AFM experiments could be repeated in lamin ko cells, and the structure and organisation of the nuclear lamina could be compared between wild type and ATM ko cells, using light microscopy. Alternatively, the increased nuclear stiffness may be related to cytoplasmic functions of ATM which are rapidly being uncovered (Perry and Kleckner, 2003; Shiloh and Ziv, 2013; Yang et al., 2011). Indeed, given that ATM is suggested to be mechanoresponsive (Kumar et al., 2014), it is possible that ATM may regulate the cytoskeleton, which could in turn affect nuclear rigidity, for example by regulating the tension of the actin cap which sits over the nucleus (Khatau et al., 2009). Cytoplasmic vs nuclear function of ATM in nuclear rigidity could thus be investigated through the expression of ATM constructs that are targeted to or excluded from the nucleus.

Chapter 4 : Nuclear F-actin promotes nuclear re-organisation after cell division

4.1 Introduction

The previous chapter developed and instrumented several imaging techniques to study nuclear and chromatin structure. This chapter uses these methods to gain insight into the role of nuclear F-actin in nuclear re-organisation after cell division.

Cell division is a fundamental process which maintains tissue homeostasis and when misregulated, drives pathologies such as cancer. Research into this field is therefore an important aspect of cell biology. Although the mechanisms of chromosome formation and segregation have been well defined (Du Toit, 2014; Gibcus et al., 2018), our understanding of chromatin de-condensation remains limited and warrants further research (reviewed in section 1.4). Indeed, an accessible chromatin structure is required for DNA repair, gene transcription and DNA replication and therefore, understanding how chromatin de-condenses after cell division is important for all nuclear processes (Antonin and Neumann, 2016; Lima-de-Faria and Jaworska, 1968; Ziv et al., 2006). In addition, studying the re-organisation of chromatin after cell division gives great insight into the 3D structure of chromatin and therefore gene regulation. Indeed, chromatin is at its most mobile in the first 2 hrs after cell division, when TADs are re-established (Thomson et al., 2004), thus nuclear positioning and high order chromatin structure may be linked to the process of chromatin de-condensation.

Chromatin de-condensation is also temporally related to the reformation of the nuclear envelope and an increase in nuclear volume (Philpott et al., 1991; Wright, 1999). Whether chromatin compaction effects the size of the nucleus is yet to be determined. However, given the correlation between nuclear expansion and chromatin de-compaction after mitosis, these processes may be linked. Likewise, the expansion of the nucleus may impact the organisation of chromatin, by providing spatial boundarys in which chromatin can be organised. Therefore, the expansion of the nucleus and chromatin de-condensation may impact each other in a two-way relationship. Importantly, nuclear volume changes will affect the concentration of nuclear proteins, thereby effecting the kinetics of nuclear reactions and the formation of nuclear bodies (Hancock, 2004; Mao et al., 2011). Therefore, research into mechanisms which govern chromatin de-condensation and nuclear expansion may shed light on the mechanisms which produce and maintain chromatin structure.

Observations from Robert Grosse's laboratory identified the transient formation of nuclear actin filaments that emerge after cell division. These filaments were visualised using several actin binding probes (Baarlink et al., 2017), including a nuclear actin chromobody (nAC). This consists of the variable heavy (V_HH) domain of an actin specific antibody, fused to an NLS and GFP (Figure4-1A) (Plessner et al., 2015), and therefore can be used to visualise both G- and F-actin. This construct was used to produce stable cell lines, thus permitting live cell nuclear actin imaging. These experiments revealed the formation of nuclear F-actin upon the completion of cytokinesis, which dynamically rearranges for a period of ~60-90 minutes during early G1, before rapidly disassembling (Figure 4-1B)

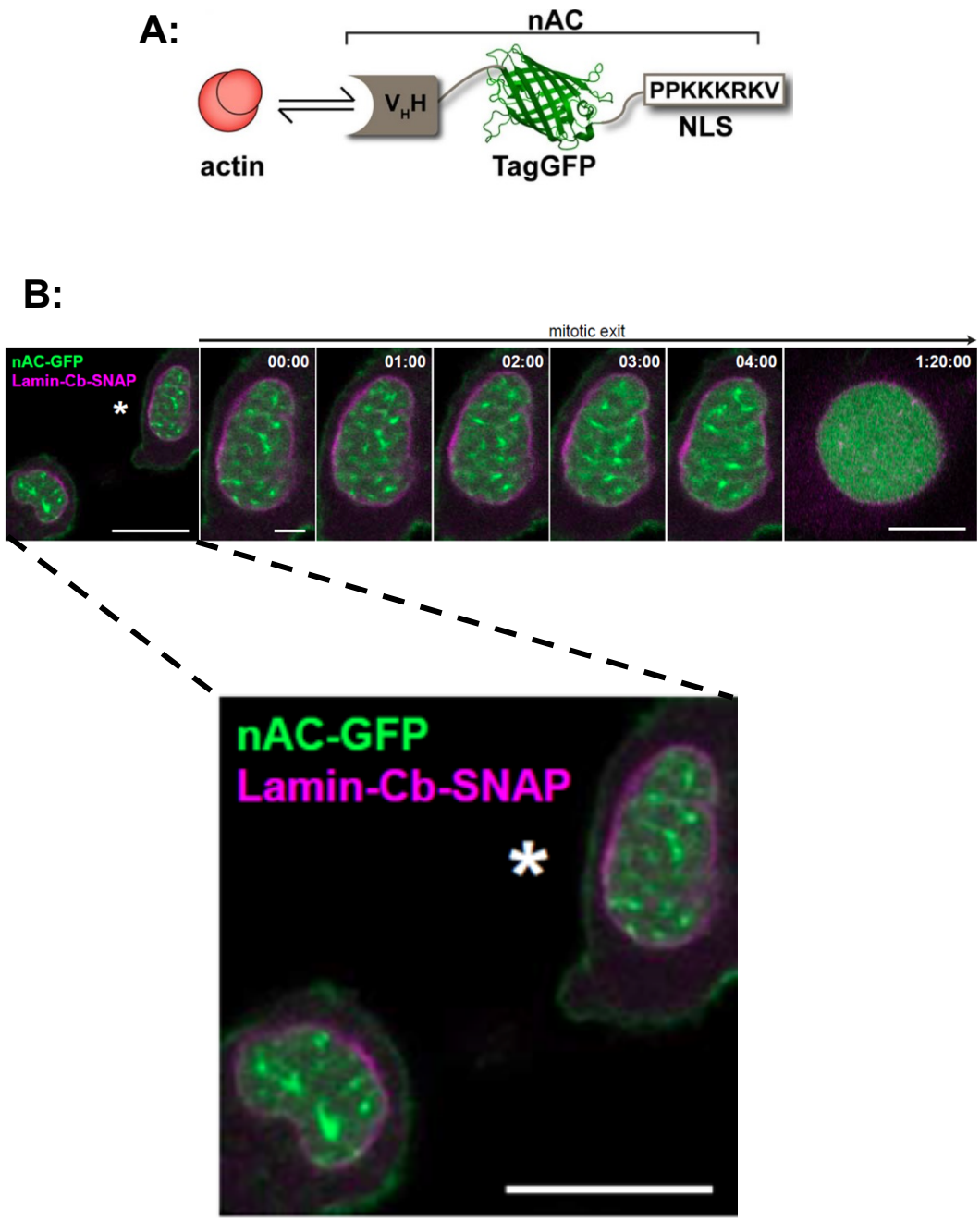

Figure 4-1 Nuclear F-actin arises after mitosis.

***A**, shows a schematic representation of the nuclear actin chromobody (nAC) protein; composed of the variable heavy domain (V_HH) of an actin specific antibody, tagged to a nuclear localisation sequence (NLS) and GFP (Plessner et al., 2015). **B**, shows still images from a live cell imaging video at the indicated time points, shown in minutes. Actin is visualised in green using GFP-nAC, and the nuclear lamina is visualized in purple using Lamin-Cb-SNAP. Below, shows a zoomed in image of the cells indicated by the dashed line. This figure was produced in Robert Grosse's laboratory, Marburg, Germany (Baarlink et al., 2017).*

The appearance of these filaments coincides with formation of new domains at the nuclear periphery, nuclear expansion, as well as global and epigenetic changes to chromatin structure. It is thus conceivable that nuclear F-actin is involved in these processes. Indeed, several instances of nuclear F-actin have now been identified (Baarlink et al., 2013; Belin et al., 2015b; Miyamoto et al., 2011; Plessner et al., 2015), some of which uncover a role for nuclear F-actin in chromosome mobility (Chuang et al., 2006; Spichal et al., 2016a). The results in this chapter addresses these possibilities with three main aims.

Chapter aims:

1. Understand the role of nuclear F-actin in post-mitotic chromatin de-condensation.
2. Determine whether nuclear F-actin affects chromatin remodelling after cell division.
3. Understand the role of nuclear F-actin in post-mitotic nuclear expansion.

4.2 Results

To investigate the function of nuclear F-actin after cell division, several genetic systems, which specifically manipulate nuclear F-actin, were developed in Robert Grosse's laboratory, and used throughout this thesis (Baarlink et al., 2017). Briefly, this work used NIH-3T3 cells which contain doxycycline regulated plasmids expressing NLS and flag- tagged wild type (WT) or mutant (R62D) actin, hereafter referred to as NLS-actin^{WT} and NLS-actin^{R62D} cells. Upon addition of doxycycline, these constructs are expressed, and through the NLS, traffic into the nucleus. The R62D mutation produces a form of actin monomer which is unable to polymerise, thus its overexpression dilutes the pool of incorporable actin in the nucleus and largely inhibits actin filament formation. For some experiments, an additional system was used, relying on actin depletion through overexpression of the actin export protein exportin 6. This was used in transient experiments due to constitutive lethality.

4.2.1 Nuclear F-actin promotes post-mitotic chromatin de-condensation

Given the appearance of nuclear actin filaments during a period where chromatin is de-condensing, experiments were conducted to determine the role of nuclear F-actin in post-mitotic chromatin de-compaction.

4.2.1.1 MNase assay

Micrococcal nuclease (MNase, derived from Staphylococcus aureus) digestion was used to assess chromatin accessibility biochemically. This assay utilises the ability of micrococcal nuclease to cut linker DNA, where more compact chromatin is less accessible, and is consequently cut less efficiently. Optimisation experiments were conducted to determine a suitable incubation time with the enzyme. The 5 minute timepoint was chosen, due to high retrieval of mono-nucleosomes and the distinct digestion of larger nucleosome fragments (Figure 4-2A). Once determined, NLS-actin^{WT} and NLS-actin^{R62D} cells were synchronised in mitosis and harvested 45 minutes post-mitotic release, in order to examine chromatin accessibility early in the process of chromatin de-condensation. Collected pellets were used in the MNase assay and results were analysed on an agarose gel. Quantification of these gels showed that in NLS-actin^{R62D} cells, fewer mono-nucleosomes and increased di-, tri- and tetra- nucleosomes were retrieved from the assay (Figure 4-2B). This suggests higher DNA compaction when nuclear actin polymerisation is inhibited.

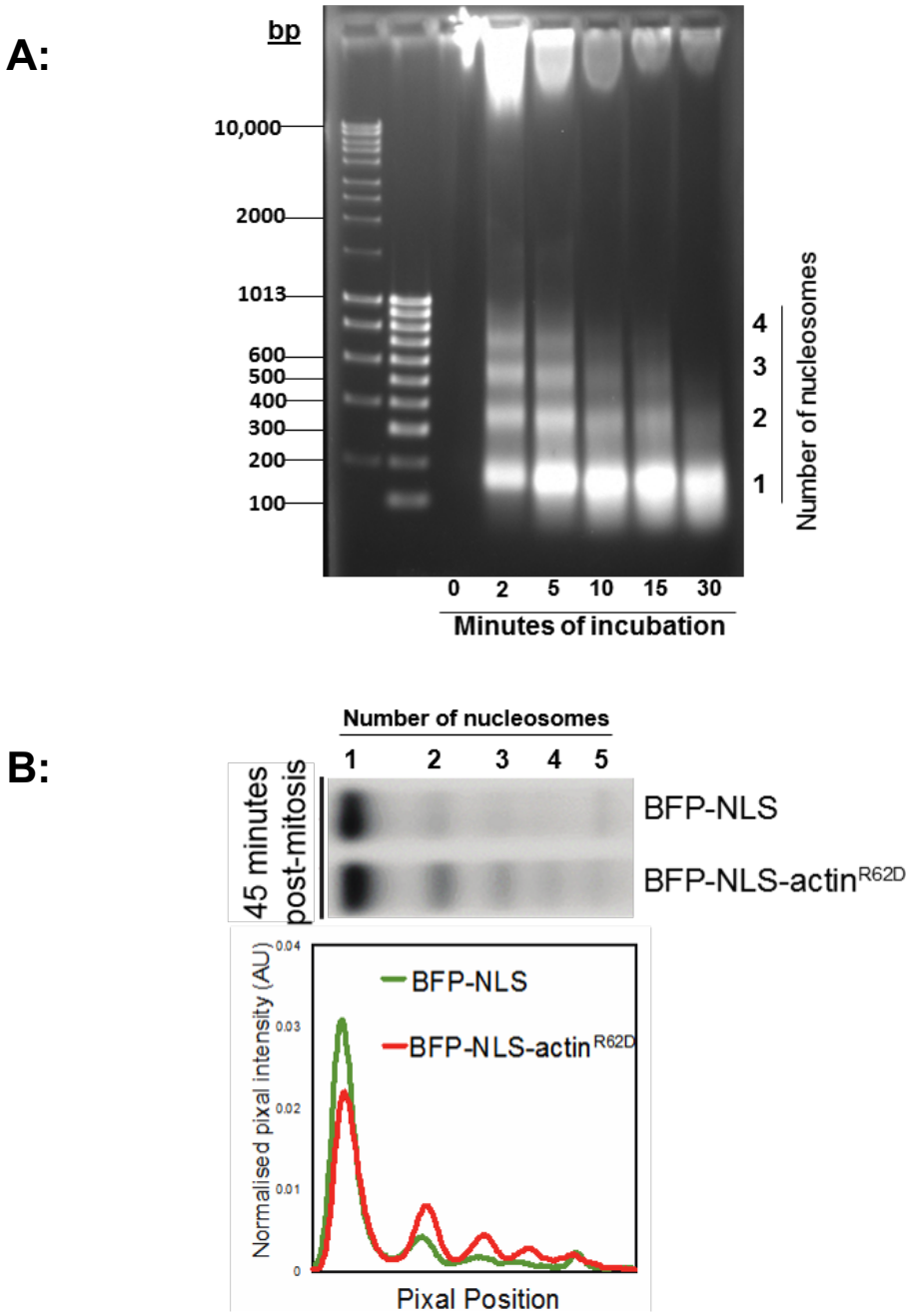

Figure 4-2 MNase assay shows decreased chromatin accessibility in actin mutant cells.

A, *is an agarose gel showing the results of an MNase optimisation experiment to determine the appropriate incubation time with the enzyme (micrococcal nuclease). 8x10^6 NIH-3T3 cells were used in the assay, and aliquoted into 6x100µl aliquots. 200 gel units of the enzyme were added to each aliquot, and the reaction was stopped at the time points shown. The 5-minute time point was chosen for future experiments. DNA lengths are shown as base pairs (bp).* ***B (top),*** *is a representative image of an agarose gel showing results of the MNase assay, comparing* NLS-actin^{WT}/NLS-actin^{R62D} *cells that were collected 45 minutes post-mitotic release. DNA lengths are shown as base pairs (bp). Experiment was performed in three independent repeats.* ***B (bottom),*** *shows the quantification of the relative band intensities of the gel shown in b top. Values were normalised to the total lane intensity, in arbitrary units (AU). Quantification used a MATLAB tool, made by Dr Stephen Cross.*

4.2.1.2 Electron microscopy

In light of these results, several approaches were used to measure chromatin compaction in intact cells. Firstly, electron microscopy (EM) was used to visualise and quantify the amount of condensed chromatin in cryo-preserved samples. Cells were synchronised in mitosis and high pressure frozen 1 hr post-mitotic release. This timepoint was chosen due to it coinciding with nuclear F-actin formation. To prepare for EM, cells were then embedded in resin and cut into 70nm sections. To aid visualisation of heterochromatin, sections were stained with uranyl acetate and lead citrate, resulting in enhanced contrast, and the detection of a heterochromatin associated dark stain in the nucleus. Figure 4-3A shows an example of an EM image of NLS-actin^{WT} and NLS-actin^{R62D} cells. Consistent with previous reports (Kalverda et al., 2008), condensed chromatin in the NLS-actin^{WT} nuclei is preferentially localised to the nuclear periphery, as well as regions surrounding the nucleolus. However, for the actin mutant nuclei, in addition to this localisation there was also substantial proportions of condensed chromatin found in the nucleoplasm (Figure 4-3A zoom). Condensed chromatin was quantified, as per chapter 3, revealing significantly more condensed chromatin in multiple NLS-actin^{R62D} nuclei (Figure 4-3B), confirming initial observations (Figure 4-2B). Interestingly, this increase is refined to nucleoplasmic heterochromatin, as the thickness and distribution heterochromatin surrounding the nuclear membrane was unaffected (Figure 4-3C). In addition, significantly increased condensed chromatin was also observed in cells over-expressing exportin 6 (Figure 4-3D) and the actin destabilising protein cofilin-1 (Figure 4-3E). Thus, when nuclear F-actin formation is inhibited by two independent mechanisms (Figure 4-3A-D), or their dynamic turnover is disrupted (Figure 4-3E), post-mitotic chromatin de-condensation is reduced.

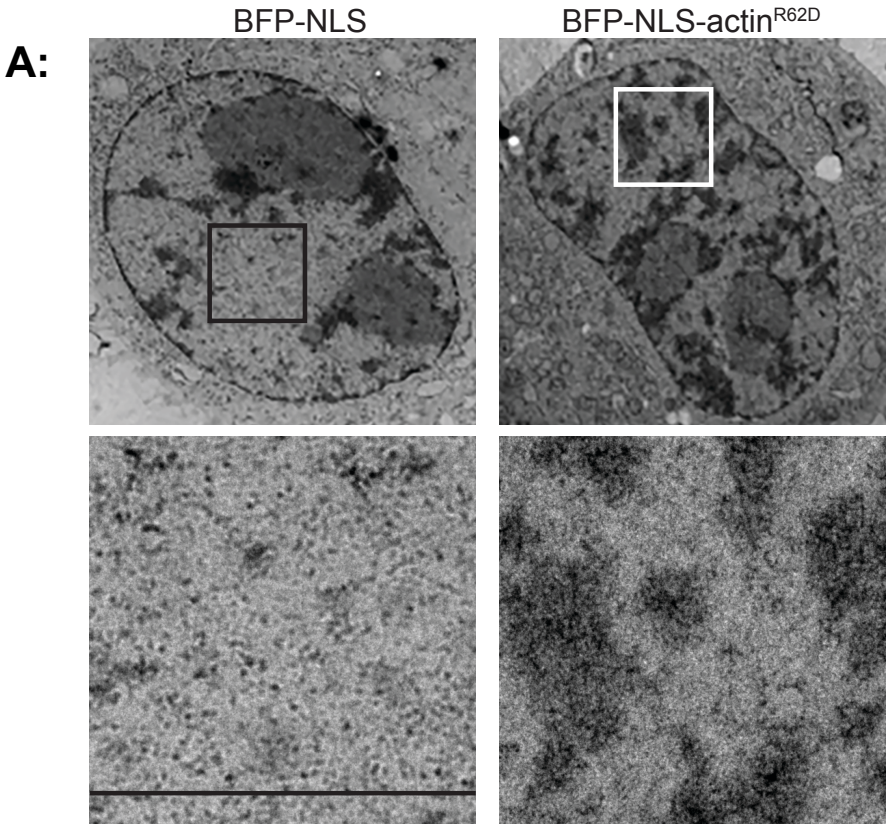
A:
BFP-NLS
BFP-NLS-actin^{R62D}

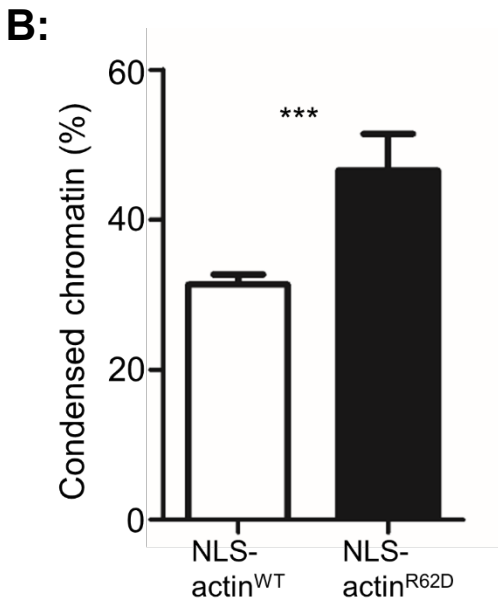
B:
Condensed chromatin (%)
60
40
20
0
***
NLS-actin^{WT}
NLS-actin^{R62D}

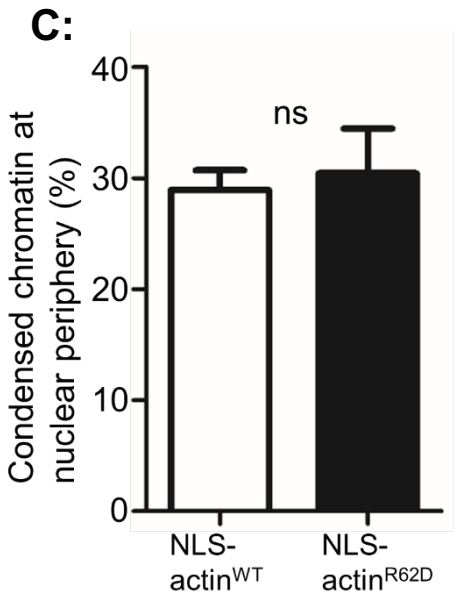
C:
Condensed chromatin at nuclear periphery (%)
40
30
20
10
0
ns
NLS-actin^{WT}
NLS-actin^{R62D}

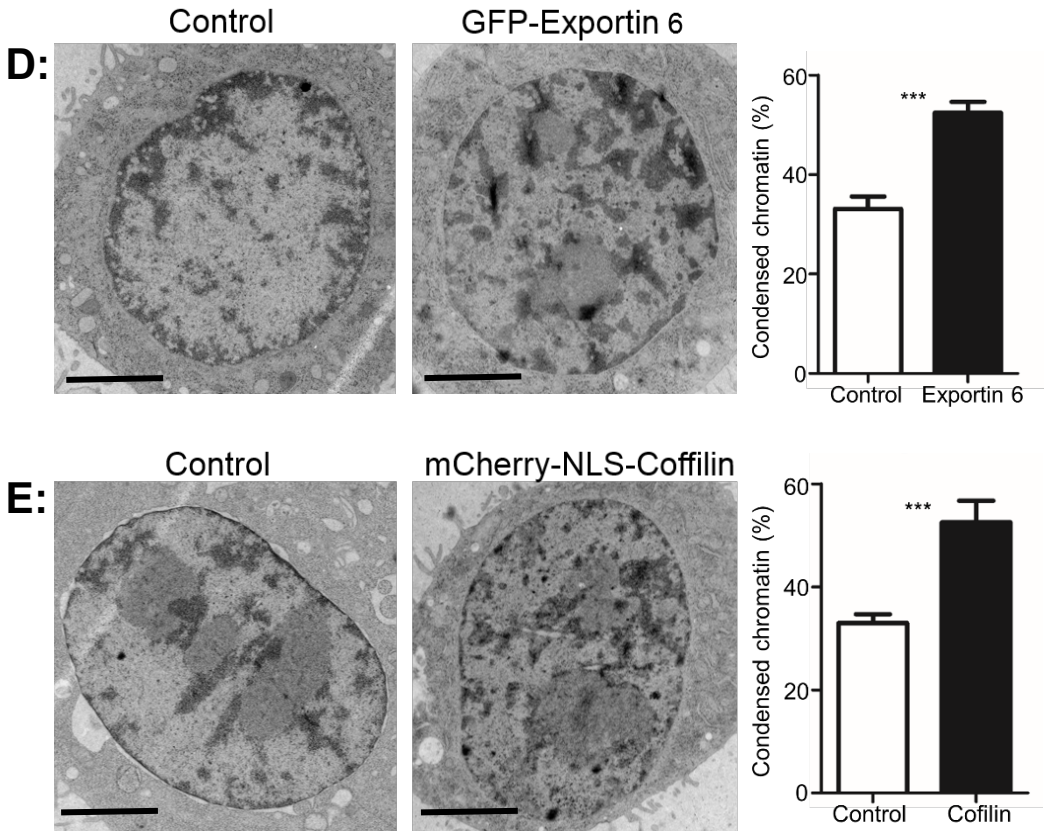

Figure 4-3 Electron microscopy shows an increase in condensed chromatin in post mitotic cells unable to polymerise or turnover nuclear actin.

The images within this figure were taken at 2900x using a transmission electron microscope (TEM), using samples of cells which were high pressure frozen 1 hr after mitotic shake off. Scale bars= 2µm. Error bars on graphs show SEM. ***A,*** *shows a representative image of NLS-actin^{WT}/NLS-actin^{R62D} cells. Top panel shows the whole nucleus, bottom panel is a higher magnification of the region highlighted, to show heterochromatin in the nucleoplasm.* ***B-C****, shows quantification of condensed chromatin as a percentage of the whole nucleus minus the nucleolus area (b) or within 5% of the nuclear edge (c). n>30 in two independent repeats. p=0.0002, Student's t-test.* ***D left****, shows a representative image of 3T3 cells which have been transfected with a control or GFP exportin 6 plasmid, right; shows quantification of the percentage of condensed chromatin, as a percentage of the nuclear area, excluding the nucleolus. N>16 in two independent repeats. p=0.0001, Student's t-test.* ***D****, right; shows a representative image of 3T3 cells which have been transfected with control or mCherry-NLS-Coffilin plasmid, right; shows quantification of the percentage of condensed chromatin within the cell types images, as a percentage of the nuclear area, excluding the nucleolus. N>16 in two independent repeats. p=0.0005, Student's t-test. Image quantification used a Fiji plugin, made by Dr Stephen Cross.*

4.2.1.3 Fluorescence lifetime imaging (FLIM)

Fluorescence lifetime imaging (FLIM) was next used to confirm these findings, by quantitatively measuring chromatin compaction, through the detection of fluorescence resonance energy transfer (FRET) (Ishikawa-Ankerhold et al., 2012). Chapter 3 discussed the development of a FLIM system, which detects FRET between two nucleosomes, where histone H2B is tagged with GFP and mCherry. It thus follows that chromatin condensation leads to increased FRET between histones, and therefore low fluorescence lifetime (Tau) values. Here, this technique was used to visually and quantitatively compare chromatin compaction in NLS-actin^{WT} and NLS-actin^{R62D} post-mitotic cells. As shown (Figure 4-4A-B), NLS-actin^{R62D} cells have lower Tau values compared to the NLS-actin^{WT} cells, thus higher FRET and reduced chromatin de-compaction after mitosis. Experiments were also conducted in the parental FLIM cell line (H2B^{2FP}), in the presence and absence of FLAG-exportin 6 expression, which was detected using an ANTI-Flag-405 co-stain. Figure 4-4C shows that the FLAG-exportin6 transfection and co-stain had no discernible effect on the GFP fluorescence lifetime in the absence of mCherry-H2B. However, when mCherry-H2B is also present, a decreased fluorescence lifetime in cells transfected with exportin6 was observed (Figure 4-4D-E). This again highlights the higher level of DNA compaction when nuclear F-actin formation is inhibited after mitosis. Therefore, through the use of biochemical and imaging techniques and using different methods of cell preservation, a novel role for nuclear F-actin in chromatin de-compaction after mitosis was identified.

A:

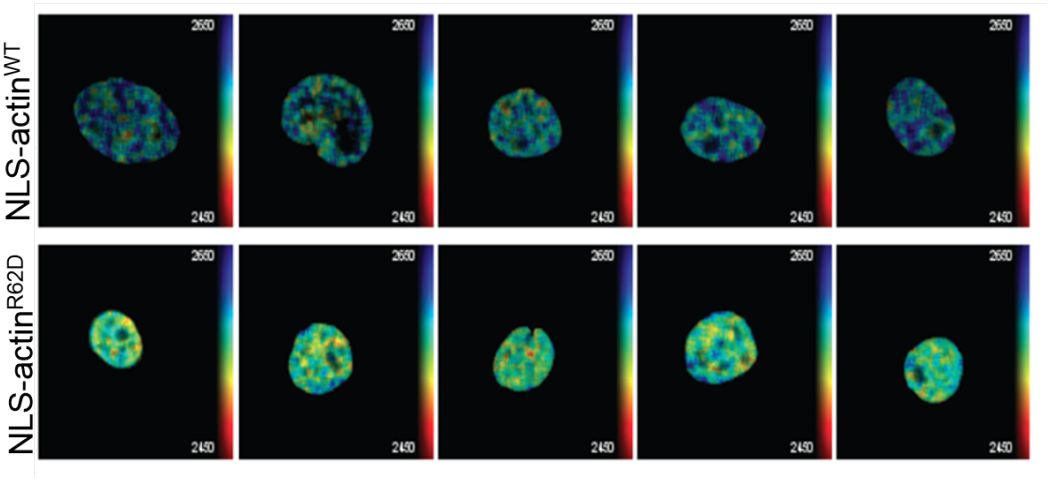
NLS-actin^{WT}
NLS-actin^{R62D}
2650
2450

B:

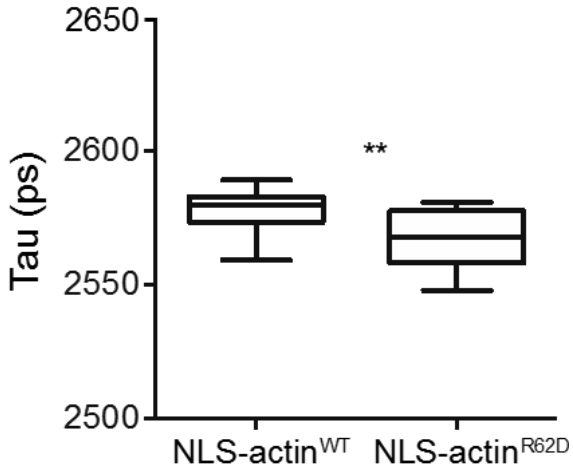
Tau (ps)
2650
2600
2550
2500
**
NLS-actin^{WT}
NLS-actin^{R62D}

C:

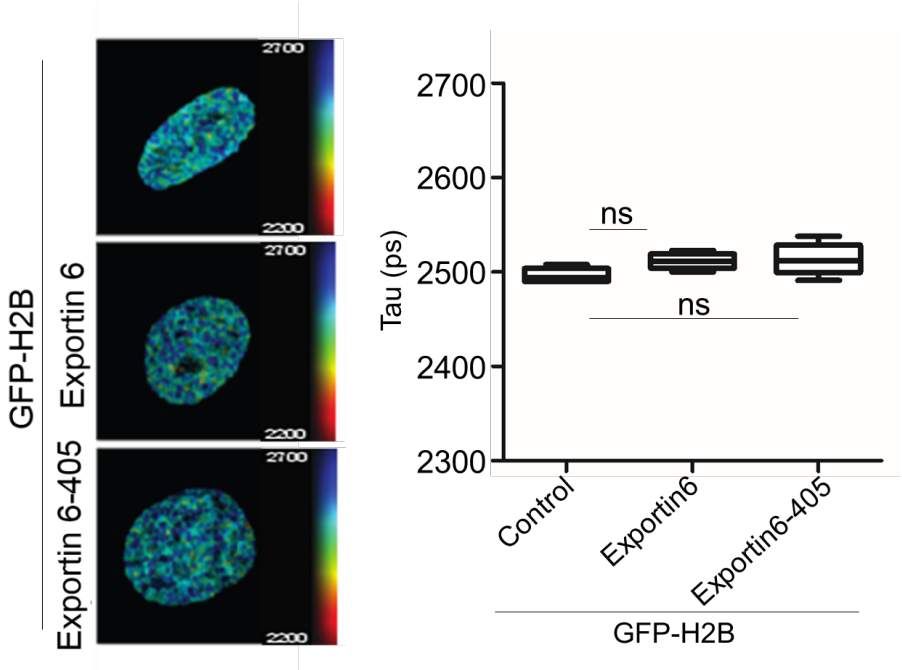
GFP-H2B
Exportin 6
Exportin 6-405
2700
2300
Tau (ps)
2700
2600
2500
2400
2300
ns
ns
Control
Exportin6
Exportin6-405
GFP-H2B

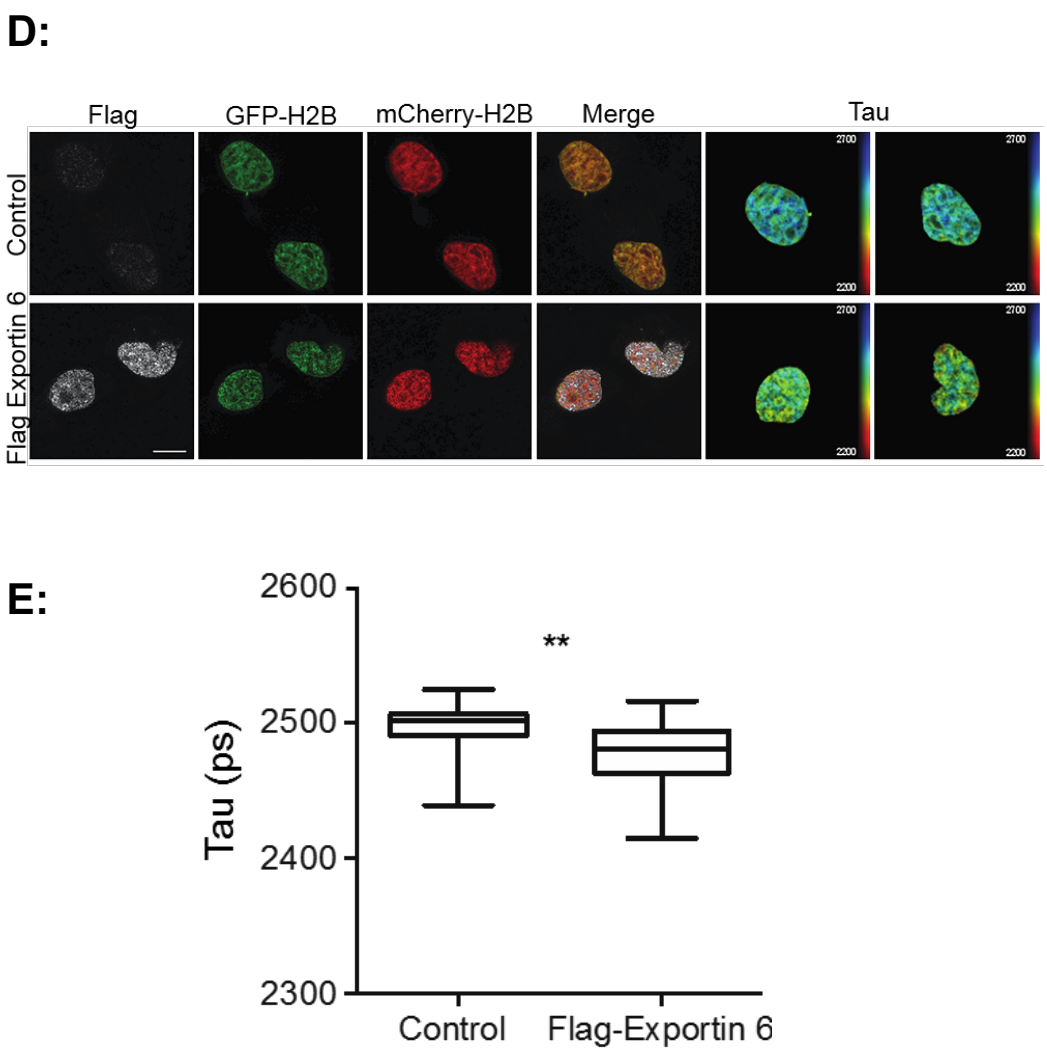

Figure 4-4 Fluorescence lifetime imaging (FLIM) shows reduced fluorescence lifetime in cells unable to polymerise nuclear actin after cell division.

This figure shows the results from several FLIM experiments. In all cases, cells were synchronized into mitosis and fixed in paraformaldehyde 1 hr post release. Post mitotic cells were selected by eye. Fluorescence lifetime maps are shown, where each pixel has a colour dictated by its fluorescence lifetime value, and its intensity determined by the GFP intensity. Colour coded scale bar represents GFP fluorescence lifetime. ***A,*** *shows a panel of a fluorescence lifetime maps, of post-mitotic NLS-actin^{WT}/NLS-actin^{R62D} cells expressing GFP and mCherry H2B.* ***B****, shows a box plot representing the range in GFP-H2B lifetime (Tau) from post-mitotic NLS-actin^{WT}/NLS-actin^{R62D} cells, as seen in a. n≥20 from two biological repeats. ** indicates p=0.0016, Student's t-test.* ***C left****, shows fluorescence lifetime maps of cells expressing GFP-H2B, with and without the expression of exportin 6 and a 405-secondary antibody. Right shows a box plot of the pooled fluorescent lifetime values, of these cells. N=5, one biological repeat, ns indicates p>0.05, Student's t-test.* ***D,*** *shows post-mitotic NIH-3T3 cells, expressing GFP and mCherry H2B, which were stained with ANTI-Flag-405 (channels are indicated). Control and exportin 6 transfected cells are indicated. The final panel shows fluorescence lifetime maps.* ***E,*** *shows a box plot of the pooled fluorescence lifetime values, of the cells shown in d. n≥30, from three biological repeats. ** indicates p=0.0021, Student's t-test.*

4.2.2 Nuclear F-actin promotes histone modifications that are associated with chromatin de-condensation

4.2.2.1 Histone modifications

In light of these results, and the contribution of epigenetic remodelling during chromatin de-condensation, a role for nuclear F-actin in chromatin de-condensation was next investigated. Given the requirement of H3S10 de-phosphorylation and H4K16 acetylation during chromatin de-compaction (Lau et al., 2016; Wilkins et al., 2014), these histone modifications were compared in NLS-actin^{WT} and NLS-actin^{R62D} cells. For Western blotting, NLS-actin^{WT} and NLS-actin^{R62D} cells were collected 45 and 120 minutes post-mitotic release, due to these timepoints coinciding with nuclear actin filament formation and disassembly (Baarlink et al., 2017). In NLS-actin^{WT} cells, a clear decrease in H3S10ph and an increase in H4K16ac, between these two-time points, was observed. However, in NLS-actin^{R62D} cells, there was very little decrease in H3S10ph, or increase in H4K16ac, between these two-time points (Figure 4-5A). This was also observed by immunofluorescence (Figure 4-5B-C), in cells fixed 1 hr after mitotic release.

Upon confirmation that both methods of analysis produce consistent results, immunofluorescence was used to compare the levels of other histone modifications in NLS-actin^{WT} and NLS-actin^{R62D} cells. The chosen modifications are generally associated with condensed (H3K27me3, H3K9me2, H3K9me3) or de-condensed (H4pan acetylation) chromatin, but do not necessarily bare relevance to the process of chromatin de-compaction. Results here were more subtle, thus image quantification was used to compare these data. Out of these modifications, the only significant change was H3K9me3 (Figure 4-5D), which was elevated in NLS-actin^{R62D} cells and was interestingly most pronounced at the nuclear periphery (Figure 4-5F).

A:

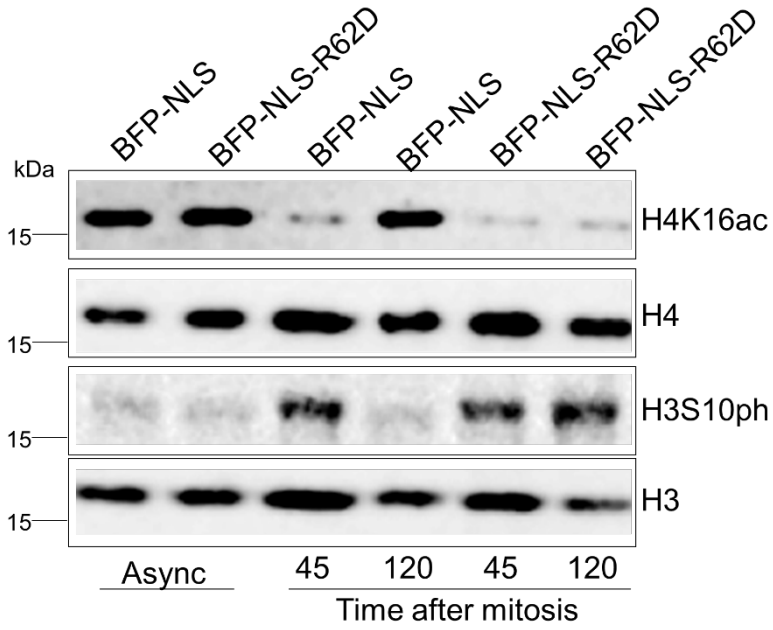
BFP-NLS
BFP-NLS-R62D
BFP-NLS
BFP-NLS
BFP-NLS-R62D
BFP-NLS-R62D
kDa
15
H4K16ac
15
H4
15
H3S10ph
15
H3
Async
45
120
45
120
Time after mitosis

B:

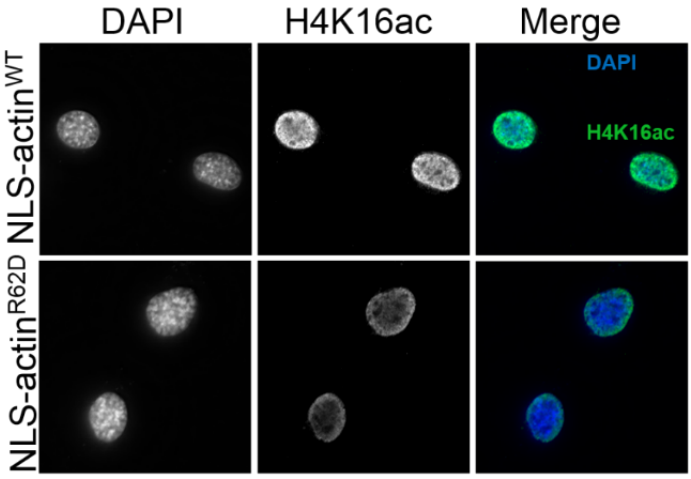
DAPI
H4K16ac
Merge
NLS-actinWT
NLS-actinR62D
DAPI
H4K16ac

C:

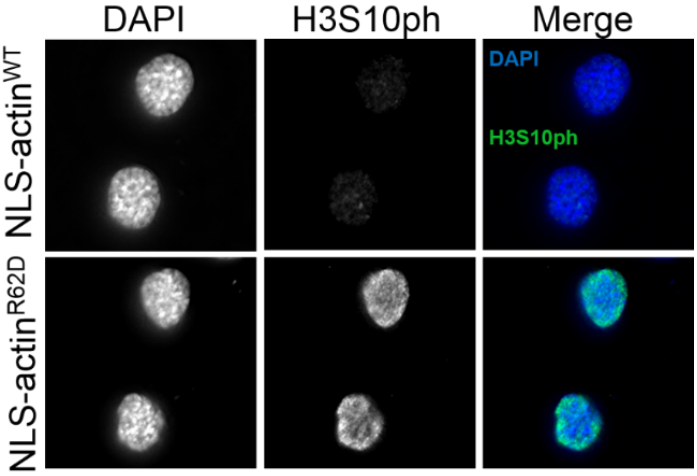
DAPI
H3S10ph
Merge
NLS-actinWT
NLS-actinR62D
DAPI
H3S10ph

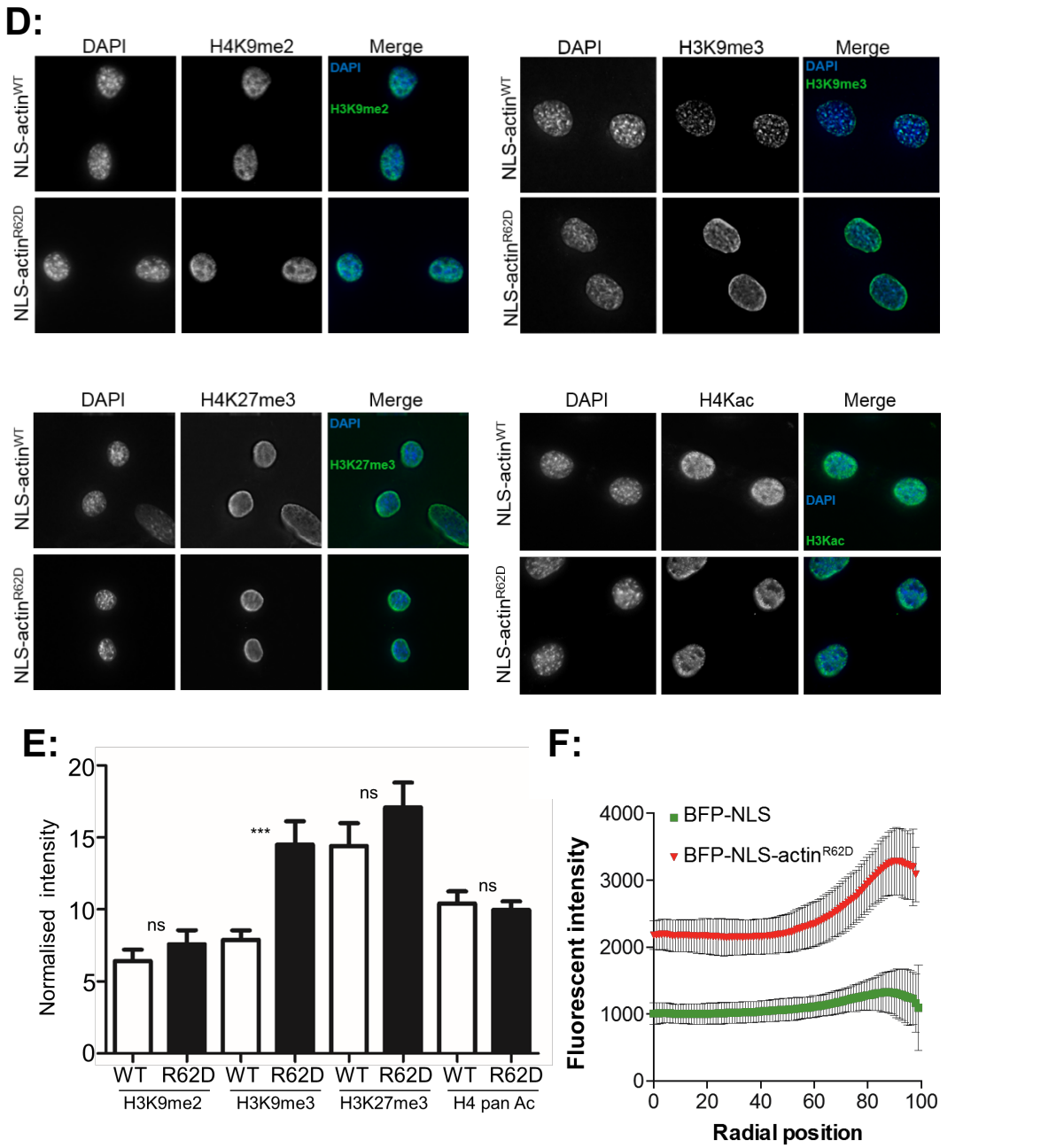

Figure 4-5 Nuclear F-actin promotes chromatin re-modelling.

***A**, shows a Western blot of samples prepared from NLS-actin^{WT} and NLS-actin^{R62D} cells which were collected 45 and 120 minutes after mitotic shake off. Protein ladder is shown in kDa. Western samples were prepared by myself and separated on a polyacrylamide gel by Abderrahmane Kaidi. **B-D,** shows images of post-mitotic NLS-actin^{WT} and NLS-actin^{R62D} cells which were taken at 60x on a widefield microscope. Cells were fixed 1 hr post mitotic release and stained with the antibodies shown. **E**, shows the corresponding quantification of the nuclear intensity, normalized to the nuclear area, of the indicated histone modifications shown in D. n>54, three biological repeats, *** indicates p<0.0002, ns indicates p>0.05, Student's t-test. Error bars show SEM. **F**, shows a graph which measures H3K9me3 fluorescence intensity as a function of nuclear position, from the cells shown in D (H3K9me3). Here, 0 is the center of the nucleus and 100 is the nuclear periphery. Data are pooled from all cells, were the red and green lines show the mean fluorescence intensity at each radial position. Error bars are SEM. n>54, three biological repeats. Radial analysis used a MATLAB plugin, made by Dr Stephen Cross.*

4.2.2.2 Chromatin modifiers

The reduction of H4K16ac may be related to the players that modify this residue. KAT5 is a histone acetyltransferase that has a broad substrate specificity, which includes H4K16 (Taylor et al., 2013). In NLS-actin^{WT} post-mitotic cells, KAT5 is highly accumulated in the nucleus (Figure 4-6A), which is correlated with the ability to re-establish H4K16ac after mitosis (Figure 4-5A-B). In the actin mutant cells, KAT5 nuclear intensity is markedly reduced, where it is found most strongly at the nuclear periphery (Figure 4-6A). These results may thus explain the reduced ability to re-establish H4K16ac in the actin mutant cells.

In relation to H3S10ph, the increase in the actin mutant cells could be attributed to decreased accumulation of the protein phosphatases PP1 and PP2A, the main phosphatases that de-phosphorylate this residue (Grallert et al., 2015; Schmitz et al., 2010). This possibility was investigated by immunofluorescence. No significant difference in the levels of these proteins were observed between NLS-actin^{WT} and NLS-actin^{R62D} cells (Figure 4-6B-C), suggesting that inhibition of nuclear F-actin does not affect the localisation of these proteins. Despite this, no data were gathered to measure the activity of these proteins, thus they cannot be excluded as players that contribute to this phenotype. Another protein which affects the phosphorylation of H3S10 is the protein kinase Aurora B (Hendzel et al., 1997), which was found to be significantly higher in NLS-actin^{R62D} cells (Figure 4-6D), potentially explaining the increased H3S10ph.

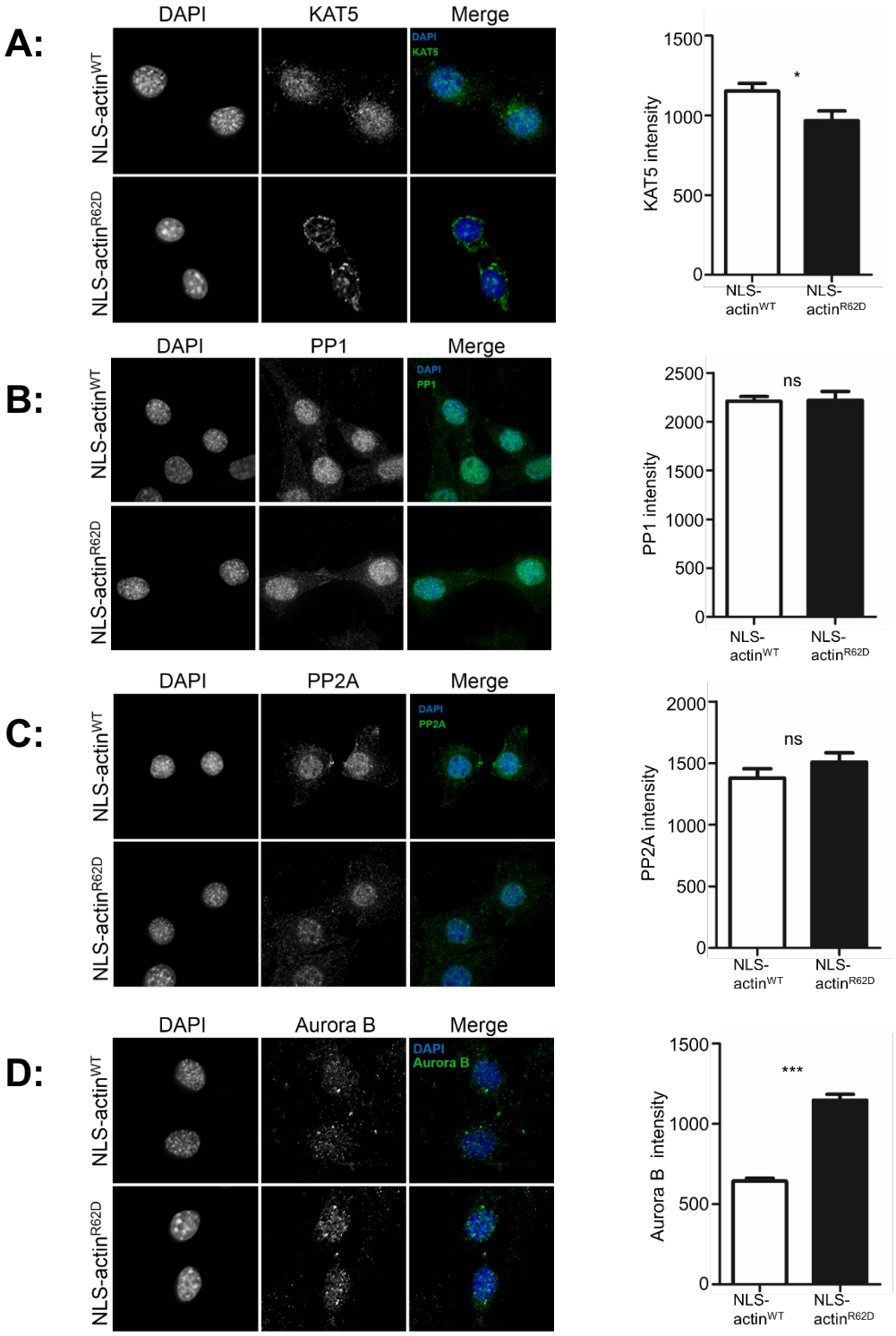

Figure 4-6 Nuclear F-actin regulates chromatin modifying enzymes.

A-D left, *shows images of post-mitotic NLS-actin^{WT} and NLS-actin^{R62D} cells which were fixed and stained with the antibodies shown (A=KAT5, B= PP1, C= PP2A, D= Aurora B). Images were taken at 60x on a widefield microscope.* ***A-D right,*** *shows the corresponding quantification of the nuclear intensity, normlaised to the nuclear area, of the indicated proteins shown in A-D. n>54, three biological repeats. *** indicates p<0.0001, * indicates p=0.0196, ns indicates p>0.05, Student's t-test. Error bars show SEM.*

4.2.3 Regulation of Aurora B

Given that the removal of Aurora B from chromatin is important for chromatin de-condensation (Ramadan et al., 2007), and NLS-actin^{R62D} cells have elevated Aurora B and defective chromatin de-condensation, it is conceivable that nuclear F-actin may be involved in the removal of Aurora B. VCP is a AAA + protein family member which promotes the extraction of Aurora B from chromatin (Ramadan et al., 2007). Consistent with this, pharmacological inhibition of VCP results in increased nuclear levels of both Aurora B and H3S10ph (Figure 4-7A-B). In this respect, inhibition of nuclear F-actin resembles VCP inhibition, where it increases both H3S10ph and Aurora B. Interestingly, VCP inhibition also results in a decrease of H4K16ac (Figure 4-7C), which was reduced in the NLS-actin^{R62D} cells. Consistent with the recruitment of histone deacetylases by H3S10ph (Wilkins et al., 2014), reduced H4K16ac may therefore be a consequence of Aurora B accumulation and its continued phosphorylation of H3S10. Therefore, it is possible that the results in section 4.2.2.1 can be explained by nuclear F-actin regulating the activity or localisation of VCP. Indeed, VCP nuclear intensity was reduced in the actin mutant cells (Figure 4-7D).

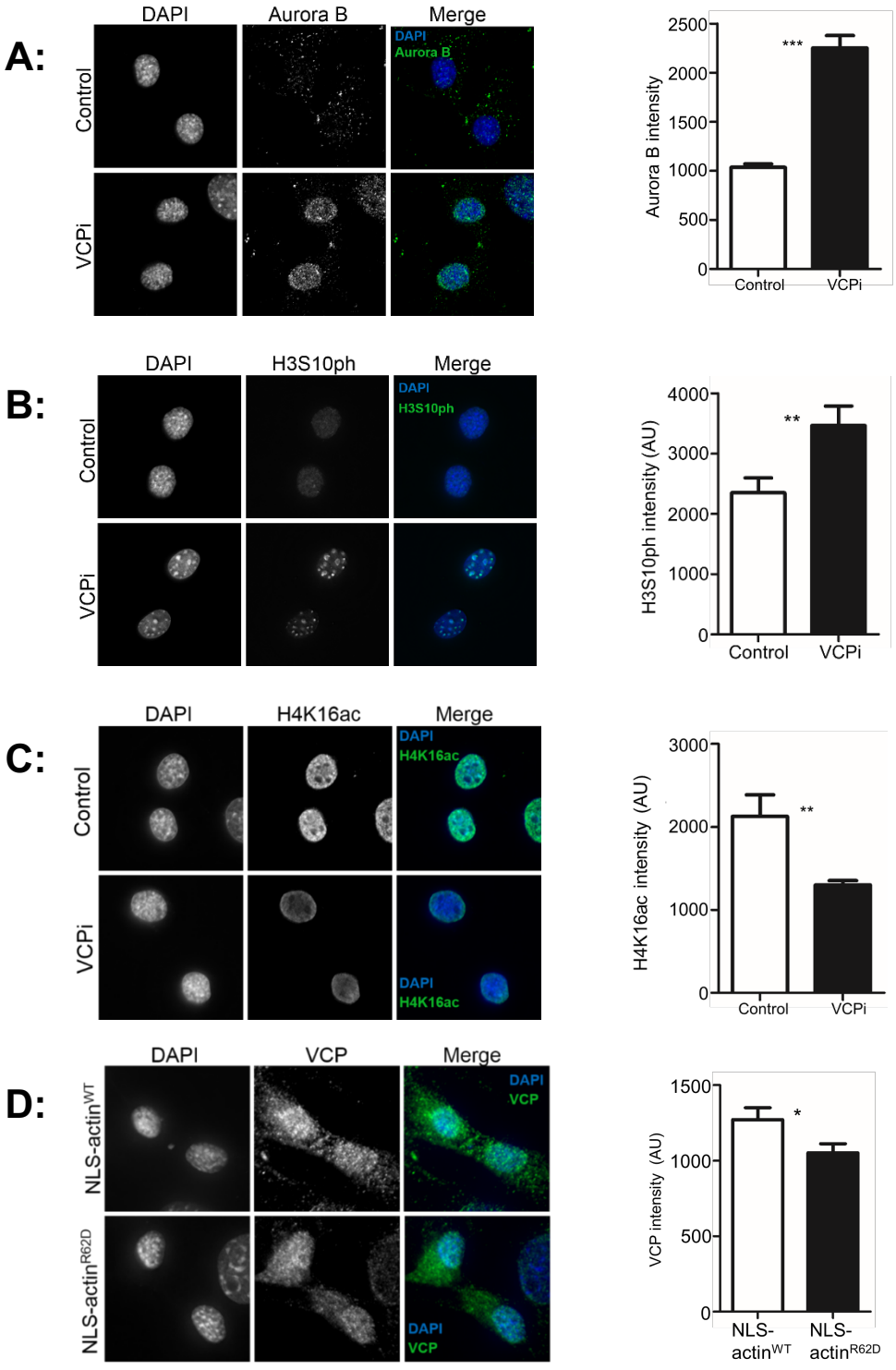

Figure 4-7. Nuclear F-actin regulates VCP.

A-D left, *shows images of post-mitotic NIH-3T3 cells which were fixed and stained with the antibodies shown (A= Aurora B, B= H3S10ph, C= H4K16ac, D= VCP). Images were taken at 60x on a widefield microscope. A-C were treated with DMSO or 30nM VCPi for 10 hrs before being fixed.* ***A-D right,*** *shows the corresponding quantification of the nuclear intensity, normlaised to the nuclear area, of the indicated proteins shown in A-D. n>60, three biological repeats, *** indicates p<0.0001, ** indicates p=0.0018 (B) or p=0.0012 (C), * indicates p=0.0149, Student's t-test. Error bars show SEM.*

4.2.4 Nuclear F-actin promotes post-mitotic nuclear expansion

In addition to chromatin de-condensation, these nuclear actin filaments also arise during a time where the nucleus is expanding. Therefore, experiments were conducted to assess the role of nuclear F-actin in post-mitotic nuclear expansion. To investigate this, NLS-actin^{WT} and NLS-actin^{R62D}, which express mCherry-H2B, were imaged as they exited mitosis. IMARIS software was then used to make 3D nuclear projections (using the mCherry channel) and measure the nuclear volume at several timepoints after anaphase. These results are shown in figure 4-8A, revealing that nuclear expansion was severely impaired in the actin mutant cells. These experiments were also repeated in cells overexpressing exportin 6, giving the same results (Figure 4-8B).

It is conceivable that these results may be a consequence of chromatin de-condensation. Alternatively, nuclear F-actin may have a direct role in expanding the nucleus after cell division. Although these hypotheses are experimentally challenging to uncouple, live cell imaging of 3T3 cells expressing mCherry-H2B and GFP-nAC suggest that nuclear F-actin may have a function at the nuclear periphery. This can be observed in figure 4-8C, where nuclear protrusions were found to arise from the surface of the nucleus during nuclear expansion, which temporally localised with nuclear actin filaments.

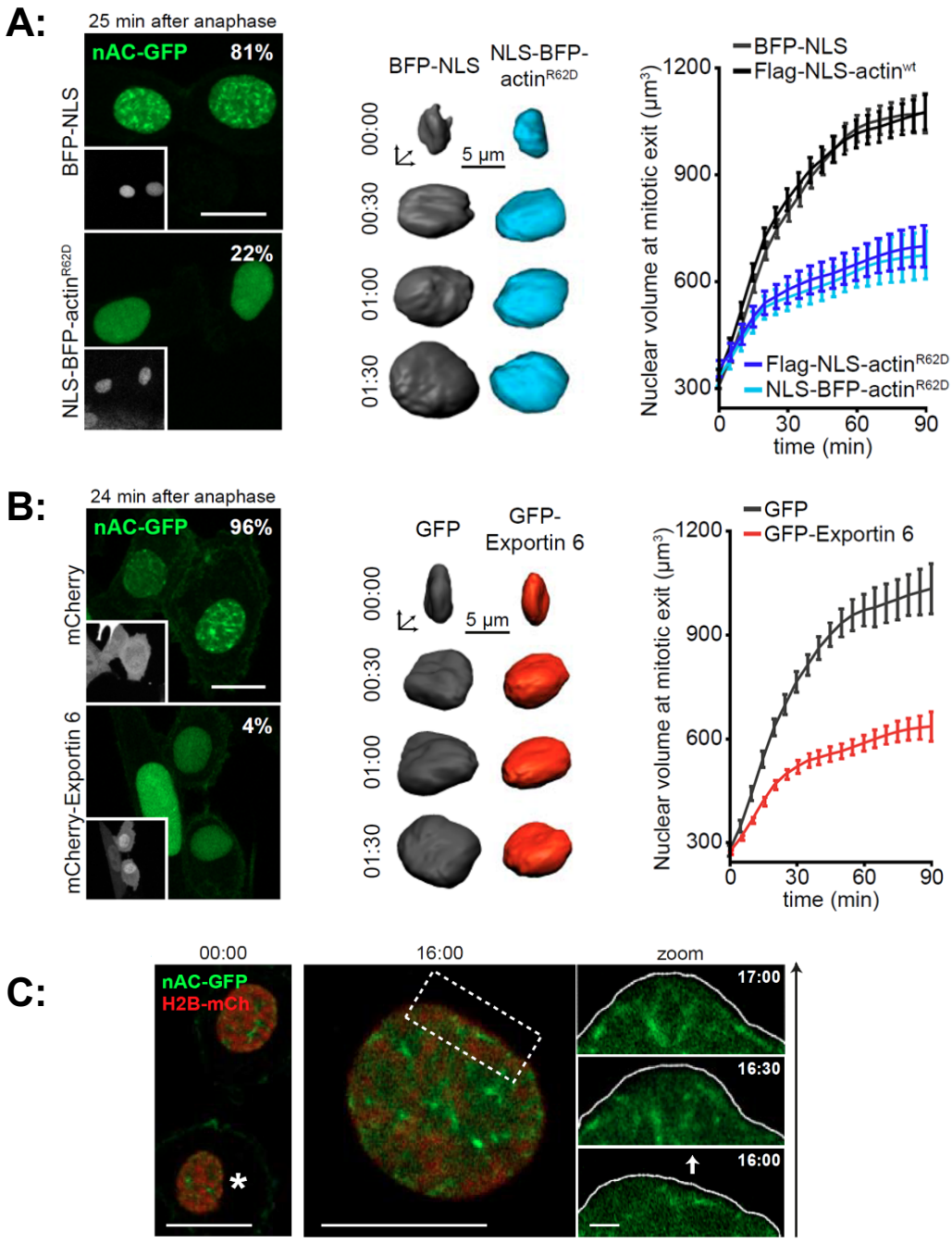

Figure 4-8 Nuclear F-actin promotes nuclear expansion.

A-B *shows three panels. The first panel shows images from a live cell imaging video of NLS-actin^{WT} and NLS-actin^{R62D} cells (A) or control and exportin 6 overexpressing cells (B) which have exited mitosis. The number indicates the percentage of cells with nuclear actin filaments. The middle panel shows 3D projections of these nuclei, at the indicated times after anaphase. The final panel shows quantification of nuclear volume at the indicated times after anaphase.* ***C,*** *shows NIH3T3 cells stably expressing nAC-GFP and H2B-mCherry during mitotic exit. The asterisk indicates the nucleus shown for the additional time points. The dashed rectangles indicate areas of dynamic nuclear protrusions, shown magnified over time (minutes). The arrows indicate the direction of protrusions. The data in this figure were generated in Professor Robert Grosse's lab, Marburg, Germany.*

4.2.4.1 Nuclear F-actin promotes nuclear protrusions

The nuclear protrusions described above spatially and temporally coincide with nuclear actin filaments (Figure 4-8C), suggesting that nuclear F-actin may be involved in producing these protrusions. To investigate this, atomic force microscopy (AFM) was used to image the surface of NLS-actin^{WT} and NLS-actin^{R62D} cells. NLS-actin^{WT} and NLS-actin^{R62D} cells were synchronised in mitosis and fixed 1 hr post-mitotic release. Cells were prepared for AFM, and the nucleus was imaged over a 5 μm region. This showed a significantly rougher surface over the nuclear region of the NLS-actin^{WT} cells (Figure 4-9A), potentially representing the nuclear protrusions seen by live cell imaging. In addition, AFM was also used in a different mode to simultaneously measure nuclear stiffness and surface topology, showing that the NLS-actin^{WT} nuclei were significantly rougher and less stiff (Figure 4-9B). Given that chapter 3 identified that nuclear stiffness is related to the extent of chromatin compaction, these experiments likely identify increased chromatin compaction and decreased surface roughness in the actin mutant cells.

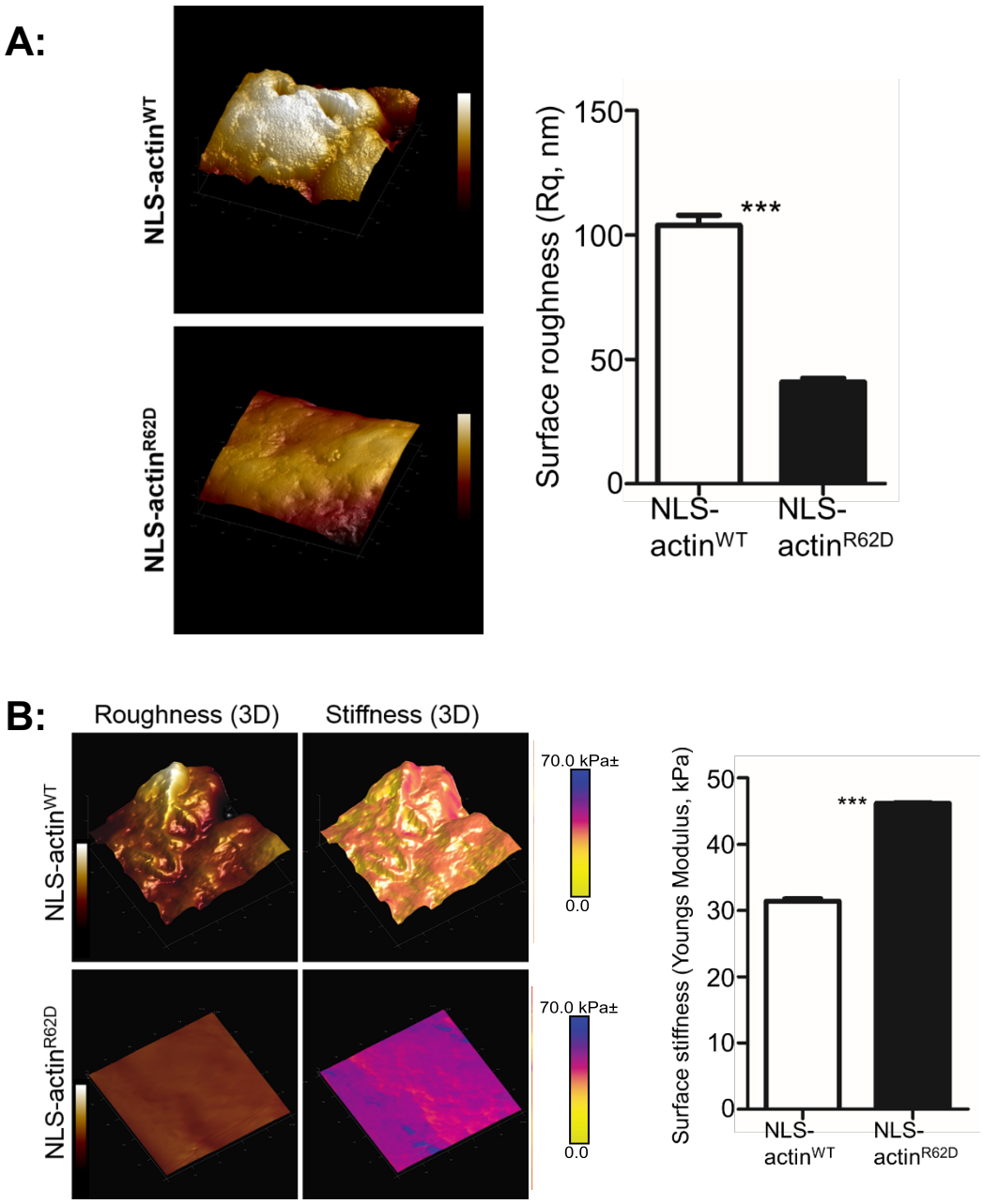

Figure 4-9 Polymerisation of nuclear F-actin affects nuclear stiffness and roughness.

The data in this figure were obtained from NLS-actin^{WT} and NLS-actin^{R62D} cells which were synchronised in mitosis and fixed 1 hr post-mitotic release. Cells were dehydrated and dried to critical point for atomic force microscopy (AFM). ***A,*** *shows an image which was acquired from a 5x5µm region over the NLS-actin^{WT} and NLS-actin^{R62D} nucleus. Scale bar shows height (nm). Right, shows quantification of the surface roughness, which is calculated by determining the Rq of the sample (nm), using AFM software. N=5, two biological repeats. *** indicates p<0.0001.* ***B****, shows two panels. The first panel shows an image which was acquired from a 5x5µm region over the NLS-actin^{WT} and NLS-actin^{R62D} nucleus. Scale bar/colour code shows height (nm). The second panel shows this same region, but the scale bar/colour code represents surface stiffness (Youngs Modulus/YM, kPa). Right shows a graph comparing YM between NLS-actin^{WT} and NLS-actin^{R62D} cells. N=5, two biological repeats. *** indicates p<0.0001. AFM imaging was in collaboration with Dr Robert Harniman.*

To confirm that this difference was not caused by cytoplasmic variation between the two cell types, these experiments were repeated using isolated nuclei from post-mitotic NLS-actin^{WT} and NLS-actin^{R62D} cells. These experiments showed the same results as the whole cells, revealing a significantly flatter surface of R62D nuclei (Figure 4-10-A/C). In light of this, and the fluorescence imaging which observed actin filaments at the nuclear periphery, it suggests that nuclear F-actin promotes nuclear protrusions. However, previous data showed that the NLS-actin^{WT} cells differ from the NLS-actin^{R62D} cells in two ways; NLS-actin^{WT} cells produce nuclear actin filaments, but they also show increased chromatin de-compaction. To tease apart which of these factors is responsible for the differences in nuclear surface roughness, AFM was again used. Here, NLS-actin^{WT} cells were synchronised in mitosis and nuclei were isolated 5 hrs post-mitotic release, by which time nuclear F-actin had disassembled (Baarlink et al., 2017). At release, one of these samples was treated with the HDAC inhibitor Trichostatin A (TSA), to induce chromatin de-compaction (Hizume et al., 2010; Rao et al., 2007). This showed that chromatin decompaction in the absence of nuclear F-actin does not increase nuclear surface roughness (Figure 4-10B/D), therefore suggesting that it is the nuclear actin filaments, not the compaction state of chromatin, that promoted the change in nuclear surface roughness.

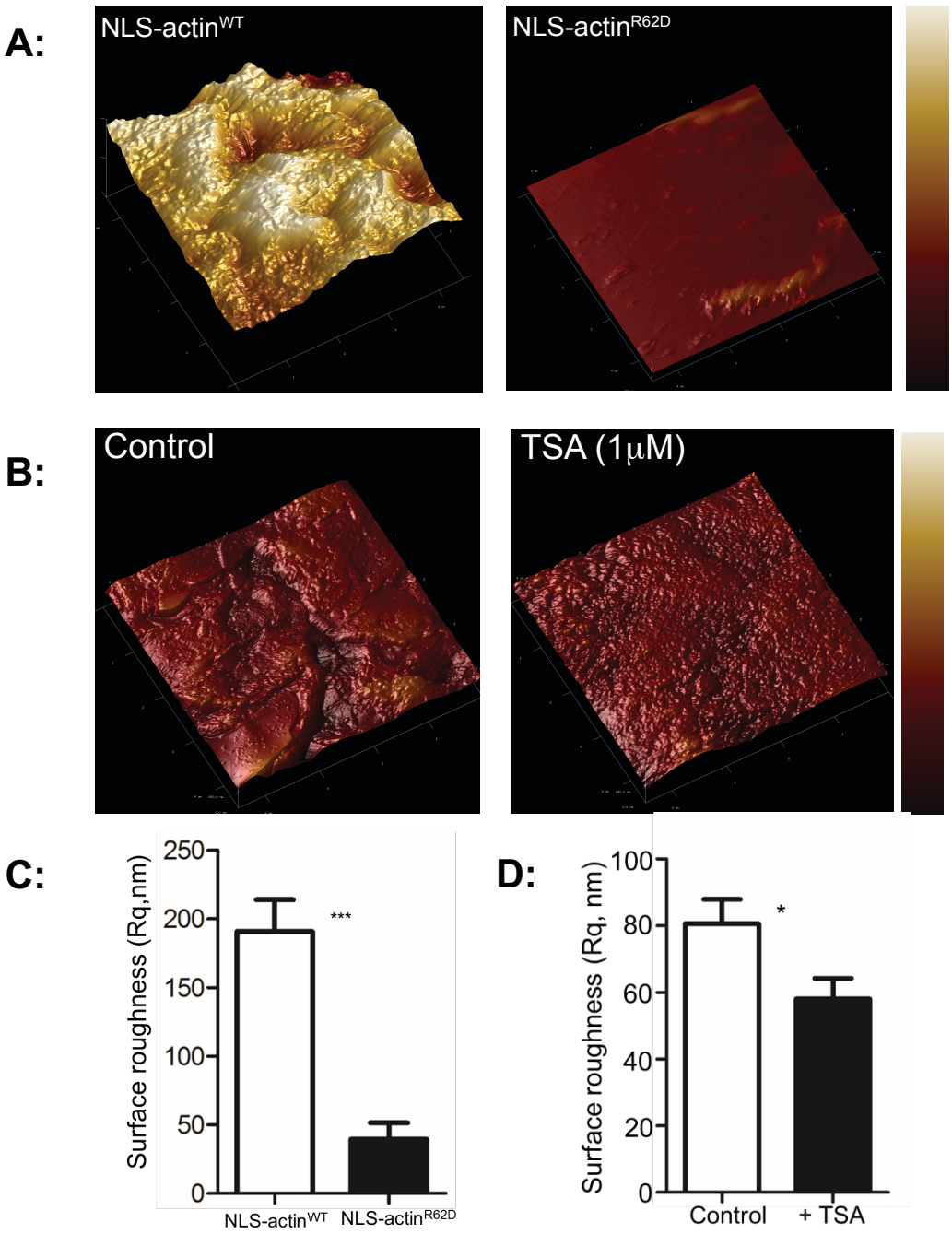

Figure 4-10 Nuclear F-actin promotes nuclear protrusions.

A, *NLS-actin^{WT} and NLS-actin^{R62D} cells which were synchronised in mitosis. 1 hr post-mitotic release, nuclei were isolated and were seeded onto PLL-coated cover slips. AFM was used to image a 5x5μm region of the surface of these nuclei. Scale bar shows height (nm).* ***B,*** *NIH-3T3 cells were synchronised in mitosis and treated with DMSO or 1μM Trichostatin A (TSA) at mitotic release. 5 hrs post-mitotic release, nuclei were isolated and were seeded onto PLL-coated cover slips. AFM was used to image a 5x5μm region of the surface of these nuclei. Scale bar shows height (nm).* ***C-D****, shows quantification of the surface roughness, which is calculated by determining the Rq of the sample (nm), using AFM software. N=9 (C), two biological repeats. *** indicates p<0. 0001. N=7 (D), two biological repeats. * indicates p=0.035. AFM imaging was in collaboration with Dr Robert Harniman.*

4.2.5 Re-establishment of nuclear bodies

Given the role of nuclear F-actin in de-condensing chromatin and expanding the nucleus, it is conceivable that inability to polymerise nuclear actin after cell division may also perturb the formation and organisation of nuclear bodies. Perhaps most obvious is the formation of the nucleolus, a dense organelle which is the site of rRNA synthesis. To address this, NLS-actin^{WT} and NLS-actin^{R62D} cells were stained with nucleolin, a prominent protein in the nucleolus (Tajrishi et al., 2011). Nucleoli were then counted, revealing no significant difference in the mean number of nucleoli per cell (Figure 4-11A), suggesting the formation of the nucleolus was not perturbed.

Next, given the defects in chromatin condensation, the heterochromatin associated Polycomb body (Pirrotta and Li, 2012) was also imaged by light microscopy. To visualise this, cells were stained with the polycomb repressive complex 1 protein, BMI1 (Abdouh et al., 2016). The nuclear intensity was then measured, revealing no significant difference in its localisation or nuclear level between the two cell types (Figure 4-11B).

Finally, given the role of actin in expanding the nucleus, it is possible that this will also affect the accumulation of nuclear lamina components, which lie below the nuclear membrane. Cells were thus stained with lamin A/C, a key component of the nuclear lamina, and imaged by light microscopy. No significant difference in the peripheral intensity was observed (Figure 4-11C). In addition, the fluorescent intensity of lamin A/C at each radial position was measured (where 0 is the centre of the nucleus, 100 is the nuclear periphery), showing the same profile between the two cell types, thus the distribution of lamin A/C is also not affected (Figure 4-11D).

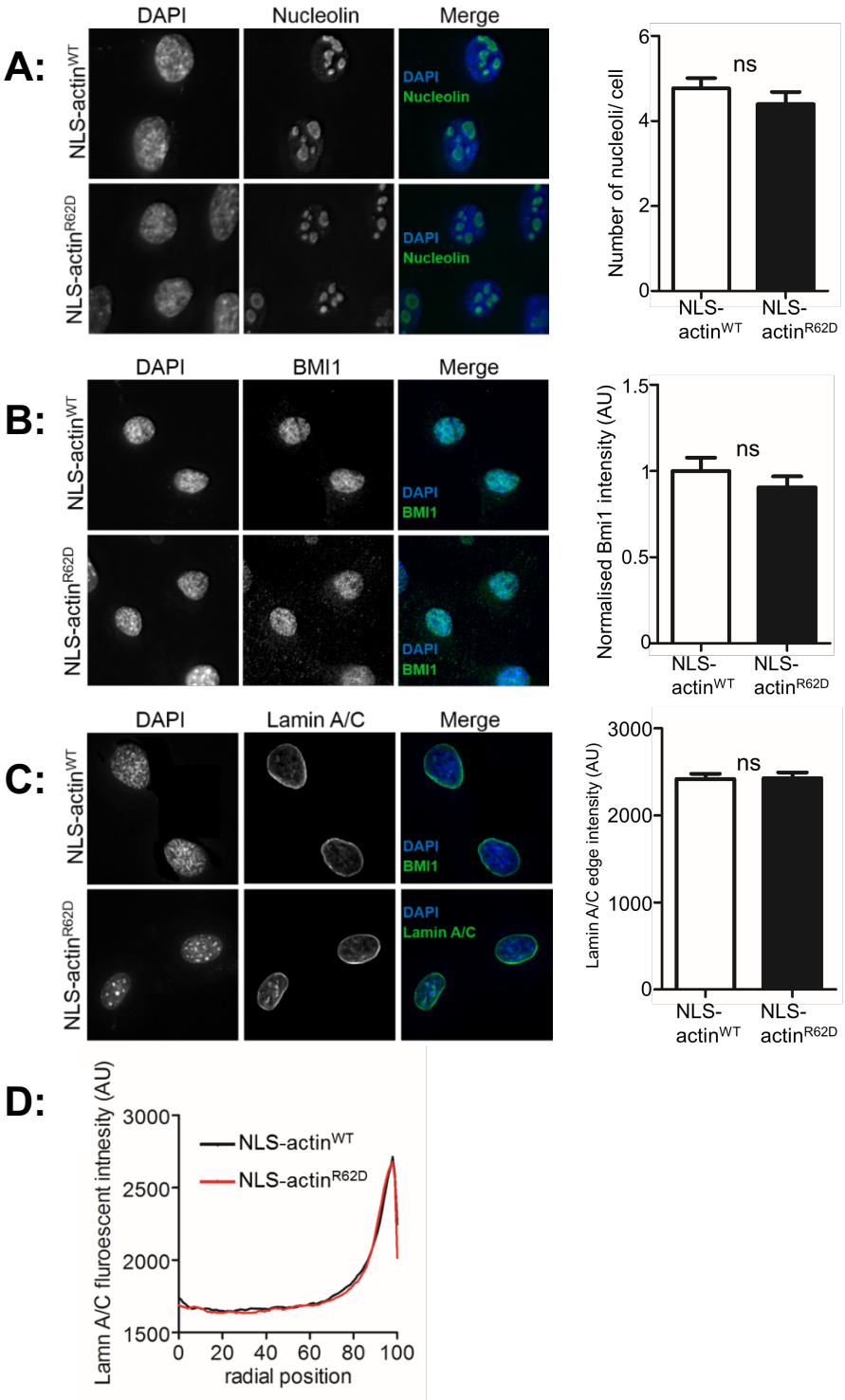

Figure 4-11 Nuclear F-actin does not affect the formation of nuclear bodies.

A-C left, *shows images of post-mitotic NLS-actin^{WT} and NLS-actin^{R62D} cells which were fixed 1 hr after mitotic release and stained with the antibodies shown (A= nucleolin, B= BMI1, C= Lamin A/C). Images were taken at 60x on a widefield microscope.* ***A-C right*** *shows the corresponding quantification of the number of nucleoli (A), nuclear intensity, normalised to the nuclear area (B) and edge intensity, defined as the pixels within 10% of the nuclear area from the nuclear periphery (C). n>30, three biological repeats, ns indicates p>0.05. Error bars show SEM.* ***D****, shows a graph of lamin A/C fluorescence intensity as a function of nuclear position. Here, 0 is the centre of the nucleus and 100 is the nuclear periphery.*

4.3 Discussion

In summary, the results in this chapter provide evidence that nuclear F-actin promotes chromatin de-condensation and nuclear expansion after cell division. Although previous work has pointed to a role for nuclear F-actin in chromosome mobility in budding yeast (Spichal et al., 2016b), this is the first evidence that nuclear F-actin can modulate global chromatin structure. This may set a precedent for future research investigating the role of filamentous actin in the nucleus. Other examples of nuclear F-actin structures are during serum stimulation (Baarlink et al., 2013), cell spreading (Plessner et al., 2015), cellular re-programming (Miyamoto et al., 2011) and DNA damage (Belin et al., 2015b). During each of these instances, it is likely that chromatin structure is altered, for example to induce activation of developmental or early response genes (Baarlink et al., 2013; Miyamoto et al., 2011), but this was not investigated. Further research may thus identify a general role for nuclear F-actin in regulating chromatin structure.

The data presented used FLIM, EM, enzymic digestion and immunofluorescence to show that inhibition of nuclear F-actin after cell division results in increased chromatin compaction, the implications of which are identified in the next chapter. Given that the nucleus is reorganised during this period it is conceivable that this would also result in problems in re-compartmentalising the genome after cell division. Indeed, the nucleus is highly mobile in early G1, during the re-establishment of territories, TADs and LADs (Thomson et al., 2004; Zullo et al., 2012) and therefore, it is possible that failure to de-condense chromatin will affect these processes. Alternatively, it may be that nuclear F-actin is primarily involved in spatially organising the genome, thus the increase in chromatin compaction detected in these experiments is in fact caused by failure to compartmentalise. Indeed, lamin A/C incorporates into the nuclear membrane in early G1, during the re-establishments of LADs. In the absence of these lamins heterochromatin at the nuclear periphery is lost and gained in the nucleoplasm, resulting in heterochromatin structures similar to what has been observed (Moir et al., 2000; Teresa R Luperchio, 2018).

In relation to the regulation of chromatin remodelling by nuclear F-actin, this work showed that actin mutant cells had limited removal of H3S10ph and re-establishment of H4K16ac after cell division. Given the association of these histone

modifications with chromatin de-condensation (Hendzel et al., 1997; Iizuka et al., 2006b; Ramadan et al., 2007), these results may simply be a consequence of the increased chromatin compaction. Indeed, other histone modifications which are not related to chromatin de-condensation were not affected. However, these results also showed that NLS-actin^{R62D} cells have increased nuclear levels of Aurora B and decreased KAT5, potentially explaining the increased H3S10ph and decreased H4K16ac, respectively. These results further suggest that these observations may be related; inhibition of VCP, which removes Aurora B from chromatin, mimicked inhibition of nuclear F-actin, in relation to these modifications. Therefore, nuclear F-actin may have a more direct involvement in chromatin remodelling, and promote the extraction of Aurora B by VCP, leading to the removal of H3S10ph and the acetylation of H4K16. Indeed, actin is a component of many chromatin associated proteins, where it has been found to also impact their mobility. Therefore, it is conceivable that actin polymerisation may be involved in chromatin re-modelling. However, phosphorylation of H3S10 is not sufficient to form mitotic chromosomes, (Van Hooser et al., 1998), thus its removal after cell division is unlikely to drive chromatin de-condensation, and therefore this is most likely not the primary function of these nuclear actin filaments.

In light of these results, it is possible that nuclear F-actin is involved in intranuclear transport, similar to in the cytoplasm. Indeed, myosins are present in the nucleus, bind chromatin remodelling complexes (Bettinger et al., 2004; Cairns et al., 1998; Peterson et al., 1998), and have been previously shown to affect the localisation of RNAP II (Chuang et al., 2006; Serebryannyy et al., 2016b). Further, nuclear F-actin and myosins have been found to promote the relocation of genes during heterochromatic DNA repair (Caridi et al., 2018). Future research may thus identify a role for nuclear myosins at mitotic exit, of which myosin 1C (NM1) is a promising candidate, due to its previously identified roles in chromosome mobility (Fomproix and Percipalle, 2004). However, given the small filament length and comparatively low concentration of nuclear actin, a transport system analogous to that in the cytoplasm is unlikely to exist. Whether short distance transport along nuclear actin filaments is involved in chromatin remodelling is yet to be determined.

This chapter also identified a role for nuclear F-actin in expanding the nucleus after cell division, which pushes on the NE and produces protrusions, potentially stimulated by emerin which can polymerise actin filaments (Holaska et al., 2004).

This may stretch the NE and promote the addition of lipids and membrane components, which has been previously shown to increase the rate of nuclear expansion (Newport et al., 1990; Siniossoglou, 2009). This may in turn impact processes within the nucleus, as evidence suggests that the size of the cell and nucleus are linked, suggesting an importance of nuclear size in cell viability (Walters et al., 2012). It is also possible the failure to expand the nucleus affects chromatin de-condensation, by defining the space in which it can remodel. In addition, the size of the nucleus may impact diffusion gradients between the nucleus and cytoplasm and therefore affect nuclear import of proteins which may promote chromatin de-condensation. However, given that these filaments arise after competent nuclear import, evident by lamin A/C membrane incorporation (Newport et al., 1990), this will likely not have a profound affect. Alternatively, chromatin de-condensation may affect nuclear expansion, for example, by recruiting nuclear envelope components, which has been previously shown to increase the rate of nuclear expansion (Polioudaki et al., 2001). However, figure 4-10B argues against this, where it shows that the de-condensation of chromatin by addition of TSA after actin filaments have disassembled does not increase nuclear roughness. Therefore, this suggests that it is nuclear actin filaments, not chromatin de-condensation, which expands the nucleus.

In future research, it would be of interest to separate these phenotypes, and understand whether nuclear F-actin primarily functions to expand the nucleus, de-condense chromatin, or both. Indeed, the emergence of nuclear F-actin driven protrusions suggests a mechanical role for nuclear actin filaments, similar to its contractile functions within the cytoplasm and the stabilisation of the Xenopus oocyte nucleus (Bohnsack et al., 2006). The production of such forces are evident at the nuclear periphery, and provides a potential mechanism for how nuclear F-actin expands the nucleus. Whether actin exerts these ‘forces’ to chromatin to promote chromatin de-condensation, or this is a consequence of increased nuclear expansion is yet to be determined. However, the localisation of these nuclear actin filaments, which occur throughout the nucleus, suggests that the action of these filaments is not restricted to the nuclear periphery, thus nuclear F-actin may have a more direct role in chromatin de-condensation.

Chapter 5 : Consequences of nuclear F-actin assembly

5.1 Introduction

Due to the exclusion of transcriptional machinery (Gottesfeld and Forbes, 1997), loss of promotor-enhancer contacts (Gibcus et al., 2018) and the highly condensed structure of a mitotic chromosome (Antonin and Neumann, 2016), it has been thought that mitotic cells are transcriptionally inactive. Recent research however has determined that this is not the case, as low-level transcription of many genes during mitosis has now been detected (Palozola et al., 2017). After cell division, the expression of these transcripts increases dramatically, which coincides with the re-establishment of an interphase chromatin structure (Palozola et al., 2017). The de-condensation and structural re-organisation of chromatin is thus important for the binding of RNA polymerase (RNAP) and the re-activation of transcription after cell division, which is fundamental to cell viability and re-entry into the cell cycle. After mitosis, the first genes activated control cell growth and proteins important in re-building the nucleus. Subsequently, cell type specific and other genes controlling the progression to S phase are expressed (Palozola et al., 2017). Importantly, this requires phosphorylation of the Retinoblastoma (Rb) protein by the cyclin dependent kinase (CDK) 4/6 and cyclin D complex. Phosphorylation of Rb leads to the release of the transcription factor E2F, resulting in transcription of genes that facilitate escape from the restriction point to promote cell cycle commitment (Bertoli et al., 2013; Helin, 1998). The role of E2F in activating transcription of genes for S phase progression has been well defined and includes targets such as cyclin E, which in complex with CDK2, mediates the G1-S transition (Ohtani et al., 1995). The de-condensation of chromatin is therefore likely important for the activation of transcription and re-entry into the cell cycle. In addition, the chromatin landscape in G1 also affects DNA replication.

In mammalian cells, the replication timing program is determined in G1 phase of the cell cycle during the timing decision point (TDP) (Dimitrova and Gilbert, 1999). This coincides with the re-establishment of high order chromatin structure and as such, the regulation of DNA replication is temporally and spatially coupled to the re-organisation of the nucleus after cell division (Dileep et al., 2015). Indeed, the compartmentalisation of chromatin provides a spatial separation between heterochromatin and euchromatin, which are typically replicated at different times during S phase (Kim et al., 2003; Lima-de-Faria and Jaworska, 1968). Important in the temporal separation of these domains during DNA

replication is the binding of lamin B1 and RIF1 to chromatin (Cornacchia et al., 2012). Together these proteins mark the majority of the late replicating genome (Cornacchia et al., 2012; Foti et al., 2016). RIF1 coats late replicating regions forming RIF1 associated domains (RADs), which function to regulate interactions within these domains and limit interactions between domains. Loss of RIF1 therefore alters the 3D structure of chromatin, leading to dysregulated replication timing (Foti et al., 2016). Lamin B also has roles in the regulation of replication timing (Gilbert, 2002) and interacts with replication foci, potentially acting as a docking site for DNA replication (Moir et al., 1994). This highlights the link between G1 chromatin structure and DNA replication. In addition, protein complexes directly involved in DNA replication assemble onto chromatin during G1.

Firstly, this involves the licencing of DNA replication origins. In mammalian cells, there is no unanimously defining signature that marks replication origins, however they are often enriched in the histone modification H4K20me2 (Tardat et al., 2010). This modification is thought to be important in origin recognition, as a component of the origin recognition complex (ORC, composed of proteins ORC1-6) specifically interacts with this modification (Kuo et al., 2012). The binding of the ORC complex to chromatin is the first step in origin licencing, which leads the recruitment of other licensing factors including CDC6 and CDT1. Once bound, these proteins recruit the MCM2-7 DNA helicase complex (Fragkos et al., 2015; Masai et al., 2010). This marks the completion of origin licencing and is fundamental for the formation of the pre-replication complex, which forms later in G1; through recruiting proteins such as GINs, CDC45 and Treslin (Im et al., 2009). During S phase, a subset of these origins are activated by the loading of other replication factors, such as PCNA, and CDK mediated phosphorylation of the MCM helicase complex (DePamphilis, 1993). Inactive origins remain dormant as a surplus for stalled origins within the same replicon (Fragkos et al., 2015).

Replication fork stalling is referred to as replication stress, and can be initiated through a number of means including repetitive DNA sequences, high GC content and importantly, highly condensed chromatin (Zeman and Cimprich, 2014). Upon the stalling of a replication fork, single stranded DNA is formed due to the uncoupling of DNA polymerase and helicase, which continues to unwind DNA after the polymerase complex has stalled (Byun et al., 2005). This single stranded DNA is coated by the protein RPA, which acts as a signal for the protein

kinase ATR; ATR interacting protein (ATRIP) specifically interacts with RPA, bringing ATR to the site of the single strand break (Zou and Elledge, 2003). ATR subsequently phosphorylates substrates such as histone H2AX at serine 139 (Ward and Chen, 2001), RPA at serine 33 (pRPAs33) (Vassin et al., 2009) and CHK1 at serine 345 (pCHK1s345) (Zhao and Piwnica-Worms, 2001). Once activated, CHK1 induces cell cycle arrest through the inhibitory phosphorylation of the protein phosphatase CDC25 (Uto et al., 2004). The ATR pathway thus serves as a protector of genome stability, by arresting the cell cycle to allow repair or replication re-start of stalled forks (Flynn and Zou, 2011).

The previous chapter identified that polymerisation of nuclear actin after cell division is important for the expansion of the nucleus and de-condensation of chromatin. Therefore, it follows that cells unable to polymerise nuclear actin after cell division have increased chromatin compaction. It was thus hypothesised that this may result in reduced transcription and impact progression of cells through G1. Further, these defects may co-inside with the TDP and consequently perturb events necessary for DNA replication. To investigate this, the experiments in this chapter address three aims.

Chapter aims:

1. What are the effects of nuclear F-actin on G1 transcription and progress through this phase?
2. Is polymerisation of nuclear actin after mitosis important for DNA replication?
3. How does the G1 chromatin environment affect DNA replication?

5.2 Results

5.2.1 Polymerisation of nuclear actin after cell division is important for mRNA transcription in G1

In light of the results in the previous chapter, and the requirement for an accessible chromatin structure during transcription, it was hypothesised that increased chromatin compaction, as seen in the NLS-actin^{R62D} cells, may impact the re-activation of transcription after cell division. There are three eukaryotic RNAP complexes, which orchestrate transcription of different genes; RNAPI (rRNA), RNAPII (mRNA) and RNAPIII (rRNA and tRNA) (Young, 1991). The CTD tail of RNAP II controls transcription timing through phosphorylation of serine residues. This is first at serine 5 (Ser5) to initiate transcription, and then at serine 2 (Ser2) to promote transcriptional elongation (Figure 5-1A) (Phatnani and Greenleaf, 2006; Young, 1991). These modifications can thus be used as a global measure of the progress of RNAPII.

Immunofluorescence and image analysis were used to measure the nuclear intensity of these modifications in post-mitotic NLS-actin^{WT} and NLS-actin^{R62D} cells. Here it was found that there was no significant difference in RNAPIIpS5 between the two cell types (Figure 5-1B). However, NLS-actin^{R62D} cells had a significant reduction in RNAPIIpS2 (Figure 5-1C), suggesting reduced transcriptional elongation; potentially affecting the mRNA genes and non-coding regions which RNAPII transcribes.

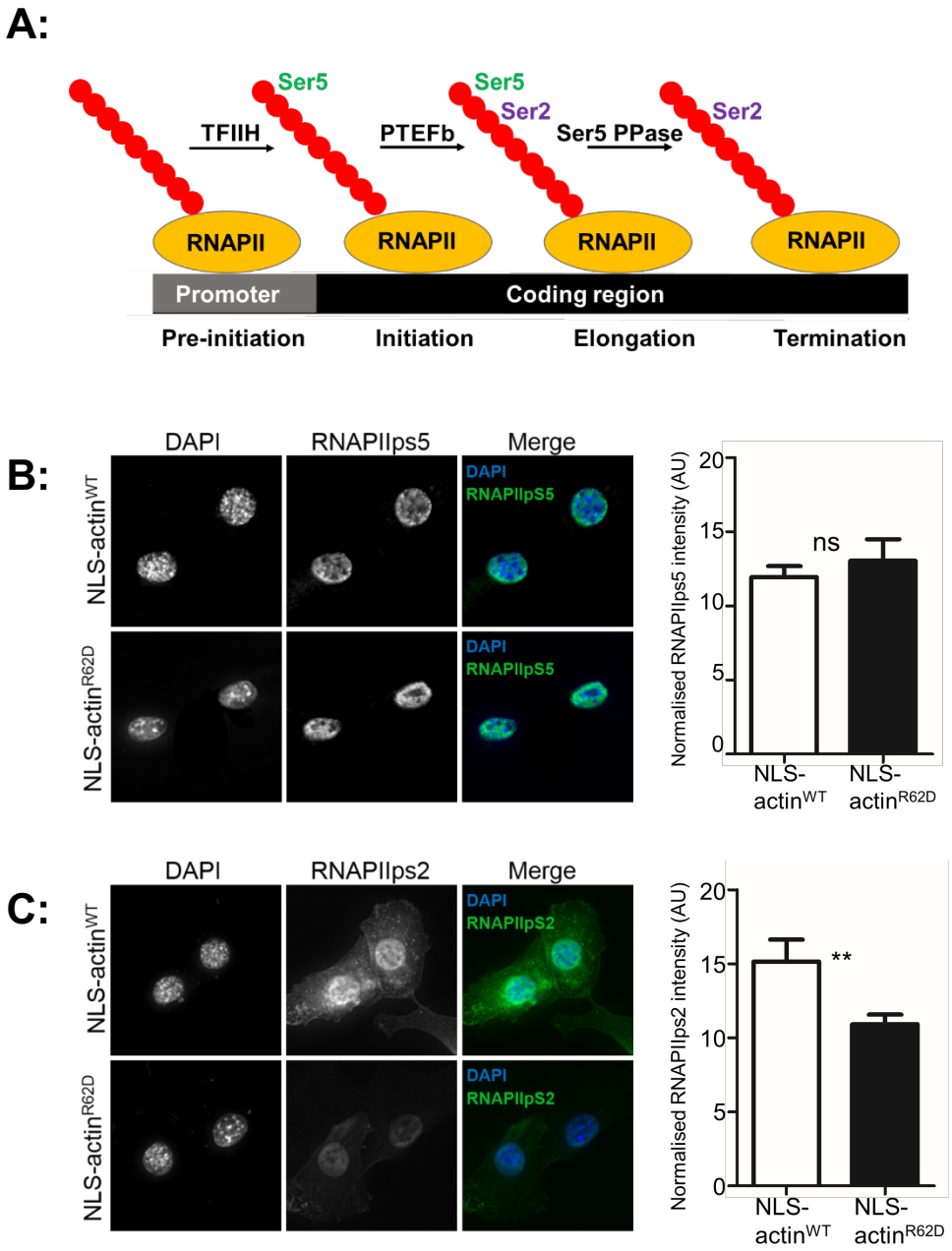

Figure 5-1. Inhibition of nuclear F-actin after cell division reduces transcriptional elongation

***A**, shows a diagram of RNA polymerase II (RNAPII) at several positions along a gene. Extending from the polymerase is a CTD tail (red) which is phosphorylated by the indicated enzymes to promote transcriptional initiation (phosphorylation at serine 5/ Ser5) and transcriptional elongation (phosphorylation at serine 2/ Ser2). The data in this figure (B-C) show images of cells taken at 60x on a widefield microscope. NIH-3T3 cells were fixed 1 hr after mitotic release and stained with DAPI to visualise the nucleus and RNAPII phosphorylation at serine 5 (RNAPIIps5, B) or serine 2 (RNAPIIps2, C). To the right of these images, is the corresponding quantification. DAPI signal was used to draw around the nucleus and measure nuclear area. The intensity of the indicated channels was then measured in this region and normlaised to the nuclear area. **B**, N>77 in three independent repeats. ns indicates p>0.05, Student's t-test. **C**, N>94 in three independent repeats. ** indicates p=.0.0094, Student's t-test.*

5.2.1.1 Inhibition of nuclear actin polymerisation after cell division does not affect global RNA production

The above experiments thus suggest that the elongation of RNAPII transcripts are reduced in NLS-actin^{R62D} cells, potentially affecting overall mRNA production. To investigate whether these cells have an overall reduction in RNA production, a nascent RNA click chemistry assay was used. Here, cells were released from mitosis and cultured in 5-ethynyl uridine (EU). This is a modified RNA nucleotide that is incorporated into RNA molecules, which are being synthesised during the time of EU incubation, and has an alkyne group to facilitate its detection. Because 80% and 15% of a cells RNA is rRNA and tRNA, respectively, this assay largely measures the levels rRNA, but also tRNA and mRNA to a lesser extent. When quantifying the EU intensity by immunofluorescence, results showed no significant difference between the two cell types (Figure 5-2). Therefore, this suggests that overall RNA production is not reduced in NLS-actin^{R62D} cells. Indeed, given that this assay largely detects rRNA, which is transcribed at the nucleolus, these results are in line with results in the previous chapter, showing that the number and size of nucleoli is not affected by the actin mutation.

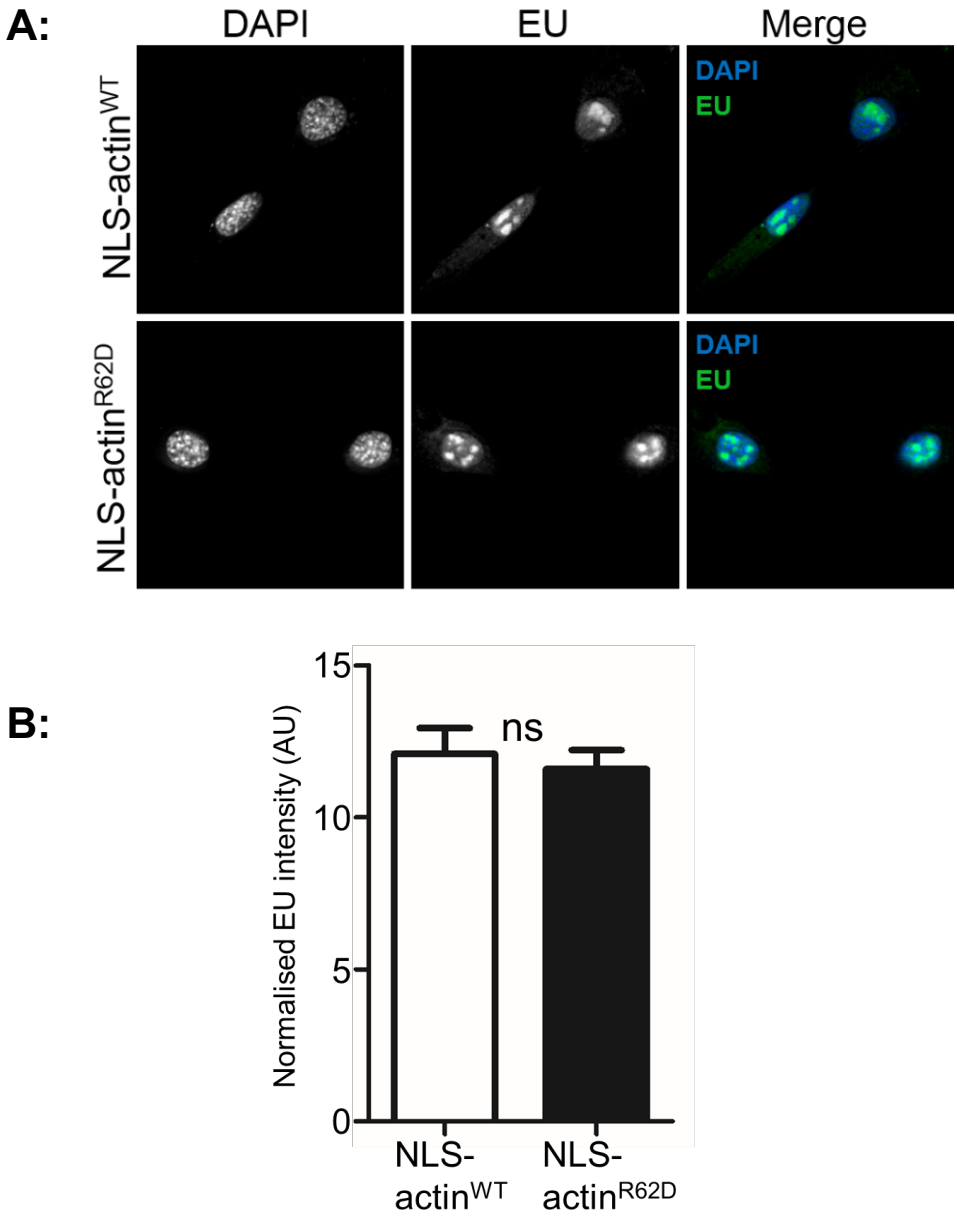

Figure 5-2. Inhibition of nuclear actin polymerisation after cell division does not affect global RNA production

***A**, shows images of cells taken at 60x on a widefield microscope. NIH-3T3 cells were synchronised in mitosis and incubated with 5-ethynyl uridine (EU) for 1 hr before being fixed. To visualise EU, which incorporates into newly synthesised RNA, click chemistry was used via an azide linked fluorophore that specifically binds an alkene group on EU. Cells were stained with DAPI to visualise the nucleus. **B**, shows quantification of the cells shown in A. DAPI signal was used to draw around the nucleus and measure nuclear area. The intensity of EU was then measured in this region and normalised to the nuclear area. N>97 in three independent repeats. ns indicates p>0.05, Student's t-test.*

5.2.1.2 Transcription and chromatin de-condensation

These results thus provide evidence that post-mitotic NLS-actin^{R62D} cells have an overall reduction in mRNA production, but not in the production of rRNA and tRNA. Although these results would have to be confirmed through additional experiments, these data do give rise to a mechanistic question; is the increased chromatin compaction after mitosis when nuclear F-actin is inhibited (chapter 4) in fact a consequence of reduced transcription of the genes necessary to de-condense chromatin, as opposed to a direct function of the actin filaments? To uncouple these possibilities, transcription was inhibited using flavopiridol, an inhibitor of PTEFb. Chromatin compaction and nuclear volume was then measured in parental cells. Results show that inhibition of transcription alone does not affect the expansion of the nucleus (Baarlink et al., 2017) or de-condensation of chromatin (Figure 5-3A-B), thus suggesting that the reduced transcription in G1 is a consequence of increased chromatin compaction, rather than the other way around.

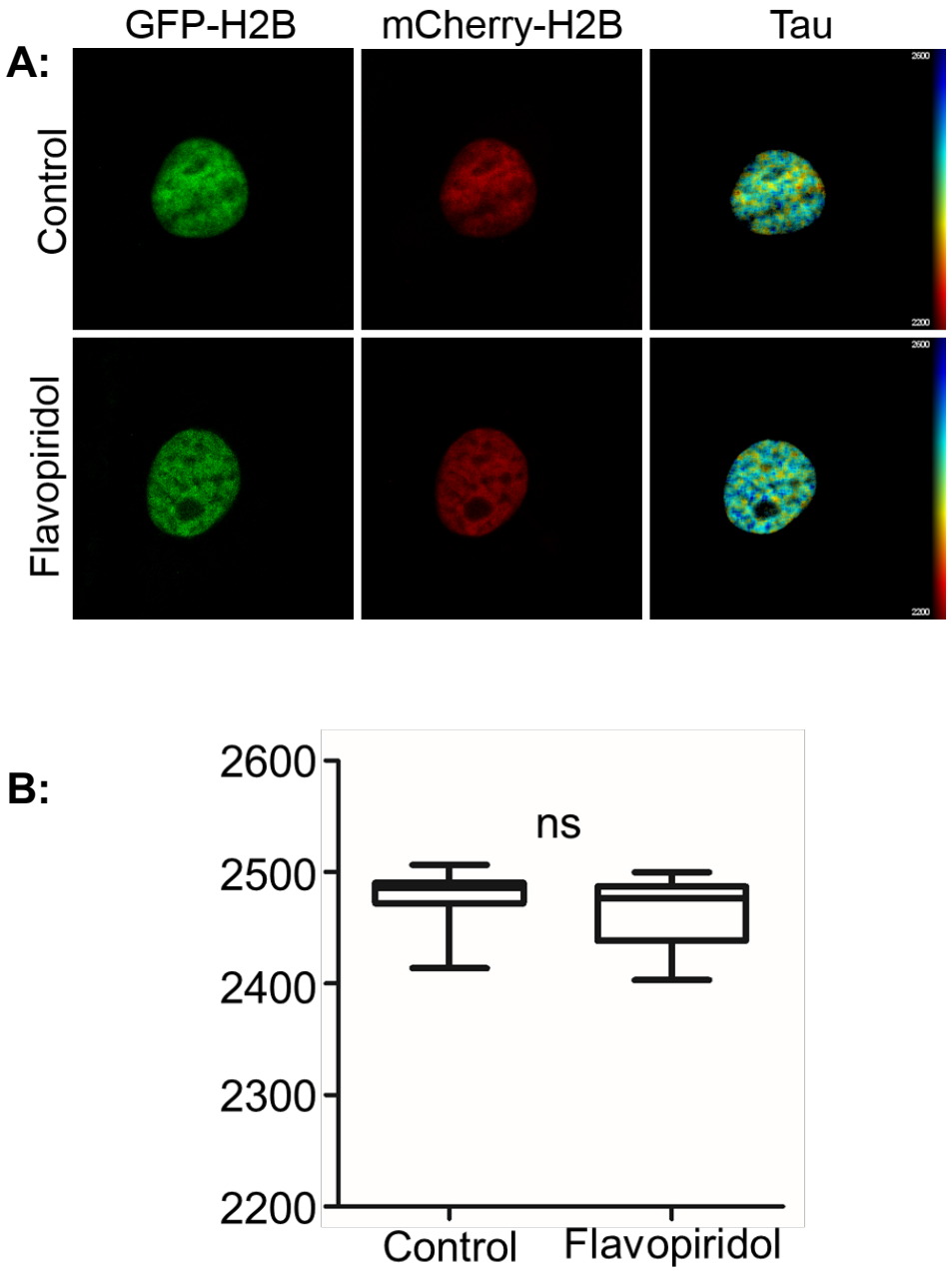

Figure 5-3. Inhibition of transcription does not affect chromatin de-condensation

***A**, shows NIH-3T3^{2FP} cells which were synchronised in mitosis, and treated with the transcriptional inhibitor Flavopiridol for 1 hr before being fixed. GFP and mCherry channels were imaged at 63X on a confocal microscope, channels are indicated. The final panel shows a merge of the fluorescent lifetime and GFP intensity maps. Scale bar shows fluorescence lifetime. **B**, shows a box plot of the fluorescence lifetime values (Tau) of the cells shown in A. N=12, two biological repeats. ns indicates p>0.05, Student's t-test.*

5.2.2 Inhibition of nuclear actin polymerisation after cell division results in reduced progression through G1

Given the requirement of active transcription in the progression from G1 to S phase, it could be speculated that the possible reduction in mRNA transcription in NLS-actin^{R62D} cells impacts G1 progression. To examine this possibility, cells were synchronised in mitosis and collected 3 hrs and 7 hrs post-mitotic release. Cells were cultured in 5-ethynyl-2'-deoxyuridine (EDU) 30 minutes before each timepoint. This is a nucleotide analogue of thymidine, similar to Brdu, which is used to detect cells in DNA synthesis. Due to the smaller size of EDU, DNA does not need to be denatured to detect it, instead it is modified with an alkyne group which reacts specifically with a fluorophore linked azide post-fixation to aid visualisation. The number of replicative cells at each of the collected time points was determined by quantifying the percentage of EDU positive cells. At the 3 hr timepoint, very few replicative cells were detected in the NLS-actin^{WT} or NLS-actin^{R62D} cells, as expected. However, at the 7 hr time point, significantly fewer replicative cells were detected in the NLS-actin^{R62D} cell population, compared to wild type (Figure 5-4A-B). Therefore, this suggests that NLS-actin^{R62D} cells progress slower through G1.

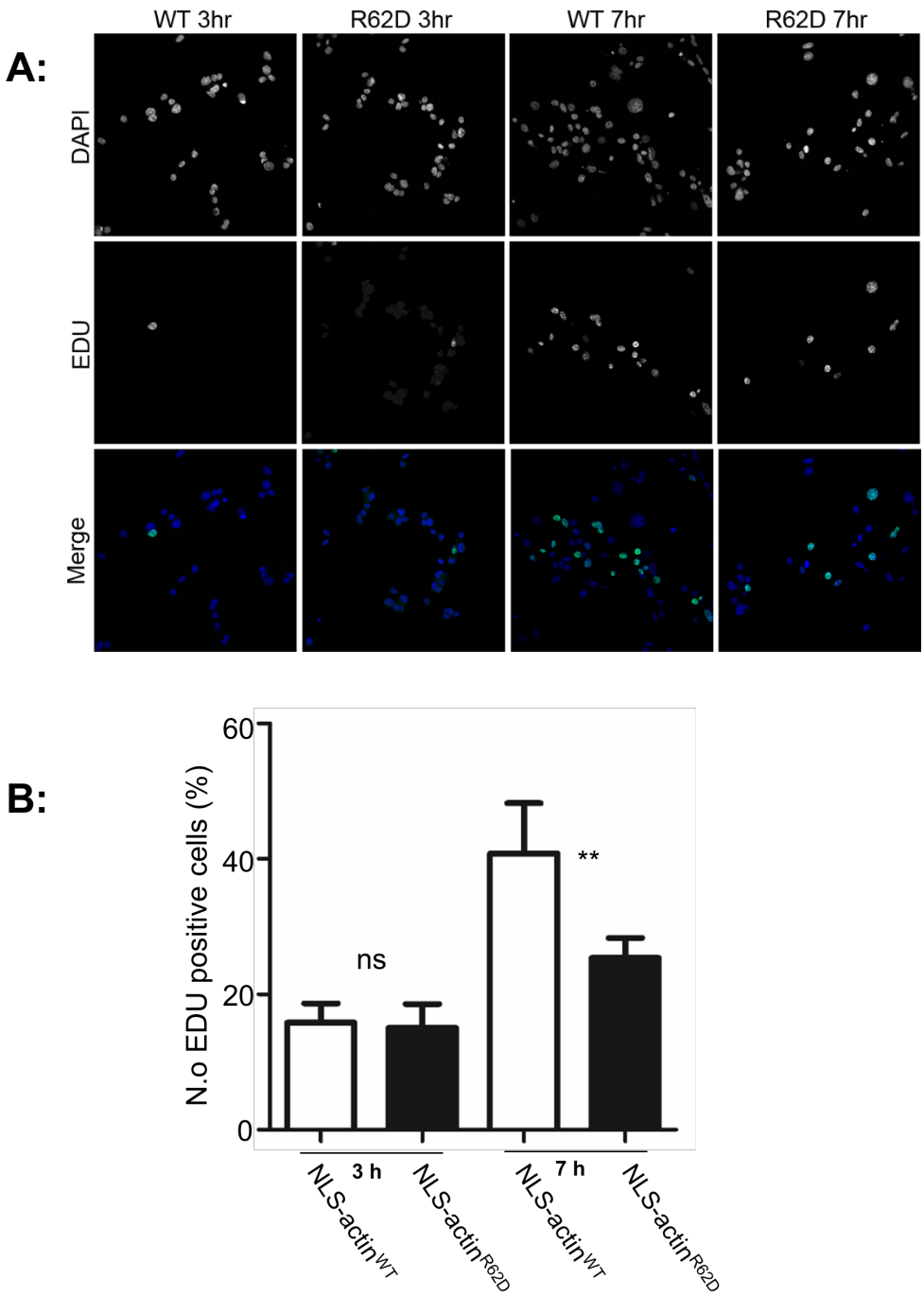

Figure 5-4. Actin mutant cells progress slower through G1

***A**, shows 10x images of cells taken on a confocal microscope. NLS-actin^{WT}/NLS-actin^{R62D} cells were synchronised in mitosis and fixed 3hrs and 7hrs post-mitotic release. 30 minutes before each timepoint, cells were cultured in 5-ethynyl-2'-deoxyuridine (EDU). EDU was detected using click chemistry, via an azide linked fluorophore which specifically interacts with the alkyne group on EDU. Cells were stained with DAPI to count the total number of cells. **B**, shows quantification of the cells shown in A, where the number of EDU positive cells at each timepoint is shown as a percentage of the total number of cells. N>100, three biological repeats. ns indicates p>0.05, ** indicates p<0.005, one-way ANOVA.*

5.2.2.1 Cyclins

The slowed progression through G1 is also supported by Western blotting to detect cyclin expression. In G1, the CDK4/6-Cyclin D complex is necessary for the activation of numerous proteins which facilitate G1 processes. Later in G1, the CDK2-Cyclin E complex is required for progression into S phase. When analysing these cyclins in mid G1 (5 hrs post-mitotic release), Western blotting showed that NLS-actin^{R62D} cells have higher levels of cyclin D, but lower levels of cyclin E (Figure 5-5A-C), suggesting an earlier biochemical state of the cell.

In addition, qPCR was conducted to compare the expression of *cyclin D* and *cyclin E* in post-mitotic cells. This showed that at the same time point in G1 (5 hrs post-mitotic release), NLS-actin^{WT} cells have higher mRNA levels of *cyclin E* and lower levels of *cyclin D* (Figure 5-5D), which is consistent with the protein analysis and again suggests that the NLS-actin^{R62D} cells are less progressed than wild type. However, although this is statistically significant, the difference is not large, and it would be unlikely to have a major effect on protein level. However, given that the Western blotting was consistent with these results, it is possible that the data normalisation to the house keeping gene, *RHOGDI*, which showed variable expression (Figure 5-5E), may explain the discrepancy of this result. Combined, these results suggest that the presumed reduced transcription in the actin mutant cells results in reduced expression of cell cycle regulators, such as cyclin E, which may in turn impact the progression of cells through G1.

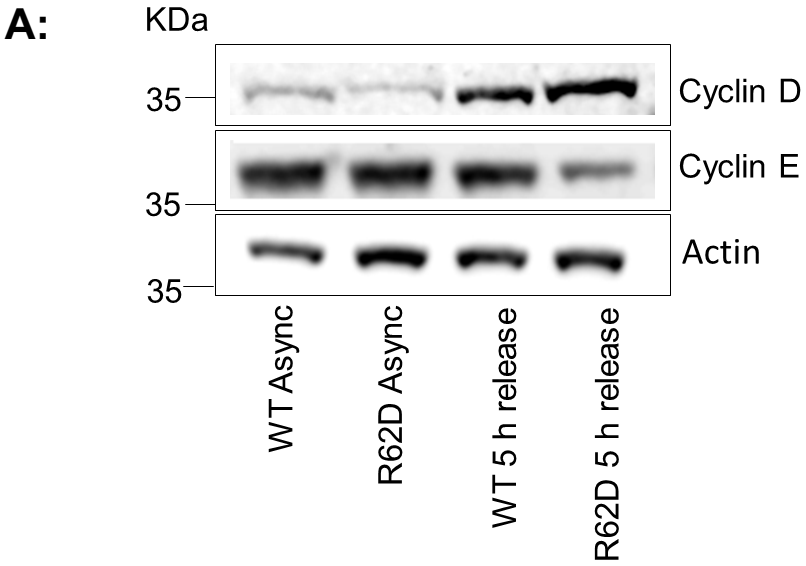
A:
KDa
35
35
35
Cyclin D
Cyclin E
Actin
WT Async
R62D Async
WT 5 h release
R62D 5 h release

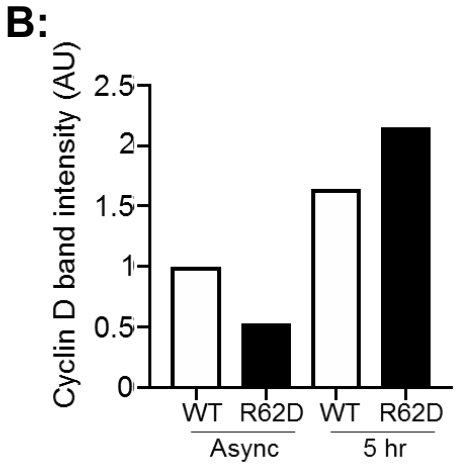
B:
Cyclin D band intensity (AU)
2.5
2
1.5
1
0.5
0
WT R62D WT R62D
Async
5 hr

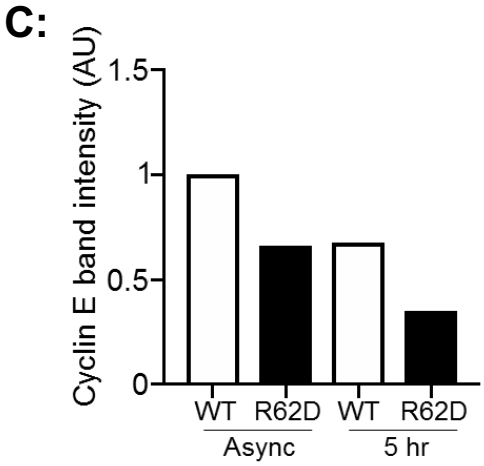
C:
Cyclin E band intensity (AU)
1.5
1
0.5
0
WT R62D WT R62D
Async
5 hr

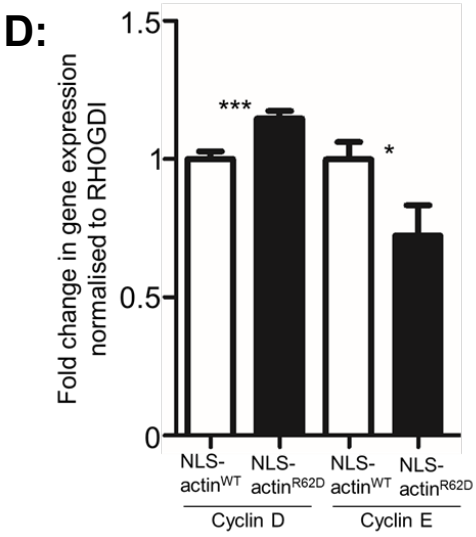
D:
Fold change in gene expression normalised to RHOGDI
1.5
1
0.5
0
***
*
NLS-actinWT
NLS-actinR62D
NLS-actinWT
NLS-actinR62D
Cyclin D
Cyclin E

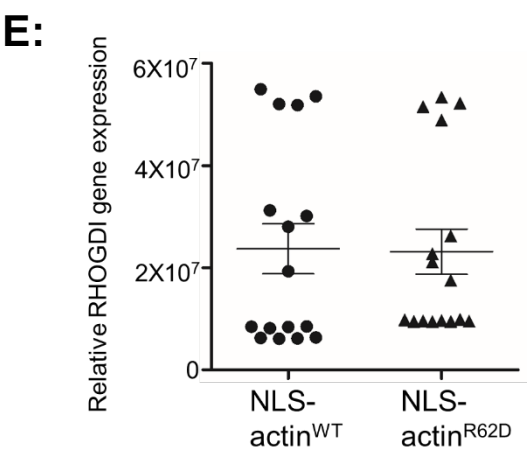
E:
Relative RHOGDI gene expression
6X10^7
4X10^7
2X10^7
0
NLS-actinWT
NLS-actinR62D

Figure 5-5. Actin mutant cells have perturbed cyclin expression

***A**, shows a Western blot of the indicated proteins. Samples were prepared by synchronising NLS-actin^{WT}/NLS-actin^{R62D} cells in mitosis, re-seeding, and then lysis to prepare Western samples 5 hrs post mitotic release. For comparison, samples were also prepared from asynchronous cells. Molecular weights are shown in kDa. **B-C**, shows the quantification of the band intensity (AU) of cyclin D (B) and cyclin E (C), in the Western blot shown in A. Lanes were normalised to the loading, and then normalised to the band intensity of the asynchronous WT. **D**, shows a graph of the fold change in gene expression of the indicated genes. Samples were prepared by synchronising NLS-actin^{WT}/NLS-actin^{R62D} cells in mitosis, re-seeding, and then lysing for RNA extraction 5 hrs post mitotic release. These samples were converted to cDNA and detection was performed in a qPCR machine. Ct values were fitted to a standard curve of known numbers of cDNA molecules. These were normalised to the number of RhoGDI molecules, which was subsequently normalised to show fold change. Results are pooled from four independent repeats performed in quadruplicate. Statistics show results from a Student's t-test, where *** indicates p=0.0009, * indicates p=0.0353. Error bars show SEM. **E**, shows a graph of RHOGDI expression. Samples were prepared as in B but left raw (i.e. no normalisation).*

5.2.2.2 Chromatin de-condensation through G1

In light of these results, experiments were next conducted to determine the chromatin compaction state at the end of G1. Indeed, it is possible that the extended G1 allows time for chromatin to de-condense in the absence of polymerised actin. To visualise and quantify chromatin compaction before entry into S phase, NLS-actin^{WT} and NLS-actin^{R62D} FLIM-cells were blocked at the G1/S boarder using thymidine. These cells were then used to take fluorescence life time measurements. This showed that global chromatin compaction between the two cell types was equivalent prior to entry into S phase (Figure 5-6A). The two cell types also show similar levels of key histone modifications by Western blotting (Figure 5-6B-C), albeit H3S10ph is still elevated in the actin mutant cell line. Combined, these results show that NLS-actin^{R62D} cells largely restore the chromatin landscape in absence of polymerised actin, albeit over a longer time.

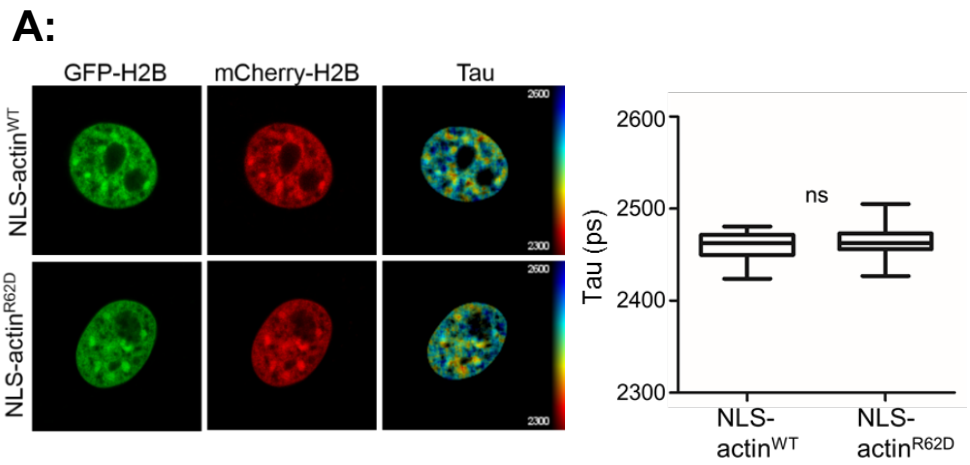
A:
GFP-H2B
mCherry-H2B
Tau
NLS-actinWT
NLS-actinR62D
2600
2300
Tau (ps)
2600
2500
2400
2300
ns
NLS-actinWT
NLS-actinR62D

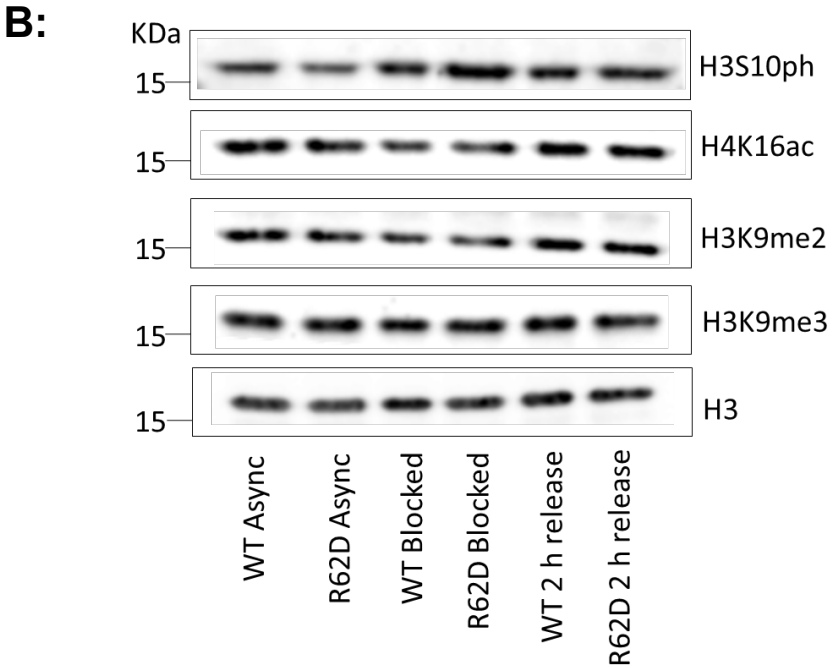
B:
KDa
15
H3S10ph
H4K16ac
H3K9me2
H3K9me3
H3
WT Async
R62D Async
WT Blocked
R62D Blocked
WT 2 h release
R62D 2 h release

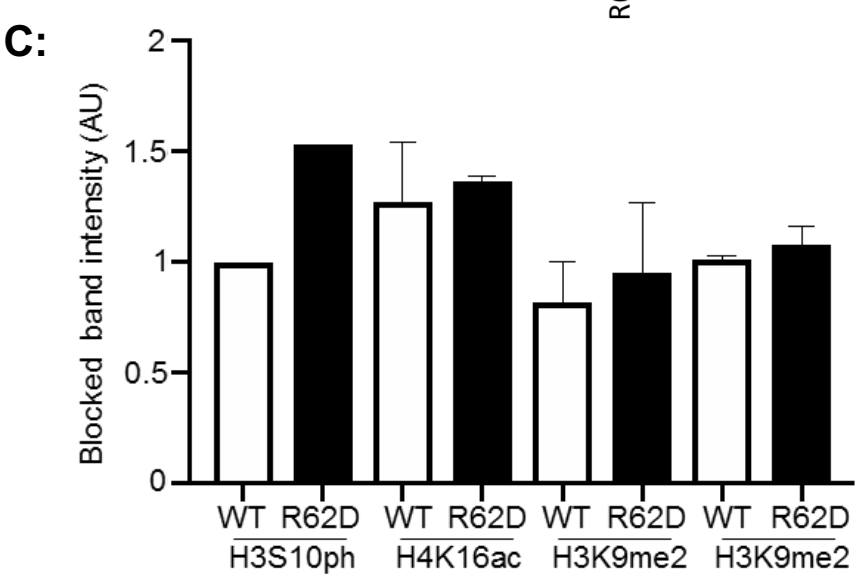
C:
Blocked band intensity (AU)
2
1.5
1
0.5
0
WT R62D
H3S10ph
WT R62D
H4K16ac
WT R62D
H3K9me2
WT R62D
H3K9me2

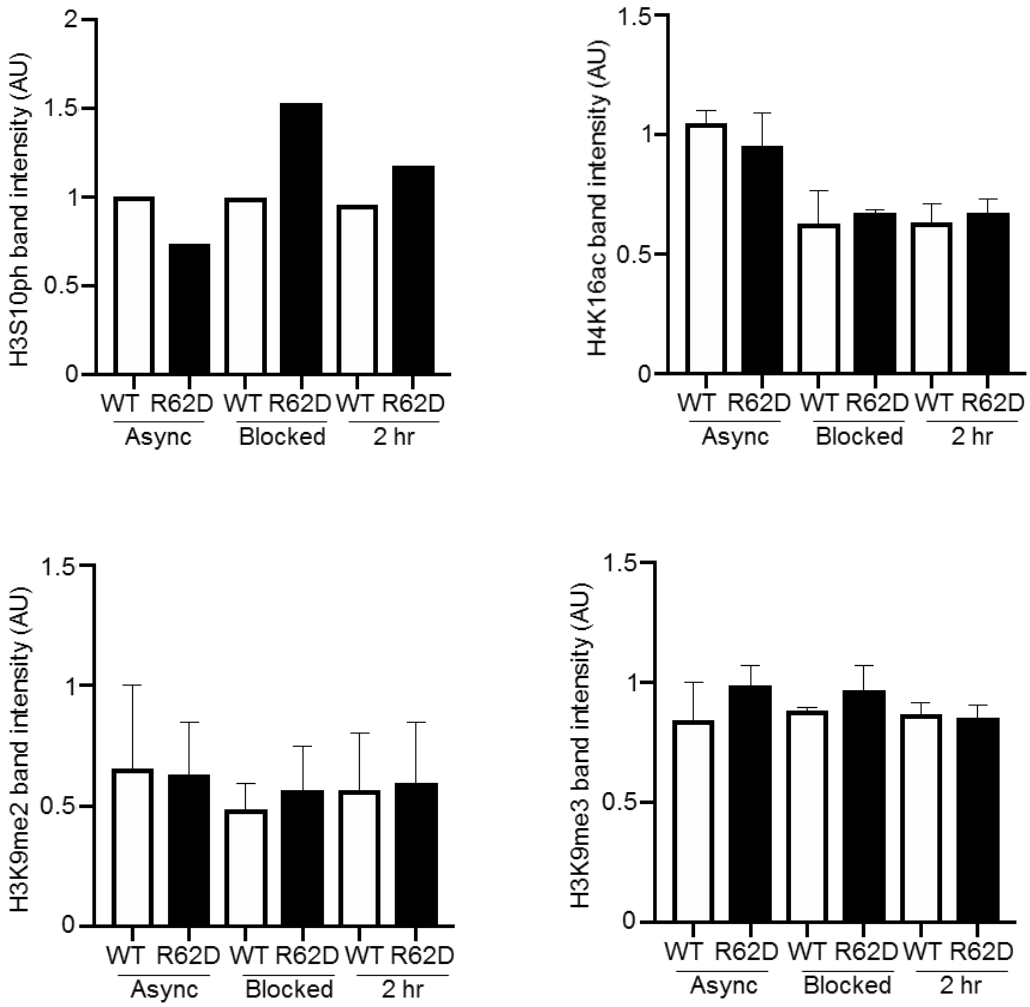

Figure 5-6. Actin mutant cells de-condense chromatin by the entry to S phase

***A left**, shows NIH-3T3^{2FP} cells which were synchronised at the G1/S border, using thymidine block for 18 hrs, before being fixed. GFP and mCherry channels were imaged at 63X on a confocal microscope, channels are indicated. The final panel shows a merge of the fluorescence lifetime and GFP intensity maps. Scale bar shows fluorescence lifetime. **A right**, shows a box plot of the fluorescence lifetime values (Tau) of the cells shown in A. N=18, two biological repeats. ns indicates p>0.05, Student's t-test. **B**, shows a Western blot of the indicated proteins. Molecular weight shown in kDa. Samples were prepared from; asynchronous cells (async), cells blocked at the G1/S border using thymidine (blocked), and cells which after being blocked in thymidine, were washed and released into S phase, and collected 2 hrs later (2 h release). **C**, shows quantification of the band intensity of the indicated proteins, at all time points shown in B. Samples were normalised to the loading, and then each protein was normalised to the WT intensity within each comparison (B top), or the band intensity of the asynchronous WT (B bottom). Data was pooled from two independent repeats, error bars show SEM.*

5.2.3 NLS-actin^{R62D} cells have dysregulated replication timing

Although the NLS-actin^{R62D} successfully de-condense chromatin by the time of entry into S phase, several lines of evidence suggest that S phase dynamics may still be affected. As mentioned in the introduction, this is because the formation of domains and protein complexes required for S phase organise in G1 during the timing decision point (TDP). Thus, it is conceivable that the perturbed organisation of chromatin in early G1 may disrupt these processes, resulting in defective DNA replication.

To examine S phase dynamics, flow cytometry was first used. Because NLS-actin^{R62D} cells have a longer G1, analysing S phase dynamics after mitotic shake off would not be a fair comparison. Thus, the actin plasmids were induced using overnight doxycycline treatment, then cells were blocked the G1/S border using a single thymidine block. Cells were then released into S phase by removal of thymidine and collected every hour for a period of 5 hrs. Propidium iodide (PI) was used to measure DNA content and EDU Click Chemistry was used to detect replicative cells. By plotting these parameters, distinct G1, S and G2 populations were identified and gated. The NLS-actin^{WT} cells showed the expected profile, where they begin replicating DNA 2 hrs post-release from thymidine, and this population gradually increases through the timepoints, until they begin to exit S phase after 5 hrs (Figure 5-7). However, the NLS-actin^{R62D} cells initiate DNA replication only 1 hr after release from thymidine and at the 2 hr time point, when the NLS-actin^{WT} cells have just started replicating, the NLS-actin^{R62D} cells reached their peak in DNA replication (Figure 5-7).

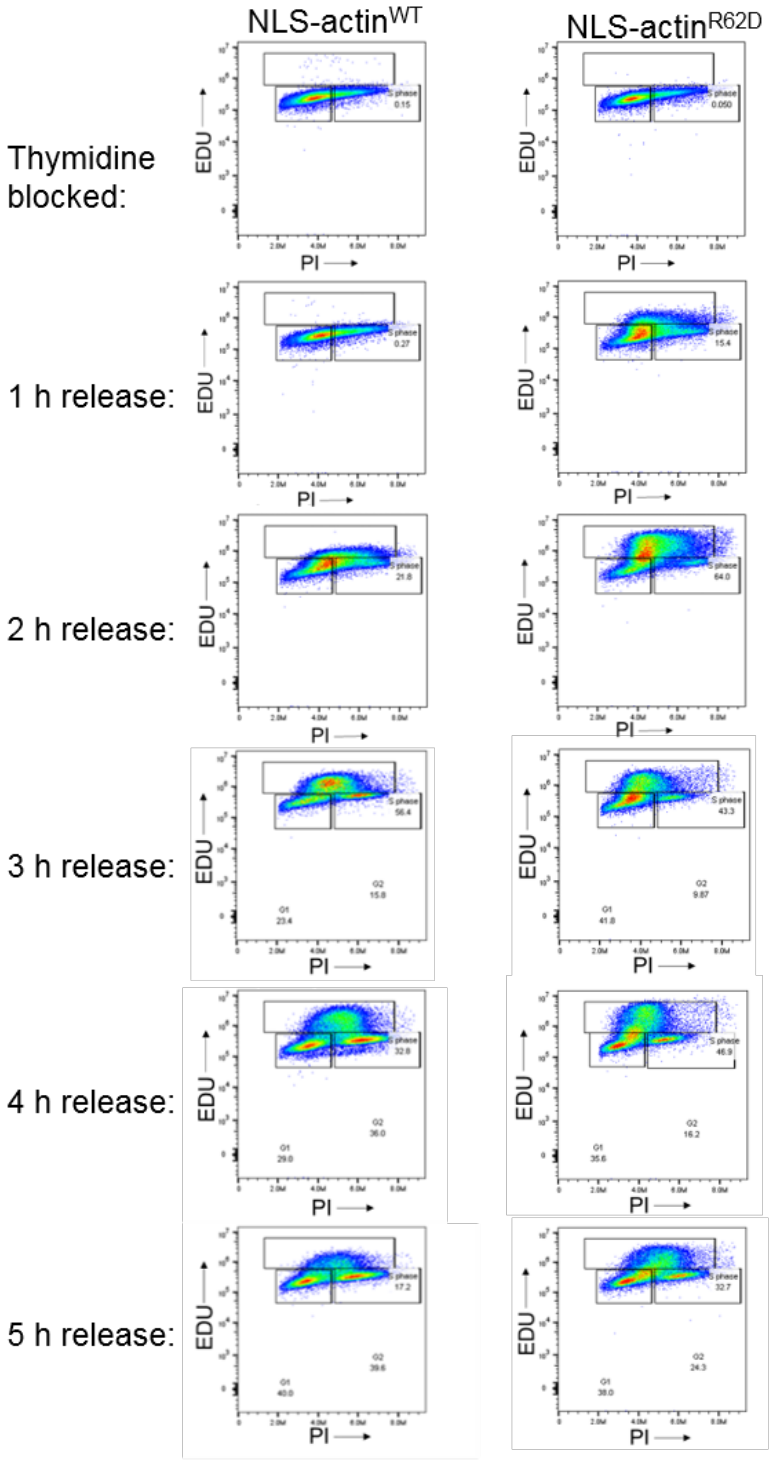

Figure 5-7. Actin mutant cells prematurely enter S phase

This figure shows representative scatter plots acquired using flow cytometry (Novocyte), from three independent repeats. NLS-actin^{WT}/NLS-actin^{R62D} cells were induced by overnight treatment with doxycycline then blocked at the G1/S boarder using thymidine. One sample continued to be cultured in thymidine (thymidine blocked). Other samples were washed and released into S phase, then collected every hour post release. Cells were cultured in 5-ethynyl-2'-deoxyuridine (EDU) 30 minutes before each timepoint. EDU was detected using click chemistry, via an azide linked fluorophore which specifically interacts with the alkyne group on EDU. For DNA content, cells were stained with propidium iodide (PI). Gates on plots show G1 (left), S (top) and G2 (right) phase.

A control experiment was also conducted where the NLS-actin^{WT} and NLS-actin^{R62D} plasmids were only induced when cells reached the G1/S border by thymidine block, and therefore NLS-actin^{R62D} cells did not passage through mitosis in absence of polymerised actin. Cells were then prepared for flow cytometry as described above. In this experiment, the cell types have similar S phase dynamics, and importantly, early initiation of DNA replication was not observed in NLS-actin^{R62D} cells (Figure 5-8). These results highlight that defective replication timing is only induced when the cells go through mitosis in the presence of the actin mutant plasmid. Therefore, the early initiation of DNA replication is not related to S phase specific actin filaments or any other influence of plasmid expression through S phase. Instead, this suggests that it is the changes to chromatin structure in G1, induced through the expression of the mutant actin (chapter 4), that disrupts DNA replication. This will be important later in this chapter.

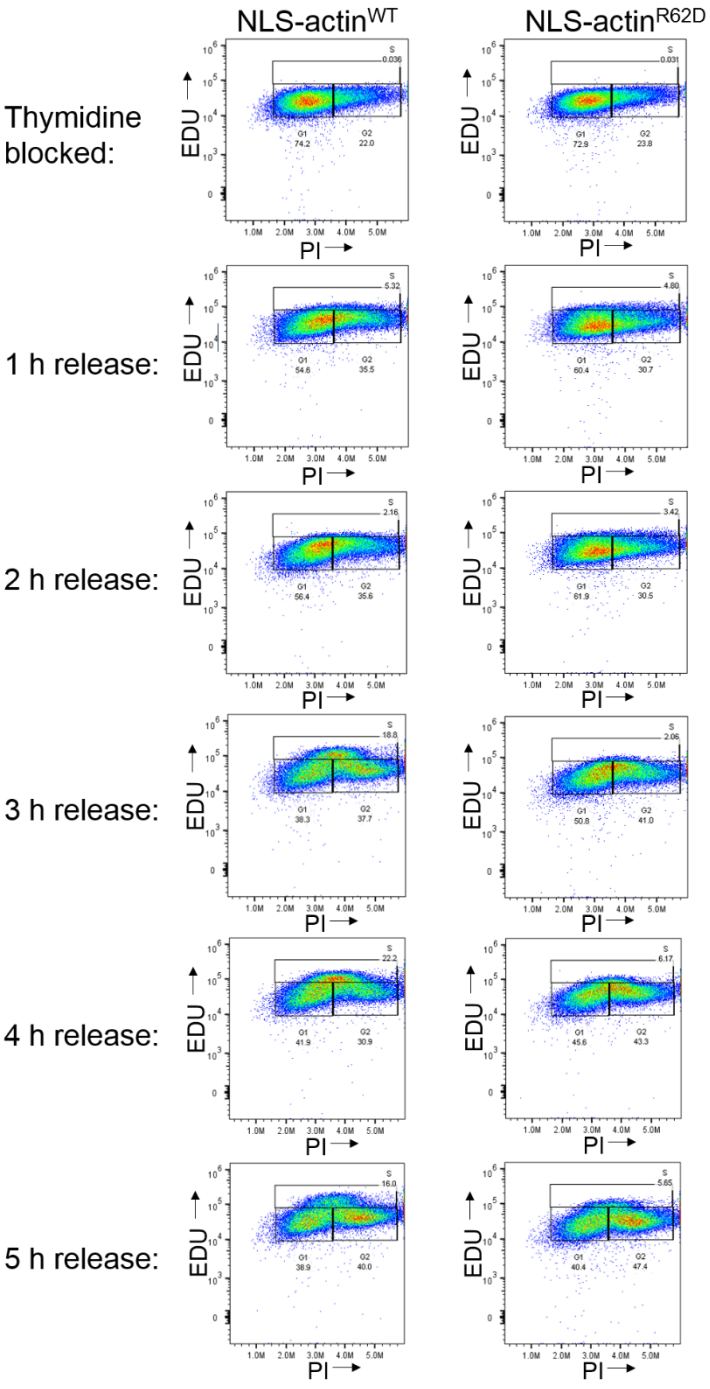

Figure 5-8. Early initiation of DNA replication is linked to mitosis

This figure shows representative scatter plots acquired using flow cytometry (Novocyte), from two independent repeats. NLS-actin^{WT}/NLS-actin^{R62D} cells were blocked at the G1/S boarder using thymidine. After incubation, cells were cultured in doxycycline to induce expression of mutant actin. After 8 hrs, samples were washed and released into S phase by removal of thymidine, then collected every hr post release. One sample continued to be cultured in thymidine (thymidine blocked). Cells were cultured in 5-ethynyl-2'-deoxyuridine (EDU) 30 minutes before each timepoint. EDU was detected using click chemistry, via an azide linked fluorophore which specifically interacts with the alkyne group on Edu. For DNA content, cells were stained with propidium iodide (PI). Gates on plots show G1 (left), S (top) and G2 (right) phase.

To compliment the flow cytometry results, cells were subjected to the same treatments as described above, but instead prepared for immunofluorescence. Here, the stage of S phase was scored based on EDU morphology and categorised into early, mid and late S phase cells (Figure 5-9A). Given the dramatic differences in replication dynamics between the cell types at the 2 hr timepoint, this timepoint was chosen. When scoring cells at this timepoint, it was found that there was a significant reduction in the number of early S phase cells and a significant increase in the number of mid and late S phase cells in the NLS-actin^{R62D} cell population (Figure 5-9B-C). These findings thus confirm defects in replication timing shown by flow cytometry and further, they reveal the early initiation of late replicating regions.

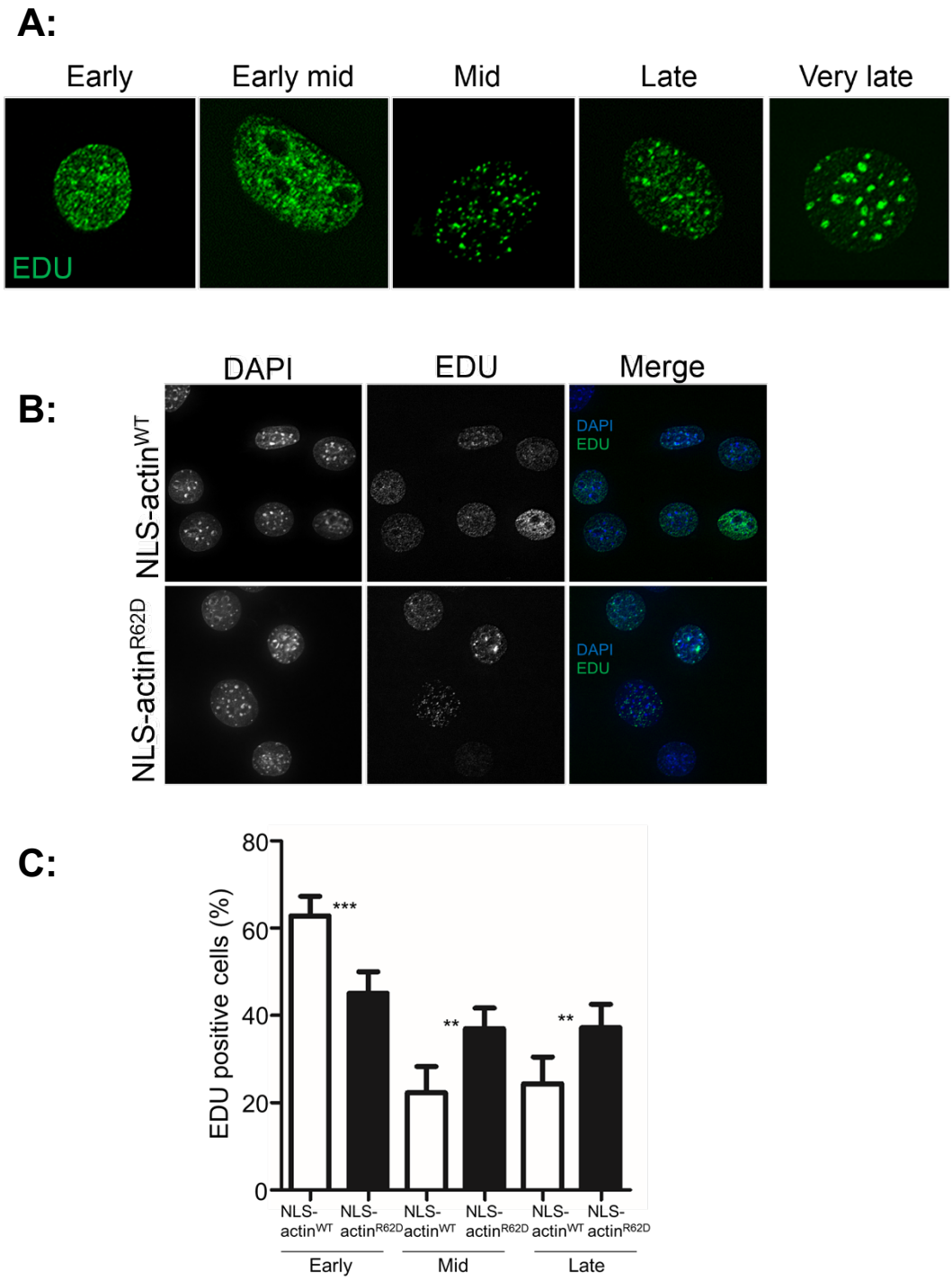

Figure 5-9. Actin mutant cells have early initiation of late replicating origins

This figure shows images of NIH-3T3 S phase cells taken at 60x with a wide field microscope. Cells were cultured in 5-ethynyl-2'-deoxyuridine (EDU) for 30 minutes before being fixed. EDU was detected using click chemistry, via an azide linked fluorophore which specifically interacts with the alkyne group on EDU. For DNA content, cells were stained with DAPI. ***A****, shows representative images of EDU morphology at the indicated phases of S phase.* ***B****, shows images of NLS-actin^{WT}/NLS-actin^{R62D} cells which were fixed 2 hrs after release from thymidine.* ***C****, shows a graph of the quantification of the percentage of cells at each stage of S phase, as seen in B. N>48, two biological repeats. *** indicates p<0.0005, ** indicates p<0.005, one-way ANOVA.*

5.2.4 NLS-actin^{R62D} cells show replication stress

In light of these results and the importance of co-ordinated replication timing in the fidelity of S phase, it could be expected that NLS-actin^{R62D} cells show signs of replication stress. As discussed in the introduction, induction of replication stress activates ATR, which phosphorylates target proteins to induce cell cycle arrest. The phosphorylation of these substrates can therefore be used to measure ATR activation, and within S phase, replication stress. To examine this, cells blocked at the G1/S border using thymidine and were collected 2 hrs after their release (i.e. the S phase population). Western samples were prepared to compare the phosphorylation of ATR specific substrates and the protein level of the ATR interacting protein, ATRIP. As shown (Figure 5-10A-B), the S phase population of NLS-actin^{R62D} cells have increased ATRIP as well as pRPAs33 and pCHK1s345. Given that these phosphorylation events are specific to ATR activity and the S phase population, these results provide evidence for increased ATR activation and thus replication stress in NLS-actin^{R62D} cells.

Another important marker of replication stress is the phosphorylation of histone H2AX (forming γH2AX), which rapidly form foci during replication stress. To visualise these foci, immunofluorescence and image analysis was used to count the number of these foci in cells released into S phase. As shown (Figure 5-10C) the number of γH2AX foci was significantly higher in the NLS-actin^{R62D} cells, providing further evidence for replication stress. Importantly, this phosphorylation is not ATR specific, as it can also be induced by ATM. However, ATM phosphorylates this residue primarily in response to DNA damage, not replication stress. Although severe replication stress can lead to DNA damage, ATR acts to prevent this. Thus, phosphorylation of H2AX in S phase is largely through the action of ATR (Marechal and Zou, 2013). It therefore follows that if the increase in γH2AX in S phase is attributed to the DNA damage specific ATM phosphorylations, then this would likely be evident before the cells enter S phase. γH2AX intensity in early G1 cells was therefore measured, where results showed no significant difference (Figure 5-10D). Therefore, this suggests that NLS-actin^{R62D} cells do not have increased DNA damage but do have an S phase specific increase in H2AX phosphorylation, providing further evidence of replication stress in these cells.

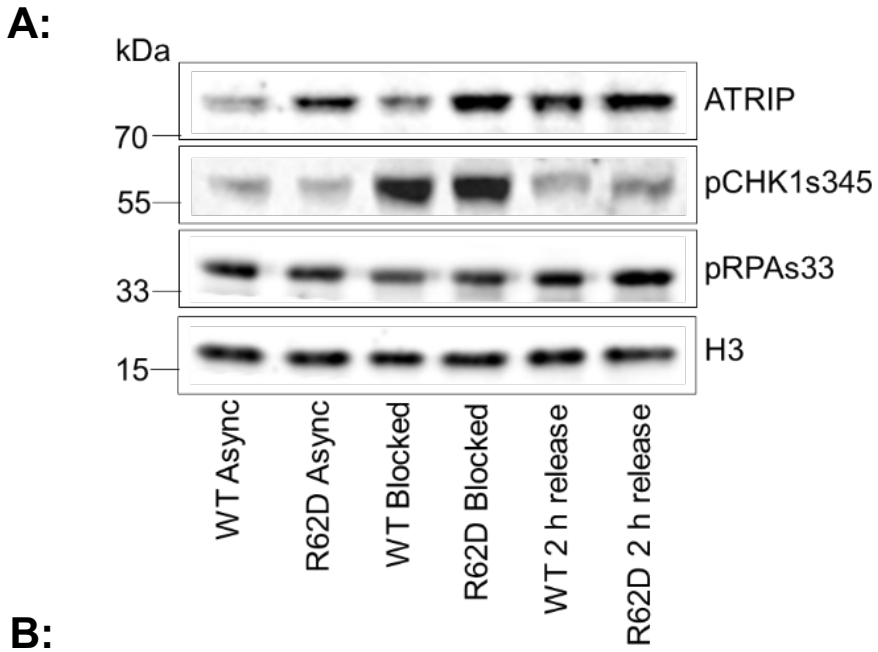
A:
kDa
70
55
33
15
ATRIP
pCHK1s345
pRPAs33
H3
WT Async
R62D Async
WT Blocked
R62D Blocked
WT 2 h release
R62D 2 h release

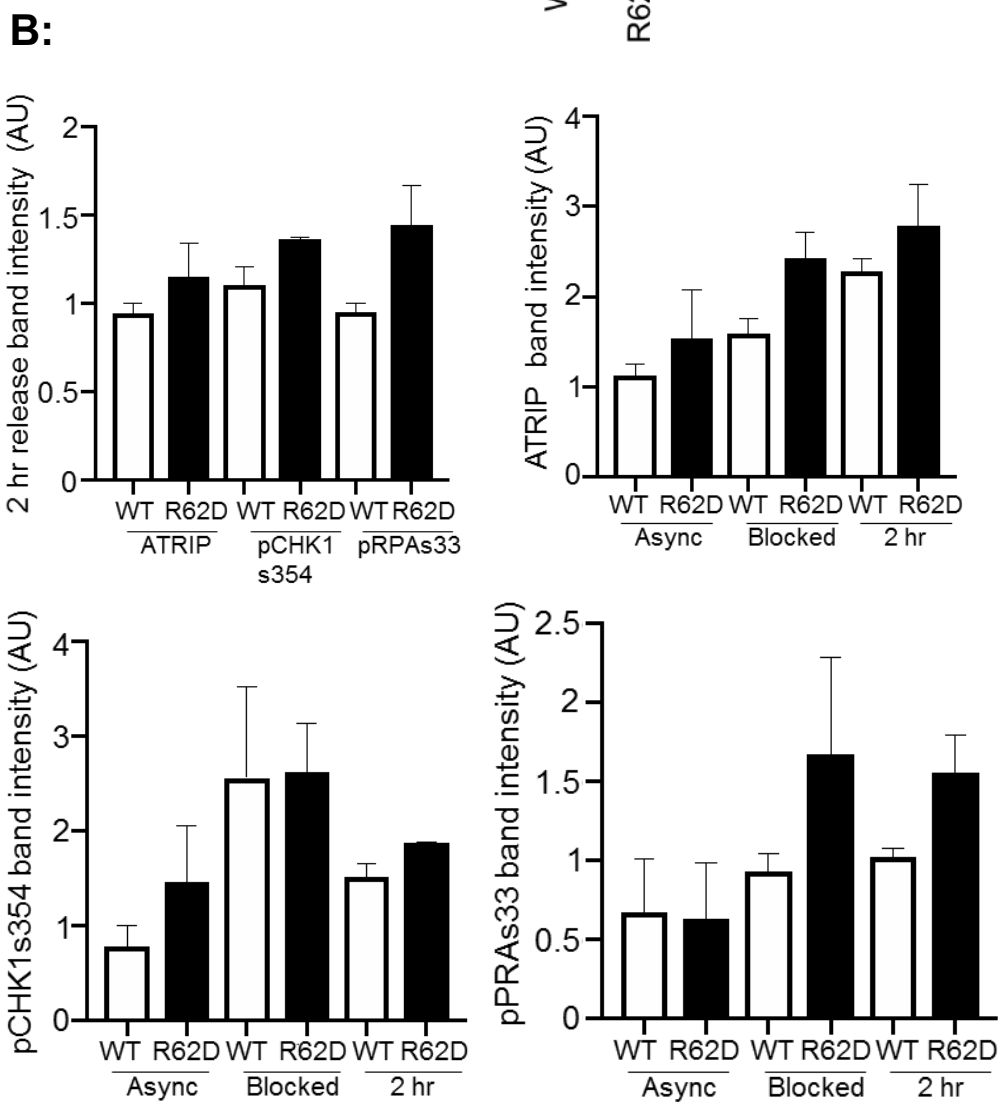
B:
2 hr release band intensity (AU)
WT R62D WT R62D WT R62D
ATRIP
pCHK1 s354
pRPAs33
ATRIP band intensity (AU)
Async
Blocked
2 hr
pCHK1s354 band intensity (AU)
pPRAs33 band intensity (AU)

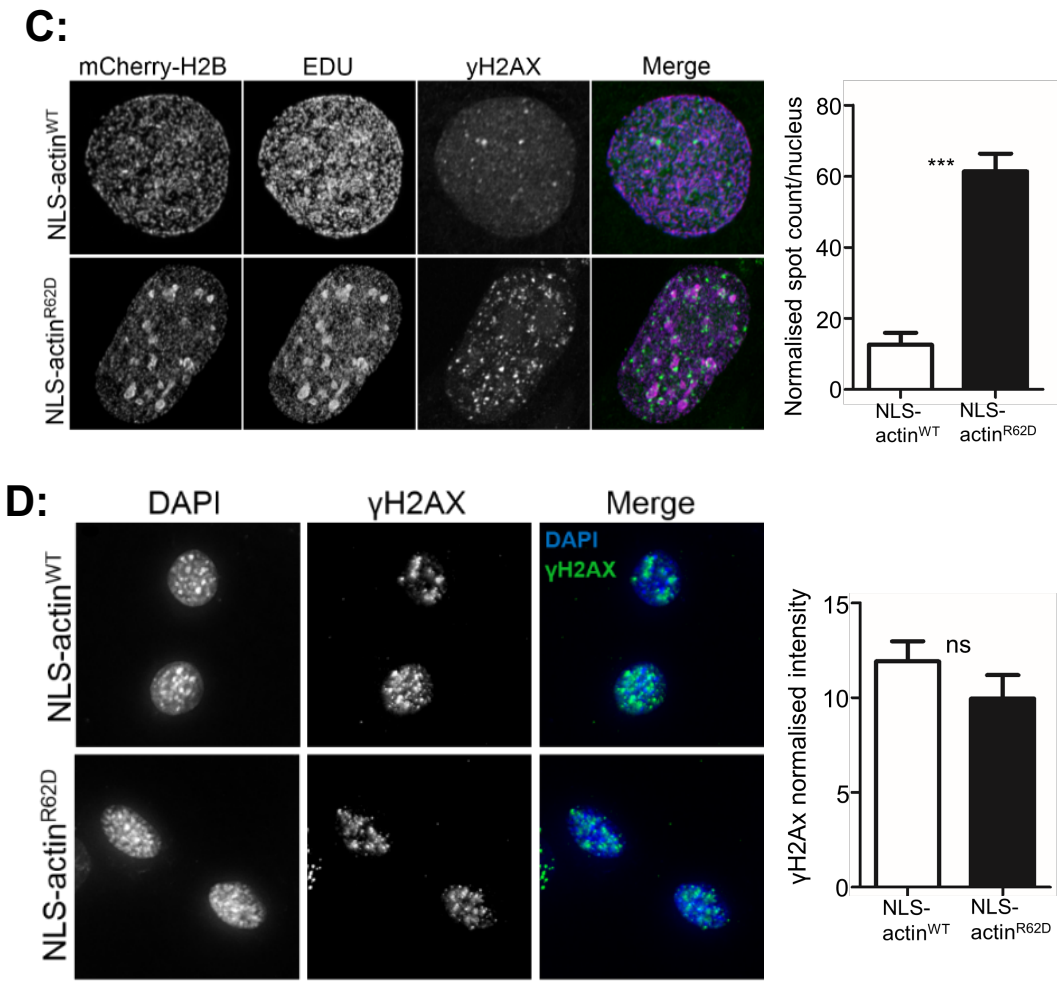

Figure 5-10. Actin mutant cells show replication stress

***A**, shows a Western blot of the indicated proteins. Molecular weights are shown in kDa. Western samples were prepared from NLS-actin^{WT}/NLS-actin^{R62D} cells which were asynchronous (async), blocked at the G1/S border using thymidine (blocked) or released into S phase and collected 2 hrs post-release (2 h release). **B**, shows quantification of the indicated proteins in the Western blot seen in A. Samples were normalised to the loading control, then normalised to the WT of each comparison (B top left), or the asynchronous WT.. Data was pooled from two independent repeats, error bars show SEM. **C left**, shows images of NLS-actin^{WT}/NLS-actin^{R62D} cells expressing mCherry H2B, taken with at 63X with a confocal microscope using HyVolution software. Cells were released from thymidine block and fixed 2 hrs later. Cells were cultured in 5-ethynyl-2'-deoxyuridine (EDU) for 30 minutes before this timepoint. EDU was detected using click chemistry, via an azide linked fluorophore which specifically interacts with the alkyne group on EDU. Cells were also stained with γH2AX. **C right**, shows quantification of the number of γH2AX foci in the cells shown in B. N>60, two biological repeats. *** indicates p<0.0005, Student's t-test. **D**, shows images of post-mitotic NLS-actin^{WT}/NLS-actin^{R62D} cells taken at 60x with a wide field microscope. Cells were fixed and stained with DAPI and γH2AX. **D right**, shows the quantification of γH2AX fluorescent intensity. DAPI signal was used to draw around the nucleus and measure nuclear area. The intensity of the indicated channels was then measured in this region and normalised to the nuclear area. N=60, two biological repeats. ns indicates p>0.05, Student's t-test.*

5.2.5 NLS-actin^{R62D} post-mitotic cells show perturbations in replication machinery

The results in this chapter provide evidence that failure to polymerise actin after cell division perturbs replication timing, resulting in replication stress. Given that the actin mutant cells have increased chromatin compaction during the period when the replication timing program is established (Dimitrova and Gilbert, 1999), it is conceivable that this would interfere with the organisation of this program. Indeed, the first step in forming a replication origin is origin licencing by the ORC complex, which binds H4K20me2 (Tardat et al., 2010). Given the perturbations in histone modifications in the previous chapter, H4K20me2 and the precursor of this methylation, H4K20me1, were examined by immunofluorescence. The results showed that NLS-actin^{R62D} cells had a significant reduction in both these modifications (Figure 5-11A). This suggests that origin licencing may be perturbed in the actin mutant cells. To test this, MCM7, a member of the MCM helicase complex which is loaded onto chromatin during origin licencing, was imaged by light microscopy. Again, the results showed a significant reduction in the nuclear levels of this protein in the actin mutant cells (Figure 5-11B). This further suggests defects in origin licencing.

Because licenced origins are the site at which the pre-replication complex forms, these data suggest that the formation of this complex may also be affected in the actin mutant cells. Indeed, CDC45, a component of the pre-replication complex, is also significantly reduced in the actin mutant cells (Figure 5-11C). Therefore, these results suggest that the increase in chromatin condensation and defects in the epigenetic landscape observed when nuclear F-actin is inhibited after mitosis (chapter 4), impairs the formation of the pre-replication complex. However, one cannot exclude the possibility that these results are a consequence of the reduced transcription in the actin mutant cells; indeed, the expression of these proteins increases during G1. These results may therefore in part explain the spatial-temporal defects in DNA replication.

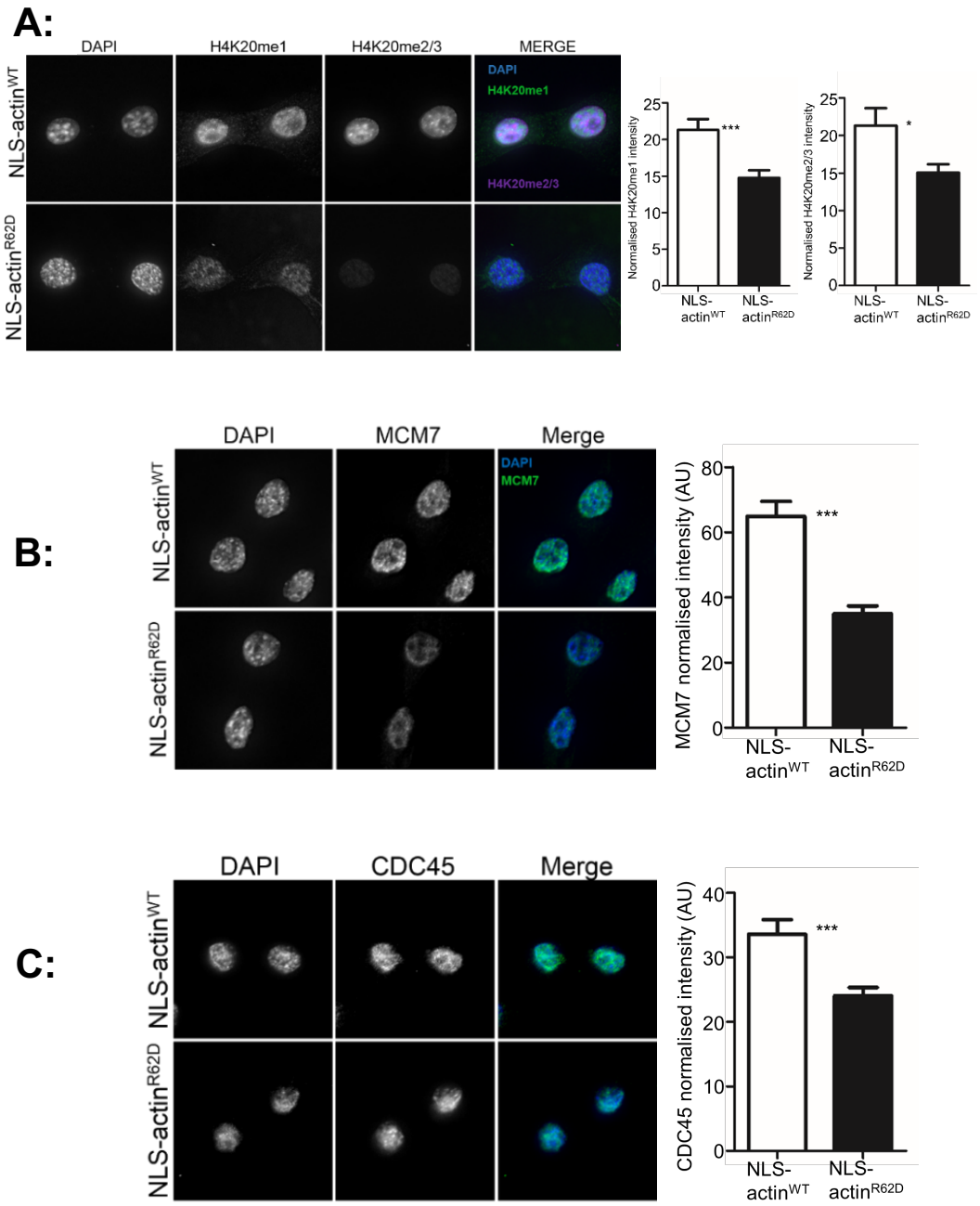

Figure 5-11. Inhibition of nuclear actin polymerisation after mitosis impairs the formation of the pre-replication complex

*This figure (**A-C**) shows images of NLS-actin^{WT}/NLS-actin^{R62D} cells which were taken at 60x with a wide field microscope. Cells were synchronised in mitosis and fixed 1 hr later. Cells were stained with DAPI and the indicated antibodies; H4K20me2/3 (A), MCM7 (B), CDC45 (C). Graphs show the quantification of fluorescent intensity. DAPI signal was used to draw around the nucleus and measure nuclear area. The intensity of the indicated channels was then measured in this region and normalised to the nuclear area. In all cases, N>100, from three independent repeats. * indicates p=0.0143, *** indicates p<0.0001, students ttest.*

5.2.5.1 Chromatin organisation

It is likely that the increase in condensed chromatin in the actin mutant cells affects the replication timing program by delaying the establishment of high order chromatin structure, given that TADs overlap with replication timing domains (Pope et al., 2014). This organisation is not only important for the separation of heterochromatin and euchromatin, which replicate at different times in S phase, but also because it effects the localisation of regulatory proteins. Here an important protein that links chromatin architecture to replication timing is RIF1, which binds heterochromatin to ensure that it is replicated late in S phase. Expression of mutant actin after cell division resembles RIF1 depletion, which results in disruption to the replication timing program. It was therefore speculated that the perturbed chromatin landscape in the actin mutant cells may affect RIF1 binding, and the formation of RIF1-associated domains. To test this, RIF1 was imaged by immunofluorescence after pre-extraction to remove non-chromatin bound RIF1. Indeed, RIF1 nuclear intensity was significantly reduced in the actin mutant cells (Figure 5-11A-B). Thus, this may explain the early replication of late replicating regions that was observed.

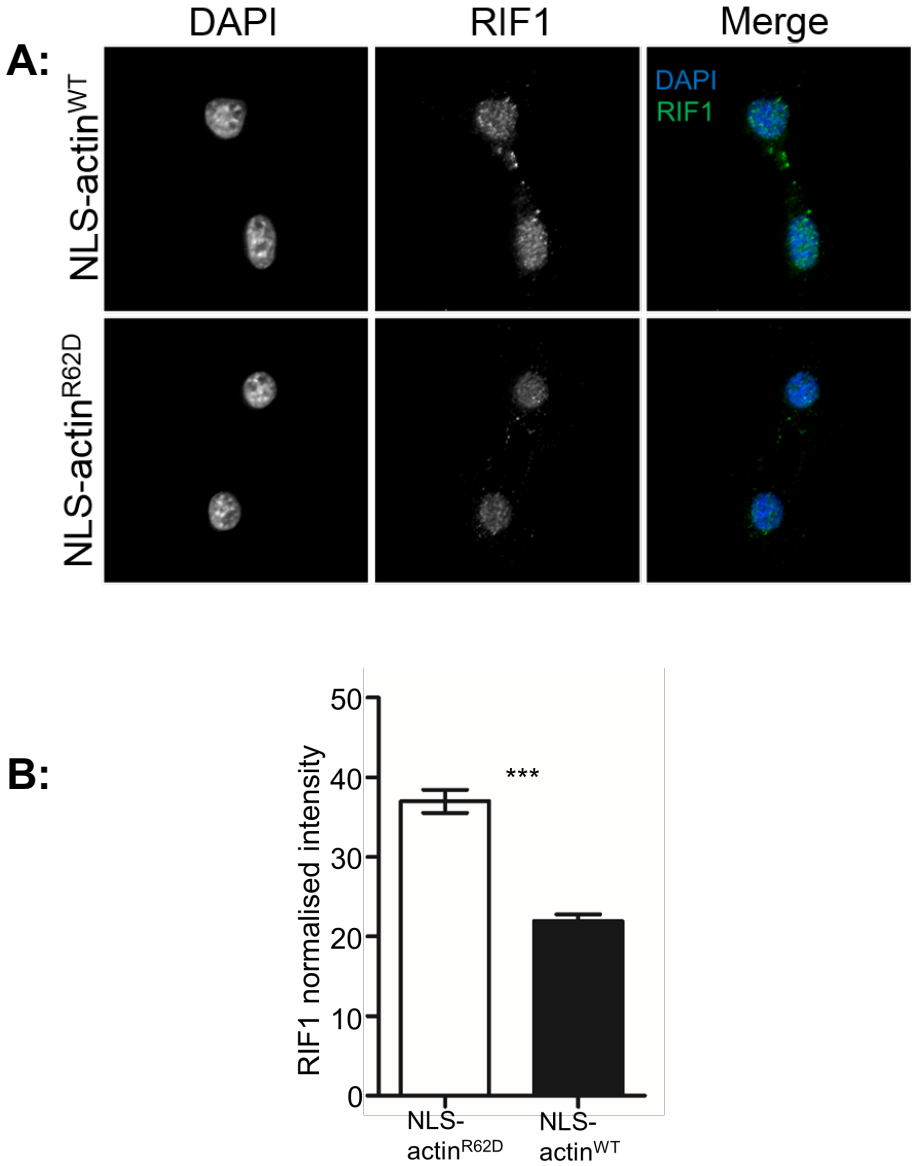

Figure 5-12. Actin mutant cells have reduced chromatin bound RIF1

***A**, shows images of NLS-actin^{WT}/NLS-actin^{R62D} cells which were taken at 60x with a wide field microscope. Cells were synchronised in mitosis. 1 hr after release, cells were incubated with pre-extraction buffer (CSK) and fixed. Cells were stained with DAPI RIF1. **B**, shows a graph of RIF1 fluorescence intensity of the cells in A. DAPI signal was used to draw around the nucleus and measure nuclear area. The intensity of RIF1 was then measured in this region and normalised to the nuclear area. N=80, from three independent repeats. *** indicates p<0.0001, Student's t-test.*

5.3 Discussion

The results in this chapter show that after cell division, polymerised actin is required for the timely reactivation of transcription and the fidelity of DNA replication. Thus, inhibition of actin filament formation reduces transcription in G1 and delays entry into S phase. These results also suggest that the alterations to the chromatin landscape, caused by inhibiting the formation of nuclear actin filaments after cell division, affects the formation of domains and complexes which regulate the spatial-temporal control of DNA replication. Subsequently, DNA replication timing becomes dysregulated and cells encounter replication stress. It is therefore tempting to speculate that nuclear actin polymerisation protects genome stability.

The reduction in RNAPII phosphorylation at serine 2, but not at serine 5, suggests that transcriptional elongation is reduced in cells unable to polymerise actin after cell division, whereas transcriptional initiation is not. Given that transcription is generally not compatible with condensed chromatin, the increased chromatin compaction in the actin mutant cells likely explains this result. It is therefore likely that overall mRNA transcription is reduced in these cells, but this will need to be tested by other methods, such as GRO-seq, which involves the sequencing of newly transcribed RNA molecules. Importantly, these changes in transcription do not explain why NLS-actin^{R62D} cells fail to de-condense chromatin, as global inhibition of transcription does not delay nuclear expansion or chromatin de-condensation. However, these results may explain why these cells progress slower through G1. Indeed, transcription increases dramatically as cells exit mitosis, and is required for the expression of cell cycle regulators that promote progress through the cell cycle (Palozola et al., 2017). Given that cyclin E expression is important for the G1-S transition (Ohtani et al., 1995), and it is also reduced at the protein level in NLS-actin^{R62D} cells, reduced expression of these regulators due to increased chromatin compaction may explain the change in cell cycle phase distribution. Alternatively, the slowed G1 phase may not be a result of decreased transcription, and instead be caused the cell finding alterative mechanisms to de-condense chromatin in absence of nuclear actin. Indeed, chromatin appears to be decondensed by the time NLS-actin^{R62D} cells enter S phase.

Upon entry into S phase, NLS-actin^{R62D} cells prematurely initiate DNA replication. In fact, 2 hrs after thymidine release, when the NLS-actin^{WT} cells have just started replicating, NLS-actin^{R62D} cells have reached their peak in DNA replication. Further, visualisation of EDU foci at this time point revealed that the flow cytometry data is not simply showing the early initiation of a normal replication timing program; NLS-actin^{R62D} cells were replicating early mid and late regions at the same time, whereas the NLS-actin^{WT} cells were largely replicating early replication domains. The deregulation of replication timing was not observed when the mutant actin was expressed after cells exit mitosis. Therefore, this suggests that the early initiation of DNA replication in NLS-actin^{R62D} cells is a result of alterations that occur after cell division. Indeed, euchromatin is generally replicated early during DNA replication, whereas heterochromatin is replicated late (Kim et al., 2003; Lima-de-Faria and Jaworska, 1968), highlighting the importance of chromatin structure on DNA replication. Therefore, alterations to this organisation, for example caused by increased chromatin compaction, may affect the ability to separate the activation of these domains. To investigate this possibility, repli-seq (Marchal et al., 2018) could be used to identify regions which prematurely replicate in the actin mutant cells. Subsequently, the location of these regions after cell division could be determined using GFP-dCas9 CRISPR or FISH and compared between the two cell types. If the hypothesis is correct, regions which are inappropriately replicated in S phase, will also be spatially disorganised in G1. Further, this spatial mis organisation may affect the binding of RIF1 to these regions, which was reduced in NLS-actin^{R62D} cells. In the absence of RIF1 binding, activation of these origins would not be repressed, thus these domains would replicate early in S phase.

The results in this chapter also showed that the licencing of DNA origins was perturbed in NLS-actin^{R62D} cells. This is again likely due to the perturbed G1 chromatin environment. Indeed, chapter 4 identified a potential role for nuclear F-actin in chromatin re-modelling, and results in this chapter further suggest this, showing that H4K20 methylation was also reduced in cells unable to polymerise nuclear actin. This may in turn have an effect on the later stages of DNA replication, as the ORC complex interacts with this modification (Kuo et al., 2012), which is required for the recruitment of licencing factors such as CDT1 and MCM7, as well as pre-replication components. Thus, the reduced H4K20me1/2 in NLS-actin^{R62D} cells could have a consequential effect on the

other parts of this pathway. This may in turn effect DNA replication, by affecting the number and distribution of replication origins.

The flow cytometry data also showed that although NLS-actin^{R62D} cells enter DNA replication quicker, they appear to pause in S phase and ultimately progress slower through this phase. This profile suggests that the cells are experiencing replication stress, which was confirmed by the results showing increased activation of the ATR pathway in NLS-actin^{R62D} (Flynn and Zou, 2011). It is therefore expected that this replication stress is due to the defective replication timing program. Future experiments would involve analysis of DNA fibres, which are extracted from cells that have been by pulse labelled with fluorescent nucleotides, to gain insight into replication dynamics and stalled replication forks (Merrick et al., 2004). In addition, the dysregulation of DNA replication could result in collisions between RNA and DNA polymerases, and the production of DNA-RNA hybrids that induce replication stress (Helmrich et al., 2011). Such structures require cleavage by the enzyme RNase H (Gomez-Gonzalez et al., 2009), which may therefore be elevated in in NLS-actin^{R62D} cells. The successful activation and cell cycle arrest induced by the ATR pathway suggests that errors in DNA replication may be repaired. However, it is possible that some regions remain un-replicated or errors may not be detected and escape cell cycle checkpoints. If this is the case, mutations may be propagated to daughter cells during the next mitosis, thus making nuclear actin polymerisation a factor which is important for genome stability and therefore health and disease.

Recent work has also shown that polymerisation of nuclear actin after cell division is important for DNA replication (Parisis et al., 2017). This showed that inhibition of nuclear actin polymerisation after cell division reduced S phase progression and induced γH2AX foci in both mammalian cells and a Xenopus system, similar to what has been observed in this chapter. However, Parisis et al explained these findings as mis-organisation of NPCs, which affects nuclear transport and therefore DNA replication. It cannot be excluded that nuclear transport is altered in NLS-actin^{R62D} cells, and this may affect DNA replication, but no evidence for this is provided in this thesis. The discrepancy between these studies may be explained by the different methods which were used to inhibit actin filament formation; indeed, Parisis et al used pharmacological inhibitors which affect both nuclear and cytoplasmic actin, whereas this thesis used genetic inhibition to specifically interfere with nuclear F-actin formation.

Chapter 6 : General discussion

The work in this thesis developed from observations in Robert Grosse's laboratory, which identified the emergence of nuclear actin filaments after cell division. Given the appearance of these filaments during a time when the nucleus is expanding, and chromatin is de-condensing, this thesis aimed to understand the role for nuclear F-actin in these processes. As such, several ways of measuring chromatin compaction and nuclear structure were developed, most notably a chromatin fluorescence lifetime imaging approach (Chapter 3). Using these methods, and genetic manipulation to inhibit nuclear F-actin formation, it was found that failure to polymerise nuclear actin after cell division results in cells with smaller nuclei, and increased chromatin compaction. This is the first evidence that nuclear F-actin can modulate global chromatin structure and provides a potential mechanism for how the nucleus expands after cell division (Chapter 4). Given the requirement for chromatin de-condensation in processes such as transcription and DNA replication, it was hypothesised that the increase in chromatin compaction when nuclear F-actin is inhibited may affect these processes. Indeed, the results in Chapter 5 show that the emergence of nuclear F-actin after cell division is required for the timely co-ordination of DNA replication. This is in agreement with previous reports showing that the DNA replication timing program is established in early G1 (Dimitrova and Gilbert, 1999). Specifically, the results suggest that failure to organise the genome after cell division affects the binding of DNA replication factors to chromatin, resulting in dysregulated DNA replication and replication stress. Failure to repair damage induced during DNA replication can potentially result in the propagation of errors to daughter cells. Combined, the results in this thesis suggest a model where nuclear F-actin re-organises the nucleus and protects genome integrity (Figure 6-1).

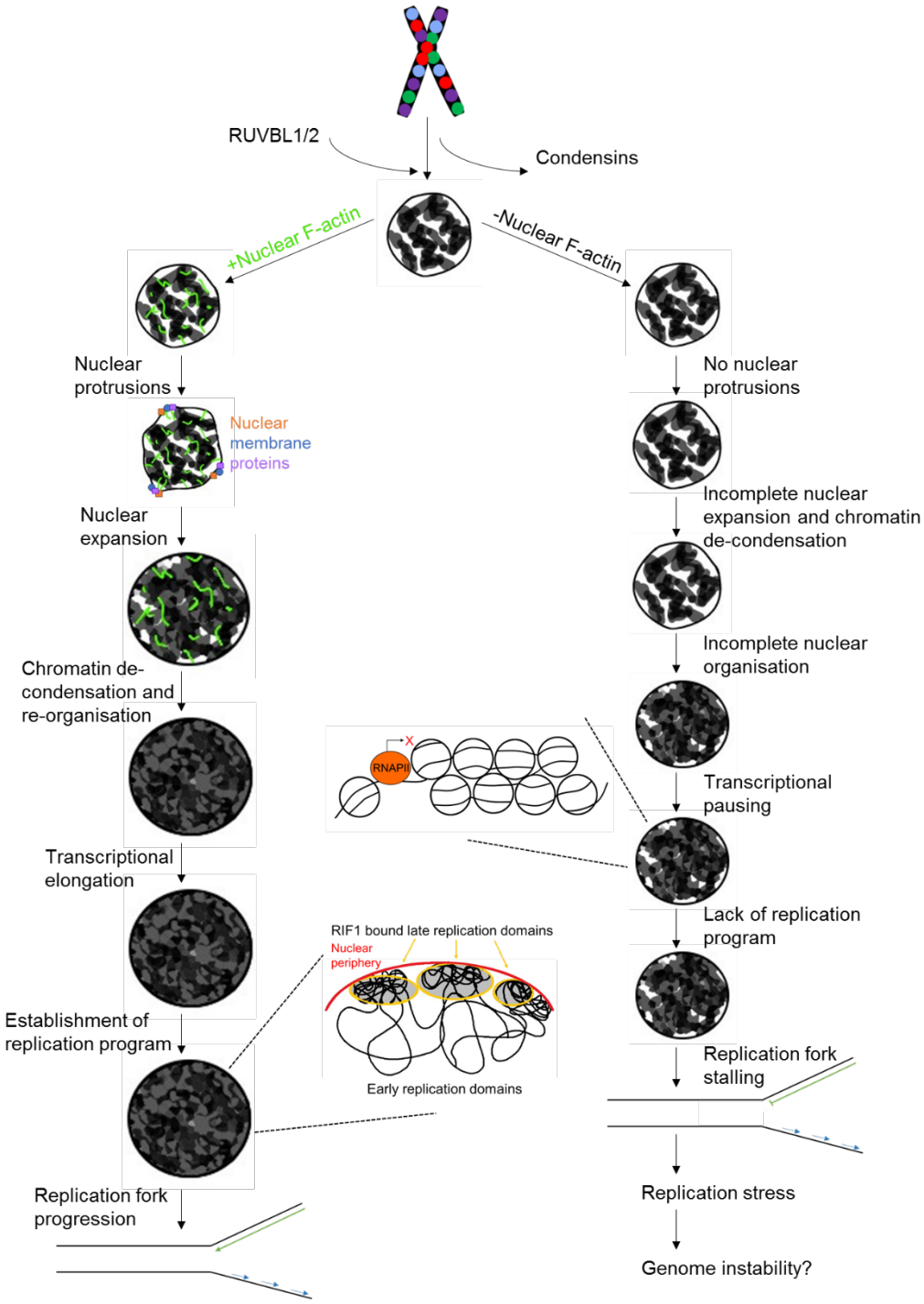
RUVBL1/2
Condensins
+Nuclear F-actin
-Nuclear F-actin
Nuclear protrusions
No nuclear protrusions
Nuclear membrane proteins
Nuclear expansion
Incomplete nuclear expansion and chromatin de-condensation
Incomplete nuclear organisation
Chromatin de-condensation and re-organisation
RNAPII
Transcriptional pausing
Transcriptional elongation
Lack of replication program
RIF1 bound late replication domains
Nuclear periphery
Establishment of replication program
Replication fork stalling
Early replication domains
Replication fork progression
Replication stress
Genome instability?

Figure 6-1. Thesis model.

This figure shows a model which summarises the results within this thesis. After mitosis, the nuclear envelope reforms around chromosomes, which are partially de-condensed by the removal of condensins and the expression of proteins such as RUVBL1/2. ***Left*** *shows the emergence of nuclear F-actin (green), which pushes on the nuclear membrane, forming nuclear protrusions which may increase the incorporation of nuclear membrane proteins (orange/green/purple) into the nuclear membrane. This results in nuclear expansion. These filaments also promote the de-condensation and re-organisation of chromatin, which provides accessibility to RNAPII, resulting in transcriptional re-activation. In addition, this organisation provides a basis for the separation of replication timing domains, which are bound by proteins such as RIF1 to establish a replication timing program. This ensures the fidelity of DNA replication.* ***Right*** *shows the sequence of events in absence of nuclear F-actin. Nuclear protrusions are not produced, leading to reduced nuclear expansion. Chromatin is also not fully de-condensed, which causes obstruction to the progression of RNAPII and an overall reduction in transcriptional elongation. Failure to de-condense chromatin likely affects the establishment of replication timing domains, reducing the binding of RIF1 to chromatin, resulting in a disrupted replication timing program. Thus, when cells enter S phase, origins fire simultaneously, resulting in replication stress, which if unrepaired, can result in genome instability.*

In light of this model, methods which visualise chromosomal translocations, such as karyotyping and chromosome paints, or DNA sequencing, could be used to identify mutations which arise in cells unable to polymerise nuclear actin. It thus follows that future experiments may reveal that failure to polymerise nuclear actin after cell division could be a source of mutations which are observed in disease. Indeed, changes in gene expression are driving factors during the transformation of a normal to tumour cell. Research investigating the mechanisms which promote this altered transcriptional landscape has largely focused on mutations which evoke the activation of proto-oncogenes (Anderson et al., 1992), and the silencing of tumour suppressor genes (Klein, 1988; Levine et al., 1991). More recent work has shown that mutations in non-coding DNA and genes which regulate the epigenome are also common. These changes also result in altered gene expression, for example by the activation of DNA methyltransfereses (Samudio-Ruiz and Hudson, 2012) as well as mutation of enhancer sequences (Weinhold et al., 2014) and regulatory non-coding RNAs (Lopez-Serra and Esteller, 2012). Thus, if the replication stress observed in the actin mutant cells produces errors during DNA replication which are not repaired, this could affect the expression of these key cancer driving genes and regulatory regions. In addition to mutations and epigenetic regulation, it is now appreciated that changes to the 3D structure of chromatin are important in progression to cancer (Corces and Corces, 2016). This is related to the ability of DNA to form loop structures at CTCF boundaries, ultimately forming topologically associated domains (TADs). These structures impact gene regulation through the interaction of sequences that are otherwise distant within the linear DNA sequence (Dixon et al., 2012). Alterations in this structure can therefore influence gene expression and the development of cancer. Given that nuclear F-actin arises during the establishment of this architecture, it is possible that cells unable to polymerise nuclear actin have alterations in this landscape, which could in turn promote cancer progression. Alternatively, actin polymerisation may drive cancer development in a different context, though its ability to dramatically alter chromatin structure, and potentially alter gene expression.

Future research may thus identify a role for nuclear F-actin in compartmentalising the genome after cell division. Indeed, cell division is known to be important in establishing nuclear architecture; genes readily switch radial compartments during early G1, reaching stability by mid G1 and positionally changing only subtly through interphase (Thomson et al., 2004), thus mitosis is required to re-

locate chromosomes to the nuclear periphery (Finlan et al., 2008). In addition, chromatin de-condensation has been shown to impact gene position (Therizols et al., 2014). Despite this knowledge, the mechanisms which produce the 3D organisation of chromatin after cell division remain incompletely understood. Given that nuclear F-actin arises whilst this organisation is established, it tempting to speculate that nuclear F-actin may be involved in these processes. This may involve the fundamental properties of filamentous actin, including contractile and transport roles identified within the cytoplasm (Mogilner and Oster, 1996). In relation to this thesis, nuclear actin was suggested to have a mechanical function at the nuclear periphery, and potentially in de-condensing chromatin. Therefore, it is possible that nuclear F-actin is involved in the physical movement of chromatin, to organise the genome into specific domains, for example at the nuclear periphery. This is further suggested by studies which observe chromatin re-arrangements in the region occupied by nuclear actin filaments (Serebryannyy et al., 2016c) and actin dependent repositioning of gene loci (Dundr et al., 2007). An alternative model to explain how nuclear F-actin may impact chromatin architecture is by acting as a transport mechanism for the delivery of proteins which subsequently organise the genome; indeed, myosins and actin binding proteins are present in the nucleus. In addition, given that actin is a component of chromatin re-modelling complexes (Bettinger et al., 2004; Cairns et al., 1998; Peterson et al., 1998) and its polymerisation has been shown to be involved in the movement of RNA polymerase (Serebryannyy et al., 2016c), one cannot exclude the possibility that these complexes also require the polymerisation of nuclear F-actin. Investigating these possibilities would not only expand on the findings within this thesis, but could also give insights into intranuclear trafficking, and the regulation and establishment of the 3D genome. In this case, actin polymerisation may be a general requirement for nuclear homeostasis. This remains an exciting avenue for the future and is now technically feasible using techniques such as HiC and FISH (Dekker, 2006; Williamson et al., 2014).

The results in this thesis may also have broader implications in the maintenance of chromatin compaction. Results showed that nuclear F-actin de-condenses chromatin after cell division, and this has also been observed following calcium induced actin filament formation during interphase (data not shown; submitted for publication), thus suggesting potential implications of nuclear F-actin in neuronal signalling. Therefore, actin may have a general role in chromatin de-

condensation. Indeed, previous studies have shown co-localisation of nuclear F-actin and heterochromatin (Serebryannyy et al., 2016c). Further, signal induced nuclear F-actin formation often coincides with local or global chromatin de-condensation, for example in DNA damage and the initiation of transcriptional responses (Baarlink et al., 2013; Belin et al., 2015a; Miyamoto et al., 2011). Finally, it has been postulated that emerin polymerises actin into short actin filaments which form a cortical network below the inner nuclear membrane, linked together by proteins such as 4.1 and α-spectrin (Holaska et al., 2004). These actin filaments may be involved in the maintenance of peripheral heterochromatin. If actin does indeed have general functions in the regulation of chromatin compaction and nuclear positioning, this could impact many disease processes. Indeed, over 180 different mutations occur in the α-actin gene (Laing et al., 2009), leading to a range of pathologies, which may be in part explained by nuclear functions of polymerised actin.

Although actin filaments are not observed in the nucleus in resting conditions, this does not exclude the possibility that short actin filaments, below the detection limit, are present in the nucleus and maintain nuclear and chromatin structure. Indeed, nuclear actin filaments bundle to stabilise the nucleus of large nuclei (Feric and Brangwynne, 2013), such as the Xenopus oocyte (Bohnsack et al., 2006), and thus shorter filaments may be required to maintain the integrity of smaller the nuclei. The ability to resolve such structures is a future challenge which could provide insight into the regulation of chromatin structure. Indeed, whether nuclear F-actin physically interacts with chromatin has not yet been determined, as co-localisation studies have used light microscopy which is limited by resolution. Further, the majority of actin visualisation involves the use of novel actin biding probes, such as the nAC, which have not been fully explored. The use of the gold standard actin visualising dye phalloidin, removes these issues, but requires cell fixation and is limited to detecting filaments which contain at least seven actin subunits (Kristo et al., 2016). Therefore, to visualise actin at high resolution in its native state, EM is required. Given the transient and dynamic nature of nuclear actin filaments, this will likely require electron tomography to capture nuclear actin filaments, spanning different focal planes. In addition, given the comparatively smaller size of nuclear actin filaments, it is possible that visualisation by EM requires staining, for example using biotinylated or HRP linked phallloidin, which are amenable to gold labelling and DAB precipitation, respectively. By combing EM mediated actin visualisation with

newly developed methods to visualise chromatin by EM (Ou et al., 2017), this could answer questions as to how nuclear F-actin mechanistically regulates chromatin.

A potential problem with standard TEM is that the samples are not truly native, as although samples can be cryo-preserved, cells will later go through a harsh sample preparation process that includes the staining with heavy metals, such as osmium and lead, to produce contrast. This could in turn affect the stability of these structures. To circumvent these issues, a more complex system, referred to as cryo-FIB-SEM (Schertel et al., 2013) can be used. Here, frozen samples are eroded by a focused ion beam (FIB), and the surface is imaged by scanning electron microscopy (SEM). 3D reconstructions are then produced by combining images from serial sections. This method therefore allows cellular structures to be visualised in their truly native state. The ability to visualise actin in its native state may answer questions about the structure of nuclear actin filaments, as well as providing strong evidence for their presence within the nucleus, which has historically been a debated topic.

In addition, research investigating the regulation of nuclear actin filaments would provide further evidence and a more uniform method to manipulate its polymerisation. As discussed in the introduction, actin monomers are polymerised through the use of actin nucleators (Weston et al., 2012). Within this work, depletion of multiple actin nucleators did not affect the polymerisation of nuclear actin after cell division. Further, silencing of emerin, which can polymerise actin in vitro (Holaska et al., 2004), did not affect the formation of these filaments (Baarlink et al., 2017). Although a nucleator was not identified, this does not exclude the possibility that a novel actin binding protein may stimulate nuclear F-actin formation. For example, EZH2 is a polycomb protein which promotes H3K27 methylation (Vire et al., 2006) and also has also been found to regulate actin polymerisation (Su et al., 2005). It is thus conceivable that nuclear actin polymerisation may be controlled by novel residential proteins, which have duel functions in both chromatin re-modelling and actin polymerisation. Further, given that under certain conditions, such as high salt concentration, actin can polymerise in absence of actin nucleators, it is possible that nuclear F-actin forms spontaneously after cell division. For example, the small nuclear volume of post-mitotic cells may promote the clustering of actin monomers or effect the balance of ions and salts within the nucleus. Interestingly,

Mass Spec results from a biotin-phalloidin pull down, identified Coffilin-1 as a cell cycle regulated nuclear F-actin disassembly protein (Baarlink et al., 2017). It is thus speculated that the rate limiting step in post-mitotic nuclear actin filaments is their disassembly. Future work may thus identify new pathways which promote the polymerisation and de-polymerisation of nuclear actin, the discovery of which will have a great impact in understanding the interplay between chromatin organisation and nuclear F-actin.

Chapter 7 : Appendix

7.1 Hooke's law

$$F = kx$$

Equation 7-1. Hooke's law

Where F is the force (N), k is the spring constant (N/m) and x is the deformation/deflection (m).

7.2 Atomic force microscopy (AFM) image resolution

$$Resolution = \frac{No\ of\ pixels}{Area\ imaged}$$

Equation 7-2. Resolution of an AFM image

Where no of pixels is the number of pixels (e.g. 256x256, 500x500) and the area imaged is the total scan area (e.g. 2.5μm or 5μm).

7.3 Resolution limits of a light microscope

$$Abbe\ resolution_{xy} = \frac{\lambda}{2NA}$$

Equation 7-3. Abbe's equation

Where λ is the wave length of light (nm) and NA is the numerical aperture.

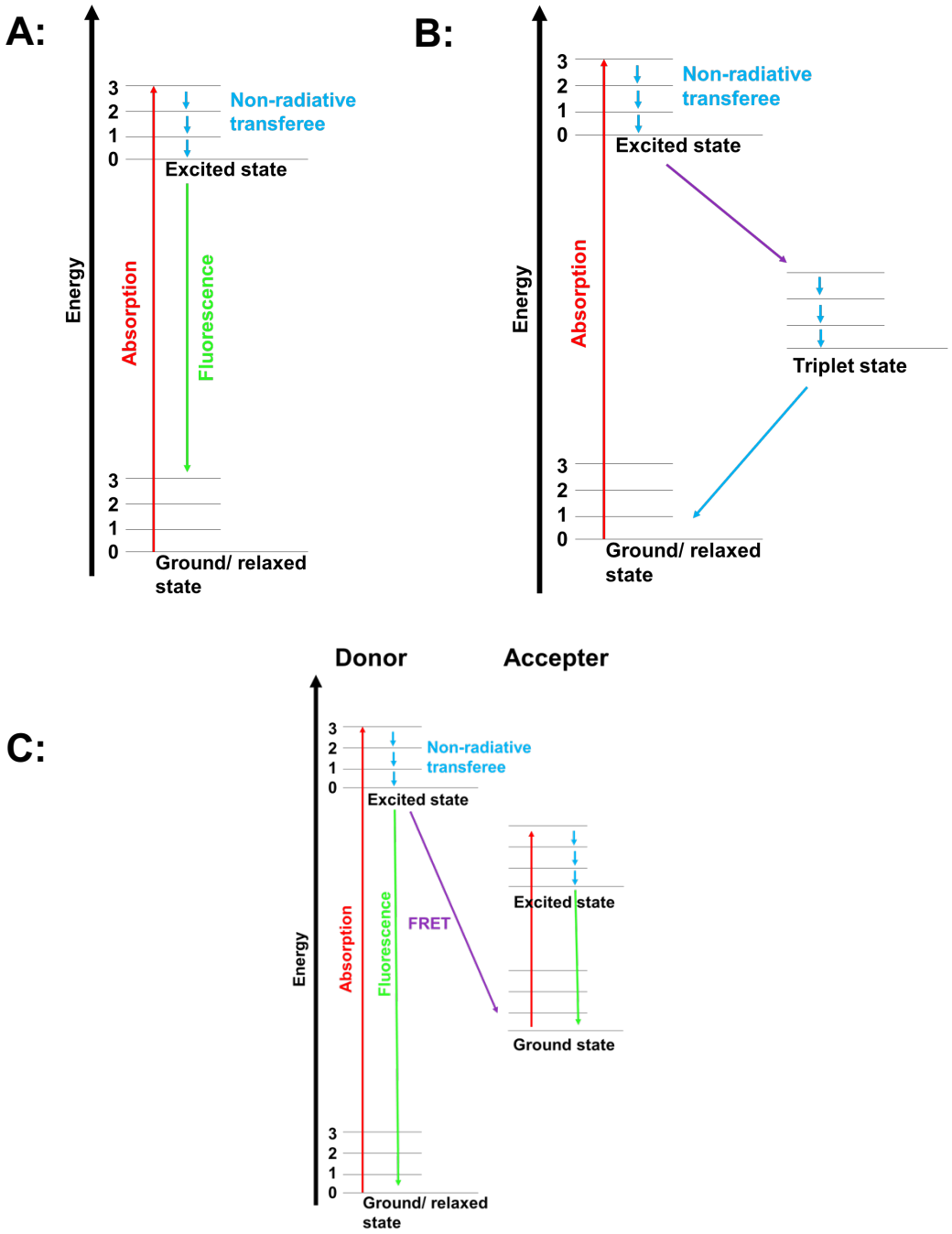

Figure 7-1. Jablonski diagrams of fluorescence, intersystem crossing and FRET

This figure shows adaptations of Jablonski diagrams to show the exchange of energy during fluorescence (A), intersystem crossing (B) and FRET (C). When a photon hits a fluorescent molecule, electrons become excited to a higher energy level (red arrow). Energy first decreases through heat loss/vibrational energy (non-radiative transfer, blue arrows) then relaxes in one of three ways: through the release of a photon and emission of fluorescence (A), conversion to an unstable triplet state which relaxes back to ground by another non-radiative transfer step (B), or by transfer of this energy to excite a neighbouring fluorophore (C). In the latter context, the molecule transferring the energy is known as the donor, and the molecule which absorbs this energy is the accepter.

A:

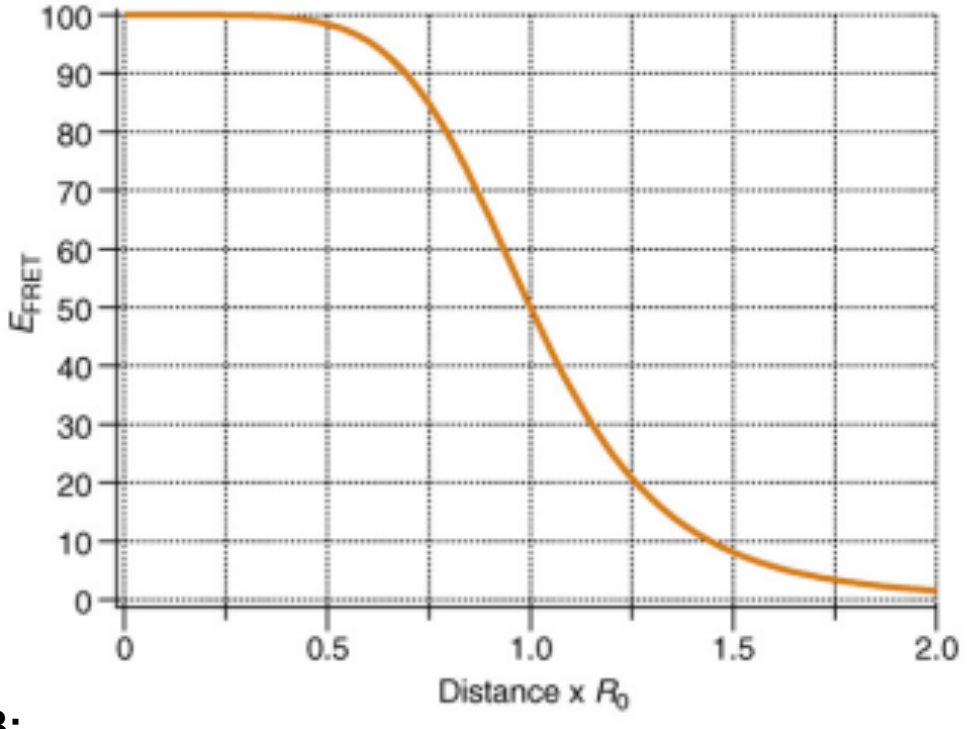

B:

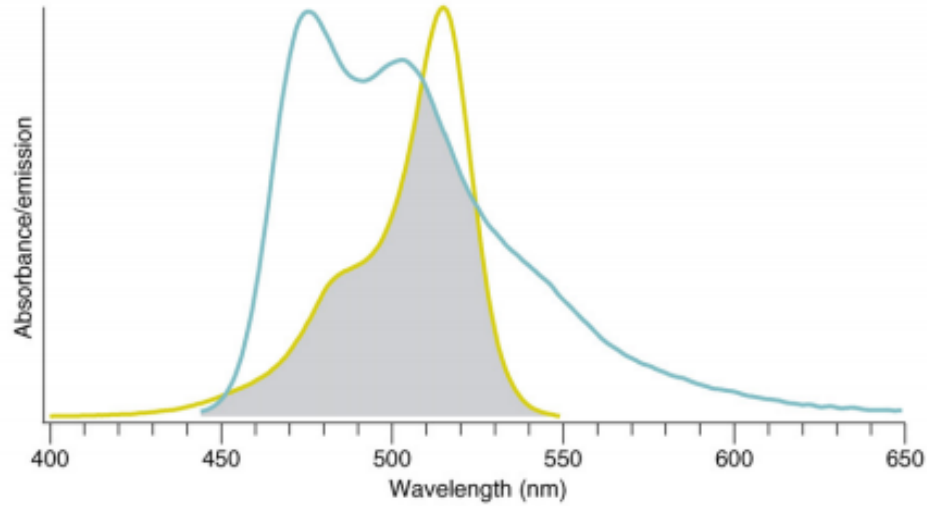

Figure 7-2. Factors which influence FRET efficiency

The images in this figure were taken from Piston et al, 2007. ***A****, shows a graph showing the effect of distance on FRET efficiency.* R_0 *is defined as the characteristic distance at which FRET efficiency is 50% (1.0 on the X axis). At distances less than* R_0*, FRET efficiency is very high (orange curve), whereas it is very low at distances above* R_0 *(no FRET above* $1.5R_0$*).* ***B****, shows a graph showing the spectral overlap between the emission spectra of CFP (blue line, donor) and the excitation spectra of YFP (accepter, yellow line). The grey area indicates the spectral overlap.*

7.4 FRET efficiency

$$E_{FRET} = \frac{1}{[1+(r/R_0)^6]}$$

Equation 7-4. Förster theory

Where R_0 is the distance at which FRET efficiency is at 50% and r is the distance between two molecules.

7.5 Fluorescence lifetime

$$\tau = \frac{1}{k_r + k_{nr}}$$

Equation 7-5. Fluorescence lifetime

The fluorescence lifetime (Tau: τ) is defined as the inverse sum of rates of relaxation from the excited state. Where, k_r is the radiative rate constant and k_{nr} is the non-radiative rate constant, i.e. the sum of internal conversion (energy relaxed as heat) and conversion to a triplet state.

7.6 Chromatin FLIM

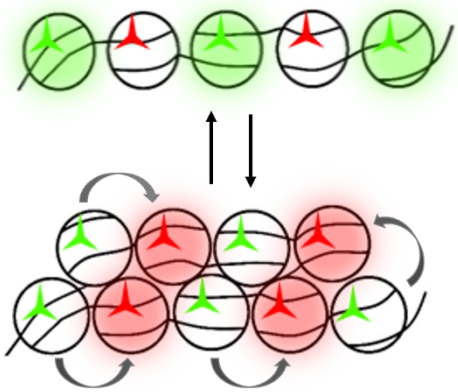

Figure 7-3. Chromatin FLIM

This figure shows a diagram to illustrate the chromatin FLIM approach. Histone H2B was labelled with GFP (donor, green) and mCherry (accepter, red), and FRET is able to occur between nucleosomes. When chromatin is de-condensed (top), nucleosomes are further apart, leading to low FRET and a high fluorescence lifetime of the donor fluorophore. When chromatin compacts (bottom), nucleosomes become in closer proximity to one another, leading to an increase in FRET, and a decrease in the GFP fluorescence lifetime.

7.7 Conversion of fluorescence lifetime to FRET efficiency

$$FRET\ efficiency = 1 - \frac{Tau\ pixel}{Tau\ donor}$$

Equation 7-6. Conversion of fluorescence lifetime to FRET efficiency

Where Tau pixel is the fluorescence lifetime in each pixel, and Tau donor is the mean fluorescence lifetime of the donor, in absence of the acceptor.

Chapter 8 : References

Abdouh, M., Hanna, R., El Hajjar, J., Flamier, A., and Bernier, G. (2016). The Polycomb Repressive Complex 1 Protein BMI1 Is Required for Constitutive Heterochromatin Formation and Silencing in Mammalian Somatic Cells. J Biol Chem *291*, 182-197.
Adams, R.R., Maiato, H., Earnshaw, W.C., and Carmena, M. (2001). Essential roles of Drosophila inner centromere protein (INCENP) and aurora B in histone H3 phosphorylation, metaphase chromosome alignment, kinetochore disjunction, and chromosome segregation. J Cell Biol *153*, 865-880.
Anderson, D.J., and Hetzer, M.W. (2007). Nuclear envelope formation by chromatin-mediated reorganization of the endoplasmic reticulum. Nat Cell Biol *9*, 1160-1166.
Anderson, M.W., Reynolds, S.H., You, M., and Maronpot, R.M. (1992). Role of proto-oncogene activation in carcinogenesis. Environ Health Perspect *98*, 13-24.
Antonin, W., and Neumann, H. (2016). Chromosome condensation and decondensation during mitosis. Curr Opin Cell Biol *40*, 15-22.
Arganda-Carreras, I., Kaynig, V., Rueden, C., Eliceiri, K.W., Schindelin, J., Cardona, A., and Sebastian Seung, H. (2017). Trainable Weka Segmentation: a machine learning tool for microscopy pixel classification. Bioinformatics *33*, 2424-2426.
Baarlink, C., Plessner, M., Sherrard, A., Morita, K., Misu, S., Virant, D., Kleinschnitz, E.M., Harniman, R., Alibhai, D., Baumeister, S*., et al.* (2017). A transient pool of nuclear F-actin at mitotic exit controls chromatin organization. Nat Cell Biol *19*, 1389-1399.
Baarlink, C., Wang, H., and Grosse, R. (2013). Nuclear actin network assembly by formins regulates the SRF coactivator MAL. Science *340*, 864-867.
Bajar, B.T., Wang, E.S., Zhang, S., Lin, M.Z., and Chu, J. (2016). A Guide to Fluorescent Protein FRET Pairs. Sensors (Basel) *16*.
Bannister, A.J., and Kouzarides, T. (2011). Regulation of chromatin by histone modifications. Cell Res *21*, 381-395.
Barrington, C., Finn, R., and Hadjur, S. (2017). Cohesin biology meets the loop extrusion model. Chromosome Res *25*, 51-60.
Belin, B.J., Lee, T., and Mullins, R.D. (2015a). Correction: DNA damage induces nuclear actin filament assembly by Formin-2 and Spire-1/2 that promotes efficient DNA repair. Elife *4*.
Belin, B.J., Lee, T., and Mullins, R.D. (2015b). DNA damage induces nuclear actin filament assembly by Formin -2 and Spire-(1/2) that promotes efficient DNA repair. [corrected]. Elife *4*, e07735.
Bertoli, C., Skotheim, J.M., and de Bruin, R.A. (2013). Control of cell cycle transcription during G1 and S phases. Nat Rev Mol Cell Biol *14*, 518-528.
Bettinger, B.T., Gilbert, D.M., and Amberg, D.C. (2004). Opinion - Actin up in the nucleus. Nat Rev Mol Cell Bio *5*, 410-415.
Bickmore, W.A., and van Steensel, B. (2013). Genome architecture: domain organization of interphase chromosomes. Cell *152*, 1270-1284.
Boettiger, A.N., Bintu, B., Moffitt, J.R., Wang, S., Beliveau, B.J., Fudenberg, G., Imakaev, M., Mirny, L.A., Wu, C.T., and Zhuang, X. (2016). Super-resolution imaging reveals distinct chromatin folding for different epigenetic states. Nature *529*, 418-422.
Bohnsack, M.T., Stuven, T., Kuhn, C., Cordes, V.C., and Gorlich, D. (2006). A selective block of nuclear actin export stabilizes the giant nuclei of Xenopus oocytes. Nat Cell Biol *8*, 257-263.
Bonder, E.M., Fishkind, D.J., and Mooseker, M.S. (1983). Direct measurement of critical concentrations and assembly rate constants at the two ends of an actin filament. Cell *34*, 491-501.
Bonenfant, D., Towbin, H., Coulot, M., Schindler, P., Mueller, D.R., and van Oostrum, J. (2007). Analysis of dynamic changes in post-translational modifications of human histones during cell cycle by mass spectrometry. Mol Cell Proteomics *6*, 1917-1932.

Burgess, R.C., Burman, B., Kruhlak, M.J., and Misteli, T. (2014). Activation of DNA damage response signaling by condensed chromatin. Cell Rep *9*, 1703-1717.
Burke, B., and Ellenberg, J. (2002). Remodelling the walls of the nucleus. Nat Rev Mol Cell Biol *3*, 487-497.
Byun, T.S., Pacek, M., Yee, M.C., Walter, J.C., and Cimprich, K.A. (2005). Functional uncoupling of MCM helicase and DNA polymerase activities activates the ATR-dependent checkpoint. Genes Dev *19*, 1040-1052.
Cairns, B.R., Erdjument-Bromage, H., Tempst, P., Winston, F., and Kornberg, R.D. (1998). Two actin-related proteins are shared functional components of the chromatin-remodeling complexes RSC and SWI/SNF. Molecular Cell *2*, 639-651.
Cameron, R.S., Liu, C.D., Mixon, A.S., Pihkala, J.P.S., Rahn, R.J., and Cameron, P.L. (2007). Myosin16b: the COOH-tail region directs localization to the nucleus and overexpression delays S-phase progression. Cell Motil Cytoskel *64*, 19-48.
Caridi, C.P., D'Agostino, C., Ryu, T., Zapotoczny, G., Delabaere, L., Li, X., Khodaverdian, V.Y., Amaral, N., Lin, E., Rau, A.R*., et al.* (2018). Nuclear F-actin and myosins drive relocalization of heterochromatic breaks. Nature *559*, 54-60.
Casella, J.F., Flanagan, M.D., and Lin, S. (1981). Cytochalasin D inhibits actin polymerization and induces depolymerization of actin filaments formed during platelet shape change. Nature *293*, 302-305.
Champoux, J.J. (2001). DNA topoisomerases: structure, function, and mechanism. Annu Rev Biochem *70*, 369-413.
Chang, C.J., Goulding, S., Earnshaw, W.C., and Carmena, M. (2003). RNAi analysis reveals an unexpected role for topoisomerase II in chromosome arm congression to a metaphase plate. J Cell Sci *116*, 4715-4726.
Chen, I., and Ting, A.Y. (2005). Site-specific labeling of proteins with small molecules in live cells. Curr Opin Biotechnol *16*, 35-40.
Chuang, C.H., Carpenter, A.E., Fuchsova, B., Johnson, T., de Lanerolle, P., and Belmont, A.S. (2006). Long-range directional movement of an interphase chromosome site. Current Biology *16*, 825-831.
Chubb, J.R., Boyle, S., Perry, P., and Bickmore, W.A. (2002). Chromatin motion is constrained by association with nuclear compartments in human cells. Current Biology *12*, 439-445.
Clapier, C.R., Iwasa, J., Cairns, B.R., and Peterson, C.L. (2017). Mechanisms of action and regulation of ATP-dependent chromatin-remodelling complexes. Nat Rev Mol Cell Biol *18*, 407-422.
Clark, T.G., and Merriam, R.W. (1977). Diffusible and bound actin nuclei of Xenopus laevis oocytes. Cell *12*, 883-891.
Collette, K.S., Petty, E.L., Golenberg, N., Bembenek, J.N., and Csankovszki, G. (2011). Different roles for Aurora B in condensin targeting during mitosis and meiosis. J Cell Sci *124*, 3684-3694.
Cooke, C.A., Heck, M.M., and Earnshaw, W.C. (1987). The inner centromere protein (INCENP) antigens: movement from inner centromere to midbody during mitosis. J Cell Biol *105*, 2053-2067.
Corces, M.R., and Corces, V.G. (2016). The three-dimensional cancer genome. Current Opinion in Genetics & Development *36*, 1-7.
Cornacchia, D., Dileep, V., Quivy, J.P., Foti, R., Tili, F., Santarella-Mellwig, R., Antony, C., Almouzni, G., Gilbert, D.M., and Buonomo, S.B. (2012). Mouse Rif1 is a key regulator of the replication-timing programme in mammalian cells. EMBO J *31*, 3678-3690.
Cramer, L. (2008). Organelle transport: dynamic actin tracks for myosin motors. Curr Biol *18*, R1066-1068.

Cremer, T., Cremer, M., Dietzel, S., Muller, S., Solovei, I., and Fakan, S. (2006). Chromosome territories--a functional nuclear landscape. Curr Opin Cell Biol *18*, 307-316.
Crisp, M., Liu, Q., Roux, K., Rattner, J.B., Shanahan, C., Burke, B., Stahl, P.D., and Hodzic, D. (2006). Coupling of the nucleus and cytoplasm: role of the LINC complex. J Cell Biol *172*, 41-53.
Dai, J., Sultan, S., Taylor, S.S., and Higgins, J.M. (2005). The kinase haspin is required for mitotic histone H3 Thr 3 phosphorylation and normal metaphase chromosome alignment. Genes Dev *19*, 472-488.
de Lanerolle, P. (2012). Nuclear actin and myosins at a glance. Journal of Cell Science *125*, 4945-4949.
Dekker, J. (2006). The three 'C's of chromosome conformation capture: controls, controls, controls. Nature Methods *3*, 17-21.
DePamphilis, M.L. (1993). Origins of DNA replication in metazoan chromosomes. J Biol Chem *268*, 1-4.
Dhalluin, C., Carlson, J.E., Zeng, L., He, C., Aggarwal, A.K., and Zhou, M.M. (1999). Structure and ligand of a histone acetyltransferase bromodomain. Nature *399*, 491-496.
Dileep, V., Ay, F., Sima, J., Vera, D.L., Noble, W.S., and Gilbert, D.M. (2015). Topologically associating domains and their long-range contacts are established during early G1 coincident with the establishment of the replication-timing program. Genome Res *25*, 1104-1113.
Dimitrova, D.S., and Gilbert, D.M. (1999). The spatial position and replication timing of chromosomal domains are both established in early G1 phase. Mol Cell *4*, 983-993.
Dixon, J.R., Selvaraj, S., Yue, F., Kim, A., Li, Y., Shen, Y., Hu, M., Liu, J.S., and Ren, B. (2012). Topological domains in mammalian genomes identified by analysis of chromatin interactions. Nature *485*, 376-380.
Dopie, J., Skarp, K.P., Rajakyla, E.K., Tanhuanpaa, K., and Vartiainen, M.K. (2012). Active maintenance of nuclear actin by importin 9 supports transcription. Proc Natl Acad Sci U S A *109*, E544-552.
Dorigo, B., Schalch, T., Bystricky, K., and Richmond, T.J. (2003). Chromatin fiber folding: requirement for the histone H4 N-terminal tail. J Mol Biol *327*, 85-96.
Du Toit, A. (2014). Cell cycle: regulating chromosome segregation. Nat Rev Mol Cell Biol *15*, 364-365.
Dultz, E., Zanin, E., Wurzenberger, C., Braun, M., Rabut, G., Sironi, L., and Ellenberg, J. (2008). Systematic kinetic analysis of mitotic dis- and reassembly of the nuclear pore in living cells. J Cell Biol *180*, 857-865.
Dundr, M., Ospina, J.K., Sung, M.H., John, S., Upender, M., Ried, T., Hager, G.L., and Matera, A.G. (2007). Actin-dependent intranuclear repositioning of an active gene locus in vivo. J Cell Biol *179*, 1095-1103.
Ernst, J., Kheradpour, P., Mikkelsen, T.S., Shoresh, N., Ward, L.D., Epstein, C.B., Zhang, X., Wang, L., Issner, R., Coyne, M.*, et al.* (2011). Mapping and analysis of chromatin state dynamics in nine human cell types. Nature *473*, 43-49.
Evdokimova, V.N., Gandhi, M., Nikitski, A.V., Bakkenist, C.J., and Nikiforov, Y.E. (2018). Nuclear myosin/actin-motored contact between homologous chromosomes is initiated by ATM kinase and homology-directed repair proteins at double-strand DNA breaks to suppress chromosome rearrangements. Oncotarget *9*, 13612-13622.
Farr, C.J., Antoniou-Kourounioti, M., Mimmack, M.L., Volkov, A., and Porter, A.C. (2014). The alpha isoform of topoisomerase II is required for hypercompaction of mitotic chromosomes in human cells. Nucleic Acids Res *42*, 4414-4426.
Federico, C., Scavo, C., Cantarella, C.D., Motta, S., Saccone, S., and Bernardi, G. (2006). Gene-rich and gene-poor chromosomal regions have different locations in the interphase nuclei of cold-blooded vertebrates. Chromosoma *115*, 123-128.

Feric, M., and Brangwynne, C.P. (2013). A nuclear F-actin scaffold stabilizes ribonucleoprotein droplets against gravity in large cells. Nat Cell Biol *15*, 1253-1259.
Fields, A.P., and Thompson, L.J. (1995). The regulation of mitotic nuclear envelope breakdown: a role for multiple lamin kinases. Prog Cell Cycle Res *1*, 271-286.
Finlan, L.E., Sproul, D., Thomson, I., Boyle, S., Kerr, E., Perry, P., Ylstra, B., Chubb, J.R., and Bickmore, W.A. (2008). Recruitment to the nuclear periphery can alter expression of genes in human cells. Plos Genet *4*, e1000039.
Fischle, W., Tseng, B.S., Dormann, H.L., Ueberheide, B.M., Garcia, B.A., Shabanowitz, J., Hunt, D.F., Funabiki, H., and Allis, C.D. (2005). Regulation of HP1-chromatin binding by histone H3 methylation and phosphorylation. Nature *438*, 1116-1122.
Fiserova, J., Efenberkova, M., Sieger, T., Maninova, M., Uhlirova, J., and Hozak, P. (2017). Chromatin organization at the nuclear periphery as revealed by image analysis of structured illumination microscopy data. J Cell Sci *130*, 2066-2077.
Flynn, R.L., and Zou, L. (2011). ATR: a master conductor of cellular responses to DNA replication stress. Trends Biochem Sci *36*, 133-140.
Fomproix, N., and Percipalle, P. (2004). An actin-myosin complex on actively transcribing genes. Exp Cell Res *294*, 140-148.
Foti, R., Gnan, S., Cornacchia, D., Dileep, V., Bulut-Karslioglu, A., Diehl, S., Buness, A., Klein, F.A., Huber, W., Johnstone, E.*, et al.* (2016). Nuclear Architecture Organized by Rif1 Underpins the Replication-Timing Program. Mol Cell *61*, 260-273.
Fragkos, M., Ganier, O., Coulombe, P., and Mechali, M. (2015). DNA replication origin activation in space and time. Nat Rev Mol Cell Biol *16*, 360-374.
Francis, L.W., Gonzalez, D., Ryder, T., Baer, K., Rees, M., White, J.O., Conlan, R.S., and Wright, C.J. (2010). Optimized sample preparation for high-resolution AFM characterization of fixed human cells. J Microsc *240*, 111-121.
Garcia, B.A., Barber, C.M., Hake, S.B., Ptak, C., Turner, F.B., Busby, S.A., Shabanowitz, J., Moran, R.G., Allis, C.D., and Hunt, D.F. (2005). Modifications of human histone H3 variants during mitosis. Biochemistry *44*, 13202-13213.
Gavet, O., and Pines, J. (2010). Progressive activation of CyclinB1-Cdk1 coordinates entry to mitosis. Dev Cell *18*, 533-543.
Gibcus, J.H., Samejima, K., Goloborodko, A., Samejima, I., Naumova, N., Nuebler, J., Kanemaki, M.T., Xie, L., Paulson, J.R., Earnshaw, W.C.*, et al.* (2018). A pathway for mitotic chromosome formation. Science *359*.
Giet, R., and Glover, D.M. (2001). Drosophila aurora B kinase is required for histone H3 phosphorylation and condensin recruitment during chromosome condensation and to organize the central spindle during cytokinesis. J Cell Biol *152*, 669-682.
Gilbert, D.M. (2002). Replication timing and transcriptional control: beyond cause and effect. Current Opinion in Cell Biology *14*, 377-383.
Gomez-Gonzalez, B., Felipe-Abrio, I., and Aguilera, A. (2009). The S-Phase Checkpoint Is Required To Respond to R-Loops Accumulated in THO Mutants. Molecular and Cellular Biology *29*, 5203-5213.
Goodarzi, A.A., Noon, A.T., Deckbar, D., Ziv, Y., Shiloh, Y., Lobrich, M., and Jeggo, P.A. (2008). ATM signaling facilitates repair of DNA double-strand breaks associated with heterochromatin. Mol Cell *31*, 167-177.
Gottesfeld, J.M., and Forbes, D.J. (1997). Mitotic repression of the transcriptional machinery. Trends Biochem Sci *22*, 197-202.
Grallert, A., Boke, E., Hagting, A., Hodgson, B., Connolly, Y., Griffiths, J.R., Smith, D.L., Pines, J., and Hagan, I.M. (2015). A PP1-PP2A phosphatase relay controls mitotic progression. Nature *517*, 94-98.
Grosse, R., and Vartiainen, M.K. (2013). To be or not to be assembled: progressing into nuclear actin filaments. Nat Rev Mol Cell Biol *14*, 693-697.

Guilluy, C., Osborne, L.D., Van Landeghem, L., Sharek, L., Superfine, R., Garcia-Mata, R., and Burridge, K. (2014). Isolated nuclei adapt to force and reveal a mechanotransduction pathway in the nucleus. Nat Cell Biol *16*, 376-381.
Gunesdogan, U., Jackle, H., and Herzig, A. (2014). Histone supply regulates S phase timing and cell cycle progression. Elife *3*, e02443.
Guttinger, S., Laurell, E., and Kutay, U. (2009). Orchestrating nuclear envelope disassembly and reassembly during mitosis. Nat Rev Mol Cell Biol *10*, 178-191.
Hagting, A., Den Elzen, N., Vodermaier, H.C., Waizenegger, I.C., Peters, J.M., and Pines, J. (2002). Human securin proteolysis is controlled by the spindle checkpoint and reveals when the APC/C switches from activation by Cdc20 to Cdh1. J Cell Biol *157*, 1125-1137.
Hancock, R. (2004). A role for macromolecular crowding effects in the assembly and function of compartments in the nucleus. J Struct Biol *146*, 281-290.
Helin, K. (1998). Regulation of cell proliferation by the E2F transcription factors. Curr Opin Genet Dev *8*, 28-35.
Helmrich, A., Ballarino, M., and Tora, L. (2011). Collisions between Replication and Transcription Complexes Cause Common Fragile Site Instability at the Longest Human Genes. Molecular Cell *44*, 966-977.
Hendzel, M.J., Wei, Y., Mancini, M.A., Van Hooser, A., Ranalli, T., Brinkley, B.R., Bazett-Jones, D.P., and Allis, C.D. (1997). Mitosis-specific phosphorylation of histone H3 initiates primarily within pericentromeric heterochromatin during G2 and spreads in an ordered fashion coincident with mitotic chromosome condensation. Chromosoma *106*, 348-360.
Hetzer, M., Meyer, H.H., Walther, T.C., Bilbao-Cortes, D., Warren, G., and Mattaj, I.W. (2001). Distinct AAA-ATPase p97 complexes function in discrete steps of nuclear assembly. Nat Cell Biol *3*, 1086-1091.
Hirano, H., and Matsuura, Y. (2011). Sensing actin dynamics: structural basis for G-actin-sensitive nuclear import of MAL. Biochem Biophys Res Commun *414*, 373-378.
Hirano, T., Kobayashi, R., and Hirano, M. (1997). Condensins, chromosome condensation protein complexes containing XCAP-C, XCAP-E and a Xenopus homolog of the Drosophila Barren protein. Cell *89*, 511-521.
Hizume, K., Araki, S., Hata, K., Prieto, E., Kundu, T.K., Yoshikawa, K., and Takeyasu, K. (2010). Nano-scale analyses of the chromatin decompaction induced by histone acetylation. Arch Histol Cytol *73*, 149-163.
Ho, C.Y., Jaalouk, D.E., Vartiainen, M.K., and Lammerding, J. (2013). Lamin A/C and emerin regulate MKL1-SRF activity by modulating actin dynamics. Nature *497*, 507-511.
Hofmann, W.A., Stojiljkovic, L., Fuchsova, B., Vargas, G.M., Mavrommatis, E., Philimonenko, V., Kysela, K., Goodrich, J.A., Lessard, J.L., Hope, T.J.*, et al.* (2004). Actin is part of pre-initiation complexes and is necessary for transcription by RNA polymerase II. Nature Cell Biology *6*, 1094-U1018.
Holaska, J.M., Kowalski, A.K., and Wilson, K.L. (2004). Emerin caps the pointed end of actin filaments: evidence for an actin cortical network at the nuclear inner membrane. PLoS Biol *2*, E231.
Hsu, J.Y., Sun, Z.W., Li, X., Reuben, M., Tatchell, K., Bishop, D.K., Grushcow, J.M., Brame, C.J., Caldwell, J.A., Hunt, D.F.*, et al.* (2000). Mitotic phosphorylation of histone H3 is governed by Ipl1/aurora kinase and Glc7/PP1 phosphatase in budding yeast and nematodes. Cell *102*, 279-291.
Hu, P., Wu, S., and Hernandez, N. (2004). A role for beta-actin in RNA polymerase III transcription. Genes Dev *18*, 3010-3015.
Iida, K., and Yahara, I. (1986). Reversible Induction of Actin Rods in Mouse C3h-2k Cell by Incubation in Salt Buffers and by Treatment with Nonionic Detergents. Experimental Cell Research *164*, 492-506.

Iizuka, M., Matsui, T., Takisawa, H., and Smith, M.M. (2006a). Regulation of replication licensing by acetyltransferase Hbo1. Mol Cell Biol *26*, 1098-1108.
Iizuka, T., Fudou, R., Jojima, Y., Ogawa, S., Yamanaka, S., Inukai, Y., and Ojika, M. (2006b). Miuraenamides A and B, novel antimicrobial cyclic depsipeptides from a new slightly halophilic myxobacterium: taxonomy, production, and biological properties. J Antibiot (Tokyo) *59*, 385-391.
Im, J.S., Ki, S.H., Farina, A., Jung, D.S., Hurwitz, J., and Lee, J.K. (2009). Assembly of the Cdc45-Mcm2-7-GINS complex in human cells requires the Ctf4/And-1, RecQL4, and Mcm10 proteins. Proc Natl Acad Sci U S A *106*, 15628-15632.
Ishikawa-Ankerhold, H.C., Ankerhold, R., and Drummen, G.P. (2012). Advanced fluorescence microscopy techniques--FRAP, FLIP, FLAP, FRET and FLIM. Molecules *17*, 4047-4132.
Johansen, K.M., and Johansen, J. (2006). Regulation of chromatin structure by histone H3S10 phosphorylation. Chromosome Res *14*, 393-404.
Kabsch, W., Mannherz, H.G., Suck, D., Pai, E.F., and Holmes, K.C. (1990). Atomic structure of the actin:DNase I complex. Nature *347*, 37-44.
Kaiser, T.E., Intine, R.V., and Dundr, M. (2008). De Novo Formation of a Subnuclear Body. Science *322*, 1713-1717.
Kalverda, B., Roling, M.D., and Fornerod, M. (2008). Chromatin organization in relation to the nuclear periphery. FEBS Lett *582*, 2017-2022.
Kaszas, E., and Cande, W.Z. (2000). Phosphorylation of histone H3 is correlated with changes in the maintenance of sister chromatid cohesion during meiosis in maize, rather than the condensation of the chromatin. J Cell Sci *113 (Pt 18)*, 3217-3226.
Kelly, A.E., Ghenoiu, C., Xue, J.Z., Zierhut, C., Kimura, H., and Funabiki, H. (2010). Survivin reads phosphorylated histone H3 threonine 3 to activate the mitotic kinase Aurora B. Science *330*, 235-239.
Khanna, K.K., Lavin, M.F., Jackson, S.P., and Mulhern, T.D. (2001). ATM, a central controller of cellular responses to DNA damage. Cell Death Differ *8*, 1052-1065.
Khatau, S.B., Hale, C.M., Stewart-Hutchinson, P.J., Patel, M.S., Stewart, C.L., Searson, P.C., Hodzic, D., and Wirtz, D. (2009). A perinuclear actin cap regulates nuclear shape. Proc Natl Acad Sci U S A *106*, 19017-19022.
Kim, S.M., Dubey, D.D., and Huberman, J.A. (2003). Early-replicating heterochromatin. Genes Dev *17*, 330-335.
Kimura, K., Hirano, M., Kobayashi, R., and Hirano, T. (1998). Phosphorylation and activation of 13S condensin by Cdc2 in vitro. Science *282*, 487-490.
Kleckner, N., Zickler, D., Jones, G.H., Dekker, J., Padmore, R., Henle, J., and Hutchinson, J. (2004). A mechanical basis for chromosome function. Proc Natl Acad Sci U S A *101*, 12592-12597.
Klein, G. (1988). Tumour suppressor genes. J Cell Sci Suppl *10*, 171-180.
Kothapalli, D., Zhao, L., Hawthorne, E.A., Cheng, Y., Lee, E., Pure, E., and Assoian, R.K. (2007). Hyaluronan and CD44 antagonize mitogen-dependent cyclin D1 expression in mesenchymal cells. J Cell Biol *176*, 535-544.
Kremers, G.J., Gilbert, S.G., Cranfill, P.J., Davidson, M.W., and Piston, D.W. (2011). Fluorescent proteins at a glance. J Cell Sci *124*, 157-160.
Kristo, I., Bajusz, I., Bajusz, C., Borkuti, P., and Vilmos, P. (2016). Actin, actin-binding proteins, and actin-related proteins in the nucleus. Histochem Cell Biol *145*, 373-388.
Kumar, A., Mazzanti, M., Mistrik, M., Kosar, M., Beznoussenko, G.V., Mironov, A.A., Garre, M., Parazzoli, D., Shivashankar, G.V., Scita, G*., et al.* (2014). ATR mediates a checkpoint at the nuclear envelope in response to mechanical stress. Cell *158*, 633-646.

Kuo, A.J., Song, J., Cheung, P., Ishibe-Murakami, S., Yamazoe, S., Chen, J.K., Patel, D.J., and Gozani, O. (2012). The BAH domain of ORC1 links H4K20me2 to DNA replication licensing and Meier-Gorlin syndrome. Nature *484*, 115-119.
Laing, N.G., Dye, D.E., Wallgren-Pettersson, C., Richard, G., Monnier, N., Lillis, S., Winder, T.L., Lochmuller, H., Graziano, C., Mitrani-Rosenbaum, S.*, et al.* (2009). Mutations and polymorphisms of the skeletal muscle alpha-actin gene (ACTA1). Hum Mutat *30*, 1267-1277.
Lakowicz, J.R. (2006). Principles of Fluorescence Spectroscopy.
Lammerding, J., Fong, L.G., Ji, J.Y., Reue, K., Stewart, C.L., Young, S.G., and Lee, R.T. (2006). Lamins A and C but not lamin B1 regulate nuclear mechanics. Journal of Biological Chemistry *281*, 25768-25780.
Landsverk, H.B., Kirkhus, M., Bollen, M., Kuntziger, T., and Collas, P. (2005). PNUTS enhances in vitro chromosome decondensation in a PP1-dependent manner. Biochem J *390*, 709-717.
Lau, A.C., Zhu, K.P., Brouhard, E.A., Davis, M.B., and Csankovszki, G. (2016). An H4K16 histone acetyltransferase mediates decondensation of the X chromosome in C. elegans males. Epigenetics Chromatin *9*, 44.
Lengsfeld, A.M., Low, I., Wieland, T., Dancker, P., and Hasselbach, W. (1974). Interaction of phalloidin with actin. Proc Natl Acad Sci U S A *71*, 2803-2807.
Levine, A.J., Momand, J., and Finlay, C.A. (1991). The p53 tumour suppressor gene. Nature *351*, 453-456.
Lieberman-Aiden, E., van Berkum, N.L., Williams, L., Imakaev, M., Ragoczy, T., Telling, A., Amit, I., Lajoie, B.R., Sabo, P.J., Dorschner, M.O.*, et al.* (2009). Comprehensive mapping of long-range interactions reveals folding principles of the human genome. Science *326*, 289-293.
Lima-de-Faria, A., and Jaworska, H. (1968). Late DNA synthesis in heterochromatin. Nature *217*, 138-142.
Liu, W., Tanasa, B., Tyurina, O.V., Zhou, T.Y., Gassmann, R., Liu, W.T., Ohgi, K.A., Benner, C., Garcia-Bassets, I., Aggarwal, A.K.*, et al.* (2010). PHF8 mediates histone H4 lysine 20 demethylation events involved in cell cycle progression. Nature *466*, 508-512.
Lleres, D., Bailly, A.P., Perrin, A., Norman, D.G., Xirodimas, D.P., and Feil, R. (2017a). Quantitative FLIM-FRET Microscopy to Monitor Nanoscale Chromatin Compaction In Vivo Reveals Structural Roles of Condensin Complexes. Cell Reports *18*, 1791-1803.
Lleres, D., Bailly, A.P., Perrin, A., Norman, D.G., Xirodimas, D.P., and Feil, R. (2017b). Quantitative FLIM-FRET Microscopy to Monitor Nanoscale Chromatin Compaction In Vivo Reveals Structural Roles of Condensin Complexes. Cell Rep *18*, 1791-1803.
Lleres, D., James, J., Swift, S., Norman, D.G., and Lamond, A.I. (2009). Quantitative analysis of chromatin compaction in living cells using FLIM-FRET. J Cell Biol *187*, 481-496.
Lopez-Serra, P., and Esteller, M. (2012). DNA methylation-associated silencing of tumor-suppressor microRNAs in cancer. Oncogene *31*, 1609-1622.
Magalska, A., Schellhaus, A.K., Moreno-Andres, D., Zanini, F., Schooley, A., Sachdev, R., Schwarz, H., Madlung, J., and Antonin, W. (2014). RuvB-like ATPases function in chromatin decondensation at the end of mitosis. Dev Cell *31*, 305-318.
Mahadevan, L.C., Willis, A.C., and Barratt, M.J. (1991). Rapid histone H3 phosphorylation in response to growth factors, phorbol esters, okadaic acid, and protein synthesis inhibitors. Cell *65*, 775-783.
Mao, Y.T.S., Zhang, B., and Spector, D.L. (2011). Biogenesis and function of nuclear bodies. Trends in Genetics *27*, 295-306.
Marchal, C., Sasaki, T., Vera, D., Wilson, K., Sima, J., Rivera-Mulia, J.C., Trevilla-Garcia, C., Nogues, C., Nafie, E., and Gilbert, D.M. (2018). Genome-wide analysis of replication timing by next-generation sequencing with E/L Repli-seq. Nature Protocols *13*, 819-839.

Marechal, A., and Zou, L. (2013). DNA damage sensing by the ATM and ATR kinases. Cold Spring Harb Perspect Biol *5*.
Masai, H., Matsumoto, S., You, Z., Yoshizawa-Sugata, N., and Oda, M. (2010). Eukaryotic chromosome DNA replication: where, when, and how? Annu Rev Biochem *79*, 89-130.
Mazumdar, M., Sundareshan, S., and Misteli, T. (2004). Human chromokinesin KIF4A functions in chromosome condensation and segregation. J Cell Biol *166*, 613-620.
Mazumder, A., Roopa, T., Basu, A., Mahadevan, L., and Shivashankar, G.V. (2008). Dynamics of chromatin decondensation reveals the structural integrity of a mechanically prestressed nucleus. Biophys J *95*, 3028-3035.
McCormack, E.A., Rohman, M.J., and Willison, K.R. (2001). Mutational screen identifies critical amino acid residues of beta-actin mediating interaction between its folding intermediates and eukaryotic cytosolic chaperonin CCT. J Struct Biol *135*, 185-197.
McEvoy, J.D., Kossatz, U., Malek, N., and Singer, J.D. (2007). Constitutive turnover of cyclin E by Cul3 maintains quiescence. Mol Cell Biol *27*, 3651-3666.
Melak, M., Plessner, M., and Grosse, R. (2017). Actin visualization at a glance. J Cell Sci *130*, 525-530.
Melby, T.E., Ciampaglio, C.N., Briscoe, G., and Erickson, H.P. (1998). The symmetrical structure of structural maintenance of chromosomes (SMC) and MukB proteins: long, antiparallel coiled coils, folded at a flexible hinge. J Cell Biol *142*, 1595-1604.
Merrick, C.J., Jackson, D., and Diffley, J.F. (2004). Visualization of altered replication dynamics after DNA damage in human cells. J Biol Chem *279*, 20067-20075.
Misteli, T. (2013). The cell biology of genomes: bringing the double helix to life. Cell *152*, 1209-1212.
Miyamoto, K., Pasque, V., Jullien, J., and Gurdon, J.B. (2011). Nuclear actin polymerization is required for transcriptional reprogramming of Oct4 by oocytes. Genes Dev *25*, 946-958.
Mizuno, H., Kawahara, Y., Wu, J., Katayose, Y., Kanamori, H., Ikawa, H., Itoh, T., Sasaki, T., and Matsumoto, T. (2011). Asymmetric distribution of gene expression in the centromeric region of rice chromosome 5. Front Plant Sci *2*, 16.
Mogilner, A., and Oster, G. (1996). Cell motility driven by actin polymerization. Biophys J *71*, 3030-3045.
Moir, R.D., Montaglowy, M., and Goldman, R.D. (1994). Dynamic Properties of Nuclear Lamins - Lamin-B Is Associated with Sites of DNA-Replication. Journal of Cell Biology *125*, 1201-1212.
Moir, R.D., Yoon, M., Khuon, S., and Goldman, R.D. (2000). Nuclear lamins A and B1: different pathways of assembly during nuclear envelope formation in living cells. J Cell Biol *151*, 1155-1168.
Morton, W.M., Ayscough, K.R., and McLaughlin, P.J. (2000). Latrunculin alters the actin-monomer subunit interface to prevent polymerization. Nat Cell Biol *2*, 376-378.
Murakoshi, H., and Shibata, A.C.E. (2017). ShadowY: a dark yellow fluorescent protein for FLIM-based FRET measurement. Sci Rep *7*, 6791.
Murga, M., Jaco, I., Fan, Y., Soria, R., Martinez-Pastor, B., Cuadrado, M., Yang, S.M., Blasco, M.A., Skoultchi, A.I., and Fernandez-Capetillo, O. (2007). Global chromatin compaction limits the strength of the DNA damage response. J Cell Biol *178*, 1101-1108.
Nagano, T., Lubling, Y., Varnai, C., Dudley, C., Leung, W., Baran, Y., Mendelson Cohen, N., Wingett, S., Fraser, P., and Tanay, A. (2017). Cell-cycle dynamics of chromosomal organization at single-cell resolution. Nature *547*, 61-67.
Newport, J.W., Wilson, K.L., and Dunphy, W.G. (1990). A lamin-independent pathway for nuclear envelope assembly. J Cell Biol *111*, 2247-2259.

Nishida, E., Iida, K., Yonezawa, N., Koyasu, S., Yahara, I., and Sakai, H. (1987). Cofilin Is a Component of Intranuclear and Cytoplasmic Actin Rods Induced in Cultured-Cells. P Natl Acad Sci USA *84*, 5262-5266.
Oberdoerffer, P. (2015). Stop relaxing: How DNA damage-induced chromatin compaction may affect epigenetic integrity and disease. Mol Cell Oncol *2*, e970952.
Ohtani, K., DeGregori, J., and Nevins, J.R. (1995). Regulation of the cyclin E gene by transcription factor E2F1. Proc Natl Acad Sci U S A *92*, 12146-12150.
Olmos, Y., Hodgson, L., Mantell, J., Verkade, P., and Carlton, J.G. (2015). ESCRT-III controls nuclear envelope reformation. Nature *522*, 236-239.
Otterbein, L.R., Graceffa, P., and Dominguez, R. (2001). The crystal structure of uncomplexed actin in the ADP state. Science *293*, 708-711.
Ou, H.D., Phan, S., Deerinck, T.J., Thor, A., Ellisman, M.H., and O'Shea, C.C. (2017). ChromEMT: Visualizing 3D chromatin structure and compaction in interphase and mitotic cells. Science *357*.
Padilla-Parra, S., Auduge, N., Tramier, M., and Coppey-Moisan, M. (2015). Time-domain fluorescence lifetime imaging microscopy: a quantitative method to follow transient protein-protein interactions in living cells. Cold Spring Harb Protoc *2015*, 508-521.
Palozola, K.C., Donahue, G., Liu, H., Grant, G.R., Becker, J.S., Cote, A., Yu, H.T., Raj, A., and Zaret, K.S. (2017). Mitotic transcription and waves of gene reactivation during mitotic exit. Science *358*, 119-122.
Parisis, N., Krasinska, L., Harker, B., Urbach, S., Rossignol, M., Camasses, A., Dewar, J., Morin, N., and Fisher, D. (2017). Initiation of DNA replication requires actin dynamics and formin activity. Embo Journal *36*, 3212-3231.
Pascual-Garcia, P., Debo, B., Aleman, J.R., Talamas, J.A., Lan, Y., Nguyen, N.H., Won, K.J., and Capelson, M. (2017). Metazoan Nuclear Pores Provide a Scaffold for Poised Genes and Mediate Induced Enhancer-Promoter Contacts. Mol Cell *66*, 63-76 e66.
Paulson, J.R., and Laemmli, U.K. (1977). The structure of histone-depleted metaphase chromosomes. Cell *12*, 817-828.
Pederson, T. (2010). "Compact" nuclear domains: Reconsidering the nucleolus. Nucleus-Austin *1*, 444-445.
Pendleton, A., Pope, B., Weeds, A., and Koffer, A. (2003). Latrunculin B or ATP depletion induces cofilin-dependent translocation of actin into nuclei of mast cells. Journal of Biological Chemistry *278*, 14394-14400.
Perry, J., and Kleckner, N. (2003). The ATRs, ATMs, and TORs are giant HEAT repeat proteins. Cell *112*, 151-155.
Pestic-Dragovich, L., Stojiljkovic, L., Philimonenko, A.A., Nowak, G., Ke, Y., Settlage, R.E., Shabanowitz, J., Hunt, D.F., Hozak, P., and de Lanerolle, P. (2000). A myosin I isoform in the nucleus. Science *290*, 337-341.
Peterson, C.L., Zhao, Y.M., and Chait, B.T. (1998). Subunits of the yeast SWI/SNF complex are members of the actin-related protein (ARP) family. Journal of Biological Chemistry *273*, 23641-23644.
Phatnani, H.P., and Greenleaf, A.L. (2006). Phosphorylation and functions of the RNA polymerase IICTD. Gene Dev *20*, 2922-2936.
Philpott, A., and Leno, G.H. (1992). Nucleoplasmin remodels sperm chromatin in Xenopus egg extracts. Cell *69*, 759-767.
Philpott, A., Leno, G.H., and Laskey, R.A. (1991). Sperm decondensation in Xenopus egg cytoplasm is mediated by nucleoplasmin. Cell *65*, 569-578.
Pirrotta, V., and Li, H.B. (2012). A view of nuclear Polycomb bodies. Curr Opin Genet Dev *22*, 101-109.
Piston, D.W., and Kremers, G.J. (2007). Fluorescent protein FRET: the good, the bad and the ugly. Trends Biochem Sci *32*, 407-414.

Plessner, M., and Grosse, R. (2015). Extracellular signaling cues for nuclear actin polymerization. Eur J Cell Biol *94*, 359-362.
Plessner, M., Melak, M., Chinchilla, P., Baarlink, C., and Grosse, R. (2015). Nuclear F-actin formation and reorganization upon cell spreading. J Biol Chem *290*, 11209-11216.
Polioudaki, H., Kourmouli, N., Drosou, V., Bakou, A., Theodoropoulos, P.A., Singh, P.B., Giannakouros, T., and Georgatos, S.D. (2001). Histones H3/H4 form a tight complex with the inner nuclear membrane protein LBR and heterochromatin protein 1. EMBO Rep *2*, 920-925.
Pope, B.D., Ryba, T., Dileep, V., Yue, F., Wu, W., Denas, O., Vera, D.L., Wang, Y., Hansen, R.S., Canfield, T.K.*, et al.* (2014). Topologically associating domains are stable units of replication-timing regulation. Nature *515*, 402-405.
Posern, G., Sotiropoulos, A., and Treisman, R. (2002). Mutant actins demonstrate a role for unpolymerized actin in control of transcription by serum response factor. Mol Biol Cell *13*, 4167-4178.
Pranchevicius, M.C., Baqui, M.M., Ishikawa-Ankerhold, H.C., Lourenco, E.V., Leao, R.M., Banzi, S.R., dos Santos, C.T., Roque-Barreira, M.C., Espreafico, E.M., and Larson, R.E. (2008). Myosin Va phosphorylated on Ser1650 is found in nuclear speckles and redistributes to nucleoli upon inhibition of transcription. Cell Motil Cytoskeleton *65*, 441-456.
Puhka, M., Vihinen, H., Joensuu, M., and Jokitalo, E. (2007). Endoplasmic reticulum remains continuous and undergoes sheet-to-tubule transformation during cell division in mammalian cells. J Cell Biol *179*, 895-909.
Ramadan, K., Bruderer, R., Spiga, F.M., Popp, O., Baur, T., Gotta, M., and Meyer, H.H. (2007). Cdc48/p97 promotes reformation of the nucleus by extracting the kinase Aurora B from chromatin. Nature *450*, 1258-1262.
Rao, J., Bhattacharya, D., Banerjee, B., Sarin, A., and Shivashankar, G.V. (2007). Trichostatin-A induces differential changes in histone protein dynamics and expression in HeLa cells. Biochem Biophys Res Commun *363*, 263-268.
Resch-Genger, U., Grabolle, M., Cavaliere-Jaricot, S., Nitschke, R., and Nann, T. (2008). Quantum dots versus organic dyes as fluorescent labels. Nat Methods *5*, 763-775.
Reynolds, E.S. (1963). The use of lead citrate at high pH as an electron-opaque stain in electron microscopy. J Cell Biol *17*, 208-212.
Ricci, M.A., Manzo, C., Garcia-Parajo, M.F., Lakadamyali, M., and Cosma, M.P. (2015). Chromatin fibers are formed by heterogeneous groups of nucleosomes in vivo. Cell *160*, 1145-1158.
Riedl, J., Crevenna, A.H., Kessenbrock, K., Yu, J.H., Neukirchen, D., Bista, M., Bradke, F., Jenne, D., Holak, T.A., Werb, Z.*, et al.* (2008). Lifeact: a versatile marker to visualize F-actin. Nat Methods *5*, 605-607.
Risca, V.I., Denny, S.K., Straight, A.F., and Greenleaf, W.J. (2017). Variable chromatin structure revealed by in situ spatially correlated DNA cleavage mapping. Nature *541*, 237-241.
Ruchaud, S., Carmena, M., and Earnshaw, W.C. (2007). Chromosomal passengers: conducting cell division. Nat Rev Mol Cell Biol *8*, 798-812.
Samejima, K., Samejima, I., Vagnarelli, P., Ogawa, H., Vargiu, G., Kelly, D.A., de Lima Alves, F., Kerr, A., Green, L.C., Hudson, D.F.*, et al.* (2012). Mitotic chromosomes are compacted laterally by KIF4 and condensin and axially by topoisomerase IIalpha. J Cell Biol *199*, 755-770.
Samudio-Ruiz, S.L., and Hudson, L.G. (2012). Increased DNA methyltransferase activity and DNA methylation following Epidermal Growth Factor stimulation in ovarian cancer cells. Epigenetics *7*, 216-224.

Sawicka, A., and Seiser, C. (2012). Histone H3 phosphorylation - a versatile chromatin modification for different occasions. Biochimie *94*, 2193-2201.
Scheer, U., Hinssen, H., Franke, W.W., and Jockusch, B.M. (1984). Microinjection of actin-binding proteins and actin antibodies demonstrates involvement of nuclear actin in transcription of lampbrush chromosomes. Cell *39*, 111-122.
Schertel, A., Snaidero, N., Han, H.M., Ruhwedel, T., Laue, M., Grabenbauer, M., and Mobius, W. (2013). Cryo FIB-SEM: volume imaging of cellular ultrastructure in native frozen specimens. J Struct Biol *184*, 355-360.
Schindelin, J., Arganda-Carreras, I., Frise, E., Kaynig, V., Longair, M., Pietzsch, T., Preibisch, S., Rueden, C., Saalfeld, S., Schmid, B.*, et al.* (2012). Fiji: an open-source platform for biological-image analysis. Nat Methods *9*, 676-682.
Schirmer, E.C., and Foisner, R. (2007). Proteins that associate with lamins: many faces, many functions. Experimental Cell Research *313*, 2167-2179.
Schmitz, M.H., Held, M., Janssens, V., Hutchins, J.R., Hudecz, O., Ivanova, E., Goris, J., Trinkle-Mulcahy, L., Lamond, A.I., Poser, I.*, et al.* (2010). Live-cell imaging RNAi screen identifies PP2A-B55alpha and importin-beta1 as key mitotic exit regulators in human cells. Nat Cell Biol *12*, 886-893.
Schneider, C.A., Rasband, W.S., and Eliceiri, K.W. (2012). NIH Image to ImageJ: 25 years of image analysis. Nat Methods *9*, 671-675.
Schou, K.B., Schneider, L., Christensen, S.T., and Hoffmann, E.K. (2008). Early-stage apoptosis is associated with DNA-damage-independent ATM phosphorylation and chromatin decondensation in NIH3T3 fibroblasts. Cell Biol Int *32*, 107-113.
Schrank, B.R., Aparicio, T., Li, Y., Chang, W., Chait, B.T., Gundersen, G.G., Gottesman, M.E., and Gautier, J. (2018). Nuclear ARP2/3 drives DNA break clustering for homology-directed repair. Nature *559*, 61-66.
Serebryannyy, L.A., Cruz, C.M., and de Lanerolle, P. (2016a). A Role for Nuclear Actin in HDAC 1 and 2 Regulation. Sci Rep-Uk *6*.
Serebryannyy, L.A., Parilla, M., Annibale, P., Cruz, C.M., Laster, K., Gratton, E., Kudryashov, D., Kosak, S.T., Gottardi, C.J., and de Lanerolle, P. (2016b). Persistent nuclear actin filaments inhibit transcription by RNA polymerase II. J Cell Sci *129*, 3412-3425.
Serebryannyy, L.A., Yuen, M., Parilla, M., Cooper, S.T., and de Lanerolle, P. (2016c). The Effects of Disease Models of Nuclear Actin Polymerization on the Nucleus. Frontiers in Physiology *7*.
Shachar, S., and Misteli, T. (2017). Causes and consequences of nuclear gene positioning. J Cell Sci *130*, 1501-1508.
Shachar, S., Voss, T.C., Pegoraro, G., Sciascia, N., and Misteli, T. (2015). Identification of Gene Positioning Factors Using High-Throughput Imaging Mapping. Cell *162*, 911-923.
Shanbhag, N.M., Rafalska-Metcalf, I.U., Balane-Bolivar, C., Janicki, S.M., and Greenberg, R.A. (2010). ATM-dependent chromatin changes silence transcription in cis to DNA double-strand breaks. Cell *141*, 970-981.
Shiloh, Y., and Ziv, Y. (2013). The ATM protein kinase: regulating the cellular response to genotoxic stress, and more. Nat Rev Mol Cell Biol *14*, 197-210.
Shumaker, D.K., Kuczmarski, E.R., and Goldman, R.D. (2003). The nucleoskeleton: lamins and actin are major players in essential nuclear functions. Curr Opin Cell Biol *15*, 358-366.
Simon, D.N., and Wilson, K.L. (2011). The nucleoskeleton as a genome-associated dynamic 'network of networks'. Nat Rev Mol Cell Biol *12*, 695-708.
Siniossoglou, S. (2009). Lipins, lipids and nuclear envelope structure. Traffic *10*, 1181-1187.
Spector, D.L., and Lamond, A.I. (2011). Nuclear Speckles. Csh Perspect Biol *3*.

Spichal, M., Brion, A., Herbert, S., Cournac, A., Marbouty, M., Zimmer, C., Koszul, R., and Fabre, E. (2016a). Evidence for a dual role of actin in regulating chromosome organization and dynamics in yeast. J Cell Sci *129*, 681-692.
Spichal, M., Brion, A., Herbert, S., Cournac, A., Marbouty, M., Zimmer, C., Koszul, R., and Fabre, E. (2016b). Evidence for a dual role of actin in regulating chromosome organization and dynamics in yeast. Journal of Cell Science *129*, 681-692.
Stephens, A.D., Banigan, E.J., Adam, S.A., Goldman, R.D., and Marko, J.F. (2017). Chromatin and lamin A determine two different mechanical response regimes of the cell nucleus. Mol Biol Cell *28*, 1984-1996.
Stephens, A.D., Liu, P.Z., Banigan, E.J., Almassalha, L.M., Backman, V., Adam, S.A., Goldman, R.D., and Marko, J.F. (2018). Chromatin histone modifications and rigidity affect nuclear morphology independent of lamins. Mol Biol Cell *29*, 220-233.
Stewart, S.A., Kothapalli, D., Yung, Y., and Assoian, R.K. (2004). Antimitogenesis linked to regulation of Skp2 gene expression. J Biol Chem *279*, 29109-29113.
Stuven, T., Hartmann, E., and Gorlich, D. (2003). Exportin 6: a novel nuclear export receptor that is specific for profilin.actin complexes. EMBO J *22*, 5928-5940.
Su, I.H., Dobenecker, M.W., Dickinson, E., Oser, M., Basavaraj, A., Marqueron, R., Viale, A., Reinberg, D., Wulfing, C., and Tarakhovsky, A. (2005). Polycomb group protein ezh2 controls actin polymerization and cell signaling. Cell *121*, 425-436.
Tajrishi, M.M., Tuteja, R., and Tuteja, N. (2011). Nucleolin: The most abundant multifunctional phosphoprotein of nucleolus. Commun Integr Biol *4*, 267-275.
Takemoto, A., Murayama, A., Katano, M., Urano, T., Furukawa, K., Yokoyama, S., Yanagisawa, J., Hanaoka, F., and Kimura, K. (2007). Analysis of the role of Aurora B on the chromosomal targeting of condensin I. Nucleic Acids Res *35*, 2403-2412.
Talbert, P.B., and Henikoff, S. (2010). Histone variants--ancient wrap artists of the epigenome. Nat Rev Mol Cell Biol *11*, 264-275.
Tang, C.W., Maya-Mendoza, A., Martin, C., Zeng, K., Chen, S.B., Feret, D., Wilson, S.A., and Jackson, D.A. (2008). The integrity of a lamin-B1-dependent nucleoskeleton is a fundamental determinant of RNA synthesis in human cells. Journal of Cell Science *121*, 1014-1024.
Tardat, M., Brustel, J., Kirsh, O., Lefevbre, C., Callanan, M., Sardet, C., and Julien, E. (2010). The histone H4 Lys 20 methyltransferase PR-Set7 regulates replication origins in mammalian cells. Nat Cell Biol *12*, 1086-1093.
Taylor, G.C., Eskeland, R., Hekimoglu-Balkan, B., Pradeepa, M.M., and Bickmore, W.A. (2013). H4K16 acetylation marks active genes and enhancers of embryonic stem cells, but does not alter chromatin compaction. Genome Res *23*, 2053-2065.
Teresa R Luperchio, M.E.S., Xianrong Wong, Marie-Cécile Gaillard, Peter Tsang, Katja Pekrun, Robert A Ach, N Alice Yamada, James Taylor, Karen Reddy (2018). Chromosome Conformation Paints Reveal The Role Of Lamina Association In Genome Organization And Regulation. bioRxiv.
Therizols, P., Illingworth, R.S., Courilleau, C., Boyle, S., Wood, A.J., and Bickmore, W.A. (2014). Chromatin decondensation is sufficient to alter nuclear organization in embryonic stem cells. Science *346*, 1238-1242.
Thomson, I., Gilchrist, S., Bickmore, W.A., and Chubb, J.R. (2004). The radial positioning of chromatin is not inherited through mitosis but is established de novo in early G1. Current Biology *14*, 166-172.
Towbin, B.D., Gonzalez-Aguilera, C., Sack, R., Gaidatzis, D., Kalck, V., Meister, P., Askjaer, P., and Gasser, S.M. (2012). Step-wise methylation of histone H3K9 positions heterochromatin at the nuclear periphery. Cell *150*, 934-947.
Towbin, B.D., Meister, P., and Gasser, S.M. (2009). The nuclear envelope - a scaffold for silencing? Current Opinion in Genetics & Development *19*, 180-186.

Tremethick, D.J. (2007). Higher-order structures of chromatin: the elusive 30 nm fiber. Cell *128*, 651-654.
Uto, K., Inoue, D., Shimuta, K., Nakajo, N., and Sagata, N. (2004). Chk1, but not Chk2, inhibits Cdc25 phosphatases by a novel common mechanism. EMBO J *23*, 3386-3396.
Vagnarelli, P. (2012). Mitotic chromosome condensation in vertebrates. Exp Cell Res *318*, 1435-1441.
Van Hooser, A., Goodrich, D.W., Allis, C.D., Brinkley, B.R., and Mancini, M.A. (1998). Histone H3 phosphorylation is required for the initiation, but not maintenance, of mammalian chromosome condensation. J Cell Sci *111 (Pt 23)*, 3497-3506.
Vassin, V.M., Anantha, R.W., Sokolova, E., Kanner, S., and Borowiec, J.A. (2009). Human RPA phosphorylation by ATR stimulates DNA synthesis and prevents ssDNA accumulation during DNA-replication stress. J Cell Sci *122*, 4070-4080.
Vire, E., Brenner, C., Deplus, R., Blanchon, L., Fraga, M., Didelot, C., Morey, L., Van Eynde, A., Bernard, D., Vanderwinden, J.M*., et al.* (2006). The Polycomb group protein EZH2 directly controls DNA methylation. Nature *439*, 871-874.
Visa, N. (2005). Actin in transcription. Actin is required for transcription by all three RNA polymerases in the eukaryotic cell nucleus. EMBO Rep *6*, 218-219.
Wakatsuki, T., Schwab, B., Thompson, N.C., and Elson, E.L. (2001). Effects of cytochalasin D and latrunculin B on mechanical properties of cells. J Cell Sci *114*, 1025-1036.
Walters, A.D., Bommakanti, A., and Cohen-Fix, O. (2012). Shaping the nucleus: factors and forces. J Cell Biochem *113*, 2813-2821.
Wang, F., Dai, J., Daum, J.R., Niedzialkowska, E., Banerjee, B., Stukenberg, P.T., Gorbsky, G.J., and Higgins, J.M. (2010). Histone H3 Thr-3 phosphorylation by Haspin positions Aurora B at centromeres in mitosis. Science *330*, 231-235.
Wang, Y., Maharana, S., Wang, M.D., and Shivashankar, G.V. (2014). Super-resolution microscopy reveals decondensed chromatin structure at transcription sites. Sci Rep *4*, 4477.
Ward, I.M., and Chen, J. (2001). Histone H2AX is phosphorylated in an ATR-dependent manner in response to replicational stress. J Biol Chem *276*, 47759-47762.
Warren, S.C., Margineanu, A., Alibhai, D., Kelly, D.J., Talbot, C., Alexandrov, Y., Munro, I., Katan, M., Dunsby, C., and French, P.M. (2013). Rapid global fitting of large fluorescence lifetime imaging microscopy datasets. PLoS One *8*, e70687.
Watson, J.D., and Crick, F.H. (1953). Molecular structure of nucleic acids; a structure for deoxyribose nucleic acid. Nature *171*, 737-738.
Webster, M., Witkin, K.L., and Cohen-Fix, O. (2009). Sizing up the nucleus: nuclear shape, size and nuclear-envelope assembly. J Cell Sci *122*, 1477-1486.
Wei, Y., Mizzen, C.A., Cook, R.G., Gorovsky, M.A., and Allis, C.D. (1998). Phosphorylation of histone H3 at serine 10 is correlated with chromosome condensation during mitosis and meiosis in Tetrahymena. Proc Natl Acad Sci U S A *95*, 7480-7484.
Wei, Y., Yu, L., Bowen, J., Gorovsky, M.A., and Allis, C.D. (1999). Phosphorylation of histone H3 is required for proper chromosome condensation and segregation. Cell *97*, 99-109.
Weinhold, N., Jacobsen, A., Schultz, N., Sander, C., and Lee, W. (2014). Genome-wide analysis of noncoding regulatory mutations in cancer. Nat Genet *46*, 1160-1165.
Weintraub, A.S., Li, C.H., Zamudio, A.V., Sigova, A.A., Hannett, N.M., Day, D.S., Abraham, B.J., Cohen, M.A., Nabet, B., Buckley, D.L*., et al.* (2017). YY1 Is a Structural Regulator of Enhancer-Promoter Loops. Cell *171*, 1573-1588 e1528.
Welch, W.J., and Suhan, J.P. (1985). Morphological-Study of the Mammalian Stress Response - Characterization of Changes in Cytoplasmic Organelles, Cytoskeleton, and Nucleoli, and Appearance of Intranuclear Actin-Filaments in Rat Fibroblasts after Heat-Shock Treatment. Journal of Cell Biology *101*, 1198-1211.

Weston, L., Coutts, A.S., and La Thangue, N.B. (2012). Actin nucleators in the nucleus: an emerging theme. J Cell Sci *125*, 3519-3527.
Wilkins, B.J., Rall, N.A., Ostwal, Y., Kruitwagen, T., Hiragami-Hamada, K., Winkler, M., Barral, Y., Fischle, W., and Neumann, H. (2014). A cascade of histone modifications induces chromatin condensation in mitosis. Science *343*, 77-80.
Williamson, I., Berlivet, S., Eskeland, R., Boyle, S., Illingworth, R.S., Paquette, D., Dostie, J., and Bickmore, W.A. (2014). Spatial genome organization: contrasting views from chromosome conformation capture and fluorescence in situ hybridization. Gene Dev *28*, 2778-2791.
Wright, S.J. (1999). Sperm nuclear activation during fertilization. Curr Top Dev Biol *46*, 133-178.
Wu, S., Wang, W., Kong, X., Congdon, L.M., Yokomori, K., Kirschner, M.W., and Rice, J.C. (2010). Dynamic regulation of the PR-Set7 histone methyltransferase is required for normal cell cycle progression. Genes Dev *24*, 2531-2542.
Yamazaki, S., Yamamoto, K., de Lanerolle, P., and Harata, M. (2016). Nuclear F-actin enhances the transcriptional activity of beta-catenin by increasing its nuclear localization and binding to chromatin. Histochem Cell Biol *145*, 389-399.
Yang, D.Q., Halaby, M.J., Li, Y., Hibma, J.C., and Burn, P. (2011). Cytoplasmic ATM protein kinase: an emerging therapeutic target for diabetes, cancer and neuronal degeneration. Drug Discov Today *16*, 332-338.
Ye, Y. (2006). Diverse functions with a common regulator: ubiquitin takes command of an AAA ATPase. J Struct Biol *156*, 29-40.
Young, R.A. (1991). RNA polymerase II. Annu Rev Biochem *60*, 689-715.
Zeman, M.K., and Cimprich, K.A. (2014). Causes and consequences of replication stress. Nat Cell Biol *16*, 2-9.
Zeug, A., Woehler, A., Neher, E., and Ponimaskin, E.G. (2012). Quantitative intensity-based FRET approaches--a comparative snapshot. Biophys J *103*, 1821-1827.
Zhang, L., Eugeni, E.E., Parthun, M.R., and Freitas, M.A. (2003). Identification of novel histone post-translational modifications by peptide mass fingerprinting. Chromosoma *112*, 77-86.
Zhao, H., and Piwnica-Worms, H. (2001). ATR-mediated checkpoint pathways regulate phosphorylation and activation of human Chk1. Mol Cell Biol *21*, 4129-4139.
Zhao, K.J., Wang, W.D., Rando, O.J., Xue, Y.T., Swiderek, K., Kuo, A., and Crabtree, G.R. (1998). Rapid and phosphoinositol-dependent binding of the SWI/SNF-like BAF complex to chromatin after T lymphocyte receptor signaling. Cell *95*, 625-636.
Zheng, C., and Hayes, J.J. (2003). Intra- and inter-nucleosomal protein-DNA interactions of the core histone tail domains in a model system. J Biol Chem *278*, 24217-24224.
Ziv, Y., Bielopolski, D., Galanty, Y., Lukas, C., Taya, Y., Schultz, D.C., Lukas, J., Bekker-Jensen, S., Bartek, J., and Shiloh, Y. (2006). Chromatin relaxation in response to DNA double-strand breaks is modulated by a novel ATM- and KAP-1 dependent pathway. Nat Cell Biol *8*, 870-876.
Zou, L., and Elledge, S.J. (2003). Sensing DNA damage through ATRIP recognition of RPA-ssDNA complexes. Science *300*, 1542-1548.
Zullo, J.M., Demarco, I.A., Pique-Regi, R., Gaffney, D.J., Epstein, C.B., Spooner, C.J., Luperchio, T.R., Bernstein, B.E., Pritchard, J.K., Reddy, K.L*., et al.* (2012). DNA sequence-dependent compartmentalization and silencing of chromatin at the nuclear lamina. Cell *149*, 1474-1487.